

**EFFECT OF SPATIAL AND TEMPORAL VARIABILITY
IN OCEANIC PROCESSES ON AIR-SEA FLUXES
OF CARBON DIOXIDE**

by

Piotr Trela

Submitted in partial fulfilment of the requirements
for the degree of Doctor of Philosophy

at

**Dalhousie University
Halifax, Nova Scotia
August, 1996**

© Copyright by Piotr Trela, 1996



National Library
of Canada

Acquisitions and
Bibliographic Services Branch

395 Wellington Street
Ottawa, Ontario
K1A 0N4

Bibliothèque nationale
du Canada

Direction des acquisitions et
des services bibliographiques

395, rue Wellington
Ottawa (Ontario)
K1A 0N4

Your file *Votre référence*

Our file *Notre référence*

The author has granted an irrevocable non-exclusive licence allowing the National Library of Canada to reproduce, loan, distribute or sell copies of his/her thesis by any means and in any form or format, making this thesis available to interested persons.

L'auteur a accordé une licence irrévocable et non exclusive permettant à la Bibliothèque nationale du Canada de reproduire, prêter, distribuer ou vendre des copies de sa thèse de quelque manière et sous quelque forme que ce soit pour mettre des exemplaires de cette thèse à la disposition des personnes intéressées.

The author retains ownership of the copyright in his/her thesis. Neither the thesis nor substantial extracts from it may be printed or otherwise reproduced without his/her permission.

L'auteur conserve la propriété du droit d'auteur qui protège sa thèse. Ni la thèse ni des extraits substantiels de celle-ci ne doivent être imprimés ou autrement reproduits sans son autorisation.

ISBN 0-612-16005-X

Canada

Name

PIOTR TRELA

Dissertation Abstracts International is arranged by broad, general subject categories. Please select the one subject which most nearly describes the content of your dissertation. Enter the corresponding four-digit code in the spaces provided.

OCEANOGRAPHY

SUBJECT TERM

0416

U·M·I

SUBJECT CODE

Subject Categories

THE HUMANITIES AND SOCIAL SCIENCES

COMMUNICATIONS AND THE ARTS

Architecture 0729
 Art History 0377
 Cinema 0900
 Dance 0378
 Fine Arts 0357
 Information Science 0723
 Journalism 0391
 Library Science 0399
 Mass Communications 0708
 Music 0413
 Speech Communication 0459
 Theater 0465

EDUCATION

General 0515
 Administration 0514
 Adult and Continuing 0516
 Agricultural 0517
 Art 0273
 Bilingual and Multicultural 0282
 Business 0688
 Community College 0275
 Curriculum and Instruction 0727
 Early Childhood 0518
 Elementary 0324
 Finance 0277
 Guidance and Counseling 0519
 Health 0680
 Higher 0745
 History of 0520
 Home Economics 0278
 Industrial 0521
 Language and Literature 0279
 Mathematics 0280
 Music 0522
 Philosophy of 0998
 Physical 0523

Psychology 0325
 Reading 0335
 Religious 0327
 Sciences 0714
 Secondary 0533
 Social Sciences 0534
 Sociology of 0340
 Special 0529
 Teacher Training 0530
 Technology 0710
 Tests and Measurements 0288
 Vocational 0747

LANGUAGE, LITERATURE AND LINGUISTICS

Language
 General 0679
 Ancient 0289
 Linguistics 0290
 Modern 0291

Literature
 General 0401
 Classical 0294
 Comparative 0295
 Medieval 0297
 Modern 0298
 African 0316
 American 0591
 Asian 0305
 Canadian (English) 0352
 Canadian (French) 0355
 English 0593
 Germanic 0311
 Latin American 0312
 Middle Eastern 0315
 Romance 0313
 Slavic and East European 0314

PHILOSOPHY, RELIGION AND THEOLOGY

Philosophy 0422
 Religion
 General 0318
 Biblical Studies 0321
 Clergy 0319
 History of 0320
 Philosophy of 0322
 Theology 0469

SOCIAL SCIENCES

American Studies 0323
 Anthropology
 Archaeology 0324
 Cultural 0326
 Physical 0327

Business Administration
 General 0310
 Accounting 0272
 Banking 0770
 Management 0454
 Marketing 0338
 Canadian Studies 0385

Economics
 General 0501
 Agricultural 0503
 Commerce-Business 0505
 Finance 0508
 History 0509
 Labor 0510
 Theory 0511
 Folklore 0358
 Geography 0366
 Gerontology 0351
 History
 General 0578

Ancient 0579
 Medieval 0581
 Modern 0582
 Black 0328
 African 0331
 Asia, Australia and Oceania 0332
 Canadian 0334
 European 0335
 Latin American 0336
 Middle Eastern 0333
 United States 0337
 History of Science 0585
 Law 0398
 Political Science
 General 0615
 International Law and Relations 0616
 Public Administration 0617
 Recreation 0814
 Social Work 0452

Sociology
 General 0626
 Criminology and Penology 0627
 Demography 0938
 Ethnic and Racial Studies 0631
 Individual and Family Studies 0628
 Industrial and Labor Relations 0629
 Public and Social Welfare 0630
 Social Structure and Development 0700
 Theory and Methods 0344
 Transportation 0709
 Urban and Regional Planning 0999
 Women's Studies 0453

THE SCIENCES AND ENGINEERING

BIOLOGICAL SCIENCES

Agriculture
 General 0473
 Agronomy 0285
 Animal Culture and Nutrition 0475
 Animal Pathology 0476
 Food Science and Technology 0359
 Forestry and Wildlife 0478
 Plant Culture 0479
 Plant Pathology 0480
 Plant Physiology 0817
 Range Management 0777
 Wood Technology 0746

Biology

General 0306
 Anatomy 0287
 Biostatistics 0308
 Botany 0309
 Cell 0379
 Ecology 0329
 Entomology 0353
 Genetics 0369
 Limnology 0793
 Microbiology 0410
 Molecular 0307
 Neuroscience 0317
 Oceanography 0416
 Physiology 0433
 Radiation 0821
 Veterinary Science 0778
 Zoology 0472

Biophysics

General 0786
 Medical 0760

EARTH SCIENCES

Biogeochemistry 0425
 Geochemistry 0996

Geodesy 0370
 Geology 0372
 Geophysics 0373
 Hydrology 0388
 Mineralogy 0411
 Paleobotany 0345
 Paleontology 0426
 Paleozoology 0985
 Polynology 0427
 Physical Geography 0368
 Physical Oceanography 0415

HEALTH AND ENVIRONMENTAL SCIENCES

Environmental Sciences 0768
 Health Sciences
 General 0566
 Audiology 0300
 Chemotherapy 0992
 Dentistry 0567
 Education 0350
 Hospital Management 0769
 Human Development 0758
 Immunology 0982
 Medicine and Surgery 0564
 Mental Health 0347
 Nursing 0569
 Nutrition 0570
 Obstetrics and Gynecology 0380
 Occupational Health and Safety
 Therapy 0354
 Ophthalmology 0381
 Pathology 0571
 Pharmacology 0419
 Pharmacy 0572
 Physical Therapy 0382
 Public Health 0573
 Radiology 0574
 Recreation 0575

Speech Pathology 0460
 Toxicology 0383
 Home Economics 0386

PHYSICAL SCIENCES

Pure Sciences
 Chemistry
 General 0485
 Agricultural 0749
 Analytical 0486
 Biochemistry 0487
 Inorganic 0488
 Nuclear 0738
 Organic 0490
 Pharmaceutical 0491
 Physical 0494
 Polymer 0495
 Radiation 0754
 Mathematics 0405

Physics
 General 0605
 Acoustics 0986
 Astronomy and Astrophysics 0606
 Atmospheric Science 0608
 Atomic 0748
 Electronics and Electricity 0607
 Elementary Particles and High Energy 0798
 Fluid and Plasma 0759
 Molecular 0609
 Nuclear 0610
 Optics 0752
 Radiation 0756
 Solid State 0611
 Statistics 0463

Applied Sciences
 Applied Mechanics 0346
 Computer Science 0984

Engineering
 General 0537
 Aerospace 0538
 Agricultural 0539
 Automotive 0540
 Biomedical 0541
 Chemical 0542
 Civil 0543
 Electronics and Electrical 0544
 Heat and Thermodynamics 0548
 Hydraulic 0545
 Industrial 0546
 Marine 0547
 Materials Science 0794
 Mechanical 0548
 Metallurgy 0743
 Mining 0551
 Nuclear 0552
 Packaging 0549
 Petroleum 0765
 Sanitary and Municipal System Science 0554
 Geotechnical 0428
 Operations Research 0796
 Plastics Technology 0795
 Textile Technology 0994

PSYCHOLOGY

General 0621
 Behavioral 0584
 Clinical 0622
 Developmental 0620
 Experimental 0623
 Industrial 0624
 Personality 0625
 Physiological 0989
 Psychological 0349
 Psychometrics 0632
 Social 0451



Ani, Oldze i Rouzicom dedykuję

TABLE OF CONTENTS

Table of Contents	v
List of Figures	vii
List of Tables	x
Abstract	xi
List of Symbols	xii
Acknowledgments	xvii
Chapter 1: General Introduction	1
Chapter 2: Effects of Spatial Fluctuations in Oceanic Properties on Air-Sea Fluxes of CO₂	
2.1 Introduction	8
2.2 Data	10
2.3 Nonlinear Effects on Partial Pressure of CO ₂	12
2.4 Effects of Spatial Fluctuations on Partial Pressure of CO ₂ in the Surface Ocean	22
2.5 Implications for the Direct Estimates of Air-Sea Fluxes of CO ₂	32
2.6 Implications for Transient Box Models	34
2.7 Other Issues	41
2.8 Concluding Remarks	44
Chapter 3: Temporal Fluctuations in Oceanic Properties in the Labrador Sea: Effect on Air-Sea Fluxes of CO₂	
3.1 Introduction	46
3.2 Approach	49
3.3 Description of the Model	52
3.4 Annual Cycles of Biogeochemical Variables	69
3.5 Partial Pressure and Air-Sea Fluxes of CO ₂	84
3.6 Estimates of the CO ₂ Fluxes by <i>Tans et al.</i> [1990]	98

3.7	Concluding Remarks	99
Chapter 4: Sensitivity of Air-Sea Fluxes of CO₂ in the Labrador Sea to Changes in Oceanic Processes		
4.1	Introduction	101
4.2	Approach	104
4.3	Sensitivity of Air-Sea Fluxes of CO ₂ to Changes in Oceanic Processes	105
4.4	Medium-Term Effects of Alterations in Processes Determining Air-Sea Fluxes of CO ₂	143
4.5	Concluding Remarks	153
Chapter 5: Effects of Temporal Fluctuations in Oceanic Properties on Air-Sea Fluxes of CO₂ in High-CO₂ Environments		
5.1	Introduction	157
5.2	Approach	159
5.3	The Covariance and the Nonlinearity Terms under Various Atmospheric Partial Pressures of CO ₂	161
5.4	Sensitivity of Future Fluxes of CO ₂ to Physical and Biogeochemical Processes	169
5.5	Some Consequences for Carbon Modelling	171
5.6	Concluding Remarks	175
Chapter 6: Concluding Remarks: Summary and Suggestions for Further Work		
Appendix A: Sensitivity of the Estimates of the Nonlinear Effects to the Computational Procedure		
		183
Appendix B: Computation of Vertical Exchanges and the Surface-Layer Temperature in the Labrador Sea		
		188
Appendix C: Details of Biogeochemical Components of the Model of the Labrador Sea		
		194
References		212

LIST OF FIGURES

Figure 2-1 (a) Partial pressure of CO ₂ (p) as a function of temperature (T). (b) Second derivative of p with respect to T (d^2p/dT^2) as a function of T .	14
Figure 2-2 The nonlinear contribution associated with normal distribution of temperature, as a function of its mean and standard deviation	19
Figure 2-3 Partial pressure of CO ₂ as a function of temperature and dissolved inorganic carbon.	20
Figure 2-4 The nonlinear contribution as a function of the standard deviations of temperature, dissolved inorganic carbon, and partial pressure of carbon dioxide at the regional scale	25
Figure 2-5 Partition of the global GEOSECS data into boxes recreating the horizontal structure of several carbon box models from the literature	27
Figure 2-6 The global nonlinear error associated with models with various numbers of boxes	28
Figure 3-1 Components of the one-dimensional model of oceanic properties affecting the transfer of CO ₂ between the atmosphere and the ocean	53
Figure 3-2 Annual cycles of the input variables: (a) thickness of layer 1 and layer 2, (b) air temperature, (c) windspeed, (d) cloud cover, (e) humidity, (f) precipitation	54
Figure 3-3 Computed annual cycles of (a) oceanic temperature, (b) salinity, (c) vertical diffusive mixing velocities	61
Figure 3-4 Annual cycles of the modelled oceanic properties and air-sea fluxes of CO ₂ in the surface layer and the intermediate layer: (a) nutrients, (b) phytoplankton concentration, (c) zooplankton concentration, (d) total alkalinity, (e) dissolved inorganic carbon, (f) air-sea difference in the partial pressure of CO ₂ and the gas-transfer coefficient, (g) air-sea fluxes of CO ₂	71

Figure 3-5 Comparison of the modelled properties with the observational data: (a) the surface-layer nutrient concentration ($\text{NO}_3 + \text{NO}_2$), (b) the surface-layer chlorophyll concentration, (c) the surface-layer concentration of dissolved inorganic carbon.	76
Figure 3-6 Effects of the fluctuations in the oceanic properties on the air-sea fluxes of CO_2 at various time scales	89
Figure 3-7 Distribution of the estimates of \bar{F} , the annual average fluxes of CO_2 as a function of the number of observations used to compute a given estimate	93
Figure 3-8 Distribution of the estimates of the seasonal means of the gas-transfer coefficient (K) and the partial pressure of CO_2 in the surface-layer (p_1), as a function of the number of observations used to compute a given estimate: (a) Estimates of the seasonal mean of K during the cold season. (b) Estimates of the seasonal mean of p_1 during the cold season. (c) Estimates of the seasonal mean of K during the warm season. (d) Estimates of the seasonal mean of p_1 during the warm season.	95
Figure 4-1 Effects of alterations in physical parameters of the model on the partial pressure of CO_2 in the surface layer: (a) effects of the changes in the depth or timing of the deep winter convection, (b) effects of the changes in the depth of the surface layer thickness in summer, (c) effects of the changes in the duration of the summer stratification of the water column on the partial pressure of CO_2	111
Figure 4-2 Effects of hypothetical increases in the ratio of the production of CaCO_3 to the gross primary production	119
Figure 4-3 Effects of modifications in the photosynthesis parameters (α^{chl} and P_m^{chl}) on the seawater properties affecting the air-sea fluxes of CO_2 (a) phytoplankton concentration in the surface layer, (b) dissolved inorganic carbon concentration in the surface layer and in the intermediate layer, (c) air-sea fluxes of CO_2	124
Figure 4-4 Effects of changes in the production-independent component of respiration on the partial pressure of CO_2	129

Figure 4-5 Effects of changes in the zooplankton parameters on the dissolved inorganic concentration in the surface layer	131
Figure 4-6 The partial pressure of atmospheric CO ₂ at Sable Island	135
Figure 4-7 (a) The gas-transfer coefficient as a function of instantaneous windspeeds (b) Partial pressures of CO ₂ in the surface layer computed with the gas-transfer coefficient as a function of instantaneous windspeeds and “smoothed” windspeeds used in the standard run. (c) Air-sea fluxes of CO ₂ computed using instantaneous windspeeds, before and after “smoothing” to remove the day-to-day variations in these fluxes	139
Figure 4-8 The temporal nonlinear contribution, c_t , as a function of standard deviations of the properties of the surface layer of the Labrador Sea: (a) dissolved inorganic carbon, (b) partial pressure of CO ₂	144
Figure 4-9 Evolution of the air-sea fluxes of CO ₂ following hypothetical changes in the photosynthesis parameters.	148
Figure 5-1 Values of the covariance term (ΔF_a) and the nonlinearity term (ΔF_b) as a function of atmospheric partial pressure of CO ₂	163
Figure 5-2 Annual cycles of (a) dissolved inorganic carbon and (b) partial pressure of CO ₂ in the surface waters of the Labrador Sea at the atmospheric partial pressure of CO ₂ of 335 μ atm and 840 μ atm	164
Figure 5-3 The second derivative of partial pressure of CO ₂ (p) with respect to the concentration of dissolved inorganic carbon C , as function of $p(C)$	166
Figure 5-4 Evolution of the air-sea fluxes of CO ₂ following hypothetical increase in α^{chl} and P_m^{chl} by 50% throughout the simulation for the partial pressure of atmospheric CO ₂ (p_a) of 840 μ atm.	170
Figure C-1 The photosynthesis parameters as a function of the nitrate concentration (a,b) and seawater temperature (c,d) in the Labrador Sea	199
Figure C-2 The photosynthesis parameters in the open Labrador Sea as a function of time	201

LIST OF TABLES

Table 2-1 Partial pressure of CO ₂ and the nonlinear contribution at the regional scale	24
Table 2-2 Partial pressure of CO ₂ and the nonlinear contribution associated with various model idealizations of the global ocean	29
Table 2-3 Buffer factors and the nonlinear correction associated with different definitions of the buffer factor	39
Table 3-1 The nonlinear contribution to the oceanic partial pressure of CO ₂ and the air-sea CO ₂ fluxes at the annual and the seasonal time-scales	87
Table 4-1 Sensitivity of the air-sea CO ₂ fluxes to changes in the model parameters or inputs	107
Table 4-2 (a) Departures of the annual air-sea CO ₂ fluxes and of the day of the onset of nutrient limitation from the values in the standard run as a result of changes in the photosynthesis parameters	123
Table 4-2 (b) Departures of the covariance term (ΔF_a) and the carbonate nonlinearity term (ΔF_b) from their standard values as a result of changes in the photosynthesis parameters	123
Table A-1 Sensitivity of global estimates of partial pressure of CO ₂ and the nonlinear error in selected model representations	184
Table B-1 Temperatures and salinities of the waters adjacent to the Labrador Sea (based on <i>Ikeda</i> [1987]).	189
Table B-2 Fitted parameters of the present model and model of <i>Ikeda</i> [1987].	193
Table B-3 Inter-annual and annual variabilities in temperature and salinity	193

ABSTRACT

Air-sea fluxes of CO_2 depend on the gas-transfer coefficient (K) and the air-sea difference in the partial pressure of CO_2 (Δp). If K and Δp covary, the mean air-sea flux of CO_2 will differ from the flux computed from means of K and Δp . The difference is termed here *the covariance term*. Moreover, the partial pressure of CO_2 in seawater (p) is a nonlinear function of several seawater properties, such as temperature (T), salinity (S), concentration of dissolved inorganic carbon (C) and alkalinity (A). As a result of this nonlinearity, air-sea fluxes computed using mean values of p for a range of seawater conditions will differ from the fluxes calculated using p computed from corresponding means of T , S , C and A . The difference is termed here *the carbonate nonlinearity term*. Any study of air-sea fluxes of CO_2 , whether based on observations or models, should, ideally, select time and space scales such as to minimize both these terms.

In this thesis, I quantify the covariance and the nonlinearity terms at various spatial and temporal scales and explore implications of these results for studies of air-sea fluxes of CO_2 . The spatial component of the nonlinearity term is examined using data collected during the Geochemical Ocean Sections Study (GEOSECS). Standard deviation of p is a good indicator of the magnitude of the nonlinearity term. Failing to consider the spatial fluctuations at the global scale may bias direct estimates of global oceanic uptake of CO_2 upward by 3.0 Gt C y^{-1} (=65% of total emissions of anthropogenic CO_2 in 1973). Partitioning the global dataset into subsets representing high- and low-latitude waters reduces the bias to 1.4 Gt C y^{-1} .

To study the temporal components of the covariance and the nonlinearity terms a new ecosystem model of the Labrador Sea is developed. The model is used to simulate the annual cycles of K , T , S , C and A . When the annual means of these properties are used to compute air-sea fluxes of CO_2 , both the covariance and the nonlinearity terms are neglected. This results in overestimation of the air-sea fluxes by $2.4 \text{ mol C m}^{-2} \text{ y}^{-1}$ (=300% of the estimated total annual uptake of anthropogenic CO_2 for the Labrador Sea) compared with the best estimate from the ecosystem model. The overestimation would increase markedly in CO_2 -rich environments. Partitioning the annual cycle into warm and cold seasons reduces the overestimation severalfold.

The Labrador Sea model is used to rank the importance of various oceanic processes for air-sea CO_2 flux. Effects of changes in these processes on the CO_2 flux would be larger in CO_2 -rich environments.

LIST OF SYMBOLS

Notation	Quantity, Units
α^{chl}	initial slope of the chlorophyll-normalized photosynthesis-light curve, $\text{mg C (mg chl)}^{-1} (\text{W m}^{-2})^{-1}$.
γ_A	alkalinity-to-carbon ratio in biogenic matter, $\text{meq. (mmol C)}^{-1}$.
γ_N	nutrient-to-carbon ratio in biogenic matter, $\text{mmol N (mmol C)}^{-1}$.
Γ	CaCO_3 to organic carbon production ratio, $\text{mmol CaCO}_3 (\text{mmol C})^{-1}$.
ϵ_c	recycled fraction of phytoplankton excretion, dimensionless.
ϵ_l	recycled fraction of phytoplankton losses, dimensionless.
ϵ_m	recycled fraction of zooplankton losses, dimensionless.
θ	carbon-to-chlorophyll ratio, $\text{mg C (mg chl)}^{-1}$.
u	piston velocity, m d^{-1} .
Λ	Irlev parameter, $(\text{mg C m}^{-3})^{-1}$.
μ	reciprocal of e -folding time for anthropogenic CO_2 production, when the production is assumed to grow exponentially, yr^{-1} .
ξ	buffer factor, dimensionless.
$\Delta\xi$	nonlinear correction of buffer factor (the difference in buffer factor between a nonuniform and a uniform ocean).
σ	biomass-specific gross phytoplankton growth, d^{-1} .
a	assimilation efficiency of zooplankton, dimensionless.
a	area weight (fraction of the area of the global ocean), dimensionless.
A	total alkalinity, meq m^{-3} , $\mu\text{eq kg}^{-1}$.
A	proportionality coefficient linking the piston velocity with windspeed, $\text{m d}^{-1}(\text{m s}^{-1})^{-2}$.
B	phytoplankton biomass, mmol C m^{-3} .
B_o	threshold prey concentration, mmol C m^{-3} .
B	number of boxes composing the global ocean.
c	nonlinear contribution to the partial pressure of CO_2 , μatm .
c_t	temporal nonlinear contribution, μatm .

C	dissolved inorganic carbon, mmol m^{-3} , $\mu\text{mol kg}^{-1}$.
δC	small departure from the actual values of C , $\mu\text{mol kg}^{-1}$.
d_i	diffusivity across the bottom of layer i , m^2d^{-1} .
D	daylength, hr.
E	specific excretion rate, d^{-1} .
\mathcal{E}	excretion as a fraction of the gross phytoplankton growth σ , dimensionless.
E	nonlinear error, μatm .
$f_{ij}^d(X_i, X_j)$	diffusive flux of a property X from layer i to layer j . ($= -f_{ji}^d(X_i, X_j)$), mmol m^{-2} .
$f_{ij}^e(X_i, X_j)$	flux of a property X from layer i to layer j caused by entrainment, mmol m^{-2} .
F	air-sea flux of CO_2 , $\text{mol m}^{-2} \text{yr}^{-1}$, $\text{mmol m}^{-2} \text{d}^{-1}$.
F_a	air-sea flux of CO_2 computed without accounting for the covariance between K and Δp , ($= \overline{K \Delta p}$), $\text{mol m}^{-2} \text{yr}^{-1}$.
F_b	air-sea flux of CO_2 computed without accounting for the covariance between K and Δp , or for the nonlinearity of the carbonate system, ($= \overline{K \Delta p(\overline{K}, \overline{T}, \overline{S}, \dots)}$), $\text{mol m}^{-2} \text{yr}^{-1}$.
F_x	anthropogenic air-sea flux of CO_2 , $\text{mol m}^{-2} \text{yr}^{-1}$.
^{14}F	air-sea flux of ^{14}C $\text{mol m}^{-2} \text{yr}^{-1}$.
\overline{F}	average air-sea flux of CO_2 , $\text{mol m}^{-2} \text{yr}^{-1}$.
ΔF_a	the covariance term, the component of air-sea fluxes of CO_2 associated with the covariance between K and Δp . ($F_a - \overline{F} = \overline{K' \Delta p'}$), $\text{mol m}^{-2} \text{yr}^{-1}$.
ΔF_b	the carbonate nonlinearity term, the component of air-sea fluxes of CO_2 associated with the nonlinearity of the carbonate system, $= F_b - F_a = -\overline{K}c$, $\text{mol m}^{-2} \text{yr}^{-1}$.
$\Delta \overline{F}_{p_a}$	change in \overline{F} as a result of a change in a biogeochemical process (at a given value of p_a).
g	specific grazing rate, d^{-1} .
g_m	maximum specific grazing rate, d^{-1} .

h	entrainment/detrainment velocity, m d^{-1} .
h^+	entrainment velocity, m d^{-1} .
h^-	detrainment velocity, m d^{-1} .
H	thickness of a layer or a box, m .
\mathbf{H}_a	depth of surface ocean water containing the same amount of dissolved inorganic carbon as the preindustrial atmosphere, m .
$\mathbf{H}_m, \mathbf{H}_d$	depths of the mixed layer and the deep ocean, respectively, m .
\mathbf{H}^*	the effective mixed-layer depth (H_m increased to reflect transfer of carbon from the mixed layer into the deep ocean), m .
i	input of the anthropogenic CO_2 into the ocean-atmosphere system, mol yr^{-1} .
I_o	irradiance just below the sea surface, (W m^{-2}).
I_k	photoadaptation parameter, $= P_m^{chl} / \alpha^{chl}$, W m^{-2} .
k_i	diffusive mixing velocity across the bottom of layer i , m d^{-1} .
$\mathbf{k}_{i,j}$	transfer coefficients from reservoir i to reservoir j , yr^{-1} .
\bar{K}	gas-transfer coefficient, $\text{mol CO}_2 \text{ m}^{-2} \text{ yr}^{-1} \mu\text{atm}^{-1}$.
\bar{K}	average gas-transfer coefficient, $\text{mol CO}_2 \text{ m}^{-2} \text{ yr}^{-1} \mu\text{atm}^{-1}$.
\mathcal{K}	vertical attenuation coefficient for irradiance, m^{-1} .
\mathcal{K}_w	attenuation coefficient of water, m^{-1} .
\mathcal{K}^{chl}	attenuation coefficient of chlorophyll and co-varying substances, $\text{m}^{-1} (\text{mg chl m}^{-3})^{-1}$.
\mathcal{K}_x	attenuation coefficient of all substances other than chlorophyll, m^{-1} .
\mathbf{K}_b	number of regions composing a box.
\mathbf{K}_r	number of individual samples within a region.
l	specific loss rate of phytoplankton d^{-1} .
L_i	proportionality constant converting difference in density between adjacent layers into diffusivity d_i , $\text{m}^2 \text{ d}^{-1} (\text{kg m}^{-3})^{1.5}$.
m	zooplankton specific loss rate, d^{-1} .
\mathbf{M}_a	mass of the atmosphere, mol .
\mathbf{n}	number of regions composing the global ocean, $\mathbf{n}=1, \dots, \mathbf{R}$.
N	nitrate concentration, nmol m^{-3} .

N_i	departure from N_{i0} due to uptake of anthropogenic CO_2 , mol.
N_{i0}	amount of preindustrial carbon in i th reservoir, mol.
p	partial pressure of CO_2 in seawater, μatm .
δp	small departure from the actual values of p associated with departure in C by δC , μatm .
p_1	partial pressure of CO_2 in the surface layer, μatm .
$\overline{p(T, S, \dots)}$	average value of the partial pressure, μatm .
$p(\overline{T}, \overline{S}, \dots)$	partial pressure calculated from the average seawater properties, μatm .
p_a	atmospheric partial pressure of CO_2 , μatm .
$\overline{p_a}$	average atmospheric partial pressure of CO_2 , μatm .
p_{a0}	preindustrial partial pressure of CO_2 , μatm .
p_e	model estimate of p_t , μatm .
p_m	partial pressure in the mixed layer, μatm .
p_t	true value of mean partial pressure in the global surface ocean, μatm .
Δp	air-sea difference in the partial pressure of CO_2 , $= p_a - p$, μatm .
\mathcal{P}	concentration of phosphates, $\mu\text{mol kg}^{-1}$.
$P(z)$	primary production at depth z , $\text{mg C m}^{-3} \text{ hr}^{-1}$.
P_m^{chl}	assimilation number, $\text{mg C (mg chl)}^{-1} \text{ hr}^{-1}$.
P_T	daily primary production for a layer, $\text{mg C m}^{-2} \text{ d}^{-1}$.
r	coefficient of correlation, dimensionless.
r^2	coefficient of determination, dimensionless.
\mathbf{r}_a	fraction of anthropogenic CO_2 remaining in the atmosphere, dimensionless.
R	specific respiration rate of phytoplankton d^{-1} .
R_d	dark respiration as a fraction of gross growth rate, dimensionless.
R_L	enhancement of the dark respiration in light, dimensionless.
R_o	specific maintenance respiration rate of phytoplankton (the rate when production is zero), d^{-1} .
\mathcal{R}	isotopic ratio of ^{14}C to ^{12}C , dimensionless.
\mathbf{R}_b	total number of regions per box b .
$s(X)$	standard deviation of a property X .

S	salinity, dimensionless.
S_r	number of samples per region r .
Sc	Schmidt number, dimensionless.
Si	silicate, $\mu\text{mol kg}^{-1}$.
T	temperature, $^{\circ}\text{C}$.
v	phytoplankton sinking velocity, m d^{-1} .
w	windspeed, m s^{-1} .
Z	zooplankton biomass, mol C m^{-3} .

Subscripts referring to the biogeochemical model of the Labrador Sea:

1	surface layer.
2	intermediate layer.
3	deep layer.
a	atmosphere.
i	a given layer.
j	a layer below layer i , $j = i + 1$.
o	preindustrial.

Superscripts:

Single prime indicates fluctuating component, departure of individual value from the mean.

Overbar indicates mean properties.

ACKNOWLEDGMENTS

I am very grateful to Dr. Shubha Sathyendranath and Dr. Trevor Platt for their patience, invaluable advice and guidance during the course of this thesis. I am indebted to Dr. Robert Moore, Dr. Dan Kelley and Dr. John Cullen, the other three members of my supervisory committee, for their advice in the course of the thesis work. I also thank Dr. Taro Takahashi, the external examiner, for the time and attention he spent on my thesis and for many helpful comments.

I am grateful to all the scientific and technical staff at the Biological Oceanographic Division of the Bedford Institute of Oceanography for their support. I would also like to thank Dr. John Lazier and other members of the Ocean Circulation Division of the Bedford Institute of Oceanography for providing me with the data and their insights into the physical oceanography of the Labrador Sea.

Financial support during the course of this work was provided by the Natural Sciences and Engineering Research Council through operating grants to Dr. Shubha Sathyendranath and Dr. Trevor Platt.

Thanks also go to my friends: Ravi, Margareth, Vivian and others who helped me with my work and made my years in Halifax memorable.

Finally, I would like to thank Anna and my parents for their love, support, patience and understanding and Olga for brightening the sky with her smile.

Chapter 1.

General Introduction

The oceans are an important component of the global carbon cycle. This was true historically, when the carbon cycle was undisturbed, and is true in the present, when the cycle is perturbed by the activity of man. The role of the oceans in the global carbon cycle has, therefore, been the subject of intense research involving observations and modelling.

Observational studies contribute to our understanding of the carbon cycle in two ways. First, they provide direct estimates of the air-sea exchanges of CO₂ from the observed fields of oceanic partial pressure of CO₂ and the gas transfer-coefficient [*Tans et al.*, 1990; *Lefevre*, 1995; *Takahashi et al.*, 1995]. Second, the observed seawater properties describing the carbonate system, as well as the distribution of tracers, are used to constrain carbon models [e.g., *Oeschger et al.*, 1975; *Siegenthaler*, 1983; *Shaffer and Sarmiento*, 1995].

Models are constructed to test our understanding of the carbon cycle in the past and at present, and to predict the evolution of this cycle in the future. The first objective is achieved by diagnostic models, the second by transient models.

Diagnostic models use sets of physical and biogeochemical constraints to identify important physical and biogeochemical mechanisms controlling carbon fluxes in the oceans [*Rintoul*, 1992]. Into this category fall the models of *Knox and McElroy* [1984], *Sarmiento and Toggweiler* [1984], *Siegenthaler and Wenk* [1984], *Volk and Liu* [1988], *Taylor et al.* [1991], and *Shaffer and Sarmiento* [1995]. The spatial resolution of diagnostic models varies from the local to the global. These models are not designed to examine the evolution of the carbon cycle over long time scales: their temporal coverage is limited to periods during which a quasi-steady state can be assumed. Therefore, diagnostic models describe either past periods in which

a quasi-steady state of the carbon cycle prevailed (e.g., the preindustrial and the glacial periods), or “snapshots” of the present carbon cycle. In the latter case, the premise is that the accumulation of anthropogenic CO₂ in the ocean-atmosphere system during the simulated period is very small and has a negligible effect on the carbon cycle.

Processes crucial to the oceanic carbon cycle are identified and the spatial and temporal scales relevant to these processes are evaluated using diagnostic models. This information is then used to formulate another class of carbon models that examine transient changes in the carbon cycle. Transient models typically operate at the global scale and simulate periods from the preindustrial times to the present time, and are often extended into the 21st century.

These models range from simple ones with a few compartments, such as the box and box-diffusion models of *Craig* [1957], *Keeling* [1973], *Oeschger et al.* [1975], *Hoffert et al.* [1981], *Bacastow and Björkström* [1981], *Siegenthaler* [1983], *Peng and Broecker* [1991], *Joos et al.* [1991], *Craig and Holmen* [1995] and *Jain et al.* [1995] to the three-dimensional (3-D), ocean general-circulation models (OGCM) with a resolution of a few degrees latitude [e.g., *Maier-Reimer and Hasselmann*, 1987; *Toggweiler et al.*, 1989; *Sarmiento et al.*, 1992; and *Taylor*, 1995]. Despite their superior spatial and temporal resolution, the 3-D models are not likely to replace simple box-models completely, because their complexity and computational requirements limit their applications, particularly when comprehensive sensitivity analyses are required [*Shaffer and Sarmiento*, 1995].

In spite of recent advances in this field, some aspects of the carbon cycle in the air-sea system have received little attention in the past. For example, we do not know how best deal with fluctuations in properties determining air-sea fluxes. All studies, whether they be based on observations or models, have to choose some minimal spatial and temporal scales and to ignore fluctuations in the studied quantities at smaller scales. But to optimize the studies, it is important to select the scales of study such as to minimize errors from finer-scale fluctuations in the field.

In this thesis, I explore fluctuations in the ocean carbon cycle, the biogeochemical processes responsible for these fluctuations and their implications for our understanding of the role of the oceans in climate change.

Let us begin by looking at factors that influence the flux of CO_2 across the ocean-atmosphere interface. Air-sea flux of CO_2 (F) is driven by the air-sea difference in the partial pressure of CO_2 (Δp), with the rate controlled by the gas-transfer coefficient (K):

$$F = K \Delta p = K(p_a - p), \quad (1 - 1)$$

where p_a and p are the partial pressures of CO_2 in air and in seawater, respectively. The gas-transfer coefficient K is primarily a function of windspeed. The partial pressure of CO_2 in seawater is a function of several seawater properties, such as temperature (T), salinity (S), alkalinity (A), and concentrations of dissolved inorganic carbon (C), phosphates (\mathcal{P}) and silicates (Si): $p = p(T, S, A, C, \mathcal{P}, Si)$. (Note that other seawater properties may affect p indirectly, for example, a decrease in nitrate concentration increases alkalinity.)

The dependence of p on these properties is nonlinear. As a result, the mean partial pressure of CO_2 may be different from the partial pressure computed from the mean properties of seawater, with the difference termed here the *nonlinear contribution c*:

$$c = \overline{p(T, S, C, \dots)} - p(\overline{T}, \overline{S}, \overline{C}, \dots) \neq 0, \quad (1 - 2)$$

where the overbars denote mean values.

Spatial and temporal variability in K and Δp introduces nonlinear effects in the air-sea exchange of CO_2 . To quantify these effects, instantaneous values of K and Δp are first decomposed into mean and fluctuating components:

$$K = \overline{K} + K', \quad (1 - 3)$$

$$\Delta p = \overline{\Delta p} + \Delta p', \quad (1 - 4)$$

where, as before, the overbars denote means, and the primes denote fluctuating components. The quantity $\overline{\Delta p}$ can be further decomposed using equation (1-2):

$$\overline{\Delta p} = \overline{(p_a - p)} = \overline{p_a} - \overline{p} = \overline{p_a} - (p(\overline{T}, \overline{S}, \dots) + c). \quad (1-5)$$

The average flux of CO₂ can now be expressed as

$$\begin{aligned} \overline{F} &= \overline{K \Delta p} \\ &= \overline{(\overline{K} + K')(\overline{\Delta p} + \Delta p')} \\ &= \overline{K} \overline{\Delta p} + \overline{K' \Delta p'} \\ &= \underbrace{\overline{K} [\overline{p_a} - p(\overline{T}, \overline{S}, \dots)]}_{F_b} + \underbrace{(-\overline{K}c)}_{\Delta F_b} + \underbrace{\overline{K' \Delta p'}}_{\Delta F_a} \end{aligned} \quad (1-6)$$

In other words, the mean air-sea flux of CO₂ is the sum of three terms:

1. $F_b = \overline{K} [\overline{p_a} - p(\overline{T}, \overline{S}, \dots)]$, is the term associated with the means: \overline{K} and \overline{T} , \overline{S} , and so on;
2. $\Delta F_a = \overline{K' \Delta p'}$ is the *covariance term*. If there is any covariance between K and Δp , the mean air-sea CO₂ flux will differ from the flux associated with average values of K and Δp .
3. $\Delta F_b = -\overline{K}c$ is the *carbonate nonlinearity term*. As a result of the nonlinearity in the carbonate system, the partial pressure of a uniform ocean would be different from the mean partial pressure of an ocean whose properties fluctuate in space and time, even if the averages of the seawater properties in both cases were identical.

Estimates of air-sea flux of CO₂ from surface-ocean data and from carbon models neglect ΔF_a and, often, ΔF_b . Little work has been done to quantify ΔF_a or ΔF_b , or to evaluate strategies to minimize potential errors in estimated air-sea flux of CO₂ associated with these two terms.

The conclusions drawn from averaged observations may be misleading if the observations do not reflect variations in the relevant properties at all the pertinent

time and space scales. For example, by assuming uniformity of oceanic properties at some temporal and spatial scales, global carbon models implicitly neglect the covariance term (ΔF_a) and the carbonate nonlinearity term (ΔF_b) at small scales. As a result, systematic errors in the estimates of the air-sea fluxes of CO_2 are introduced. One expects these errors to be larger in box models with coarse spatial and temporal resolution, although the errors may persist to a smaller degree in 3-D models as well.

It is easy to see that nonlinear effects can be a source of error in models that ignore them. But what are the consequences for the real ocean? There is always a certain degree of variability in the real ocean. If there is a change in this variability, say in temperature, due to changes in horizontal mixing, or in dissolved inorganic carbon and alkalinity, due to changes in spatial or temporal patterns of nutrient utilization by oceanic biota, the net air-sea flux of CO_2 could change. In other words, if nonlinear effects are important, the net flux of CO_2 between the oceans and the atmosphere can also be modified by altering the fluctuations around the mean properties, rather than the means themselves. This is contrary to the common, tacit, assumption that a change in the role of the oceans in global carbon cycles requires a modification in the mean properties of the world ocean.

In this thesis, I quantify the magnitude of the errors arising from estimating mean fluxes of CO_2 from mean oceanic properties (i.e., from neglecting ΔF_a and ΔF_b) using oceanic data (Chapter 2) and one-dimensional model simulations (Chapters 3). I discuss ways to reduce these errors (Chapters 2 and 3).

Since this work focuses on spatial and temporal variability in the oceanic properties controlling the air-sea fluxes of CO_2 , it seems worthwhile to explore which processes are responsible for this variability. In general, the variability in oceanic properties reflects spatial and temporal patterns in the underlying oceanic processes:

- physico-chemical processes, such as air-sea exchanges and water mixing, and

- biogeochemical processes involved in the formation, sinking and decomposition of biogenic matter.

Changes in these processes may affect the mean and the fluctuating components of the fluxes. I use an ecosystem model of the Labrador Sea to test the sensitivity of the various components of air-sea CO₂ fluxes (i.e., \overline{F} , ΔF_a and ΔF_b) to these physical, chemical and biological processes (Chapter 4).

This analysis is then extended to examine future, CO₂-rich, environments (Chapter 5). Sensitivity of the CO₂ fluxes to variability in oceanic processes may be altered in future environments. This is because the nonlinearity in the carbonate system increases as the concentration of dissolved inorganic carbon in seawater increases over present-day levels. Therefore, the covariance and the carbonate nonlinearity terms are likely to increase in the future, as anthropogenic carbon accumulates in the ocean. I try to quantify the potential change in those terms using the Labrador Sea model.

Results of sensitivity studies can also be used to rank various physical and biological processes according to their relative importance for air-sea CO₂ fluxes. (Chapter 4). This ranking can be used for optimising other models of CO₂ fluxes in the Labrador Sea.

Some other issues associated with fluctuations in the oceanic properties are also addressed in this thesis. In addition to the systematic errors that are inherent in the use of mean values to describe nonlinear processes, there are random errors associated with imprecise determination of these means because of insufficient sampling. In Chapter 3, I examine sampling strategies to reduce these errors.

The results of this work are partitioned into four chapters, followed by a general discussion. In Chapter 2, I examine the nonlinearity of the carbonate system and evaluate the effect of spatial fluctuations in the seawater properties on the oceanic partial pressure of carbon dioxide and on air-sea fluxes of CO₂, using the data from

the Geochemical Ocean Sections Study (GEOSECS) and the Transient Tracers in the Oceans (TTO) cruises.

In Chapter 3, I describe a diagnostic model of the Labrador Sea and use it to simulate temporal fluctuations in seawater properties controlling the air-sea difference in the partial pressure of CO_2 and in the gas-transfer coefficient. The importance of covariance between Δp and K , and the consequences of the nonlinearity of the carbonate system, for the air-sea fluxes of CO_2 in the Labrador Sea are then evaluated.

In Chapter 4, I use the model of the Labrador Sea to assess the sensitivity of the air-sea CO_2 fluxes to possible changes in physical and biogeochemical processes, at present levels of atmospheric CO_2 . The sensitivity of the components of the CO_2 fluxes associated with the means and with the fluctuations in the oceanic properties are evaluated. I also examine the evolution of the CO_2 fluxes over several decades after modifications in some of the oceanic processes.

In Chapter 5, I compute the components of the CO_2 fluxes associated with the fluctuations in the oceanic properties in future, CO_2 -rich environments. I assess changes in the sensitivity of air-sea fluxes of CO_2 to the oceanic properties in the future environments. Some implications of these results for the validity of tracer calibration of carbon models are also discussed.

Finally, a summary of the results and some directions for future work are presented in Chapter 6.

Chapter 2.

Effects of Spatial Fluctuations in Oceanic Properties on Air-Sea Fluxes of CO₂

2.1 Introduction

The partial pressure of CO₂ in the oceans is controlled by several seawater properties: temperature, salinity, total alkalinity, dissolved inorganic carbon, and, to a smaller extent, by other components such as the concentration of silicate and phosphate. A decrease in alkalinity or an increase in temperature or dissolved inorganic carbon tends to raise the partial pressure quasi-exponentially. An increase in salinity, silicate or phosphate concentration has a similar effect, albeit much less pronounced.

Due to the nonlinearities in these relationships, the average partial pressure of a set of seawater samples is usually different from the partial pressure calculated from the average values of the controlling seawater properties. For example, if one considers two water masses with distinct temperatures, the average partial pressure of the two water masses would be different from that associated with their average temperature. The nonlinearity of the carbonate system implies that the partial pressure of a uniform ocean would be different from that of a nonuniform ocean with the same mean properties as the uniform ocean. Since the transfer of CO₂ through the ocean-atmosphere interface is driven by the difference in partial pressure of CO₂ across this interface, an alteration of partial pressure in surface waters would affect the net flux of carbon between the ocean and the atmosphere.

In this chapter I try to assess the magnitude of the error incurred when the spatial aspect of the nonlinearity of the carbonate system is ignored. I concentrate

on the surface waters which are in direct contact with the atmosphere. The horizontal structure of existing carbon models is used to partition the data into one or more boxes and to compare the results of simple models with those of more complex models.

The results show that neglecting the nonlinearity of the carbonate system may lead to underestimating of the partial pressure of CO_2 . I examine some implications of these results for observational studies and global carbon models. Air-sea fluxes of CO_2 are estimated as the product of the difference in partial pressure between the atmosphere and the surface ocean (Δp) and the gas-transfer coefficient K . Errors in estimates of the partial pressure incurred on neglecting the nonlinear effects translate into errors in the estimate of these fluxes. If the ice-free area of the ocean is on average $340 \times 10^{12} \text{ m}^2$, and the global average gas-transfer coefficient K is $0.067 \text{ mol CO}_2 \text{ m}^{-2} \text{ yr}^{-1} \mu\text{atm}^{-1}$ [*Tans et al.*, 1990], then a difference of $1 \mu\text{atm}$ in the partial pressure, at the global scale, would lead to a change in the estimated carbon flux of about $0.27 \text{ Gt C yr}^{-1}$. This value is equivalent to 6% of the annual anthropogenic emission in the mid-1970s (the period from which most of the data used in this work originates) [*Rotty*, 1987].

In global carbon models the ocean is represented by a small number of boxes. It is assumed that the seawater properties are horizontally uniform within each box. This implies that the nonlinearity of the carbonate system is ignored within each box, and consequently the partial pressures estimated from the average properties of each box are biased with respect to the real ocean.

It is more difficult to quantify the consequences of neglecting the carbonate nonlinearity in carbon models than in direct estimates from the surface-ocean data. In carbon models the final results are influenced by dynamic interactions between carbon reservoirs in the atmosphere, the mixed layer and the deep ocean. Therefore, the consequences of nonlinearity would depend on the assumptions used in the model and the structure of the model. I compute the error caused by neglecting nonlinear

effects in some simplified models and examine the possible consequences of these effects for more realistic models.

The nonlinear effect may also modify results of diagnostic box models, which deduce the rates of mixing and of biochemical processes using a set of physical and biochemical constraints [Rintoul, 1992]. Partial pressure of CO₂ is one such constraint; hence accounting for the nonlinear effects may modify conclusions drawn from these models as well.

2.2 Data

2.2.1 Geochemical Ocean Sections Study (GEOSECS)

To estimate the nonlinear effects associated with spatial variability in oceanic properties I used mainly the Geochemical Ocean Sections Study (GEOSECS) data [as given in the GEOSECS atlases of Bainbridge, 1981; Broecker *et al.*, 1982; Weiss *et al.*, 1983]. This is the only global carbon data set available to date, and it has been widely used in studies of the global carbon cycle.

The GEOSECS data do not cover the whole ocean and represent mostly the summer seasons in both hemispheres [Takahashi *et al.*, 1981a], thus these estimates of the nonlinear effects refer to the idealized "GEOSECS ocean" and, as discussed later, probably represent a lower bound for the nonlinear effects in the real ocean.

The nonlinear effects in the mixed layer were of main interest here, as the waters in this layer are in direct contact with the atmosphere. To evaluate the properties of these waters I used the GEOSECS data from the top 49 m of the water column, corresponding to the depth ranges 0-24 m and 24-49 m in the GEOSECS carbonate data summary of Takahashi *et al.* [1981b].

I chose the 0-49 m depth range as a compromise between minimizing the influence of the deep waters and retaining a large number of observations. Using data from a greater depth range (for instance, one corresponding to a mixed layer of

75 m used in many carbon models) would introduce the risk of admitting, in areas where the mixed layer is shallow, observations that are strongly influenced by the properties of deep waters, thus being unrepresentative of waters in direct contact with the atmosphere. Using a smaller depth range in this analysis, on the other hand, would reduce the already sparse coverage of some oceanic regions.

For example, consider the case of the North Indian Ocean. In this region the average partial pressure of CO₂ for samples from 50-74 m was higher by 124 μ atm than that for samples from 0-49 m. Therefore, incorporation of the samples from the 50-74 m layer would affect strongly both the average and the variance in seawater properties within this region. Restriction of the analysis to observations from the depth range of 0-24 m, on the other hand, would leave only three samples in the whole region.

2.2.2 Transient Tracers in the Oceans (TTO)

The analysis based on the GEOSECS data was supplemented by examination of some data from the Transient Tracers in the Oceans (TTO) cruises. I used the revised version of the TTO data, compiled by P. Brewer, T. Takahashi and R. T. Williams, available at The Carbon Dioxide Information Analysis Center (CDIAC).

The TTO data were used to obtain an independent estimate of the seawater properties in the North Atlantic, the region poorly covered during the GEOSECS cruises. The TTO data were also used to assess consequences of variability in the seawater properties at local scales (comparable with the resolution of ocean general circulation models).

2.3 Nonlinear Effects on Partial Pressure of CO₂

2.3.1 Definitions

To describe the consequences of the nonlinearity of the carbon system on the oceanic partial pressure of CO₂ I use the term “nonlinear effects.” Whenever necessary I make a distinction between “nonlinear contribution” and “nonlinear error.” The first term refers to the difference in partial pressure between the real, nonuniform, waters and the waters assumed to be uniform at the scale of interest. *Nonlinear error*, on the other hand, reflects the difference between the real ocean and a partially uniform ocean. A partially uniform ocean is made up of a number of parts, each of which is assumed to be internally uniform, but distinct from the others. The word “error” is used to underscore the application of this quantity in observational studies and models, which approximate the real ocean as a set of compartments, each of which is assumed to be uniform. As a result of ignoring nonlinearity within the compartments, the estimates of partial pressure of CO₂ are subject to a systematic error. These concepts are elaborated further in the following paragraphs.

The nonlinear contribution

The nonlinear contribution c is defined here as the difference between the average partial pressure of CO₂ of a nonuniform body of water and the partial pressure that the same body of water would have if it were uniform, with the same mean composition as the nonuniform waters.

If one denotes the average value of a property X as \bar{X} , the nonlinear contribution c may be expressed as

$$c = \overline{p(T, S, A, C, Si, P)} - p(\bar{T}, \bar{S}, \bar{A}, \bar{C}, \bar{Si}, \bar{P}). \quad (2-1)$$

where p is the partial pressure of CO_2 , T is temperature, S stands for salinity, A is alkalinity, and C , Si and \mathcal{P} stand for the concentration of dissolved inorganic carbon, silicate and phosphate, respectively. A glossary of the mathematical notations appears in the introductory part of this thesis.

The first term on the right-hand side of equation (2-1) represents the partial pressure for the nonuniform case. It is computed as the average of partial pressures associated with each sample, which in turn are calculated from the individual sample values of the controlling variables. The second term is the partial pressure for the uniform case. It is computed by assuming that the seawater properties controlling the partial pressure are uniform within the body of water considered, and equal to the average values of these properties. Note that this approach assumes that the available data are truly representative of the real nonuniform ocean.

As an example, the nonlinear contribution for the case when p is a function of only temperature (with remaining seawater properties kept at average GEOSECS values) is shown in Figure 2-1a.

The partial pressure of CO_2 was computed following the scheme of *Peng et al.* [1987], which uses dissociation constants for carbonic, boric, silicic and phosphoric acids given by *Mehrbach et al.* [1973], *Lyman* [1956], *Ingri* [1959], and *Kester and Pytkowicz* [1967], respectively. Some carbon models have used an alternative set of the carbonic acid dissociation constants of *Goyet and Poisson*, [1989] (although *Takahashi et al.* [1993] have argued that the temperature dependence of the partial pressure computed using these constants is inconsistent with the values measured directly). Therefore, Figures 2-1a and 2-1b contain results derived for these constants as well (denoted by broken lines).

Consider two observations with temperatures T_I and T_J , and corresponding partial pressures p_I and p_J . The nonlinear contribution c graphically represented here as a vector $\overline{XX'}$, is the difference between the average of the partial pressures associated with the individual values of temperature ($\overline{p(T)}$) and the partial pressure computed for the average temperature ($p(\overline{T})$).

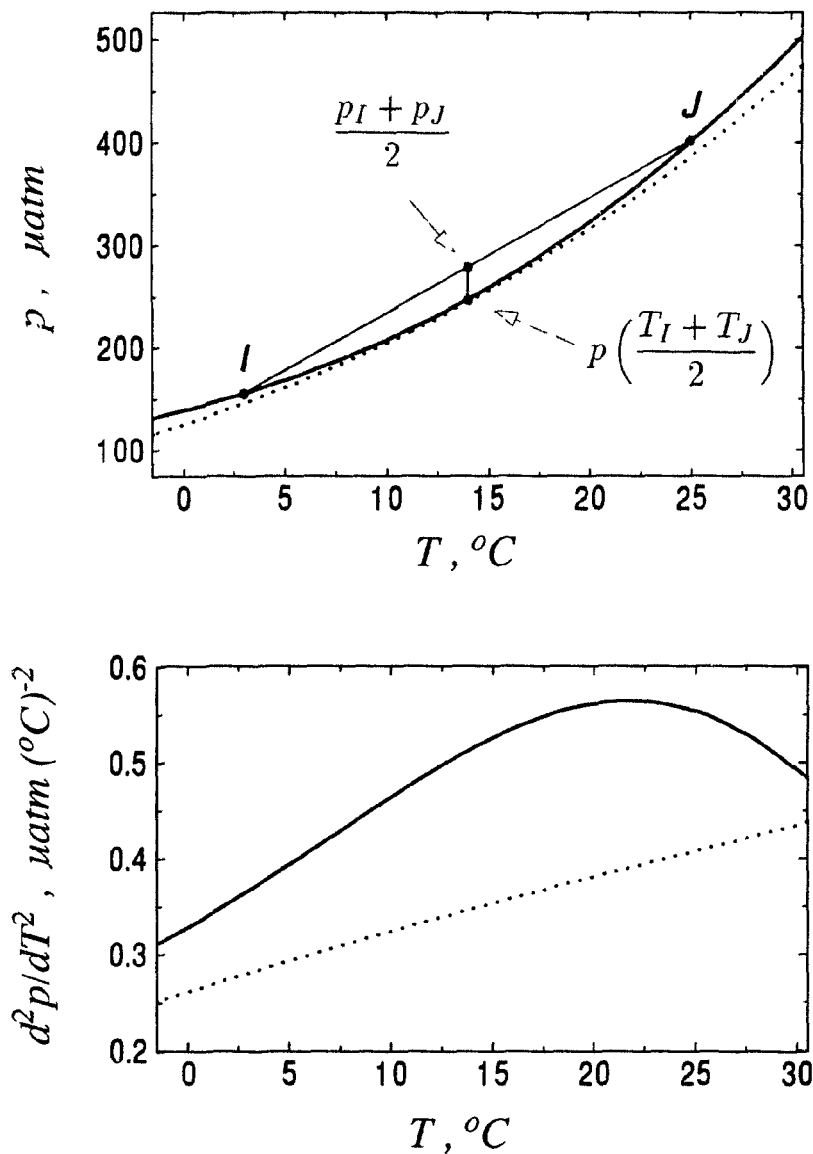


FIGURE 2-1. (a) Partial pressure of CO₂ (p) as a function of temperature (T). Note the nonlinearity of this relation: $(p_I + p_J)/2 > p[(T_I + T_J)/2]$. (b) Second derivative of p with respect to T (d^2p/dT^2) as a function of T . Solid and dashed lines represent results obtained using dissociation constants of Mehrbach *et al.* [1973] and of Goyet and Poisson [1989], respectively. Alkalinity, dissolved inorganic carbon, silicate, and phosphate concentrations are assumed to be average values in the analyzed GEOSECS data: 2320 $\mu\text{eq kg}^{-1}$, 2010 $\mu\text{mol kg}^{-1}$, 6 $\mu\text{mol kg}^{-1}$, and 0.4 $\mu\text{mol kg}^{-1}$, respectively.

The nonlinear contribution can be evaluated at various spatial scales. Let us divide the ocean into regions, each representing a certain oceanographic regime. Based on the assumption of equal weight to every observation in a region, the average of a property X for region r , \bar{X}_r , is given by

$$\bar{X}_r = \frac{\sum_{s=1}^{S_r} X_s}{S_r}, \quad (2-2)$$

where S_r is the number of samples in region r . The nonlinear contribution at the regional scale is then given by

$$c_r = \bar{p}_r - p(\bar{T}_r, \bar{S}_r, \dots) = \frac{\sum p_s(T_s, S_s, \dots)}{S_r} - p\left(\frac{\sum T_s}{S_r}, \frac{\sum S_s}{S_r}, \dots\right). \quad (2-3)$$

The same rules would apply to computation of the nonlinear contribution in the case of multiple observations within a small grid (local nonlinear contribution), or time series observations at a single station (temporal nonlinear contribution, discussed in detail in Chapter 3).

If data from two or more regions are combined into a “box,” then one has to account for different surface areas associated with regions composing such a box. I assign to each region an area weight, \mathbf{a}_r , equal to the fraction of the area of the ocean occupied by region r . Then, the average value of a property X in box b , \bar{X}_b , is given by

$$\bar{X}_b = \frac{\sum_{r=1}^{\mathbf{R}_b} (\mathbf{a}_r \bar{X}_r)}{\mathbf{a}_b}, \quad (2-4)$$

where \mathbf{R}_b denotes the total number of regions belonging to box b and \mathbf{a}_b is the area weight of box b : $\mathbf{a}_b = \sum_{r=1}^{\mathbf{R}_b} \mathbf{a}_r$.

The nonlinear contribution associated with box b , c_b , may then be calculated from

$$c_b = \bar{p}_b - p(\bar{T}_b, \bar{S}_b, \dots) = \frac{\sum_{r=1}^{\mathbf{R}_b} (\mathbf{a}_r \bar{p}_r)}{\mathbf{a}_b} - p\left(\frac{\sum_{r=1}^{\mathbf{R}_b} (\mathbf{a}_r \bar{T}_r)}{\mathbf{a}_b}, \frac{\sum_{r=1}^{\mathbf{R}_b} (\mathbf{a}_r \bar{S}_r)}{\mathbf{a}_b}, \dots\right). \quad (2-5)$$

The nonlinear errors

In box models the global ocean is divided into a finite number of horizontally uniform boxes. Within each box the nonlinear contribution is neglected, because p is estimated from the average seawater properties. The estimates of the global partial pressure from box models are therefore subject to the nonlinear error \mathbf{E} . I define \mathbf{E} as the difference between p_t , the true mean partial pressure in the global surface ocean, and p_e , the partial pressure estimated for a model ocean composed of uniform boxes:

$$\mathbf{E} = p_t - p_e. \quad (2-6)$$

Therefore, for a model representing the global ocean as a sum of \mathbf{B} boxes:

$$\mathbf{E} = \sum_{b=1}^{\mathbf{B}} (\mathbf{a}_b \bar{p}_b) - \sum_{b=1}^{\mathbf{B}} (\mathbf{a}_b p(\bar{T}_b, \bar{S}_b, \dots)). \quad (2-7a)$$

Transforming (2-7a) one may also express \mathbf{E} as the area weighted average of the nonlinear contributions associated with each box:

$$\mathbf{E} = \sum_{b=1}^{\mathbf{B}} \mathbf{a}_b (\bar{p}_b - p(\bar{T}_b, \bar{S}_b, \dots)) = \sum_{b=1}^{\mathbf{B}} (\mathbf{a}_b c_b). \quad (2-7b)$$

Note that the weights are assigned such that $\sum_{b=1}^{\mathbf{B}} \mathbf{a}_b = 1$.

Although I defined the nonlinear error with respect to the global scale, similar computations may be performed at any scale, as long as the analyzed area is represented as a collection of distinct boxes.

In section 2.4 I estimate \mathbf{E} for various models that have been used in the past. The models differ from each other in the number of boxes used, and in the demarcation of each box. However, before I analyse the actual data, I first examine how the nonlinear effects relate to the variability of seawater properties in some idealized cases.

2.3.2 Theoretical Considerations

The nonlinear effects (both the nonlinear contribution c and the nonlinear error \mathbf{E}) depend on six properties of seawater which control the partial pressure of carbon dioxide. The nonlinear dependence on so many variables makes it difficult to interpret the behavior of c and \mathbf{E} . To obtain an insight I computed c for several idealized cases. Selected properties were varied systematically within the ranges found in the surface waters of the world oceans, while the remaining properties were held constant at average values in the analyzed GEOSECS data.

Partial pressure of CO_2 as a function of a single variable

When the partial pressure p is plotted as a function of one variable at a time, it is seen that, whatever be the selected variable, p is always a convex function (i.e., the line segment between any two points of its graph lies on or above the graph and the second derivative of p is positive). Convexity of the function ensures that nonlinear contribution is positive.

As an example, I discuss p as a function of temperature T . Figure 2-1a shows that p is a convex function of T , and, consequently, the nonlinear contribution (vector XX') is always positive. It is also clear from the figure that, with increasing difference between T_I and T_J , the nonlinear contribution increases as well.

To examine the potential for nonlinear effects, I computed $d^2p(T)/dT^2$ as a measure of convexity of the function $p(T)$ (Figure 2-1b). When the dissociation constants of *Mehrbach et al.* [1973] were used, $d^2p(T)/dT^2$ reached maximum at 22°C. Therefore, if the partial pressure is controlled mainly by temperature, then the nonlinear effect will be strongest at 22°C.

Calculations with the dissociation constants of carbonic acid of *Goyet and Poisson* [1989] produced lower values of p than those in which the constants of *Mehrbach et al.* were used. The plot of $p(T)$ in this formulation has a weaker curvature. Although the value of $d^2p(T)/dT^2$ increases almost linearly with temperature, at no

point does it exceed the values calculated previously using the dissociation constants of *Mehrbach et al.* [1973]. Therefore, the nonlinear effects associated with variations in temperature are weaker when the constants of Goyet and Poisson are applied.

To analyze further the relation between nonlinear contribution and variability of temperature, I used the constants of *Mehrbach et al.* [1973] to compute c for hypothetical data, in which the temperature distribution was assumed to follow a Gaussian distribution (Figure 2-2).

The nonlinear contribution increases with standard deviation of temperature. It also increased initially with mean temperature, but this trend was reversed at higher temperatures. This reversal is consistent with the previous results showing a decline of $d^2 p(T)/dT^2$ for temperatures higher than 22°C.

Partial pressure of CO₂ as a function of two variables

Although some special cases can be conceived wherein the variability in p in natural waters is dominated by changes in a single seawater property, this is not true in general, and the computation of c usually has to take into account simultaneous variations in more than one variable. I examine the case when p is controlled by temperature and dissolved inorganic carbon.

Models of the carbon cycle often neglect the effect of silicate and phosphate [e.g., *Knox and McElroy*, 1984; *Volk and Liu*, 1988]. It is also a common practice to consider the seawater composition when all the samples are brought to a common salinity. This procedure removes most of the variability in alkalinity, which primarily depends on changes in salinity. Under these simplifying assumptions, p would be mainly a function of just two variables, temperature T and dissolved inorganic carbon C (Figure 2-3).

Note that isolines of p in the C - T coordinate frame are not equally spaced. In waters with high p , even small changes in T or C result in large changes of p and in large values of nonlinear contribution.

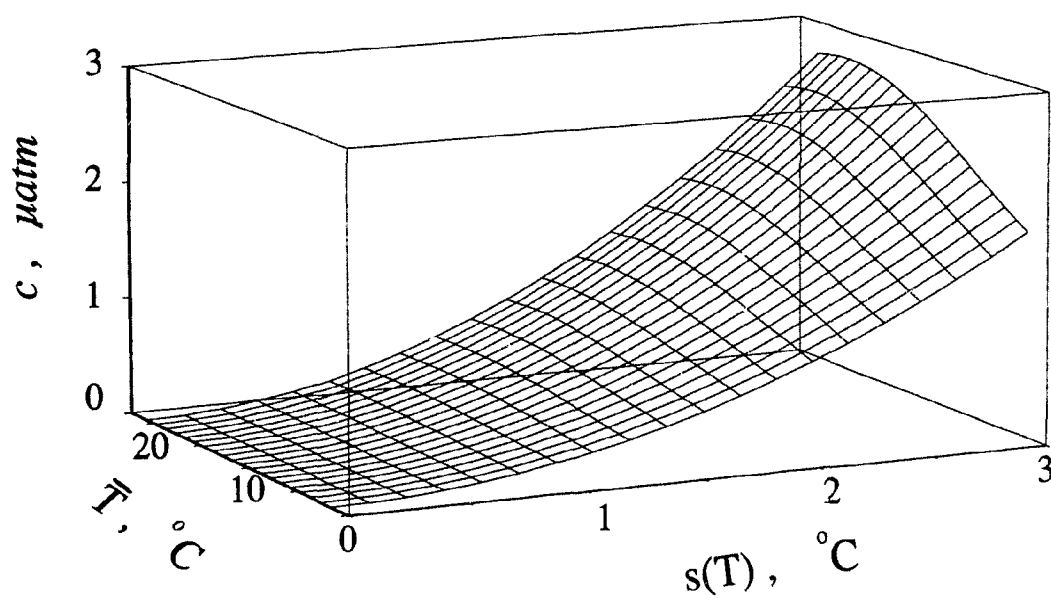


FIGURE 2-2. The nonlinear contribution (c) associated with normal distribution of temperature, as a function of its mean (\bar{T}) and standard deviation ($s(T)$). Partial pressure of CO_2 is assumed to be a function of temperature only. Alkalinity, dissolved inorganic carbon, silicate, and phosphate concentrations are as in Figure 2-1.

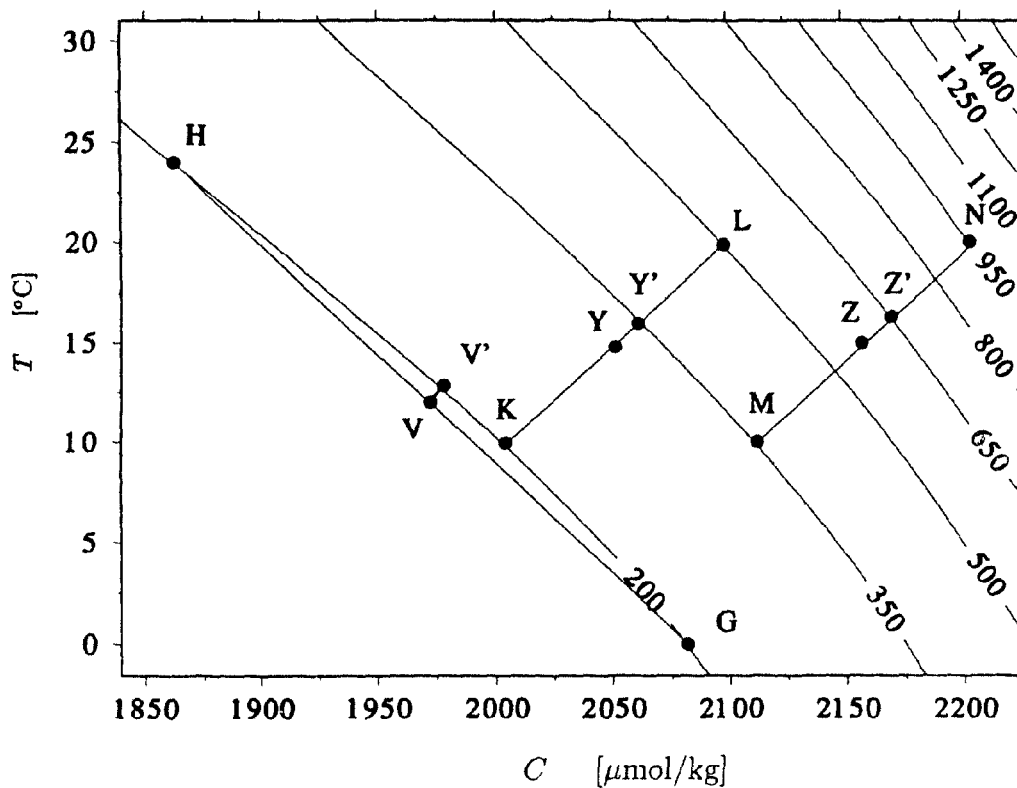


FIGURE 2-3. Partial pressure of CO_2 (p) as a function of temperature (T) and dissolved inorganic carbon (C). Note the nonlinearities of this relation: (K-L): $p_{Y'} = (p_K + p_L)/2 > p((T_K + T_L)/2, (C_K + C_L)/2) = p_Y$; (G-H): $p_{V'} = (p_G + p_H)/2 > p((T_G + T_H)/2, (C_G + C_H)/2) = p_V$; (M-N): $p_{Z'} = (p_M + p_N)/2 > p((T_M + T_N)/2, (C_M + C_N)/2) = p_Z$. Alkalinity, silicate, and phosphate concentrations are as in Figure 2-1.

Three cases are shown in Figure 2-3. In the first case (K-L), the differences in T and in C are 10°C and $95 \mu\text{mol kg}^{-1}$, respectively, the nonlinear contribution is $Y'-Y = 36 \mu\text{atm}$. In the second case (G-H), despite much larger spread in T and C (24°C and $220 \mu\text{mol kg}^{-1}$, respectively), p is constant and nonlinear contribution is smaller ($V'-V = 10 \mu\text{atm}$). In the third case (M-N), with the differences in T and C identical to the first case, but with both values of C moved toward higher concentrations, the difference in p is much larger, and the nonlinear contribution is doubled ($Z'-Z = 75 \mu\text{atm}$). Therefore, variability in C or T alone was not a good indicator of the nonlinear contribution in these cases. On the other hand, the differences in p (300, 0 and $600 \mu\text{atm}$, respectively) were closely related to the nonlinear contribution (36, 10, and $75 \mu\text{atm}$, respectively). Therefore, variability of the partial pressure seems to be a better predictor of nonlinear contribution, than variability in either T or C . I examine this relation further using the actual data in section 2.4.

Note that, typically, waters with lower temperatures tend to have higher concentrations of dissolved inorganic carbon and vice versa. As a result, the variability in the partial pressure is smaller than one would expect from the variability in C or T by itself. Therefore, one may expect the magnitude of the nonlinear contribution to be relatively small in most of the global ocean. An exception to this rule may be the upwelling zones, which are often in disequilibrium with atmospheric CO_2 , and show large variabilities in partial pressure [*Simpson and Zirino, 1980; Simpson, 1985*].

Another conclusion drawn from Figure 2-3 is that the nonlinear effects may be stronger in the future than those estimated for the present conditions. An increasing atmospheric concentration of CO_2 forces the partial pressure of the surface ocean toward higher values, mainly through an increase of inorganic carbon concentration in the surface waters. In such an environment the same variability in T and C may result in stronger nonlinear effects than in the waters with lower C (as seen in the comparison of case M-N with case K-L).

When the nonlinear contribution was examined as a function of other variables taken in pairs, similar tendencies were observed: large nonlinear effects were associated with large variations in p . Similarly, when the variations in p were small, so were values of c , sometimes even acquiring slightly negative values, as some combinations of temperature with salinity or alkalinity give rise to slightly concave isolines of p . The results of these sensitivity analyses may be used to interpret the data.

2.4 Effects of Spatial Fluctuations on Partial Pressure of CO₂ in the Surface Ocean

2.4.1 Nonlinear Contribution at Small Spatial Scales

The TTO data were used to study the nonlinear contribution at scales comparable with the resolution of the three-dimensional (3-D) carbon models. The current carbon models employ 3-D oceanic general circulation models (OGCM) with a typical resolution of several degrees. For example, the Princeton model has a resolution of 3.75° east-west and 4.5° north-south [Toggweiler *et al.*, 1989; Sarmiento *et al.*, 1992], and the Hamburg model [Maier-Reimer and Hasselmann, 1987] uses grid-size of 3.5° x 3.5° or larger.

In the subsets of the TTO data covering areas comparable to the 3.5° x 3.5° grid I found the nonlinear contribution (computed using equation 2-3) to vary from 0 up to 11 μ atm. The largest value was associated with a grid centered at 42°N, 59°W (TTO stations 243-250). This indicates that even 3-D models with high horizontal resolution are not free from the errors caused by the nonlinearities in the carbonate system, particularly given that there may also be a temporal component of nonuniformity, present even if the grid size was reduced to a single station.

2.4.2 Nonlinear Contribution at the Regional Scale

Following *Takahashi et al.* [1981b], I partitioned the GEOSECS data into 10 regions (see Table 2-1).

Each ocean was divided into a northern section (north of 10°N), an equatorial section (10°N-10°S), and a southern section (10-50°S); all waters south of 50°S were pooled into the Antarctic region. The regional averages of variables controlling partial pressure of CO₂ calculated here may differ, however, from those of *Takahashi et al.* [1981b], as only those observations were admitted in which the complete set of the controlling variables was measured, while *Takahashi et al.* used all the available data.

The area weights for the regions (Table 2-1) were based on *Moiseev* [1971]. I reduced the total area for the ocean south of 50°S given by *Moiseev* [1971] to exclude areas isolated from the atmosphere by the Antarctic sea ice. The area covered by ice was assumed to be 4×10^{12} m², which is the estimated minimum seasonal coverage of Antarctic sea-ice [*Zwally et al.*, 1983]. I chose the minimum coverage because, as already indicated, the "GEOSECS ocean" represents oceanic properties in the warm seasons, when the sea ice range is close to its minimum.

Table 2-1 summarizes my estimates of the nonlinear contribution for the 10 oceanic regions computed using the GEOSECS data. The regional values of the contribution ranged from 0.03 μ atm in the equatorial Indian Ocean to 10.9 μ atm in the North Pacific region. The equatorial Indian Ocean also had the lowest standard deviation in p , while the North Pacific region had the highest one.

I further explored this matter by plotting the nonlinear contribution as a function of standard deviation of seawater properties (Figure 2-4) within the 10 regions specified in Table 2-1.

Results of linear regression are in agreement with conclusions drawn from theoretical considerations. The nonlinear contribution was most closely correlated with the standard deviation of p . The coefficients of determination r^2 corresponding to

TABLE 2-1. Partial Pressure of CO₂ and the Nonlinear Contribution at the Regional Scale

Regions	Number of Samples S_r	Area Weight a_r	Partial Pressure of CO ₂		Nonlinear Contribution c_r
			Nonuniform Case \bar{p}_r	Uniform Case $p(\bar{T}_r, \bar{S}_r, \dots)$	
<i>GEOSECS, Atlantic:</i>					
I, 10°N-36°N	25	0.067	332.5	330.9	1.6
II, 10°S-10°N	18	0.040	357.4	357.0	0.4
III, 10°S-50°S	34	0.087	328.5	321.5	7.0
<i>GEOSECS, Pacific:</i>					
IV, 10°N-53°N	48	0.179	324.8	313.9	10.9
V, 10°S-10°N	15	0.127	379.0	376.6	2.4
VI, 10°S-50°S	38	0.183	319.6	316.3	3.3
<i>GEOSECS, Indian:</i>					
VII, North of 10°N	6	0.016	369.0	368.8	0.2
VIII, 10°S-10°N	26	0.044	360.5	360.5	0.0
IX, 10°S-50°S	30	0.126	335.8	333.3	2.5
<i>GEOSECS, Antarctic:</i>					
X, South of 50°S	38	0.131	319.8	316.4	3.4
GEOSECS global area-weighted average			335.9	331.5	4.4
<i>TTO, Atlantic:</i>					
15°N-80°N	320		291.9	281.3	10.6
- 15°N-50°N	132		330.8	324.3	6.5
- 50°N-80°N	188		264.6	259.7	4.9

Columns contain latitudinal range of regions, the number of samples available within a region, regional area weights (computed as a fraction of the area of the GEOSECS ocean, such that $\sum a_r = 1$), the partial pressures [μatm] and nonlinear contribution [μatm] computed from the data within each region. The GEOSECS data were partitioned into 10 regions as given by *Takahashi et al.* [1981b].

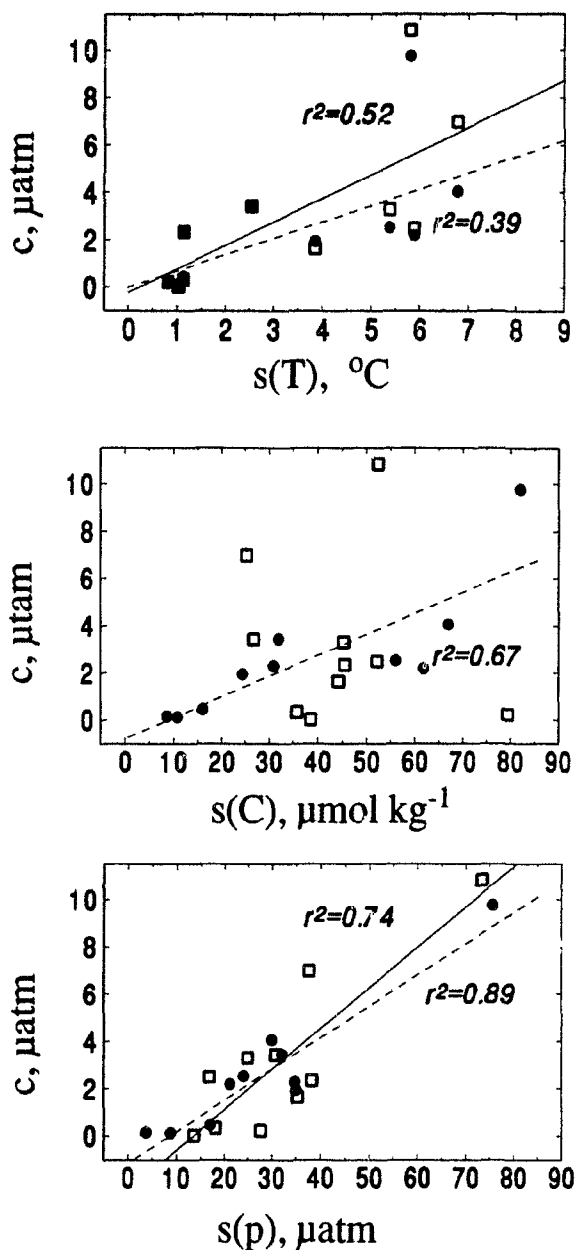


FIGURE 2-4. The nonlinear contribution as a function of the standard deviations of temperature T , dissolved inorganic carbon C , and partial pressure of carbon dioxide p at the regional scale. Regions are defined as in Table 2-1. Regional values of the nonlinear contribution c_r were computed using equation (2-3). Squares denote values calculated using the actual observations, circles represent values computed after standardization of alkalinity, dissolved inorganic carbon, silicate and phosphate concentrations, to a constant salinity of 34.78. Solid and dashed lines represent the linear regression calculated using direct and the salinity-standardized values, respectively. The regression line between the nonlinear contribution and standard deviation of dissolved inorganic carbon, direct values, is omitted, as in this case $r^2 = 0.03$.

standard deviation from direct measurements and from the salinity-standardized values were 0.74 and 0.89, respectively.

I also calculated the nonlinear contribution in the TTO data from the North Atlantic (Table 2-1). When all the TTO data were treated as belonging to a single region, the nonlinear contribution was 10.6 μatm .

When only the data south of 50°N latitude were used, the nonlinear contribution was 6.5 μatm . Both values were substantially larger than the 1.6 μatm found in the North Atlantic GEOSECS data. The GEOSECS data in the Atlantic were limited to latitudes below 36°N. Lack of data from high latitudes was responsible for the smaller regional variability of the seawater properties and, consequently, for underestimation of the regional nonlinear contribution.

In the subset of the TTO data in the Arctic waters, represented by samples collected north of 50°N, the nonlinear contribution was 4.9 μatm .

2.4.3 Model errors at the global scale

To evaluate **E**, the nonlinear error in model estimates of the global p , I recreated the horizontal structure of several carbon box models from the literature. This was accomplished by partitioning the GEOSECS data into various boxes (see Figure 2-5). The results are summarized in Table 2-2 and in Figure 2-6.

1. The simplest case considered was the representation of the surface ocean as a single box [e.g., *Revelle and Suess*, 1957; *Craig*, 1957; *Nydal*, 1968; *Oeschger et al.*, 1975; *Takahashi et al.*, 1981a; *Craig and Holmen*, 1995; *Jain et al.*, 1995]. This representation underestimated the mean partial pressure of CO_2 of the GEOSECS ocean by 10.9 μatm .

2. A few schemes for partitioning the world oceans into two boxes were examined. The nonlinear error was sensitive to how the oceans were partitioned.

Most of the two-box models in the literature separate the high-latitude waters from the rest of the ocean [e.g. *Björkström*, 1979; *Hoffert et al.*, 1981; *Knox and*

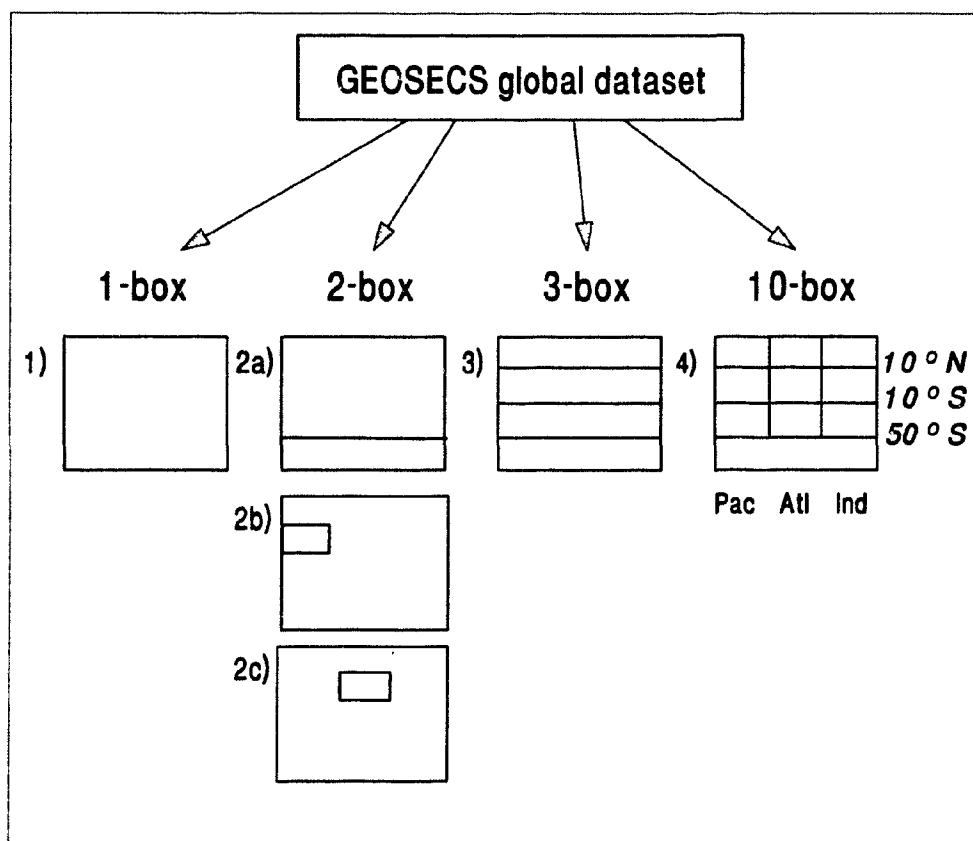


FIGURE 2-5. Partition of the global GEOSECS dataset into boxes recreating the horizontal structure of several carbon box models from the literature (see also Table 2-1 and text).

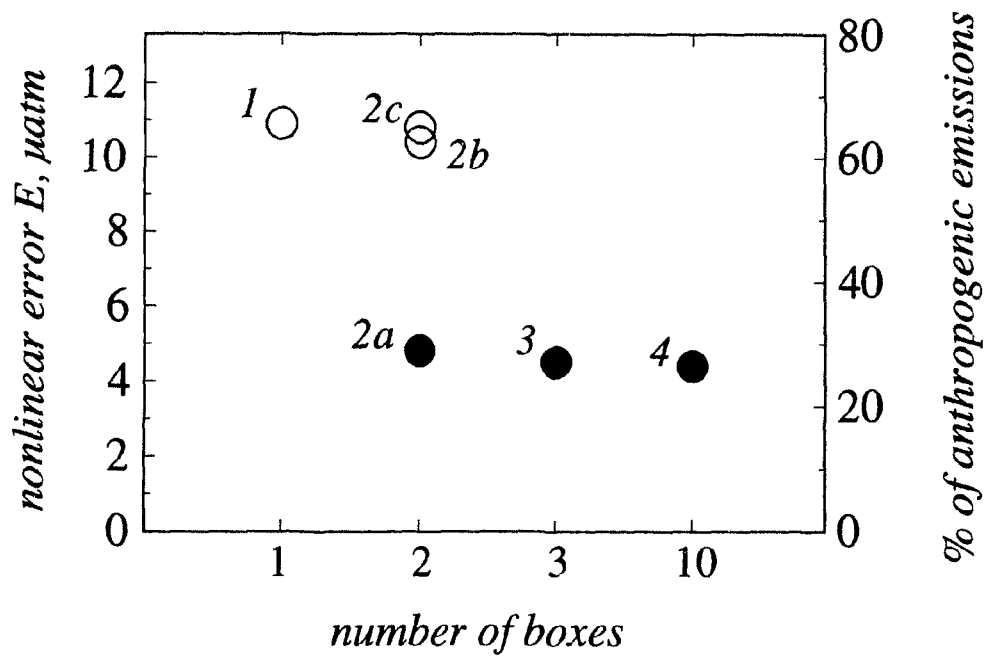


FIGURE 2-6. The global nonlinear error E associated with models with various numbers of boxes. Numbers in the graph correspond to various partitions of the global ocean described in Table 2-1 (see also Figure 2-5). Right Y-axis indicates corresponding errors in direct estimates of air-sea fluxes expressed in % of the annual anthropogenic emissions.

TABLE 2-2. Partial Pressure of CO₂ and the Nonlinear Contribution Associated With Various Model Idealizations of the Global Ocean

Model	Regions	Area Weight a_b	Partial Pressure of CO ₂		Nonlinear Contribution c_b
			Nonuniform Case \bar{p}_b	Uniform Case $p(\bar{T}_b, \bar{S}_b, \dots)$	
1. One-box model					
single global box	I-X	1.000	335.9	325.0	10.9
2. Two-box models					
(2a) with high-latitude ocean separated					
high-latitude ocean	X	0.131	319.8	316.4	3.4
balance of ocean	I-IX	0.869	338.3	333.3	5.0
$\sum a_b \dots$			335.9	331.1	4.8
(2b) with equatorial Pacific separated					
equatorial Pacific	V	0.127	379.0	376.6	2.4
balance of ocean	I-IV, VI-X	0.873	329.6	318.0	11.6
$\sum a_b \dots$			335.9	325.4	10.4
(2c) with equatorial Atlantic separated					
equatorial Atlantic	II	0.040	357.4	357.1	0.3
balance of ocean	I, III-X	0.960	335.0	323.8	11.2
$\sum a_b \dots$			335.9	325.1	10.8

Continued on the next page

TABLE 2-2. - continued

Model	Regions	Area	Partial Pressure of CO ₂		Nonlinear
		Weight \mathbf{a}_b	Nonuniform Case \bar{p}_b	Uniform Case $p(\bar{T}_b, \bar{S}_b, \dots)$	Contribution c_b
3. Three-box model with high-latitude ocean and equatorial Pacific separated					
high-latitude (as in 2a)	X	0.131	319.8	316.4	3.4
equatorial Pacific (as in 2b)	V	0.127	379.0	376.6	2.4
balance of ocean	I, II-IV, VI-IX	0.742	331.3	326.3	5.0
$\sum \mathbf{a}_b \dots$			335.9	331.6	4.5
4. 10-box model with 10 boxes corresponding to all 10 regions in Table 1-1					
$\sum \mathbf{a}_b \dots$			335.9	331.5	4.4

Models are composed of boxes, which are constructed either as a single region, or as a weighted average of several GEOSECS regions (defined in Table 1-1). " $\sum \mathbf{a}_b \dots$ " denotes the global area-weighted average of the box properties. For instance, " $\sum \mathbf{a}_b \dots$ " for the last column (box nonlinear contributions, c_b), corresponds to $\sum \mathbf{a}_b c_b$. Note that $\sum \mathbf{a}_b c_b$ corresponds to the global nonlinear error associated with a given model (**E** in the text).

McElroy, 1984; Sarmiento and Toggweiler, 1984; Siegenthaler and Wenk, 1984; Volk and Liu, 1988; Joos et al., 1991; Shaffer and Sarmiento, 1995]. As the GEOSECS data set does not cover the Atlantic north of 35°N, the high-latitude box is represented by the Antarctic region only (region X in Table 2-1). The warm waters are represented by the remaining nine regions. In this case the mean global partial pressure of CO₂ was underestimated by 4.8 μatm (model 2a in Table 2-2).

I also analyzed the nonlinear errors associated with two other two-box partitions (following *Volk and Liu [1988]*) that divide the GEOSECS ocean into the equatorial Pacific (region V) and the rest of the ocean (model 2b), or into the equatorial Atlantic (region II) and the remaining ocean (model 2c). The nonlinear errors associated with these models (10.5 and 10.8 μatm , respectively) were larger than that calculated from the model separating the high- and low-latitude waters.

3. I also tested the effect of a further increase in the number of boxes. I used three-box and 10-box partitions. The three-box partition (model 3), composed of the Antarctic and the North Pacific boxes, with the remaining regions pooled into a third box [e.g., *Volk and Liu, 1988*], underestimated the mean global p by 4.5 μatm .

In the 10-box representation all the 10 regions defined in Table 2-1 were treated as separate boxes. Most of the box models in the literature have only a few boxes representing surface waters, so this case may represent a practical upper limit for the horizontal resolution of box models. This model eliminated the errors caused by pooling data from different regions into boxes, because each box corresponded to a single region. Nevertheless, the model assumed uniformity within each of the regions and, as a result, it underestimated the mean global p by 4.4 μatm .

Two points are worth noting here. First, a large error was incurred when boxes contained regions with very different properties. Pooling the data originating from the Antarctic waters (characterized by low T , high C , and relatively low p), with those from the other parts of the ocean resulted in large values of the nonlinear error (models 1, 2b, and 2c). Second, an increase in the complexity of the model,

expressed as an increase in the number of boxes, does not necessarily lead to a reduction in the nonlinear error. If a more complex model does not have a more realistic structure than a simpler one, the associated error may remain large. Models 2b and 2c pooled together the data from warm and cold waters into single boxes, hence the structure of the models was still unrealistic. As a result, these models, despite being composed of two boxes, had the nonlinear error comparable with that of a one-box model. A strong reduction in the nonlinear error was possible only if the cold waters were isolated into a separate box (as in models 2a, 3, and 4). Once this separation was accomplished, further subdivision of the warm waters into two (model 3) or nine (model 4) boxes did not reduce the error significantly.

In Appendix A, I show that the estimates of nonlinear errors were not very sensitive to changes in the algorithm for computing p from seawater properties, or to the alternative selections of the GEOSECS data, except for employing the dissociation constants of carbonic acid proposed by *Goyet and Poisson* [1989]. Models using these constants were less prone to the nonlinear errors, with the difference being most pronounced in the case combining data from cold and warm waters into a single surface box ($4 \mu\text{atm}$ instead of $11 \mu\text{atm}$). This finding is consistent with the results obtained when p was analyzed as a function of temperature (section 2.3.2).

2.5 Implications for the Direct Estimates of Air-Sea Fluxes of CO_2

Nonlinearity of the carbonate system, coupled with nonuniform distribution of the seawater properties, may affect results of models that estimate air-sea fluxes of CO_2 directly from the mean properties of the surface ocean. In this approach [e.g., *Takahashi et al.*, 1981a] the net air-sea flux is computed directly from the difference in the partial pressure of CO_2 between the atmosphere and the ocean

$$F = K\Delta p = K(p_a - p_m), \quad (2-8)$$

where K denotes the gas transfer coefficient [$\text{mol CO}_2 \text{ m}^{-2} \text{ yr}^{-1} \mu\text{atm}^{-1}$], p_a and p_m stand for the partial pressure of CO_2 in the atmosphere and the mixed layer, respectively (both expressed in μatm).

This approach is sensitive to errors in p_m . Nonlinearity of the carbonate system results in a higher p_m than would be expected from a uniform ocean with the same mean properties as the real ocean. With $K = 0.067 \text{ mol CO}_2 \text{ m}^{-2} \text{ yr}^{-1} \mu\text{atm}^{-1}$ [Tans *et al.*, 1990], the nonlinear error of about $11 \mu\text{atm}$ for one-box models, and about $5 \mu\text{atm}$ for the more complicated models, would translate into an overestimation of the oceanic uptake by 3.0 Gt C yr^{-1} and 1.4 Gt C yr^{-1} , respectively. This corresponds to 65% and 30% of total fossil fuel emissions in 1973 [Rotty, 1987]. Thus neglecting the nonlinear errors could result in overestimation of the uptake of atmospheric carbon by the ocean, when carbon fluxes are computed from the difference in the partial pressure of CO_2 between the ocean and the atmosphere, and the oceanic p is computed from averaged seawater properties.

For example, Takahashi *et al.* [1981a] calculated a p_m of $300 \mu\text{atm}$ from globally-averaged observations of T , S , A , and C . Using the 1973 atmospheric concentration of CO_2 of $321 \mu\text{atm}$, these calculations yielded an uptake of atmospheric carbon which was greater than the whole anthropogenic carbon emission. This forced Takahashi *et al.* to consider increasing the value of the global surface-ocean temperature to 20.26°C , despite the recognition that the calculated mean temperature of 19.2°C “appears to be higher by a few degrees than the space-time average values” [Takahashi *et al.*, 1981a, p. 278] as a result of sampling mainly during the summer seasons in both hemispheres. This reservation is reinforced by the climatological data of Levitus [1982], from which one may calculate the average global ocean temperature in the 0-50 m layer to be 17.7°C . Using a more complete algorithm for calculating p (accounting for the effect of water, silicate, and phosphate dissociation) and computing the average p_m rather than the p_m associated

with mean seawater properties, would render such an upward adjustment of average temperature unnecessary. Besides, it would even allow the use of lower global temperatures, in closer agreement with the space-time average.

Note that the estimates of global p_m derived by averaging individual values of p , directly measured or calculated from the composition of every sample, are not subject to the nonlinearity error. An example of such calculation would be that of *Tans et al.* [1990], *Lefevre* [1995] and *Takahashi et al.* [1995].

2.6 Implications for Transient Box Models

Predicting the consequences of nonlinear effects is much more difficult in the case of box models in which the computed air-sea carbon flux depends on interactions between the surface ocean, the deep ocean, and the atmosphere. In this section I will discuss some transient models that are used to analyze the evolution of the carbon system with time. Diagnostic models, used to study the mechanisms that maintain a steady state, are briefly discussed in section 2.7.

Transient ocean-atmosphere models are run typically for the simulated time period extending from the preindustrial time to the present time or into the 21st century. Using as an example the transient box model composed of the atmosphere, the mixed-layer, and the deep ocean [*Bacastow and Björkström*, 1981], I next examine the consequences of nonlinear effects for such models.

2 1 Correction of the initial conditions

The initial conditions in transient models typically assume a preindustrial steady state, in which there is no net CO₂ flux between the ocean and the atmosphere. In models with a single mixed layer reservoir this condition is expressed as [e.g., *Bolin and Eriksson*, 1959]

$$\mathbf{k}_{am}N_{ao} = \mathbf{k}_{ma}N_{mo}, \quad (2-9)$$

where subscripts m and a denote the mixed layer and the atmosphere, subscript o denotes preindustrial values, \mathbf{N} is the amount of carbon in a given reservoir [mol C], \mathbf{k}_{am} and \mathbf{k}_{ma} are transfer coefficients between the atmospheric and the mixed-layer reservoirs, expressed in yr^{-1} .

To meet the condition of no net air-sea flux of CO_2 , the partial pressure of CO_2 in the surface ocean (p_m) and the atmosphere (p_a) should be equal (see (2-8)). This condition can be expressed as $p_{mo}=p_{ao}$, with p_{mo} being a function of \mathbf{N}_{mo} , and $p_{ao} = \mathbf{N}_{ao}/\mathbf{M}_a$, where \mathbf{M}_a is the mass of the atmosphere [mol].

The overall partial pressure of CO_2 in a nonuniform surface ocean is higher than that of a uniform ocean with the same average properties, by the nonlinear error \mathbf{E} (its preindustrial value being denoted \mathbf{E}_o). To correct the initial conditions for nonlinear effects one may increase \mathbf{N}_{ao} or decrease \mathbf{N}_{mo} .

In the first case the initial partial pressure of the atmosphere p_{ao} can be increased to match the p_m of the nonuniform ocean:

$$p'_{ao} = p_m(\mathbf{N}_{mo}) + \mathbf{E}_o = p_{ao} + \mathbf{E}_o, \quad (2-10)$$

where the prime denotes a quantity modified to include the nonlinear effects. The fractional change in \mathbf{N}_{ao} is given by

$$\frac{\Delta \mathbf{N}_{ao}}{\mathbf{N}_{ao}} = \frac{\mathbf{N}'_{ao} - \mathbf{N}_{ao}}{\mathbf{N}_{ao}} = \frac{p'_{ao} - p_{ao}}{p_{ao}} = \frac{\mathbf{E}_o}{p_{ao}}. \quad (2-11)$$

An increase in \mathbf{N}_{ao} would also affect the transfer coefficients according to equation (2-9). It can be shown that, for this type of model, $\mathbf{k}'_{am}/\mathbf{k}_{am} = \mathbf{N}_{ao}/\mathbf{N}'_{ao}$, that is, the ratio of the new to the old value of \mathbf{k}_{am} is inversely related to a similar ratio for \mathbf{N}_{ao} . The transfer coefficient \mathbf{k}_{ma} and other initial conditions (describing the exchange between the mixed layer and the deep ocean) are not affected by the correction of \mathbf{N}_{ao} .

If the preindustrial nonlinear effects were equal to those computed from the GEOSECS data ($\mathbf{E}_o = 10.9 \mu\text{atm}$ as in Table 2-2) and the uncorrected preindustrial

atmospheric partial pressure of CO₂ is assumed to be 280 μatm, N_{ao} would have to increase by 4% (=10.9/280).

The second option is to adjust the initial condition by decreasing N_{mo}, such that the new partial pressure, corrected for the nonlinear error E_o, would be equal to the prescribed atmospheric partial pressure:

$$p_m(N'_{mo}) + E_o = p_{ao}. \quad (2-12)$$

Due to the buffering properties of the seawater (discussed in more detail in the next subsection) a required change in partial pressure can be achieved by a much smaller fractional change in the amount of the mixed layer carbon. Typically, the fractional decrease in N_{mo} should be about 10 times smaller than the fractional increase that would be required in N_{ao}:

$$\frac{\Delta N_{mo}}{N_{mo}} \approx -\frac{1}{10} \frac{\Delta N_{ao}}{N_{ao}}. \quad (2-13)$$

In other words, to compensate for the nonlinear error, the value of N_{mo} would have to be reduced by about 0.4% (= (10.9/280)/10). This correction is much less than either the uncertainty in N_{mo} or the potential errors caused by other assumptions in box models. For all practical purposes one may assume that the changes required in the initial conditions may be significant if N_{ao} is altered to maintain equilibrium, but not if N_{mo} is modified.

2.6.2 Modifications at subsequent time steps

Once the initial conditions are set up, nonlinear effects can modify model calculations at subsequent time steps. In ocean-atmosphere models with a single surface-ocean box, accumulation of CO₂ in the atmosphere at a given time step can be represented by [e.g., Bacastow and Björkström, 1981]

$$d\mathbf{n}_a/dt = -\mathbf{k}_{am}(N_{ao} + \mathbf{n}_a) + \mathbf{k}_{ma}(N_{mo} + \xi\mathbf{n}_m) + \mathbf{i}, \quad (2-14)$$

where \mathbf{n}_a and \mathbf{n}_m represent anthropogenic carbon in the atmosphere and in the mixed layer [mol C], respectively, and \mathbf{i} is the input of the anthropogenic carbon into the ocean-atmosphere system during a given time step and ξ is the buffer factor.

The buffer factor ξ is defined as the ratio of fractional changes in p and in the concentration of dissolved inorganic carbon C :

$$\xi = \frac{\Delta p/p}{\Delta C/C}. \quad (2-15)$$

To compute the buffer factor of a water parcel using (2-15), different authors use different reference values of p and C . As a result, different numerical values of the buffer factor are obtained for the same water parcel (as discussed by *Wagener* [1979]). I calculated the buffer factors corresponding to the formulations of *Bolin and Eriksson* [1959], *Bacastow and Keeling* [1973], and *Keeling* [1973], respectively:

$$\xi_1 = \frac{\delta p/p}{\delta C/C}, \quad (2-16)$$

$$\xi_2 = \frac{(p - p_o)/p_o}{(C - C_o)/C_o}, \quad (2-17)$$

$$\xi_3 = \frac{\delta p/p_o}{\delta C/C_o}, \quad (2-18)$$

where δp denotes an increase in the partial pressure of CO_2 of a water parcel (p) if the dissolved inorganic carbon concentration of the water parcel (C) were increased by a small increment δC ; and C_o is the value of C that, at given T , S , A , S_i and P of the water parcel, would produce the preindustrial partial pressure p_o .

If the preindustrial component is removed from equation (2-14), using equation (2-9), one is left with the perturbation component:

$$d\mathbf{n}_a/dt = -\mathbf{k}_{am}\mathbf{n}_a + \mathbf{k}_{ma}\xi\mathbf{n}_m + \mathbf{i}. \quad (2-19)$$

Nonlinearity of the carbonate system may affect this perturbation component by altering the buffer factor. The effective buffer factor of a nonuniform surface ocean may be different from that of a uniform ocean with the same average properties.

I used the GEOSECS data to calculate this difference, termed here a buffer factor correction $\Delta\xi$.

Assuming $p_o = 280 \mu\text{atm}$ and using $\delta C = 0.1 \mu\text{mol kg}^{-1}$, I calculated ξ according to formulae (2-16), (2-17), and (2-18) for all GEOSECS samples. Then I repeated the procedure described in section 2.3, calculating the regional and box values of nonlinear contribution and nonlinear error described by (2-3)–(2-7) with respect to the buffer factor instead of the partial pressure. Table 2-3 contains the buffer factor calculated for the one- and two-box model representations of the surface ocean and the correction required to account for the nonlinear effects, which are ignored when uniformity within the boxes is assumed.

The calculated buffer factors differed between definitions, being smallest in the formulation of *Bolin and Eriksson* [1959] (equation 2-16) and largest when the formulation of *Keeling* [1973] (equation 2-18) was used. The nonlinear corrections followed the same pattern. Therefore, correcting for the nonlinear effects further increases the differences in buffer factor caused by its alternative formulations.

The two-box model required a smaller correction than the one-box model. The nonlinear effects for the high-latitude box were smaller than the low-latitude one, but when the TTO data from the Arctic were added to the GEOSECS data from the Antarctic, the nonlinear correction required for the modified high-latitude box was similar to that of the low-latitude box. The 10-box representation produced almost identical values of buffer nonlinear correction as the two-box representation.

2.6.3 Nonlinear effects and model estimates of oceanic uptake of anthropogenic carbon

Having computed the buffer correction for the GEOSECS data, I can now try to assess the effect of such a correction on the the estimates of oceanic carbon uptake by transient box models.

First, I analyze some simplified cases for which an analytical solution can be obtained. When an exponential growth in anthropogenic emissions (with the time

Table 2-3. Buffer Factors and the Nonlinear Correction Associated with Different Definitions of the Buffer Factor

	Buffer Factor: Uniform Case + Nonlinear Correction		
	$\xi_1 + \Delta\xi_1$	$\xi_2 + \Delta\xi_2$	$\xi_3 + \Delta\xi_3$
One-box model	9.48+0.30	9.88+0.40	10.83+0.68
Two-box model			
low-latitude box	9.10+0.12	9.57+0.16	10.63+0.30
high-latitude box	13.48+0.04	13.88+0.10	15.09+0.25
global average	9.67+0.11	10.13+0.15	11.21+0.30

The first term in each column represents the buffer factor calculated for the uniform case, the second term is the nonlinear correction (computed as the difference between the global mean buffer factor and the global mean of buffer factors computed for each box from the mean values of temperature, salinity, etc... — for the box). Formulations of buffer factor of *Bolin and Eriksson* [1959], ξ_1 , *Bacastow and Keeling* [1973], ξ_2 , and *Keeling* [1973], ξ_3 , were used (equations (2-16), (2-17) and (2-18) in the text). The one-box and the two-box models correspond to model 1 and model 2a in Table 2-2. The global average in the two-box model is an area-weighted average of the buffer factors and the buffer corrections in the low- and high-latitude boxes.

constant μ) and a constant buffer factor are assumed, the airborne fraction of anthropogenic carbon, $r_a (= \mathbf{n}_a / \int \mathbf{i} dt)$, is given by *Bacastow and Björkström* [1981]:

$$\mathbf{r}_a = 1 - \frac{1}{\mu/\mathbf{k}_{am} + \mathbf{H}_a\xi/\mathbf{H}^* + 1}, \quad (2-20)$$

where $\mathbf{H}_a = (\mathbf{N}_{ao}/\mathbf{N}_{mo})\mathbf{H}_m$, and \mathbf{H}^* for a uniform deep ocean is given by $\mathbf{H}^* = \mathbf{H}_m + \mathbf{H}_d[\mathbf{k}_{dm}/(\mu + \mathbf{k}_{dm})]$, where \mathbf{H}_m and \mathbf{H}_d are the mixed layer and the deep ocean depths, respectively, and \mathbf{k}_{dm} is the transfer coefficient between the deep ocean and the mixed layer. If one uses a constant buffer factor of $\xi = 0.64$, $\mathbf{H}_a = 69$ m, total ocean depth ($=\mathbf{H}_m + \mathbf{H}_d$) of 4200 m, $\mu = 1/22.5 \text{ yr}^{-1}$, $\mathbf{k}_{am} = 1/8.1 \text{ yr}^{-1}$, as in *Bacastow and Björkström* [1981], then for $\mathbf{H}_m = 500$ m and $\mathbf{k}_{dm} = 1/1250 \text{ yr}^{-1}$ the airborne fraction of the anthropogenic carbon in the ocean-atmosphere system would be 0.606, if the nonlinear effects were neglected.

To evaluate the consequences of nonlinearity let us assume that the nonlinear effects were constant in time and take the largest correction of the buffer factor from Table 2-3 ($\Delta\xi = 0.68$). This correction would increase r_a from 0.606 to 0.618, which corresponds to a decrease in the oceanic uptake of anthropogenic carbon by about 3%. Similar results were obtained for a box diffusion model in which the vertical distribution of carbon in the deep-ocean component of the model was assumed to be controlled by diffusion [e.g., *Oeschger et al.*, 1975]. If \mathbf{N}_{ao} were modified instead of \mathbf{N}_{mo} , r_a would increase to 0.628, and the decrease in the oceanic uptake would be less than 6%.

However, all these estimates were made for the special case in which the buffer factor was fixed and the nonlinear effects were assumed to be constant. Neither of these assumptions is realistic, particularly when the model simulation time is extended into the future. In reality, when the equilibrium partial pressure of CO_2 of the air-sea system increases, so does the buffer factor. The nonlinear effects can then be incorporated by the addition of a nonlinear buffer correction $\Delta\xi$ to the computed values of the uniform buffer factor. Consequences of such a correction would depend on:

- the structure of the model (number and delineation of boxes),
- the way the uniform buffer factor is computed (i.e., which formula is used to calculate ξ ; see equations 2-16, 2-17 and 2-18), and
- the time dependency of $\Delta\xi$ (as will be shown in Chapter 5, the nonlinear effects increase in environments with elevated partial pressure of CO_2 .)

Consequently, a more complete assessment of the role of nonlinearity for the results of carbon box models would require running a particular model with a time-dependent buffer factor and prescribing the nonlinear effects for the entire simulation period.

One could consider using a high-resolution 3-D model to obtain insights into changes in the nonuniformity of the seawater properties in time. By pooling data from the model's individual grid points into larger groups one might observe changes of nonlinear effects at successive time steps.

2.7 Other Issues

2.7.1 Nonlinear Effects in the Diagnostic Box Models

The nonlinear effect may also modify results of diagnostic box models. These models are constructed to deduce the rates of mixing and biochemical processes using a set of physical and biochemical constraints [Rintoul, 1992], usually assuming various steady states. Partial pressure of CO_2 is one of these constraints which can be modified by nonlinear effects. Introduction of a nonlinear correction in these models would require making assumptions about the degree of variability of seawater properties in different hypothetical steady states.

2.7.2 Nonlinear Effects in the Real Ocean

So far, the results have been interpreted in the context of carbon models. However, the nonlinear effects also have relevance in the real ocean.

Mixing in the real ocean may be regarded as "physical averaging." Horizontal mixing of different water masses, by homogenization of the seawater properties, usually decreases the overall p of surface waters. For instance, if points I and J on Figure 2-1a represent properties of two water masses, then the water mass created by mixing of these two water masses would typically have lower partial pressure than the average partial pressure of the parent water masses. In general, a well-mixed surface ocean would have a lower overall p than a nonuniform ocean with the same average properties, and consequently could be a stronger sink, or a weaker source, of atmospheric CO_2 .

A number of biogeochemical processes, gas exchange with the atmosphere, upwelling of deep waters, biological activity, etc., affect the distribution of seawater properties. The effect of these processes on the carbon fluxes between the atmosphere and the ocean may be changed, even without any change in the overall intensity of these processes, by merely altering their spatial distribution. For instance, without any change in the amount of new nutrients utilized by phytoplankton, an alteration of its distribution (e.g., a change in location of phytoplankton blooms) may alter the variance in seawater properties and therefore increase or decrease the capacity of surface waters to absorb atmospheric CO_2 .

2.7.3 Representativeness of the GEOSECS Data

The estimates of the nonlinear effects based on GEOSECS data are conservative and are likely to be on the lower side of the values that might be expected if a more representative data set were available. Poor coverage of some oceanic areas (e.g., Atlantic north of 35°N , coastal waters) and sampling bias toward summer seasons make the GEOSECS ocean different from the actual one. Additional data

from waters having properties which differ strongly from the values recorded in the GEOSECS surface samples would probably increase the variability of the seawater properties and consequently the nonlinear error. Incorporation of high-latitude data is likely to increase the nonlinear error as is shown by including the TTO data (Appendix A). Coastal waters, whose properties often differ from those of the open ocean, have the potential to increase the nonlinear effects but were not represented in the data set I used.

Variability in the seawater properties represented in the GEOSECS dataset reflects primarily the spatial differences between different water masses. The temporal component of variability is probably not important in this dataset, since most of the data were collected during summer seasons.

This lack of winter data may be important in high-latitude waters whose properties exhibit strong seasonal cycles. For instance, as indicated in the measurements of *Watson et al.* [1991] and in the model of *Taylor et al.* [1991], properties of seawater in high latitudes of the North Atlantic during winter are very different from those prevailing in summer. In the data used here only the postbloom situation was represented, hence a large portion of the annual variability has not been accounted for.

The differences in seawater properties between high-latitude waters and the rest of the global ocean are much larger in winter (when the water is cold and strong mixing brings carbon-rich deep waters to the surface) than in summer. Consequently, if a global dataset contained many winter data, the overall variability of seawater properties, and the nonlinear effects, would be stronger than indicated by these estimates based on the GEOSECS data. The temporal aspect of the nonlinear effects in high latitudes is explored in the next chapter using a model simulation.

2.8 Concluding Remarks

Due to the nonlinearity of the carbonate system, the partial pressure of CO_2 of nonuniform waters is different from that of uniform waters with identical mean properties. The difference, termed the nonlinear contribution c , is typically positive. However, under specific circumstances, c may take a slightly negative value. Both theoretical considerations and the analysis of the GEOSECS data indicate the largest c to be associated with the highest variability in p .

Observational studies and carbon models idealize the ocean as a set of internally uniform compartments and therefore underestimate the true value of oceanic p . The resulting nonlinear error depends on the horizontal structure of the model.

From the GEOSECS data from depths 0-49 m I estimated the magnitude of the nonlinear error to be about $11 \mu\text{atm}$ when the data from the high- and low-latitude waters are combined into a single compartment, and about $5 \mu\text{atm}$ when cold and warm waters are separated. Once the high-latitude box was isolated from the rest of the ocean, further increases in the horizontal resolution did not substantially affect the nonlinear error.

The calculations were not very sensitive to changes in the algorithm for computing p from seawater properties, or to alternative selections of data (Appendix A). The only exceptions were computations employing the dissociation constants of carbonic acid proposed by *Goyet and Poisson* [1989]. Models using these constants were less prone to the nonlinear errors when cold and warm waters were pooled into a single box ($4 \mu\text{atm}$).

My estimates of the nonlinear error based on the GEOSECS data are likely to be lower than the error expected in the real ocean. Addition of data from the Arctic region, coastal regions, and from winter months are likely to increase the estimates of the nonlinear effects. Nonlinear effects of up to $11 \mu\text{atm}$ were also found at the regional scale and even at the local scale, below the resolution of the carbon models employing 3-D oceanic general circulation models.

The consequences of the nonlinearity of the carbonate system for the estimates of the CO_2 fluxes depend on the method used. When the flux of carbon is estimated directly from the properties of the surface waters, computations based on the average partial pressure of CO_2 should be preferred to models that compute

the global partial pressure from average seawater properties, since the latter could overestimate the oceanic uptake of anthropogenic carbon (e.g., by up to 65% of fossil fuel emissions when the GEOSECS data are averaged over the global scale).

In the case of transient carbon models the impact of nonlinear effects depends on the structure of the model. In the simple box models and box diffusion models, assuming a constant buffer factor and fixing the nonlinear effects at the values computed from the GEOSECS data, a nonuniform ocean was a weaker sink of anthropogenic carbon than a uniform one. However, as the decrease was about 3%, the errors from nonlinear effects were within the uncertainty introduced by other assumptions in such simplified models. Quantification of the role of the nonlinearity for the results of more realistic carbon box models would require using a time-dependent buffer factor and prescribing time dependency of the nonlinear effects.

The nonlinearity of the carbonate system may have implications not only for models, but for the processes occurring in the real ocean as well. Horizontal and vertical mixing, gas and heat exchange with the atmosphere, precipitation and evaporation, and biological processes, all affect the distribution of properties controlling the partial pressure of CO_2 and thus modify air-sea gas exchange. In other words, carbon fluxes between the ocean and the atmosphere are affected not only by the mean intensity of biogeochemical processes, but also by their spatial distribution. The same process, depending on its spatial pattern, may either increase or decrease the nonuniformity of the seawater properties and therefore modify the capacity of the surface ocean to act as a carbon sink even if the mean intensity of this process remains unchanged.

Many of the arguments on the effects of spatial variations in oceanic properties, presented in this chapter, may also apply to temporal fluctuations in oceanic variables. The importance of the temporal fluctuations to the air-sea fluxes of CO_2 is explored in following chapters.

Chapter 3.

Temporal Fluctuations in Oceanic Properties of the Labrador Sea: Effect on Air-Sea Fluxes of CO₂

3.1 Introduction

The air-sea flux of CO₂ at any given time is obtained as the product of the gas-transfer coefficient (K) and the air-sea difference in the partial pressure of CO₂ (Δp). Therefore, if there is a covariance between K and Δp , the mean air-sea flux over a period of time would be different from the flux computed as a product of the mean values of K and Δp . Moreover, Δp is a nonlinear function of seawater properties, such as temperature, salinity, concentration of dissolved inorganic carbon and alkalinity. In the previous chapter we have seen that Δp may be affected by variations in these oceanic properties in the spatial domain. But, Δp may equally well be affected by fluctuations in these properties with time. Fluctuations in these properties with time may result in a temporal nonlinear contribution to the partial pressure of CO₂. (Note that this is a temporal analogue of the spatial nonlinear contribution discussed in Chapter 2.)

This chapter is devoted to addressing two main questions:

1. What is the effect of the covariance between the gas-transfer coefficient and the air-sea difference in partial pressure of CO₂ on air-sea exchange of CO₂, over an annual cycle?
2. Is the nonlinearity in the dependence of the partial pressure of CO₂ on the elements of the oceanic carbonate system (such as temperature T , salinity S , total alkalinity A , dissolved inorganic carbon C) important for air-sea fluxes of CO₂, over an annual time scale?

To address these questions I use a one-dimensional model of the Labrador Sea to compute two terms for this locality: the *covariance term* (used to quantify the importance of covariance between K and Δp) and the *nonlinearity term* (which quantifies the non-linear effects in the carbonate system). Formal definitions of these terms are given in section 3.5.

The importance of the covariance term has been recognized in the literature, but typically not quantified (but see *Etcheto and Merlivat*, [1988]), and, consequently, is often ignored in practical applications. I am not aware of any previous study on the magnitude of the nonlinearity term. If these terms are significant, they could potentially affect the accuracy of carbon models and conclusions drawn from observational data.

Carbon models have a finite temporal resolution, and smaller-scale temporal fluctuations in oceanic properties are, of necessity, ignored. For instance, many global carbon box models, both diagnostic [e.g., *Knox and McElroy*, 1984; *Sarmiento and Toggweiler*, 1984; *Siegenthaler and Wenk*, 1984; *Volk and Liu*, 1988; *Shaffer and Sarmiento*, 1995] and transient [e.g., *Craig*, 1957; *Keeling*, 1973; *Oeschger et al.*, 1975; *Hoffert et al.*, 1981; *Bacastow and Björkström*, 1981; *Siegenthaler*, 1983; *Joos et al.*, 1991; *Peng and Broecker*, 1991; *Craig and Holmen*, 1995; *Jain et al.*, 1995] have a temporal resolution of a year and therefore neglect both the covariance and the carbonate nonlinearity effects of seasonal and shorter-scale fluctuations.

When air-sea fluxes of CO_2 are computed directly from the time-averaged observations of partial pressure of CO_2 and windspeed [*Tans et al.*, 1990; *Lefevre*, 1995; *Takahashi et al.*, 1995], the temporal covariance between these properties below the averaging time scale is neglected. If the partial pressure of the surface ocean is computed from averaged seawater properties, that is, without accounting for variations of these properties in the course of a year the temporal effect of the carbonate nonlinearity is neglected as well.

In addition to systematic errors stemming from using averaged values to describe nonlinear processes, temporal fluctuations in oceanic properties may be a source of random errors because the averaged values themselves may be imprecise: observations of the properties affecting the air-sea flux of CO_2 are usually sparse in time, therefore the averages of these properties (computed from a small number of measurements) may differ from the true average values, if atypical values are given too much or too little weight.

This last point has been used by *Taylor et al.* [1991] as a possible explanation of the results of *Tans et al.* [1990]. *Tans et al.* computed the oceanic uptake of atmospheric CO_2 in the North Atlantic directly from the observed values of windspeed and partial pressures of CO_2 and found it to be much lower than the uptake expected from carbon models. This discrepancy led *Tans et al.* to the conclusion that there was a “missing sink” in the northern hemisphere, which they attributed to an unidentified land sink for CO_2 in the northern hemisphere. *Taylor et al.* [1991] suggested that at least a part of the discrepancy could be explained by the unrepresentativeness of the averages of oceanic properties used to compute the air-sea fluxes of CO_2 . In particular, *Taylor et al.* pointed out that *Tans et al.* excluded observations in May–June, which is the period when the seawater partial pressure of CO_2 is strongly depressed, and that this exclusion could lead to an underestimate of the annual uptake of atmospheric CO_2 .

In this chapter, I quantify the effects of the temporal *covariance term* and the *carbonate non-linearity term*, using the Labrador Sea as a case study. I investigate time-scales at which the averaging of oceanic properties becomes acceptable. I also examine different sampling strategies for minimizing both systematic and random errors. Finally, I investigate whether the data-selection scheme used by *Tans et al.* [1990] is likely to underestimate air-sea fluxes in high-latitude waters.

3.2 Approach

In this chapter, I concentrate on the effects of temporal fluctuations in the oceanic properties in high-latitude waters. These waters are important to the global carbon cycle [e.g., *Knox and McElroy*, 1984; *Sarmiento and Toggweiler*, 1984; *Siegenthaler and Wenk*, 1984], so an improved accuracy of the estimates of air-sea fluxes of CO_2 in this region should improve our understanding of the global carbon cycle. Besides, high-latitude waters are subject to very large seasonal changes; therefore, the covariance and the carbonate nonlinearity effects are likely to be large here.

From various high-latitude waters I chose the Labrador Sea to be the focus of this study. The Labrador Sea is known to be one of the high-latitude sites of deep-water formation [*Lazier*, 1980]. Surface waters in this area are mixed during winter convection with deeper waters to form the Labrador Sea Water (LSW) and part of this water is exported equatorward by Deep Western Boundary Undercurrent [*Talley and McCartney*, 1982)]. Fluctuations in the properties of the surface waters in the Labrador Sea, may therefore affect (through the covariance and the nonlinearity terms) how much inorganic carbon is exported into the deep ocean.

Another, practical, reason was the availability of oceanic data for this location in the archives of the Bedford Institute of Oceanography (BIO), which was helpful in the implementation, testing and validation of the model of the Labrador Sea.

To evaluate the importance of temporal fluctuations in high-latitude waters for air-sea fluxes of CO_2 , a one-dimensional diagnostic model of the Labrador Sea was developed first. I used a model rather than oceanic data, because observations of the oceanic properties determining air-sea fluxes of CO_2 are extremely sparse and are not sufficient to reconstruct the annual cycles of these properties in high-latitude waters. Furthermore, the same model can be used to gain insight into the processes determining these properties and to assess the sensitivity of CO_2 fluxes to hypothetical changes in these processes (see Chapter 4), as well as to estimate

changes in the covariance and the nonlinearity terms with increasing concentrations of atmospheric CO₂ (see Chapter 5).

Only a few models are available for simulating temporal changes in the oceanic properties that affect the air-sea fluxes of CO₂ in high latitudes. None of them could be used to achieve the objectives of this work without major modifications.

The model of *Evans and Parslow* [1985] does not simulate all the variables necessary to compute air-sea fluxes of CO₂ (no dissolved inorganic carbon). The model of *Peng et al.* [1987] is extremely simplified, with all biological processes reduced to a single parameter, whose value was selected to give the best match between observations and simulations of the chemical composition of seawater. The model of *Taylor et al.* [1991], whose structure is the closest to that of the model developed here, has arbitrary vertical mixing, very simplified representation of phytoplankton losses to respiration and grazing, and does not recover the magnitude of the variations in dissolved inorganic carbon observed in the Labrador Sea or in the waters around Iceland by *Takahashi et al.* [1993]. Finally, the recent model of *Antoine and Morel* [1995a] is not self-contained, since it requires an external input of chlorophyll concentration which, given the sparsity of the ship-borne data and the limited amount of the satellite data available at present, limits its utility in this context (in the application of their model for the high-latitude North Atlantic *Antoine and Morel* [1995b] had to rely on the chlorophyll cycle computed by the model of *Taylor et al.* [1991]).

Furthermore, in their original form none of these models could be used to evaluate the effect of covariance between K and Δp on the air-sea fluxes: they assume either a constant K [*Peng et al.*, 1987], or neglect the dominant effect of windspeed on K (by assuming a constant piston velocity, which makes K a function of just solubility) [*Taylor et al.*, 1991; and *Antoine and Morel*, 1995b; in the version of the model applied to the North Atlantic]. Therefore, it was necessary to develop a model that differed in some important ways from the existing ones.

The Labrador Sea model developed for this study is described in section 3.3. The model simulates the annual cycles of physical variables (temperature and salinity) and biogeochemical variables (zooplankton, phytoplankton, nutrients, dissolved inorganic carbon and alkalinity). I evaluated the reliability of the model by comparing the simulated variables with the observations in the Labrador Sea (subsection 3.4.2) and adjacent waters (subsection 3.4.3). The results are also compared with those from other models (subsection 3.4.4).

From the simulated physical and biogeochemical variables, and from prescribed atmospheric partial pressure of CO_2 and windspeeds, the annual cycles of oceanic partial pressure of CO_2 and air-sea fluxes of CO_2 are computed (section 3.5). The simulated annual cycles of oceanic variables are then used to estimate the effects of temporal fluctuations in the oceanic variables on the net air-sea flux of CO_2 .

I assess the magnitude of the covariance term and the carbonate nonlinearity term by comparing the best estimate of the air-sea fluxes in the Labrador Sea obtained by averaging daily fluxes of CO_2 with estimates based on mean values of the oceanic properties.

To find the time scales below which both the terms become negligible, the data are partitioned into shorter time-intervals and the same procedure is repeated.

In addition to the systematic errors caused *by using average values*, random errors are also caused *by estimating these average values* using a small number of observations of fluctuating properties. This problem is studied in subsection 3.5.3 in which different sampling strategies are simulated.

Finally, I investigate the representativeness of the data used in the study of *Tans et al.* [1990] to evaluate the air-sea fluxes of CO_2 in high-latitudes by mimicking their sampling strategy. The air-sea fluxes computed from this limited data set are then compared with the fluxes computed using all the data.

3.3 Description of the Model

The one-dimensional model of the Labrador Sea presented here was developed to simulate the annual cycles of mixed-layer properties that control the air-sea exchanges of CO_2 . This control is exerted either directly (temperature T , salinity S , alkalinity A , dissolved inorganic carbon C), or indirectly (nutrients N , phytoplankton B , zooplankton Z).

The model consists of three oceanic boxes, representing the surface, the intermediate and the deep waters (layers 1, 2, and 3, respectively, in Figure 3-1). This structure is similar to that of the box model used by *Ikeda* [1987] to examine heat and salt balances in the Labrador Sea. However, in the *Ikeda* model the depth of layer 1 was fixed at 30 m, whereas here it varies from 200 m in winter to 30 m in summer (Figure 3-2), following the evolution of the mixed layer described by *Shuhay* [1978]. The bases of the intermediate layer (layer 2) and the deep-ocean layer (layer 3) are fixed at 230 m, and 1430 m, respectively, as in *Ikeda* [1987].

An important feature of this structure is the presence of an intermediate layer as in the model of *Taylor et al.* [1991]. The layer acts as a "buffer zone" separating the surface layer from the carbon- and nutrient-rich deep waters and therefore affects the air-sea fluxes of CO_2 and other biogeochemical processes. This effect is not accounted for in two-layer biogeochemical models [e.g., *Evans and Parslow*, 1985; *Fasham et al.*, 1990; *Wroblewski et al.*, 1988].

In the model, the heat and salt budgets of the three oceanic layers are computed using the prescribed values of atmospheric variables, mixed-layer depth cycle and properties of the deep layer and waters adjacent to the Labrador Sea.

The model does not include sea-ice, because it is applied to the central part of the Labrador Sea, where little ice-formation occurs. Ice may affect the model indirectly, through the input of the Labrador and Greenland Current waters whose properties are affected by the formation and melting of sea-ice (see also Appendix B).

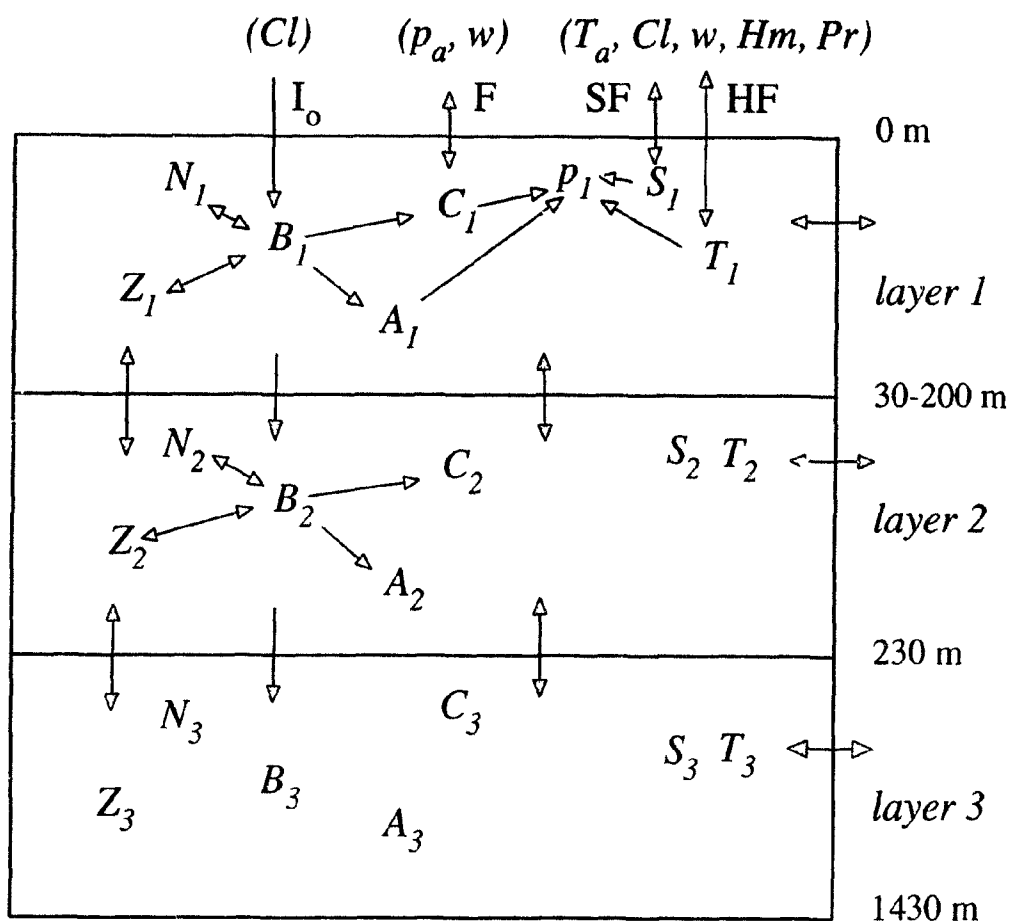


FIGURE 3-1. Components of the one-dimensional model of oceanic properties affecting the transfer of CO₂ between the atmosphere and the ocean.

Physical properties (temperature T and salinity S) and zooplankton Z are modelled in layers 1, 2, and 3, representing the surface, intermediate, and deep-ocean waters, respectively. Nutrients N , phytoplankton B , dissolved inorganic carbon C and alkalinity A are computed in layers 1 and 2 only; in layer 3 these properties have prescribed values, constant throughout the year. The seawater partial pressure of CO₂ is computed in the surface layer only (p_1). The main interactions between seawater properties are indicated by empty arrows. Exchanges between reservoirs are marked by solid arrows. The vertical exchanges between oceanic layers include: migration of Z , sinking of B , and vertical mixing (diffusive mixing, entrainment, convective overturning), which affects T , S , N , B , C and A . The horizontal mixing with adjacent waters affects mainly T and S . The air-sea exchanges include: the CO₂ flux F , the heat flux HF , the salinity flux SF and the flux of photosynthetically active radiation I_o . The atmospheric properties affecting the air-sea exchanges are given in brackets: p_a is the atmospheric partial pressure of CO₂, w is windspeed, Cl is cloud cover, Hm is humidity, T_a is air temperature and Pr is precipitation.

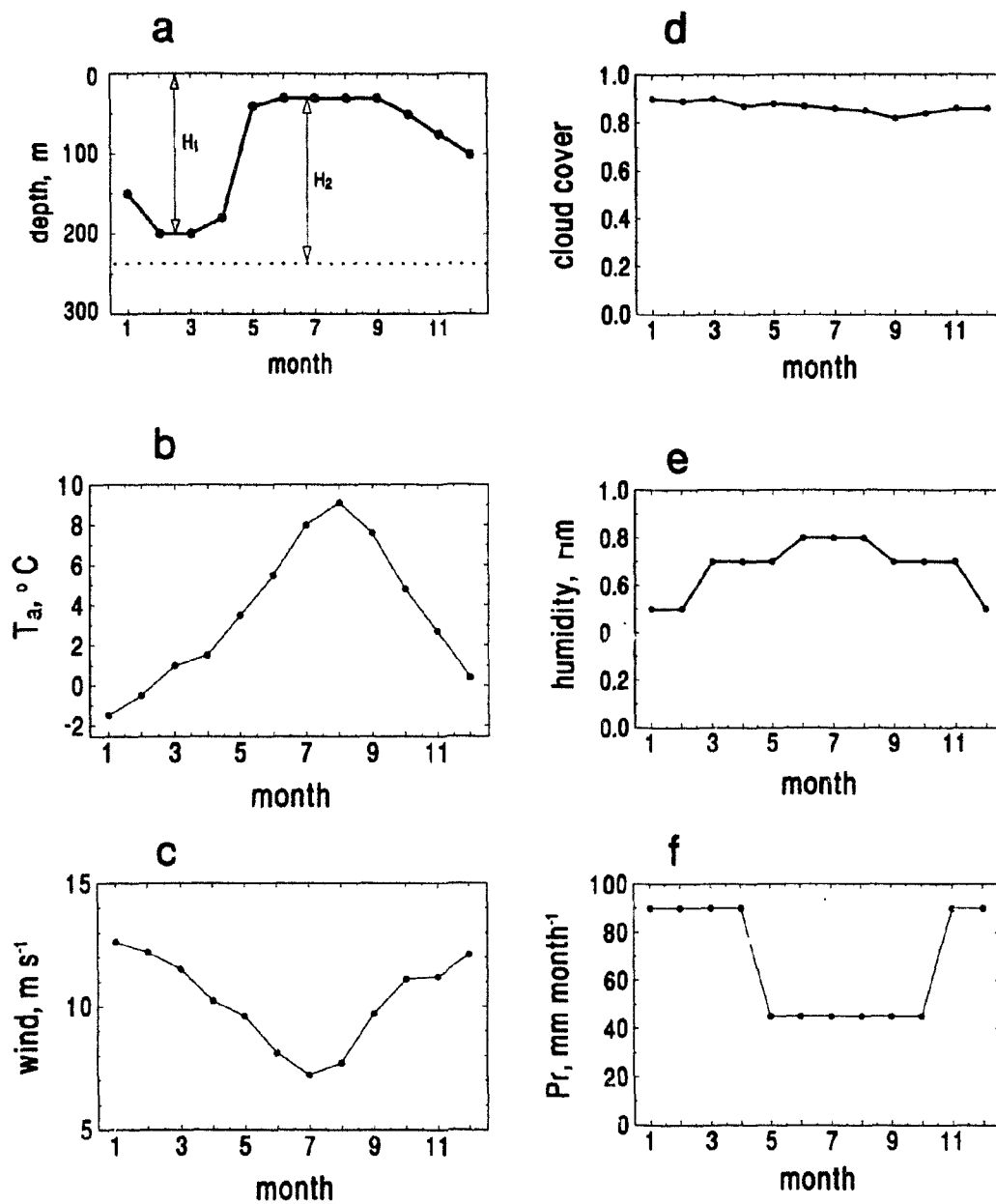


FIGURE 3-2. Annual cycles of the input variables: (a) base depth of layer 1 (solid line) and layer 2 (broken line); (b) air temperature T_a , [°C]; (c) windspeed w (at 20 m), [m s⁻¹]; (d) cloud cover Cl , dimensionless; (e) humidity Hm , dimensionless; (f) precipitation Pr [mm (month)⁻¹]. Sources: (a) based on [Shukhy, 1978]; (b), (c) and (d) from [Smith and Dobson, 1984]; (e) and (f) from [Ikeda, 1987].

In the process of computation of the heat and salt budgets, the vertical exchanges of water between the layers are established. These water exchanges, together with modelled biological processes within layers, are then used to determine the annual cycles of zooplankton, phytoplankton and nutrients (representing total biologically-usable species of nitrogen), alkalinity and dissolved inorganic carbon. Finally, air-sea fluxes of CO_2 are computed using the partial pressure of CO_2 in the surface layer (computed from the modelled temperature T , salinity S , alkalinity A and dissolved inorganic carbon C), the atmospheric partial pressure of CO_2 (prescribed), and the gas-transfer coefficient (computed from windspeed, temperature and salinity in the surface layer, which are obtained from the heat and salt budgets).

The following sections introduce the prescribed properties, as well as the methods used for computing the exchanges of water between the layers, the temperature and salinity of the surface layer, the biogeochemical variables in the two top layers and fluxes of CO_2 between the surface ocean and the atmosphere.

3.3.1 Prescribed properties

Atmospheric inputs: Several prescribed atmospheric variables are used to force the model. Windspeed, cloudiness, air temperature, humidity and precipitation are used to compute the heat and salt budgets and, eventually, the oceanic partial pressure of CO_2 (p_1). Windspeed is also used to compute the gas-transfer coefficient K , which, with p_1 and the prescribed atmospheric partial pressure of CO_2 (p_a), is used to compute the air-sea fluxes of CO_2 . Cloudiness affects also the amount of light available to phytoplankton.

Daily values of windspeed, cloudiness, air temperature, humidity and precipitation are computed using the climatological monthly averages of *Smith and Dobson* [1984] and *Baumgartner and Reichel* [1975]. For instance, monthly mean values of windspeeds for December and January are assigned to 16 December and to 16 January, respectively. The daily windspeeds for the period 17 December - 15 January are then linearly interpolated from these two values. The same procedure is applied

to the rest of the year and to the other input variables. The annual cycles of these variables are shown in Figure 3-2. (The effects of short-term variability in winds and in clouds are discussed in Chapter 4.)

The atmospheric partial pressure p_a is fixed at the global mean annual value of $335 \mu\text{atm}$ observed in late 1970s [e.g., *Bacastow and Keeling*, 1981], which corresponds to the period when the values of the deep ocean composition used here were measured.

Temperature and salinity constraints: The model is also constrained by prescribed seawater properties. Following *Ikeda* [1987], the heat and salt budgets are constrained by the values of temperature T and salinity S in the three layers on the first day of February, and by the summer differences in T and S between layers 1 and 2. Here, the February values are assumed to be: $T_1 = T_2 = 3.1^\circ\text{C}$ and $T_3 = 3.5^\circ\text{C}$, and $S_1 = S_2 = 34.65$ and $S_3 = 34.87$. Here and elsewhere in this work, the subscripts 1, 2, and 3 refer to layers 1, 2 and 3, respectively. The summer differences in T and S are $T_1 - T_2 = +3.84^\circ\text{C}$ and $S_1 - S_2 = -0.345$, respectively. The prescribed values of T and S are consistent with the averages from years 1964–1974 from Ocean Weather Station Bravo in the Labrador Sea [*Lazier and Hackett*, 1986].

Deep-layer composition: The biogeochemical composition of the deep layer is also prescribed in the model. The concentrations of nutrients N (biologically-usable nitrogen), dissolved inorganic carbon C and alkalinity A in this layer were selected to match the properties of the Labrador Sea waters in winter 1978 reported by *Anderson et al.* [1985] and the deep-ocean values from autumn 1982 in the TTO data. These values, after standardization to the mean surface-layer salinity of 34.6, are: $N_3 = 16.8 \text{ mmol m}^{-3}$, $C_3 = 2193 \text{ mmol m}^{-3}$ and $A_3 = 2350 \text{ meq m}^{-3}$.

3.3.2 Oceanic temperature, salinity, and exchanges of water between the layers

Oceanic temperature, salinity, and exchanges of water between the layers are computed from the balance of heat and salinity following the scheme of *Ikeda* [1987]. In this scheme, inputs of adjacent waters and the vertical eddy diffusivity coefficients are adjusted until the computed annual cycles of T and S meet the criteria constraining the annual and inter-annual variabilities in T and S .

The annual variability criteria require reproduction of the summer differences in temperature and salinity between layer 1 and 2 given by *Ikeda* [1987]. The inter-annual variability criteria are set here to approximate the inter-annual steady state, because the present model concentrates on simulating typical conditions. In other words, the temperatures and salinities in all three boxes are expected to change little between consecutive years of simulation.

The computed diffusivity and convective overturnings are then used to estimate vertical exchanges of other seawater properties. The computed temperature of the surface layer is used in the calculation of the partial pressure of CO_2 and the gas-transfer coefficient of CO_2 .

The main steps involved in these computations are described in the following sections. Additional details appear in Appendix B.

Temperature and salinity: The temperature and salinity of the layers evolve throughout the year depending on the air-sea fluxes, horizontal mixing and vertical mixing. The net air-sea flux of heat is computed as the sum of four components: the short-wave radiation, the long-wave radiation, the sensible heat flux and the latent heat flux. The net air-sea flux of water is calculated as the difference between precipitation and evaporation.

The long-wave radiation, fluxes of sensible and latent heat and evaporation are computed using the formulae of *Smith and Dobson* [1984], as implemented by *Ikeda*

[1987]. These formulae use humidity, wind speed and air temperature from climatological data. To compute the short-wave radiation, the clear-sky solar radiation is computed first, and then corrected for the effect of clouds, following *Platt et al.* [1990]. Precipitation is prescribed directly from climatological data.

Horizontal mixing represents inputs of adjacent waters, whose properties are given in Table B-1 (Appendix B), and are based on those of *Ikeda* [1987]. Vertical mixing is determined by entrainment, convective overturnings and diffusive mixing, which are discussed next.

Entrainment: Entrainment is associated with changes in depths of the layers. Here entrainment affects only the properties of the two top layers, since the boundary between layers 2 and 3 remains fixed throughout the year.

The entrainment velocity h [m d^{-1}] is defined as the rate of change in the thickness H_1 [m] of the surface layer:

$$h = dH_1/dt. \quad (3-1)$$

Following *Evans and Parslow* [1986] two additional functions h^+ and h^- are also defined, such that:

$h^+ = h$ and $h^- = 0$ when the depth of layer 1 increases (i.e., $\dot{h} > 0$), and

$h^+ = 0$ and $h^- = -h$ when layer 1 shallows (i.e., $\dot{h} < 0$).

The flux of a property X from layer 1 to layer 2 associated with entrainment, $f_{12}^e(X_1, X_2)$ [$\text{mmol m}^{-2} \text{ d}^{-1}$] is given by:

$$f_{12}^e(X_1, X_2) = h^-(X_1 - X_2). \quad (3-2)$$

where X_1 and X_2 are the concentrations of the property X in layers 1 and 2 [mmol m^{-3}].

Similarly, the flux from layer 2 to layer 1, $f_{21}^e(X_1, X_2)$, is given by:

$$f_{21}^e(X_1, X_2) = h^+(X_2 - X_1). \quad (3-3)$$

Note that when the boundary between the layers 1 and 2 deepens, only the properties of layer 1 are affected by entrainment (as $h^- = 0$ in (3-2)); conversely, when the boundary shallows, only the properties of the layer 2 are affected (as $h^+ = 0$ in (3-3)).

Convective overturnings: Convective overturnings are simulated here following *Ikeda* [1987]. They include shallow overturnings between the top two layers and deep overturning involving the third layer as well. *Shallow overturning* occurs whenever the layer 1 becomes denser than layer 2 resulting in complete mixing of a property X between these layers:

$$X'_1 = X'_2 = \frac{X_1 H_1 + X_2 H_2}{H_1 + H_2}, \quad (3-4a)$$

where the prime denotes concentrations of the property X after the overturning. In the present model the shallow overturning takes place between mid-December and early April.

Deep overturning is simulated following *Ikeda* [1987] by mixing the top two layers with a part of layer 3. Let us denote the thickness of layer 3 that is mixed with layers 1 and 2 as H_c [m]. The value of a property X is changed as a result of the deep overturning to X' such that:

$$X'_1 = X'_2 = \frac{X_1 H_1 + X_2 H_2 + X_3 H_c}{H_1 + H_2 + H_c}. \quad (3-4b)$$

The depth H_c is known to be variable: it may range from 0 m in years without deep convection to between 400-800 m in years with deep convection [*Lazier*, 1980; *Ikeda*, 1987]. Timing of the deep overturning may also vary. In the computations presented here the deep overturning occurs on the last day of February, as in *Ikeda* [1987], and reaches $H_c = 400$ m.

Diffusive mixing: The diffusive flux of a property X from layer 1 into layer 2 is denoted as f_{12}^d . The value of f_{12}^d is a product of the diffusive mixing velocity k_1 through the base of layer 1, expressed in m d^{-1} , and the difference in the concentrations of the property between the layers ($X_1 - X_2$) [as in *Ikeda, 1987*]:

$$f_{12}^d(X_1, X_2) = k_1(X_1 - X_2) = -f_{21}^d(X_1, X_2). \quad (3-5)$$

The diffusive mixing velocity k_1 is computed from the eddy diffusivity d_1 [$\text{m}^2 \text{d}^{-1}$] and the distance between the centers of the layers:

$$k_1 = d_1 / [0.5(H_1 + H_2)], \quad (3-6)$$

where H_1 and H_2 , both expressed in m, denote thicknesses of layers 1 and 2, respectively. The eddy diffusivity d_1 is assumed to depend on the density difference between the layers [*Munk and Anderson, 1948*]:

$$d_1 = L_1(\rho_2 - \rho_1)^{-1.5} \quad (3-7)$$

where ρ is the density [kg m^{-3}] and L_1 is a proportionality constant, expressed in $\text{m}^2 \text{d}^{-1} (\text{kg m}^{-3})^{1.5}$. Values of L_1 are estimated from the budgets of heat and salt, which depend, among other things, on the vertical exchange of water caused by diffusive mixing. To avoid unreasonably high values of d_1 when the difference in ρ is very small, the maximum value of d_1 is set at $864 \text{ m}^2 \text{d}^{-1}$ ($= 1 \times 10^{-2} \text{ m}^2 \text{s}^{-1}$), corresponding to the diffusivity in a non-stratified ocean [*Munk and Anderson, 1948*]. The computed values of the mixing velocities throughout the year are shown in Figure 3-3. The diffusive fluxes between layers 2 and 3 are computed in the same way.

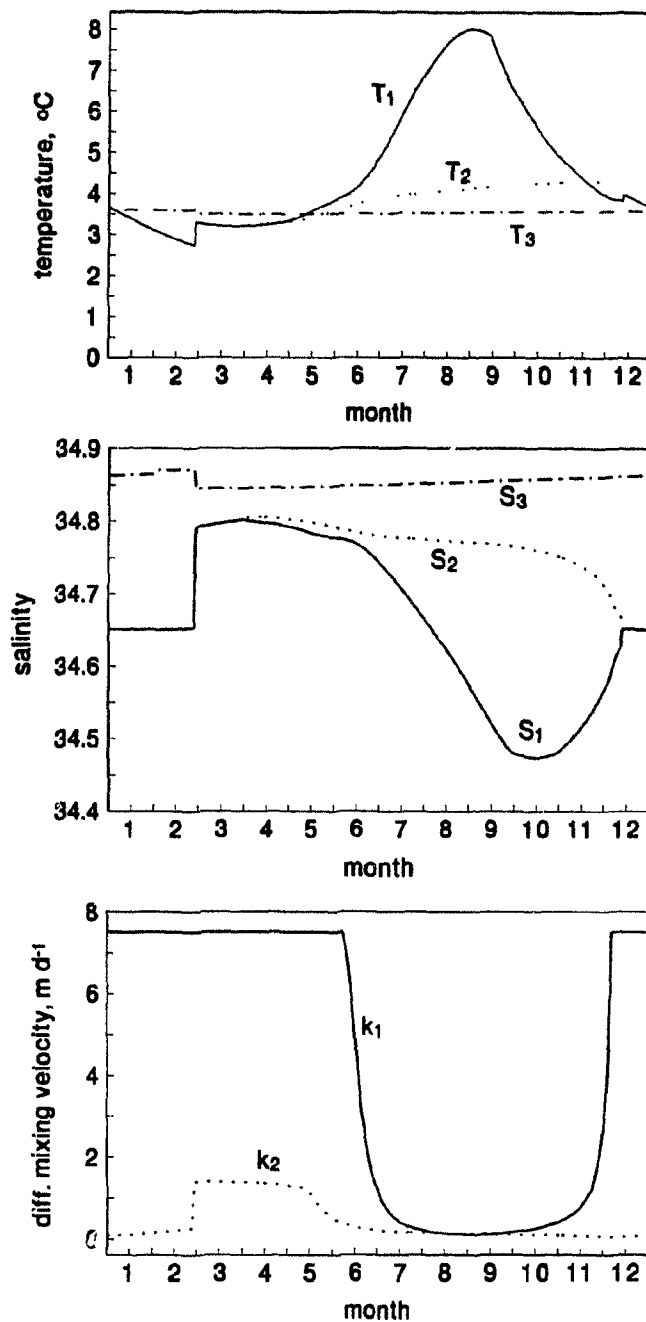


FIGURE 3-3. Computed annual cycles of (a) oceanic temperature T [$^{\circ}\text{C}$], (b) salinity S , dimensionless, in layers 1, 2, and 3; (c) vertical diffusive mixing velocities: across the base of layer 1 (k_1) and across the base of layer 2 (k_2) [m d^{-1}].

3.3.3 Daily changes in zooplankton, phytoplankton, nutrients, dissolved inorganic carbon and alkalinity

With the daily water exchanges between the layers computed, one may simulate the annual cycles of biogeochemical variables. There are five inter-dependent biogeochemical variables in layers 1 and 2 — concentrations of herbivorous zooplankton Z , phytoplankton B , nutrients N , dissolved inorganic carbon C and total alkalinity A . In layer 3, values of B , N , C and A are kept constant throughout the year at the values prescribed in 3.3.1. This simplification can be justified by the much smaller annual variations in these properties in deep waters compared with the variations in the top two layers. Two exceptions are made:

- a) Zooplankton concentration Z is modelled in all three layers, since vertical migrations may substantially affect their concentration in layer 3.
- b) In Chapter 4 (section 4.4) and Chapter 5 (section 5.4) the composition of layer 3 is allowed to change when medium-term changes are evaluated, since the small year-to-year increments in the deep-layer concentration of C , when accrued over decadal time-scale, may substantially modify annual air-sea fluxes of CO_2 .

The model is run from the initial state, in which layers 1 and 2 have the same composition as layer 3, until the annual cycles of the modelled variables stabilize. In the present model stability is attained within the first two years.

To simplify computations and interpretation of results, the biogeochemical variables are kept standardized to salinity of 34.6 (which is an average value of salinity in the surface layer obtained from the model). Addition or removal of fresh water may slightly affect the concentrations of Z , B , N , A and C , but within the range of salinity observed in the Labrador Sea, these effects translate, at the most, into $\pm 0.5\%$ differences in these properties, which does not justify further complication of the model to account for salinity-related changes in the biogeochemical variables.

The only exception is made in computations of the oceanic partial pressure of CO_2 , which might be affected not only by small variations in alkalinity (A) and dissolved inorganic carbon (C), but by variation in salinity (S) itself (through the effect of S on the dissociation constants). Values of p are therefore computed using the daily values of salinity computed by the model and the values of C and A converted to this salinity.

Changes in the modelled variables during a daily time-step are computed using the equations presented below. Before the next computational step is taken, zooplankton biomass is adjusted to represent zooplankton vertical migrations, and value of B , N , C and A are modified, when necessary, to account for convective overturning, following equations (3-4a) or (3-4b).

Zooplankton: Daily changes in concentration of zooplankton Z [mmol C m^{-3}] depend on the amount of the food assimilated and on the zooplankton losses:

$$\frac{dZ_1}{dt} = (ag_1 - m_1)Z_1, \quad (3-8a)$$

$$\frac{dZ_2}{dt} = (ag_2 - m_2)Z_2, \text{ and} \quad (3-8b)$$

$$\frac{dZ_3}{dt} = -m_3Z_3, \quad (3-8c)$$

where a denotes the zooplankton assimilation efficiency (dimensionless), g [d^{-1}] is the grazing rate, m [d^{-1}] represents zooplankton loss rate. No grazing is assumed in layer 3, since the concentration of potential food is low and zooplankton there is usually in a state of diapause, during which most of its activities, including feeding, are curtailed. For instance, *Conover* [1962] found that, after arriving into deep waters, *Calanus hyperboreus* ceased grazing and lowered its respiration severalfold. Despite the negative net growth rate, the zooplankton biomass in this layer is not reduced to zero, because it is supported by ontogenic vertical migrations of zooplankton from the top two layers.

The grazing rate g is computed as a function of the available food using the formula of Ivlev [1945]. The zooplankton loss rate m includes losses due to respiration, excretion and mortality (Appendix C).

The zooplankton concentration computed for the end of a day is then modified to reflect vertical migration. The daily migrations, pronounced in low latitudes, are unimportant or nonexistent in high latitudes [Longhurst *et al.*, 1989]. Therefore, only the ontogenic migration associated with the development cycle of zooplankton is represented. In these waters, calanoids, the dominant component of zooplankton in the Labrador Sea [Conover, 1976; Longhurst *et al.*, 1989], have a one-generation annual reproduction cycle [Conover, 1988], with younger stages reaching the surface layer in spring, feeding on phytoplankton, and gradually descending to deeper waters, where they spend the winter diapause.

In the model, the overwintering zooplankton migrates to the upper layers when the net growth rate ($ag - m$) in any of these layers becomes higher than that in the deep layer. The gradual descent is then simulated as a migration of fixed fractions of zooplankton from layer 1 and 2 into the underlying layers.

Phytoplankton: Daily changes in phytoplankton biomass B [mmolC m⁻³] are determined by the net growth of phytoplankton, losses to zooplankton grazing, and transfers of phytoplankton between the layers through sinking, diffusive mixing and entrainment:

$$\frac{dB_1}{dt} = (\sigma_1 - l_1)B_1 - g_1 Z_1 - \left[\frac{v_1}{H_1} B_1 + \frac{k_1 + h_1^+}{H_1} (B_1 - B_2) \right], \quad (3-9a)$$

and

$$\frac{dB_2}{dt} = (\sigma_2 - l_2)B_2 - g_2 Z_2 - \left[\frac{v_2}{H_2} B_2 - \frac{v_1}{H_2} B_1 + \frac{k_1 + h_1^-}{H_2} (B_2 - B_1) + \frac{k_2 + h_2^+}{H_2} (B_2 - B_3) \right], \quad (3-9b)$$

where the net growth rate is the difference between gross growth rate σ [d⁻¹] and the loss rate l [d⁻¹] caused by phytoplankton respiration and excretion (Appendix C),

v_i [m d^{-1}] is the sinking velocity in layer i ($i=1,2$), k_i denotes the mixing velocity through the base of layer i and h^+ and h^- are the functions describing the entrainment (section 3.3.2).

The normalized daily gross growth rate σ in a layer is computed by dividing the daily gross primary production in a layer, denoted as P_T [$\text{mg C m}^{-2} \text{ d}^{-1}$], by the depth of the layer H and by the phytoplankton biomass B :

$$\sigma = \frac{P_T}{12 B H}, \quad (3 - 10)$$

where B is multiplied by 12 to convert it from mmol C m^{-3} to mg C m^{-3} . The daily phytoplankton production P_T in a layer is calculated from the daylength and the noon irradiance, following *Platt et al.* [1990] and *Platt and Sathyendranath* [1991].

The noon irradiance is corrected for the presence of clouds following *Platt et al.* [1990]. For this correction I used the daily cloud cover interpolated from climatological monthly averages.

In this approach phytoplankton production depends explicitly on the amount of light available and implicitly on other limiting factors (see Appendix C for justification of this approach).

The phytoplankton production at depth z and time t , $P(z, t)$, depends on light following the formulation of *Webb et al.* [1974] and *Platt et al.* [1980]:

$$P(z, t) = (12 B / \theta) P_m^{chl} [1 - \exp(-I(z, t) / I_k)], \quad (3 - 11)$$

where θ is the carbon-to-chlorophyll ratio [$\text{mg C (mg chl)}^{-1}$], P_m^{chl} is the assimilation number (i.e., the light-saturated production normalized to chlorophyll concentration, expressed in $\text{mg C (mg chl)}^{-1} \text{ hr}^{-1}$), I_k [W m^{-2}] is the photoadaptation parameter, defined as the ratio of P_m^{chl} to α^{chl} , the chlorophyll-normalized, initial slope of the photosynthesis-light curve [$\text{mg C (mg chl)}^{-1} \text{ hr}^{-1} (\text{W m}^{-2})^{-1}$].

The effect of the limiting factors other than light, such as nutrient concentration, temperature, light history, or species composition, are represented implicitly through parameters: P_m^{chl} , α^{chl} and θ . Since the *in situ* measurements of θ are

uncertain at best [Eppley, 1980], it is assumed here that θ_1 is 50 mg C (mg chl)⁻¹ before and during the diatom spring bloom, and it increases to 75 mg C (mg chl)⁻¹ later in the season, when the phytoplankton community adapts to a higher-light and lower nutrient environment [Geider, 1987; Langdon, 1988; Cullen *et al.*, 1993] (Appendix C). In layer 2, θ_2 is assumed to be 35 mg C (mg chl)⁻¹ throughout the year, reflecting the adaptation to a lower-light, higher-nutrient environment. The carbon fluxes in the model are not sensitive to θ_2 (nor to P_m^{chl} and α^{chl} in this layer) as the primary production in layer 2 is strongly limited by the low irradiance reaching this layer.

The photosynthetic parameters P_m^{chl} and α^{chl} are based on *in situ* measurements and therefore should represent the end-result of interactions of a suite of factors affecting the chlorophyll-normalized phytoplankton production.

In addition, I use the nutrient budget of each layer to ensure that the growth rates computed for that layer do not cause the nutrient concentrations to fall below zero. In such a case, the gross growth rate is lowered to a level sufficient to maintain the nutrient values just above zero (in the computer code the threshold value was set at 0.01 mmol m⁻³).

Nutrients: Daily changes in concentration of nutrients N (representing here all biologically-usable forms of nitrogen, including nitrate, nitrite and ammonium) are determined by the removal of nutrients by gross phytoplankton growth, return of nutrients associated with the recycled portions of phytoplankton and zooplankton losses, denoted as dimensionless parameters ϵ_l and ϵ_m , respectively, and by mixing and entrainment (for more details see Appendix C):

$$\frac{dN_1}{dt} = -\gamma_N \sigma_1 B_1 + \gamma_N \epsilon_l l_1 B_1 + \gamma_N \epsilon_m m Z_1 - \left[\frac{k_{SI} + h_1^+}{H_1} (N_1 - N_2) \right], \quad (3-12a)$$

and

$$\frac{dN_2}{dt} = -\gamma_N \sigma_2 B_2 + \gamma_N \epsilon_l l_2 B_2 + \gamma_N \epsilon_m m Z_2 - \left[\frac{k_1 + h_1^-}{H_2} (N_2 - N_1) + \frac{k_2 + h_2^+}{H_2} (N_2 - N_3) \right]. \quad (3-12b)$$

The nitrogen-to-carbon molecular ratio γ_N [$\text{mmol N (mmol C)}^{-1}$] of phytoplankton depends on the availability of nutrients, species composition, and phase of phytoplankton growth [Sakshaug, 1989; Cullen *et al.*, 1993]. In this model the N:C molecular ratio of phytoplankton is assumed to be equal to the Redfield ratio of 0.15 (= 16:106) when the nutrients are abundant, and decreases to 0.10 in the nutrient-limited post-bloom phase.

Alkalinity: Alkalinity is affected by all the factors modifying the nutrient concentrations (gross growth, recycling of phytoplankton losses, recycling of zooplankton losses, mixing and entrainment), and, in addition, by the formation of CaCO_3 :

$$\frac{dA_1}{dt} = \gamma_A \sigma_1 B_1 - \gamma_A \epsilon_l l_1 B_1 - \gamma_A \epsilon_m m Z_1 - \left[\frac{k_1 + h_1^+}{H_1} (A_1 - A_2) \right] - 2\Gamma(\sigma_1 - l_1) B_1, \quad (3 - 13a)$$

and

$$\frac{dA_2}{dt} = \gamma_A \sigma_2 B_2 - \gamma_A \epsilon_l l_2 B_2 - \gamma_A \epsilon_m m Z_2 - \left[\frac{k_1 + h_1^-}{H_2} (A_2 - A_1) + \frac{k_2 + h_2^+}{H_2} (A_2 - A_3) \right] - 2\Gamma(\sigma_2 - l_2) B_2, \quad (3 - 13b)$$

where Γ is the molecular ratio of CaCO_3 to organic carbon production [$\text{mmol CaCO}_3 (\text{mmol C}_{org})^{-1}$] and the factor of two indicates removal of two equivalents of alkalinity per one mole of CaCO_3 formed.

In the standard case it was assumed that $\Gamma = 0.02 \text{ mmol CaCO}_3 (\text{mmol C}_{org})^{-1}$; consequences of higher values of Γ are explored in the sensitivity analysis (Chapter 4).

Formation of one mole of organic carbon typically increases seawater alkalinity by $\gamma_A = 0.18 \text{ meq (mmol C)}^{-1}$ (because of removal of nitrate and sulfate ions — see Appendix C), except during the nutrient-limited phase of growth, where $\gamma_A = 0.12 \text{ meq (mmol C)}^{-1}$ because of the lower N:C ratio (as indicated earlier in this

section). Formation of one mole of CaCO_3 decreases dissolved inorganic carbon by one mole and alkalinity by two equivalents.

Dissolved Inorganic Carbon: Dissolved inorganic carbon is affected by the same processes as alkalinity and, in addition, by the CO_2 flux between the atmosphere and the surface layer:

$$\frac{dC_1}{dt} = -\sigma_1 B_1 + \epsilon_1 l_1 B_1 + \epsilon_m m Z_1 - \left[\frac{k_1 + h_1^+}{H_1} (C_1 - C_2) \right] - \Gamma(\sigma_1 - l_1) B_1 + \frac{F}{H_1}, \quad (3-14a)$$

and

$$\frac{dC_2}{dt} = -\sigma_2 B_2 + \epsilon_1 l_2 B_2 + \epsilon_m m Z_2 - \left[\frac{k_1 + h_1^-}{H_2} (C_2 - C_1) + \frac{k_2 + h_2^+}{H_2} (C_2 - C_3) \right] - \Gamma(\sigma_2 - l_2) B_2, \quad (3-14b)$$

where F is the air-to-sea flux of CO_2 , here expressed in $\text{mmol C m}^{-2} \text{ d}^{-1}$.

3.3.4 Air-Sea Fluxes of CO_2

Air-sea flux of CO_2 (F) is a product of the gas transfer coefficient K [$\text{mmol C m}^{-2} \text{ d}^{-1} \mu\text{atm}^{-1}$], and Δp [μatm], the difference in the partial pressure of CO_2 between the surface ocean (p_1 ; μatm) and the atmosphere (p_a ; μatm):

$$F = K \Delta p = K(p_a - p_1) \quad (3-15).$$

The gas-transfer coefficient K is the product of the solubility, expressed in $\text{mmol C m}^{-3} \mu\text{atm}^{-1}$ and the piston velocity of a gas κ [m d^{-1}]. Solubility of CO_2 is computed following *Weiss* [1974] as a function of temperatures and salinities obtained from the model. The piston velocity of CO_2 is computed following *Wanninkhof* [1992]:

$$\kappa = A w^2 \sqrt{660 / Sc}, \quad (3-16)$$

where w is the windspeed in m s^{-1} , Sc is the dimensionless Schmidt number for CO_2 (which is the ratio of kinematic viscosity to molecular diffusivity), calculated from

the surface-layer temperature T_1 , and \mathcal{A} is the proportionality constant, expressed in $\text{m d}^{-1} (\text{m s}^{-1})^{-2}$.

For windspeeds derived from the climatological average windspeeds used in most calculations here, *Wanninkhof* [1992] gives $\mathcal{A} = 0.39 \text{ cm hr}^{-1} (\text{m s}^{-1})^{-2} = 0.094 \text{ m d}^{-1} (\text{m s}^{-1})^{-2}$. For instantaneous windspeeds, $\mathcal{A} = 0.31 \text{ cm hr}^{-1} (\text{m s}^{-1})^{-2} = 0.075 \text{ m d}^{-1} (\text{m s}^{-1})^{-2}$. The larger value of \mathcal{A} in the former case compensates for the smaller variability in w in the climatological data (the adequacy of this compensation is discussed in Chapter 4.)

The partial pressure of CO_2 in the atmosphere (p_a) is prescribed at $335 \mu\text{atm}$ (the consequences of intra-annual variability in p_a are assessed the sensitivity analysis in Chapter 4), whereas the partial pressure in the surface layer (p_1) is calculated as a function of temperature, salinity, dissolved inorganic carbon and alkalinity, using the algorithm of *Peng et al.* [1987], with the dissociation constants of carbonic and boric acids of *Mehrbach et al.* [1973] and *Lyman* [1957], respectively. For simplicity, the effect of phosphates and silicates on the partial pressure of CO_2 is not taken into consideration, because this effect is relatively small and is, to a large degree, compensated by effect of neglecting that a fraction of the biologically-usable nitrogen in seawater would be in the form of ammonia rather than as nitrates or nitrites — see Appendix C for details). The effect of uptake of nitrates (and sulfates) on the partial pressure is incorporated into changes in alkalinity.

3.4 Annual Cycles of Biogeochemical Variables

The annual cycles of the main biogeochemical variables affecting the partial pressure and the air-sea fluxes of CO_2 were simulated by the model. These variables include: zooplankton, phytoplankton, nutrients, alkalinity and dissolved inorganic carbon. Evolution of these variables during the year is described in this section with three goals in mind.

The first goal is to indicate the magnitude of fluctuations in the seawater properties determining air-sea fluxes of CO_2 . The second aim is to present the background necessary to understand the sensitivity of the air-sea CO_2 fluxes to changes in physical and biogeochemical processes, evaluated in Chapter 4. The third goal is to test the reliability of the model by comparing the simulated variables with the available *in situ* data for the Labrador Sea and with remote sensing data, measurements in adjacent waters of the North Atlantic and results of other models.

3.4.1 General features of the annual cycles

Changes in the concentration of nutrients in the surface layer (N_1) are used to identify four seasonal phases in the annual cycles of the biogeochemical variables (Figure 3-4).

The “winter” phase (end of February – mid-May) began with a deep convection, simulated here at the end of February following Ikeda [1987]. Concentrations of nutrients and other variables in layers 1 and 2 were brought close to those of the deep ocean (e.g., $N_1 > 16 \text{ mmol m}^{-3}$) and remained almost unchanged until mid-May, because phytoplankton production was strongly light-limited.

During the “spring” phase (mid-May – end of June) the shallowing surface layer and the increasing surface irradiance improved the average light conditions in the layer and triggered a spring phytoplankton bloom.

The increasing phytoplankton biomass B (which peaked at over 80 mmol C m^{-3} ($= 20 \text{ mg chl m}^{-3}$) at the end of June) depleted nutrients (N_1 : $16 \rightarrow 0.1 \text{ mmol m}^{-3}$) and markedly lowered the dissolved inorganic carbon C (by 100 mmol m^{-3}).

Alkalinity A_1 moderately increased, because of the uptake of nitrate from seawater by phytoplankton. The effect of CaCO_3 formation (lowering A and C) was small because in the standard case, the ratio of CaCO_3 production to production of organic carbon was low ($\Gamma = 0.02 \text{ mmol CaCO}_3 (\text{mmol } C_{org})^{-1}$). Consequences of possible higher production of CaCO_3 are explored in the sensitivity analysis in Chapter 4.

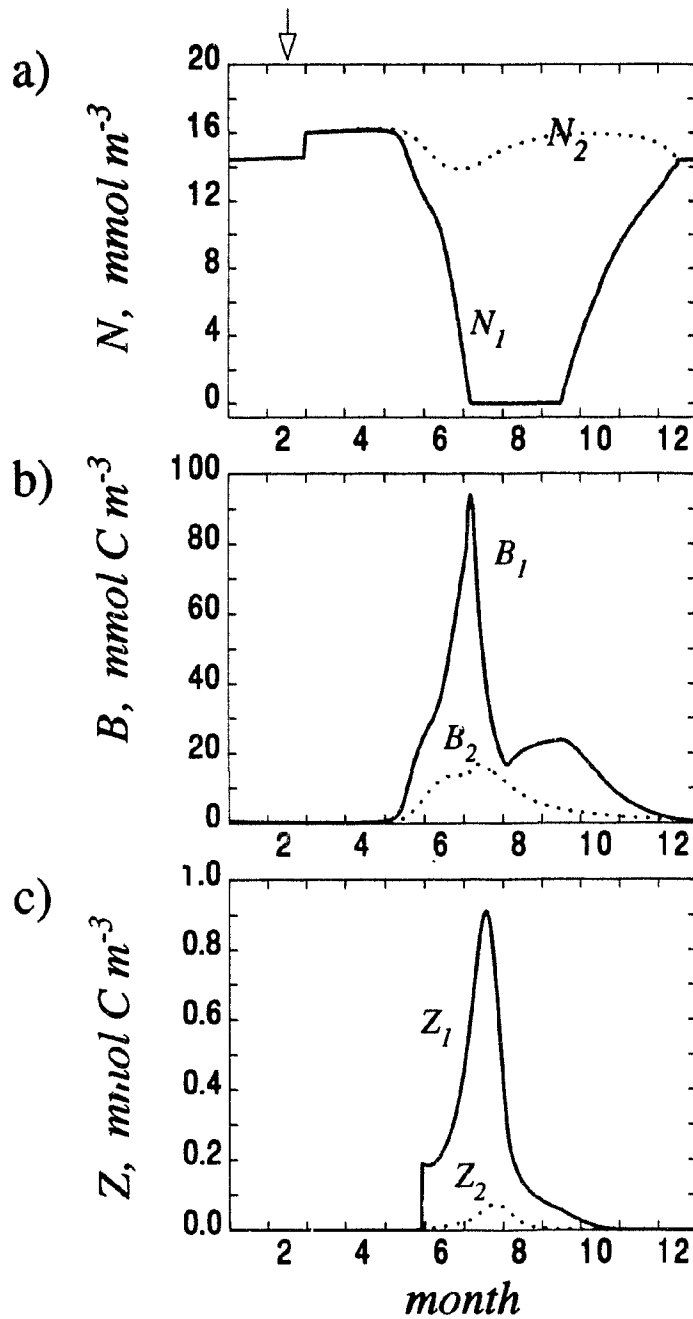


FIGURE 3-4. The annual cycles of the modelled oceanic properties and air-sea fluxes of CO_2 in the surface layer (subscript 1) and the intermediate layer (subscript 2). Empty arrows indicate the time of the simulated deep-winter convection.

- (a) Nutrients N .
- (b) Phytoplankton concentration B .
- (c) Zooplankton concentration Z .

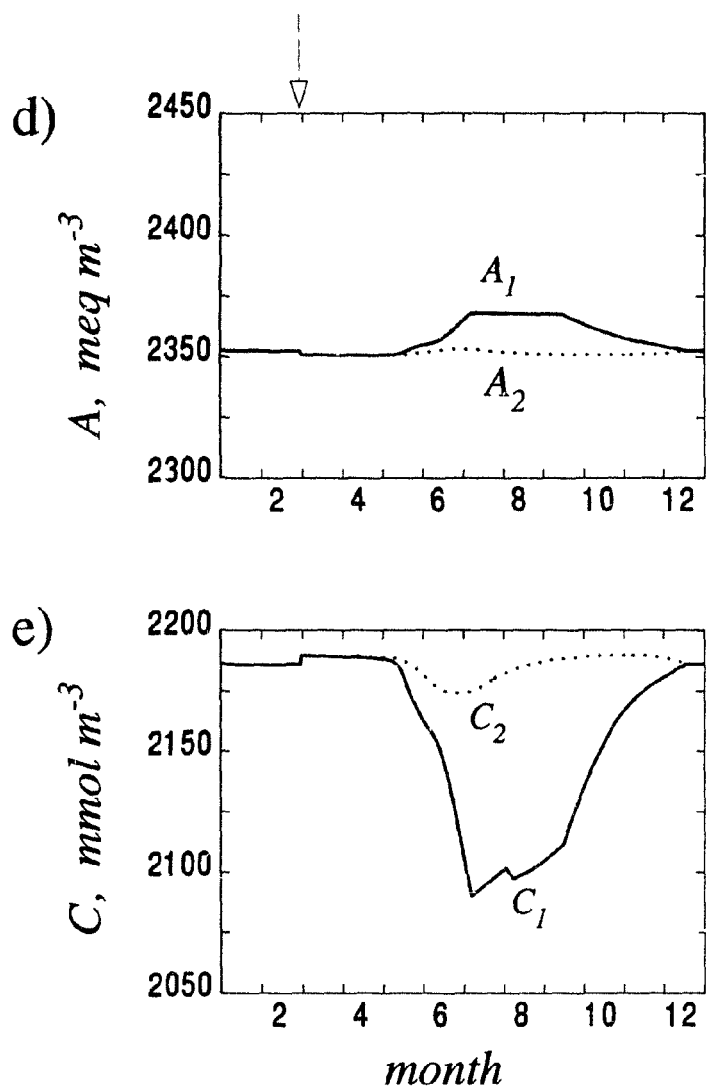


FIGURE 3-4 - continued.

(d) Total alkalinity A .

(e) Dissolved inorganic carbon C .

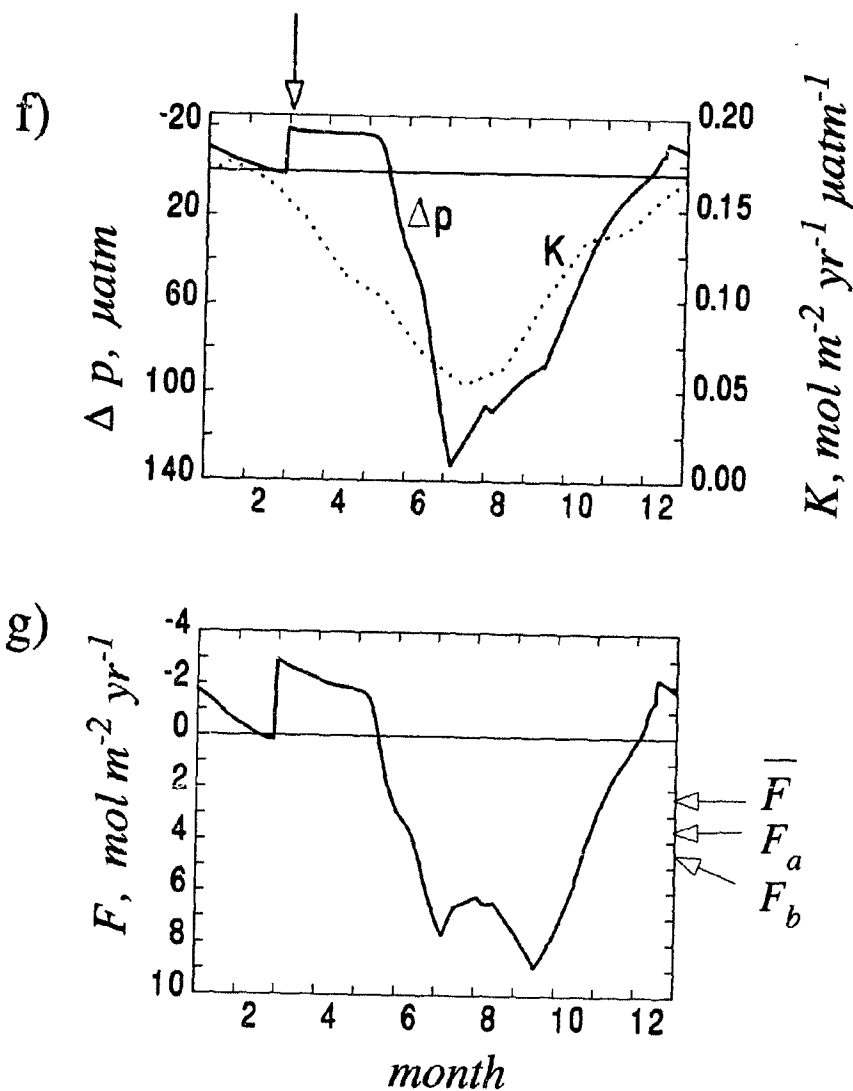


FIGURE 3-4 - continued.

- (f) Air-sea difference in partial pressure of CO_2 (Δp) and the gas-transfer coefficient K .
- (g) Air-sea fluxes of CO_2 (F): \bar{F} denotes the annual flux computed by averaging daily values of F ; F_a is the flux computed from mean values of K and Δp (equation 3-20); F_b is the flux computed from mean values of K and from p_1 calculated from mean temperature, salinity alkalinity and dissolved inorganic carbon (equation 3-22). Positive values of F correspond to the net uptake of CO_2 by the ocean.

The overwintering zooplankton migrated from the deep waters into the surface layer and increased its biomass by feeding on the developing bloom.

During the "summer" phase (July - mid-September), vertical mixing weakened, because the density stratification between layers 1 and 2 increased. Nutrients remained depleted ($N_1 < 0.1 \text{ mmol m}^{-3}$), as phytoplankton was able to remove all nutrients that could be supplied to the surface layer by the weak mixing.

The phytoplankton biomass fell sharply because of an increased sinking velocity in the declining stage of the spring bloom. Later the biomass increased slightly, because the simulated shift in the composition of phytoplankton towards a higher C:N ratio allowed uptake of additional carbon from seawater.

The concentration of dissolved inorganic carbon generally increased. The small decrease in C at the end of July was caused by the shift in the phytoplankton C:N ratio. The zooplankton concentration fell after its initial increase, reflecting diminishing food supply and continuous migration to layer 2.

The "autumn" phase (mid-September - end of February) began with the deepening of the surface layer. The phytoplankton uptake could no longer keep up with the supply of the nutrients entrained from layer 2 and nutrient concentration began to rise ($N_1: 0.1 \rightarrow 14.5 \text{ mmol m}^{-3}$). The phytoplankton concentration fell, reflecting rapidly worsening light conditions. The dissolved inorganic carbon rose, and alkalinity fell slightly, mainly in response to the entrainment of the layer 2 waters. Zooplankton continued to migrate toward deeper waters.

Finally, the concentrations of nutrients, alkalinity and dissolved inorganic carbon in the surface layer were restored to the initial values by the deep-convection event starting the next annual cycle.

In general, in the surface layer, changes in nutrients, dissolved inorganic carbon and alkalinity were dominated by biological activity from the onset of the spring bloom in early June to the decline of biological production in mid-September, and by the physical exchanges with deeper waters in the remaining part of the year.

In the intermediate layer, annual changes in the seawater variables reflected mainly the physical exchanges with the neighbouring layers and decay of organic matter imported from the surface layer, because low light limited local phytoplankton production. Most of the time, these low light levels were caused by physical constraints (low surface irradiance and absorption by water in a thick surface layer); however, during spring and summer these constraints were replaced by strong absorption of light by phytoplankton in the surface layer. In the absence of high local production, the peak in chlorophyll in mid-July reflects a pulse of organic matter sinking from the surface layer. Changes in N , C and A were linked to decomposition of the sinking organic matter and to exchanges of water with layers 1 and 3.

3.4.2 Comparison with the *in situ* data

Nutrients, phytoplankton and dissolved inorganic carbon in the surface layer, for which there are measurements from the Labrador Sea representing both the pre- and post-bloom periods, are selected for the assessment of model performance. The spread of these data over a year should be sufficient to check whether the simulated cycles of these variables during a year have realistic magnitude and timing, although not all details of the cycles could be validated because of scarcity of data, particularly in autumn and winter.

Four sources of data are used: the Imperial Oil Cruise in July 1976, the BIO primary productivity experiments 1978–1991, the TTO cruise in autumn 1982, and the BIO physical oceanography data from 1990–1994. The data are plotted alongside the simulated values on Figure 3-5.

Nutrients: The model cycle of nutrients seems to fit well to the measurements of nitrate + nitrite concentrations from the Labrador Sea (Figure 3-5 a), particularly with respect to the winter concentrations and to the timing and magnitude of nutrient decrease in during the spring bloom (late May–June). In summer, the

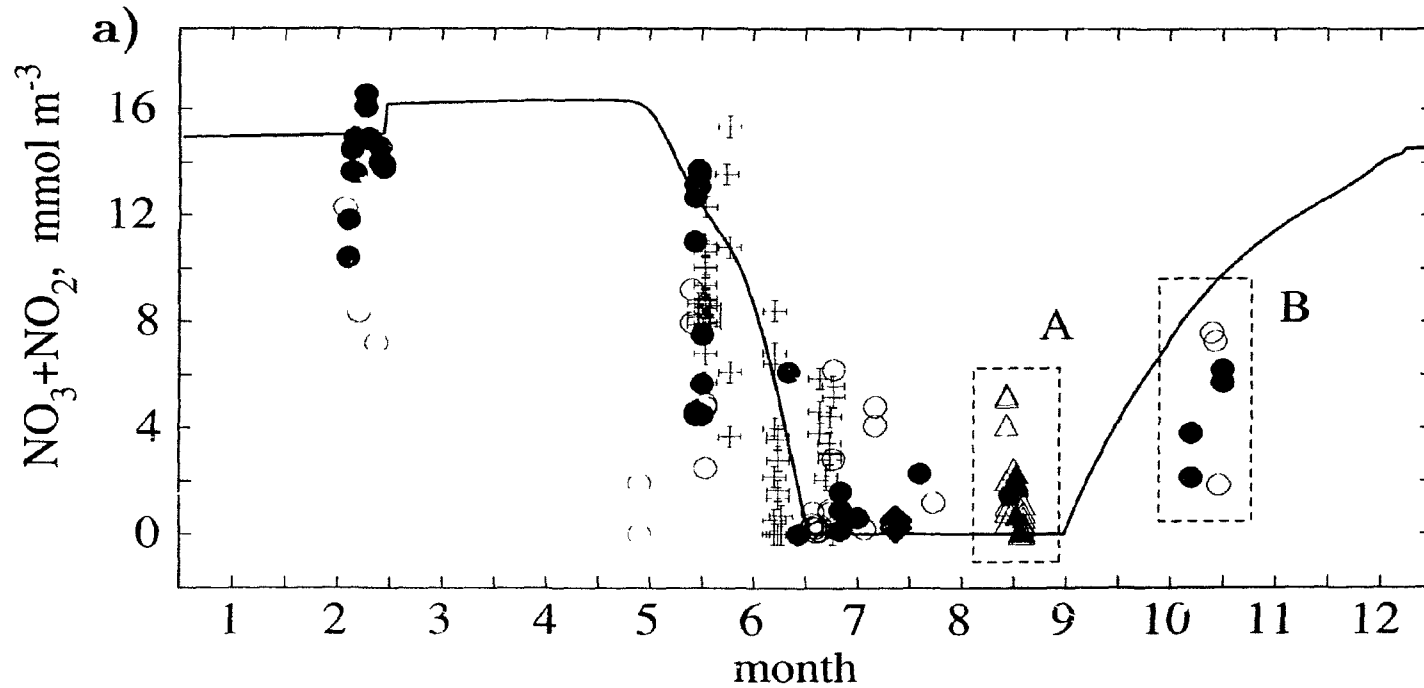


FIGURE 3-5. Comparison of the modelled properties with the observational data. Solid line represents the output of the model (the standard run), circles denote measurements from the BIO primary productivity experiments 1978-1991, triangles indicate the TTO data from 1982, crosses represent data from BIO physical oceanography cruises 1990-1994 and diamonds the data from the Imperial Oil Cruise in 1976. Filled symbols mark measurements in the central part of the Labrador Sea, while empty symbols denote the measurements from the margins of the sea.

(a) The surface-layer nutrient concentration ($\text{NO}_3 + \text{NO}_2$). Broken-line rectangles mark clusters of data "A" and "B", discussed in the text.

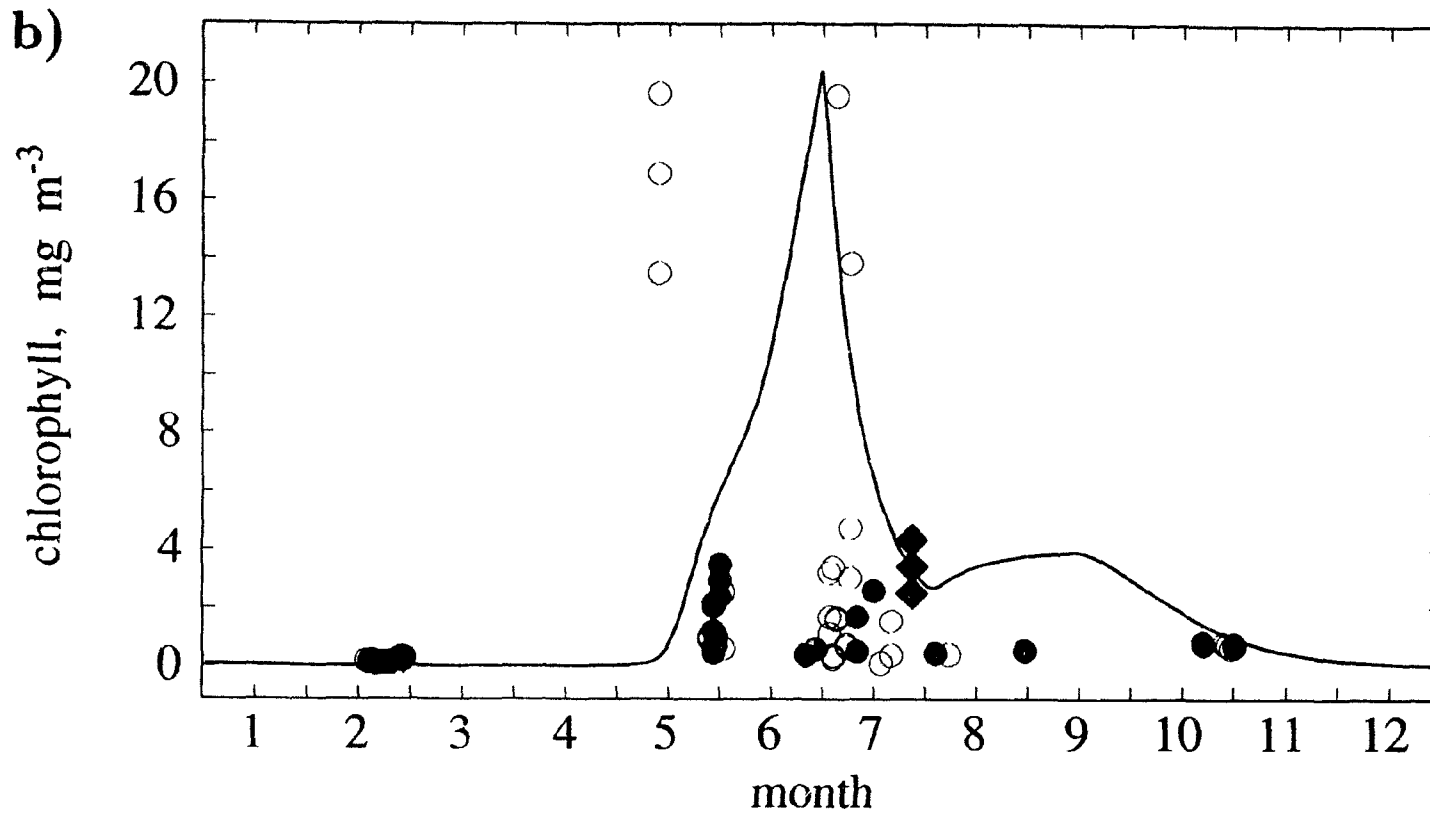


FIGURE 3-5. - continued

(b) The surface-layer chlorophyll concentration. The model values of phytoplankton biomass B_1 (solid line) were converted from mmol C m^{-3} to mg chl m^{-3} . Circles denote measurements from the BIO primary productivity experiments 1978-1991 and diamonds mark the data from the Imperial Oil Cruise in 1976. Filled symbols mark measurements in the central part of the Labrador Sea, while empty symbols denote the measurements from the margins of the sea.

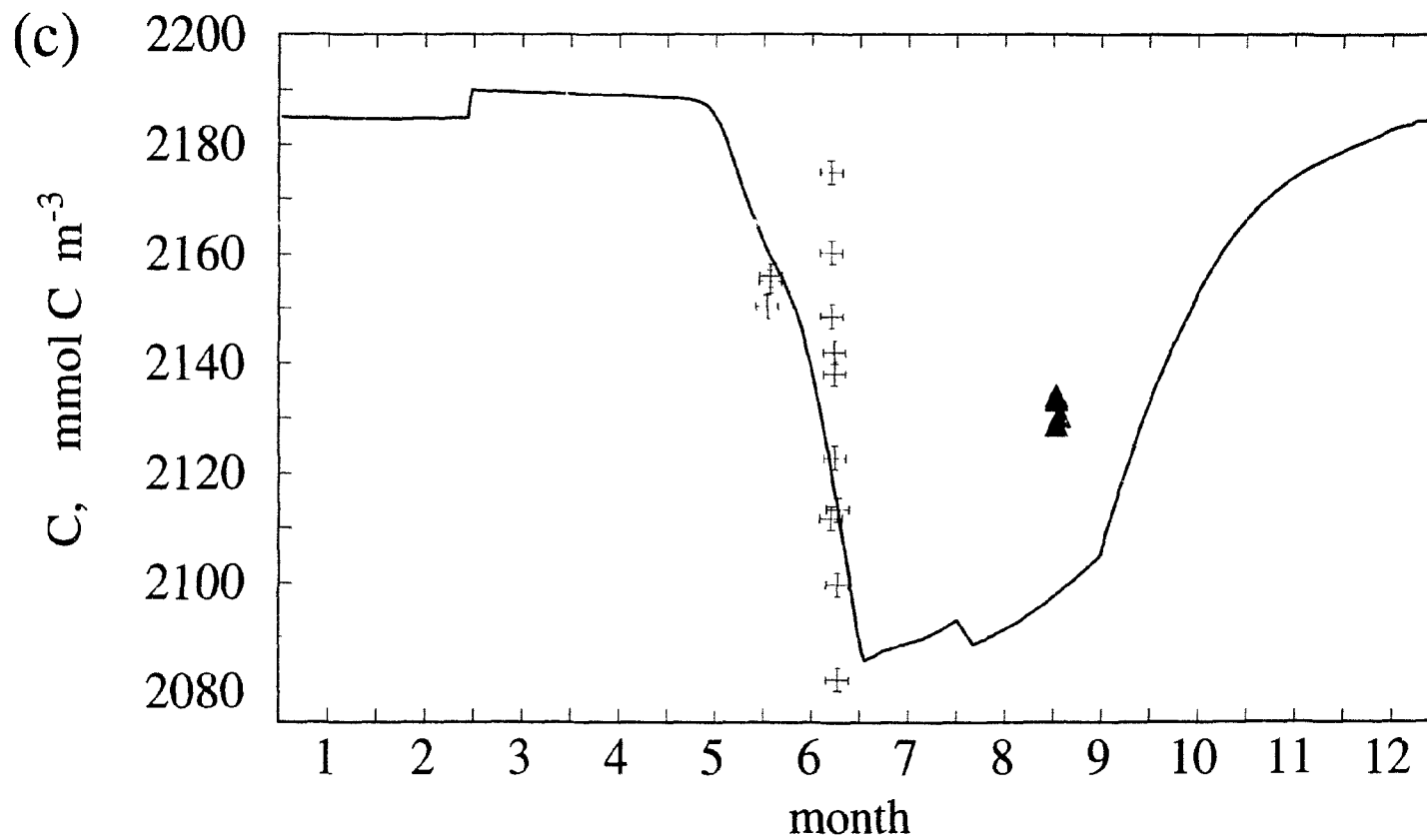


FIGURE 3-5. - continued

(c) The surface-layer concentration of dissolved inorganic carbon. Solid line represents the output of the model (the standard run), triangles indicate the TTO data from 1982 and crosses represent data from BIO physical oceanography cruises 1990-1994.

observed nutrient concentrations are usually low, as a consequence of the depletion of nutrients by phytoplankton production.

In autumn, both the observed and the simulated nutrient concentrations increase as a result of a shifting balance between diminishing biological uptake and increasing water mixing. However, it is difficult to discern the timing of the autumn mixing from the observations. This timing is important because the annual air-sea fluxes of CO_2 are sensitive to the composition of seawater in this period (as discussed in Chapter 4).

On the one hand, the somewhat elevated nutrient concentrations in early September (cluster "A" in Figure 3-5a) may be interpreted as temporary departures from the nutrient-depleted summer state. Such departures could be caused by storm events, not represented in the model forced by monthly means. Storms bring nutrients into the surface waters, and these nutrients might be sampled before phytoplankton takes them up. If this interpretation is correct, and if the October increase in nutrient concentrations (cluster "B") represents a typical time of autumn mixing, then the model simulates the mixing about one month too early.

On the other hand, the September data may be interpreted as the onset of an early autumn mixing in one year, and the October data as an indication of a late autumn mixing in another year. Then the model simulation of the nutrient cycle would fit within the range of inter-annual variations. Both the satellite data from the Labrador Sea and the *in situ* measurements in waters around Iceland (section 3.4.3), show inter-annual variability in the onset of the autumn mixing, thus lending support to this interpretation.

The nutrient data from the margins of the Labrador Sea (marked in Figure 3-5 by empty squares and triangles) are more variable than the data from the central Labrador Sea, probably because of mixing with adjacent waters, different hydrographic properties (e.g., larger influx of low-salinity waters, strong currents) and different timing of biogeochemical processes at different locations.

Chlorophyll: The simulated cycle of chlorophyll concentration broadly consistent with the observations (Figure 3-5b). The magnitude of the spring maximum in chlorophyll closely matches those measured on the margins of the Labrador Sea. The lack of a peak of similar magnitude in the central Labrador Sea data may be a result of missing the bloom, which is plausible given the small number of samples and the short duration of the bloom. Note that indirect evidence for such blooms (strong depletion of nutrients and associated uptake of inorganic carbon from seawater) are observed in these waters.

In the post-bloom phase the simulated concentration of chlorophyll cannot be validated unambiguously, although chlorophyll concentrations in the late-July data (marked as diamonds in Figure 3-5b) are of similar magnitude. These samples may be representative of the summer conditions because the sampled phytoplankton community was dominated by flagellates, which seems to be the typical composition of the post-bloom phase [MacLaren Report, 1976].

Dissolved inorganic carbon: Data on concentrations of the dissolved inorganic carbon, the last seawater variable discussed here, are limited to June, July and September. The timing and magnitude of decrease in C in June and July seem to agree with the decrease simulated by the model (Figure 3-5c).

In the TTO data from September, the dissolved inorganic carbon was higher than the values simulated by the model, which presumably reflects an input of carbon-rich deeper waters as a result of an early autumn mixing or a transient summer mixing episode, already discussed in the section on the nutrient data.

In conclusion, the simulated cycles of seawater variables are broadly consistent with the available observations from the Labrador Sea, although more data would be needed to better constrain the cycles of biogeochemical variables, particularly during the autumn mixing. Some additional constraint may be provided by analysis of oxygen data from the Labrador Sea (see suggestions for future work in Chapter 6).

3.4.3 Comparisons with other data

The model performance may be validated further by comparison of the simulated cycles of the seawater variables with satellite images and with measurements in another area of the North Atlantic with a similar hydrological regime.

The annual cycle of chlorophyll concentration can be compared with the Coastal Zone Color Scanner (CZCS) images from the area. These images indicate that the period of increased chlorophyll concentration, beginning with a bloom in June, lasts until September, although in some years this period seems to end earlier. This roughly corresponds to the period between the onset of the spring phytoplankton bloom and the termination of the elevated summer phytoplankton concentrations by autumn mixing in September.

The simulated evolution of the seawater properties in the Labrador Sea is also consistent with evolution of these properties in other waters at similar latitudes. *Takahashi et al.* [1993] compiled observations from waters around Iceland. The seasonal observations of nutrients and dissolved inorganic carbon indicate that the spring phytoplankton bloom develops in these waters in the last two weeks of May. The resulting depletion of nutrients and reduction in dissolved inorganic carbon and the partial pressure of CO_2 were of similar magnitude to those obtained from this model, particularly in the West and South Stations, whose temperature and nutrient regimes resembled most closely those of the Labrador Sea.

Elevated values of nutrient concentrations, associated with autumn mixing, were observed in August-September. There was a substantial variability between stations and between measurements at a given station in different years. Existence of such inter-annual variability in Icelandic waters (see *Takahashi et al.* [1985] and *Peng et al.* [1987]) lends some additional support to the interpretation that the timing of autumn mixing in the model falls within the range of inter-annual variability in the Labrador Sea data (3.4.2).

In conclusion, it seems that the simulated cycles of biogeochemical properties are not inconsistent with *in situ* measurements in the Labrador Sea, as well as with changes in phytoplankton concentration observed from satellites, and with the evolution in seawater properties in other North Atlantic waters at similar latitudes.

3.4.4 Comparisons with other models

The simulated seawater variables were also compared with the output of three other models from the literature dealing with high-latitude waters of the North Atlantic.

The model of *Evans and Parslow* [1985] simulates the cycles of Z , B and N in the surface layer off Newfoundland. In that model, the surface layer shallows much earlier than in the present model, reaching 25 m in April, and, consequently, the bloom occurs in April. Although not discussed explicitly, the termination of the bloom in that model is likely to be caused by a combination of high phytoplankton losses due to very strong mixing with deep waters (3 m d^{-1}) and zooplankton grazing. The evolution of the nutrient concentration is not explicitly presented by Evans and Parslow, but from the amount of nitrogen contained in the phytoplankton and zooplankton biomass given in their Figure 1, one may deduce that it never falls below 75% of its winter values of 10 mmol m^{-3} . This is clearly not the case in the Labrador Sea.

The model of *Peng et al.* [1987] was designed to fit the measurements of the concentrations of phosphates, dissolved inorganic carbon, oxygen and the oceanic partial pressure of CO_2 from around Iceland. In that model all biological processes are reduced to a single function describing the phosphate residence time in the surface layer τ , which is proportional to the prescribed depth of the surface layer divided by the prescribed surface irradiance:

$$\tau = b(H_1/I_0),$$

where b [$\text{W m}^{-3} \text{d}^{-1}$] is the proportionality parameter adjusted to fit the data. Peng *et al.* prescribed the time-dependence of b so that the spring bloom can be simulated. In their prescription of physical processes, vertical mixing is limited to the entrainment associated with changes in the prescribed surface layer depth. Such simplifications of biological and physical processes, as well as the need to fit the parameter b numerically to match the observed properties, limit applications of this model to study the sensitivity of the air-sea carbon fluxes to changes in biological processes.

Finally, in the model of Taylor *et al.* [1991], which is closest in structure to this model, the spring bloom in the Atlantic waters at 60°N began in mid-May and peaked in mid-June. This timing is similar to the one simulated here. However, the magnitude of their bloom is much lower ($< 5 \text{ mg chl m}^{-3}$), because Taylor *et al.* artificially lowered the nutrient concentration in the deep waters to simulate incomplete utilization of nitrates, possibly caused by exhaustion of other nutrients such as silicates. Application of a similar constraint in the Labrador Sea would lead to summer concentrations of nitrates of about 10 mmol m^{-3} , which are clearly too high. As a consequence, the effects of biological processes on nutrients and carbon fluxes in the model of Taylor *et al.* [1991] may be severely underestimated. Also the proposed mechanism of limiting the uptake of nitrates does not seem to hold for the Labrador Sea and for waters around Iceland: samples having high concentrations of unutilized nitrates also have high concentrations of silicates, such that silicate limitation is not likely.

3.5 Partial Pressure and Air-Sea Fluxes of CO₂

3.5.1 Annual cycles of the partial pressure and air-sea fluxes of CO₂

The annual cycles of the oceanic partial pressure p_1 and the air-sea CO₂ flux F computed by the model are shown in Figures 3-4c and 3-4f. After the deep convection, p_1 was higher than the atmospheric partial pressure, and consequently the flux of CO₂ was negative (that is, directed from sea to air). The magnitude of this flux decreased in time with decreasing gas-transfer coefficient K .

The spring phytoplankton bloom reduced p_1 sharply (by about 160 μatm) and increased F strongly (from -2 to + 8 mol CO₂ m⁻² yr⁻¹). Once the bloom ended, p_1 increased, following the increases in dissolved inorganic carbon and in temperature. The air-sea flux initially fell in response to the increase in p_1 , but this trend was reversed in late August when K increased because of stronger winds.

The autumn mixing in mid-September increased p_1 sharply by bringing carbon-rich waters to the surface layer. The gas-transfer coefficient could not compensate for this rapid increase and, consequently, the air-sea fluxes fell. By December the fluxes became negative.

In general, the air-sea fluxes of CO₂ followed mainly the cycle of the partial pressure p_1 , although changes in the gas-transfer coefficient substantially modified the evolution of the air-sea fluxes in March–April and August–September.

3.5.2 Effects of fluctuations in the oceanic properties on the partial pressure and air-sea fluxes of CO₂

Definitions of fluxes of CO₂

The daily values for the partial pressure of the surface ocean were computed using the simulated seawater temperature T , salinity S , dissolved inorganic carbon C and total alkalinity A :

$$p_1 = p(T_1, S_1, C_1, A_1). \quad (3-17)$$

As a result of the non-linearity of the carbonate system the average partial pressure is different from the partial pressure associated with the time-averages of T , S , C , and A . The difference, called here the temporal nonlinear contribution to the partial pressure of CO₂, is denoted as c_t and computed from:

$$c_t = \overline{p(T_1, S_1, \dots)} - p(\overline{T}_1, \overline{S}_1, \dots), \quad (3-18)$$

where overbars denote time-averages. Equation (3-18) is an application of equation (2-1) from Chapter 2 to the temporal, instead of the spatial, fluctuations in seawater properties.

The average air-sea flux of CO₂, denoted as \overline{F} , is given by:

$$\overline{F} = \overline{K \Delta p} = \overline{K [p_a - p(T_1, S_1, \dots)]}. \quad (3-19)$$

The value of \overline{F} serves here as the reference flux against which are compared two other carbon fluxes computed without accounting for the temporal fluctuations in oceanic properties.

The first of these fluxes, F_a , is the flux associated with the average K and the average Δp , that is, the flux computed without accounting for the covariance between K and Δp . This flux is given by:

$$F_a = \overline{K} \overline{\Delta p} = \overline{K} [\overline{p_a} - \overline{p(T_1, S_1, \dots)}]. \quad (3-20)$$

The *covariance term* is defined here as the difference between the average flux and the flux in the absence of covariance between K and Δp . It is denoted as ΔF_a :

$$\Delta F_a = \bar{F} - F_a. \quad (3-21)$$

The second flux, F_b , is computed neglecting both the covariance and the non-linearity of the carbonate system. This flux, associated with average K and average seawater T , S , C and A , may be expressed as:

$$\begin{aligned} F_b &= \bar{K} \Delta p(\bar{T}_1, \bar{S}_1, \dots) = \bar{K} [\bar{p}_a - p(\bar{T}_1, \bar{S}_1, \dots)] = \bar{K} [\bar{p}_a - \overline{p(T_1, S_1, \dots)} + c_t] \\ &= F_a + \bar{K} c_t. \end{aligned} \quad (3-22)$$

The effect of the nonlinearity of the carbonate system on the air-sea fluxes, ΔF_b , is then given by :

$$\Delta F_b = F_a - F_b = -\bar{K} c_t. \quad (3-23)$$

The term ΔF_b is the *nonlinearity term*.

Effects of fluctuations at the annual scale

The effects of the fluctuations in oceanic properties on the partial pressure of CO_2 in the Labrador Sea and air-sea fluxes of CO_2 are shown in Table 3-1. The nonlinear contribution c_t associated with annual variability of seawater properties was $7.9 \mu\text{atm}$.

The annual average air-sea flux \bar{F} was $2.2 \text{ mol CO}_2 \text{ m}^{-2} \text{ yr}^{-1}$. Without any covariance between K and Δp the calculated flux would be considerably larger ($F_a = 3.7 \text{ mol CO}_2$). The flux computed neglecting both the covariance and the nonlinearity of the carbonate system would be even greater ($F_b = 4.6 \text{ mol CO}_2 \text{ m}^{-2} \text{ yr}^{-1}$).

These results indicate that fluctuations in K , and in the seawater properties determining p_1 may have substantial effects on the air-sea fluxes of CO_2 . To put these results into perspective, one may compare the effects of covariance between K

TABLE 3-1. The nonlinear contribution to the oceanic partial pressure of CO₂ (c_t) and the air-sea CO₂ fluxes (F) at the annual and the seasonal time-scales.

Case	c_t	\bar{F}	F_a	F_b
1. annual scale	7.9	2.2	3.7	4.6
2. seasonal scale				
a) all data used:				
cold season (Nov. - April)	0.8	-1.2	-1.4	-1.3
warm season (May - Oct.)	7.0	5.6	6.1	6.7
annual average:	3.9	2.2	2.4	2.7
b) seasons as in <i>Tans et al.</i> [1990]				
cold season (Jan. - April)	1.0	-2.1	-2.3	-2.1
warm season (July - Oct.)	3.1	7.3	8.2	8.5
annual average	2.1	2.5	3.0	3.2

The temporal nonlinear contribution c_t is in μatm , fluxes F are in $\text{mol C m}^{-2} \text{ yr}^{-1}$; \bar{F} denotes the annual sum of daily fluxes, F_a is the flux computed neglecting the covariance between K and Δp , and F_b is the flux computed neglecting the covariance and the nonlinearity of the carbonate system. Case 1 presents the standard values obtained using the data from the whole year. Case 2 presents the values associated with seasonal instead of annual averages: a) with all the data partitioned into two seasons, and b) with the seasons defined by [*Tans et al.*, 1990].

and Δp (ΔF_a) and of nonlinearity of the carbonate system (ΔF_b) with the uptake of anthropogenic CO_2 by the Labrador Sea.

Based on the estimates of the 3-D model of *Maier-Reimer* [1991], in 1988 the uptake of anthropogenic CO_2 by the Labrador Sea waters, denoted here as F_x , was around $0.8 \text{ mol C m}^{-2} \text{ yr}^{-1}$ (see also Chapter 5). Then, ΔF_a is about twice the size of the anthropogenic uptake ($\Delta F_a = -1.9F_x$). The effect of the nonlinearity of the carbonate system is comparable to the anthropogenic flux ($\Delta F_b = -1.1F_x$).

Effects of fluctuations at shorter time-scales

The effects of fluctuations in the oceanic properties at progressively shorter time-scales were also evaluated. To find out at what time-scale the effects of temporal fluctuations become negligible, I partitioned the annual cycles into the six-, three-, two- and one-month periods and repeated the calculations done in the previous section for these periods.

First, the year was divided into two periods covering November–April and May–October, to represent the cold and the warm seasons, respectively. Table 3-1 contains values of c_t , \bar{F} , F_a and F_b computed for each of these seasons, and the annual sums of these fluxes.

During the cold season both the covariance between K and Δp , and the nonlinearity of the carbonate system had negligible effects on the air-sea fluxes. In the warm season these effects were stronger, since the variability in the oceanic properties during this period was larger than that in the cold season.

Overall, when a year was split into two seasons, the effects of covariance between K and Δp , and of the nonlinearity of the carbonate system on the estimates of the annual air-sea CO_2 fluxes were substantially reduced (see also Figure 3-6).

Next, the year was partitioned of into four seasons: November–January, February–April, May–July, and August–October. This partition did not reduce the effects of the covariance and the nonlinearity, compared with the two-season

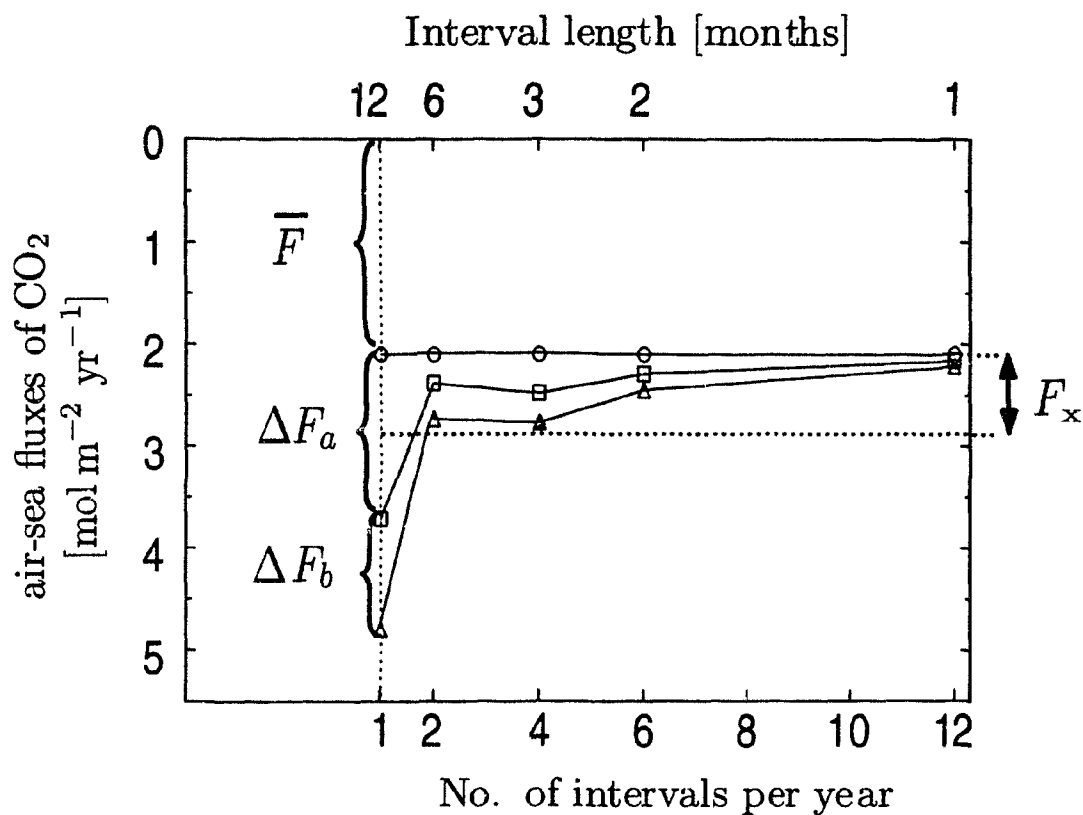


FIGURE 3-6. Effects of the fluctuations in the oceanic properties on the air-sea fluxes of CO₂ at various time scales. Symbols denote the annual sum of averages computed within intervals. For instance, at the annual scale (1 interval per year) the circle denotes \bar{F} , the square marks $F_a = \bar{K} \bar{\Delta p}$ and the triangle is $F_b = \bar{K} \Delta p(\bar{T}, \bar{S}, \dots)$ (for further explanations of this notation see Figure 3-4 and the text). At the semi-annual scale (2 intervals per year), the circle denotes the average of \bar{F} from both intervals, the square marks the average of F_a from both intervals, and so on. For comparison, the magnitude of total anthropogenic flux of CO₂ in the Labrador Sea (F_x), estimated independently from the 3-D model of *Maier-Reimer* [1991], is also shown.

partition (Figure 3-6). To achieve further reduction in these effects the annual cycle had to be partitioned into two-month and one-month periods (Figure 3-6).

Most of the reduction in the effects of the covariance and the nonlinearity was achieved by the initial partition of the annual data into warm and cold seasons. This finding is similar to the observation made in Chapter 2, where most of the reduction in the effect of the nonlinearity associated with spatial variability in seawater properties was attributed to partition of the global dataset into the high and low latitudes boxes. In general, the estimates of the air-sea fluxes of CO₂ were substantially improved, when observations from the warmer-water regime (originating from the warm season in the annual set, or from low latitudes in the global set) were separated from observations from the colder-water regime (from the cold season or from high latitudes, respectively).

Implications

These results may have implications for global carbon models which have limited temporal resolution, and for direct estimates of the air-sea fluxes of CO₂ from the measurements of oceanic properties averaged over time [*Takahashi et al.*, 1981a; *Tans et al.*, 1990; *Lefevre*, 1995; *Takahashi et al.*, 1995].

In carbon models, the systematic errors caused by neglecting the temporal covariance term and the temporal nonlinearity term can be reduced by using a shorter time step. Even using a half-year time step should reduce these errors substantially, both in diagnostic and in transient carbon models, even in the future, CO₂-rich, environments, as will be shown Chapter 5.

For the direct estimates of air-sea fluxes of CO₂ from observational data, the systematic errors could be minimized using two approaches. These approaches and their vulnerability to systematic and random errors are discussed in detail in the next section.

3.5.3 Strategies for reduction of the systematic and random errors associated with temporal fluctuations in the oceanic properties

Description of the strategies

To minimize the systematic errors associated with neglecting the covariance between K and Δp two basic strategies can be adopted:

Strategy A: Use paired observations of K and Δp to compute F , and then average the values of F to obtain the annual flux of CO_2 (\bar{F}):

$$\bar{F} \approx (\sum F_i) / \mathcal{I} = \sum (K_i \Delta p_i) / \mathcal{I}, \quad (3-24)$$

where i denotes an individual measurement of K and Δp , and \mathcal{I} is the number of individual samples used to compute the annual average. This strategy, in principle, would eliminate any systematic errors caused by the covariance (as well as by the nonlinearity).

However, this solution is often not feasible, since measurements of Δp are usually scant. Using only those measurements of K taken at the same time as Δp may lead to erroneous results if these values of K are not representative. Such cases are quite likely, given that K is a function of windspeed, which may vary rapidly.

Moreover, periods with strong winds may be underrepresented, since ship-borne observations becomes more difficult under such conditions. In other words, given a limited number of paired observations, the penalty for the elimination of this type of systematic error is the potential for a large random error.

In the future, the temporal coverage should be considerably improved with the use of buoys measuring continuously the partial pressure of CO_2 in seawater [Friederich, 1995]. However, such continuous coverage will be limited to the locations in which the buoys are deployed. For the areas without buoys, and for comparisons of CO_2 fluxes estimated from scant archive data, one could consider

an alternative strategy B that allows for a small systematic error in exchange for an improved utilization of the available data on K and Δp .

Strategy B: Estimate \bar{F} by partitioning the year into a small number of intervals and then use average values of K and Δp for each of these intervals:

$$\bar{F} \approx \left(\sum (\bar{K}_j, \overline{\Delta p}_j) \right) / \mathcal{J}, \quad (3-25)$$

where the subscript j denotes one of the intervals and \mathcal{J} is the number of intervals per year. The partitioning of the annual cycle reduces the systematic errors (although not necessarily to zero).

At the same time, this strategy allows incorporation of those observations of K which are not accompanied by corresponding measurements of Δp , thus reducing the random error.

Feasibility of the strategies

Feasibility of the two strategies depends on the number of available observations. To evaluate how many measurements are needed to reduce substantially the systematic and random errors associated with both strategies, I simulated taking a small number of measurements over a given period. For this purpose, I subsampled the calculated annual cycles of K and Δp and averaged the selected values to represent hypothetical estimates of:

- the annual mean of F (required if strategy A is used), and
- seasonal means of K and Δp (required if strategy B is used).

The experiments were then repeated, keeping the number of samples the same, but changing the time of sampling (see Figure 3-7). The whole procedure was then repeated for various numbers of measurements over the same period.

Finally, I plotted the hypothetical estimates of annual means of F , K and Δp against the number of observations of these variables per year (Fig. 3-7) or per

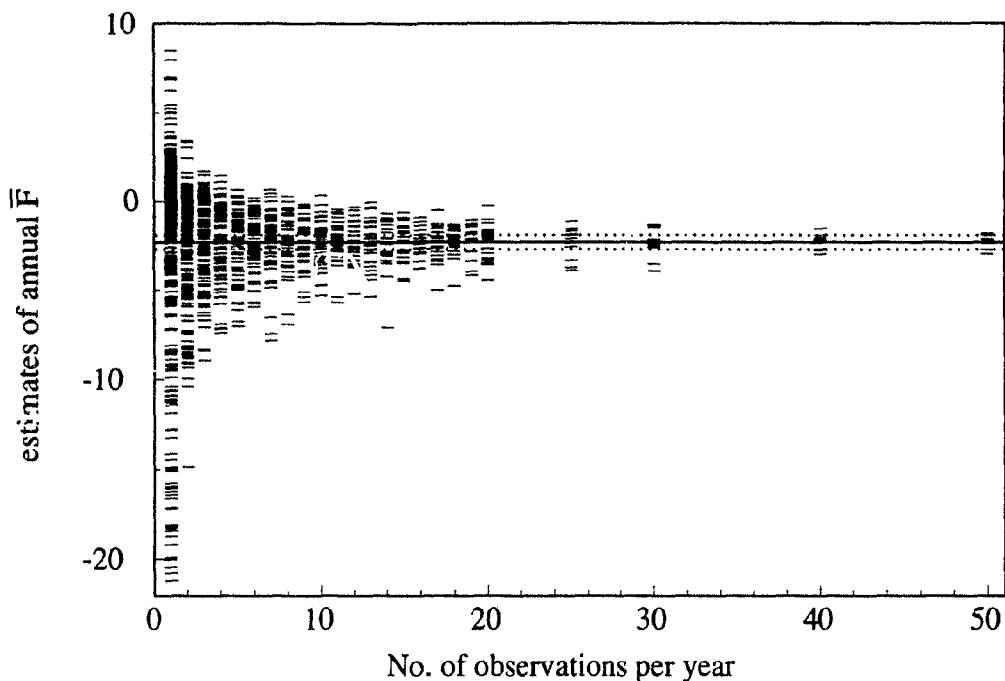


FIGURE 3-7. Distribution of the estimates of \bar{F} , the annual average fluxes of CO_2 [$\text{mol CO}_2 \text{ m}^{-2} \text{ yr}^{-1}$], as a function of the number of observations used to compute a given estimate. Each bar on the graph denotes a possible estimate of \bar{F} computed by averaging a given number of observations of $F (= K\Delta p)$. It is assumed that the observations are spread uniformly throughout the year. For instance, if two observations of F are available per season, they would be separated by $365/2 \approx 182$ days. There is one bar that represents the estimate of \bar{F} obtained by averaging F on 1 January (day 1) and F on 2 July (day 183=1+182), another that represents the estimate computed from F on 2 January and on 3 July, and so on to the bar representing the estimate from F on July 1 and on December 30. Solid line denotes the actual value of \bar{F} ; broken lines mark the estimates of \bar{F} differing from the actual value by $\pm 0.4 \text{ mol CO}_2 \text{ m}^{-2} \text{ yr}^{-1}$ (corresponding to 50% of the flux of anthropogenic CO_2 in the area).

season (Fig. 3-8). The scatter in these estimates indicates how many observations are needed to obtain reliable estimates of F , K and Δp .

Note that in these computations, realistic day-to-day fluctuations in windspeed were used (simulated as described in more detail in section 4.3.4 of Chapter 4).

Feasibility of Strategy A: First, I analysed the estimates of annual \bar{F} from individual values of F , computed from paired observations of K and Δp (Strategy A). With a single observation per year the distribution of estimates of \bar{F} simply mirrors the distribution of the daily values of the variable during the year: the standard deviation of these estimates around the true mean value is $5.7 \text{ mol CO}_2 \text{ m}^{-2} \text{ yr}^{-1}$.

With increasing number of observations the scatter in the estimates is reduced gradually (Figure 3-7): with two observations of F per year, the standard deviation was $3.1 \text{ mol CO}_2 \text{ m}^{-2} \text{ yr}^{-1}$ and with 15 observations the standard deviation was $1 \text{ mol CO}_2 \text{ m}^{-2} \text{ yr}^{-1}$. Reduction of the standard deviation to $0.4 \text{ mol CO}_2 \text{ m}^{-2} \text{ yr}^{-1}$ (which is about 50% of the anthropogenic flux of CO_2 in the Labrador Sea; see Chapter 5) would require at least 40 observations per year. In other words, to reduce the random error substantially, at least 40 concurrent measurements of K and Δp spaced throughout the year would be required if Strategy A were to be implemented.

Feasibility of Strategy B: Partitioning of the annual data into seasons was suggested as a way to reduce the systematic errors (Strategy B). Here I simulated the partition of a year into two seasons. The scatter in the estimates of the semi-annual means of the gas transfer coefficient (K) and the partial pressure of CO_2 in the surface layer (p_1) as a function of the number of measurements per 6-month season is shown in Figures 3-8 a to d.

Note that deviations in seasonal estimates of \bar{K} or p_1 from their true values may have a different effect on seasonal fluxes of CO_2 , depending on the season. For instance, a given deviation in the estimate of K in the warm season translates into 9

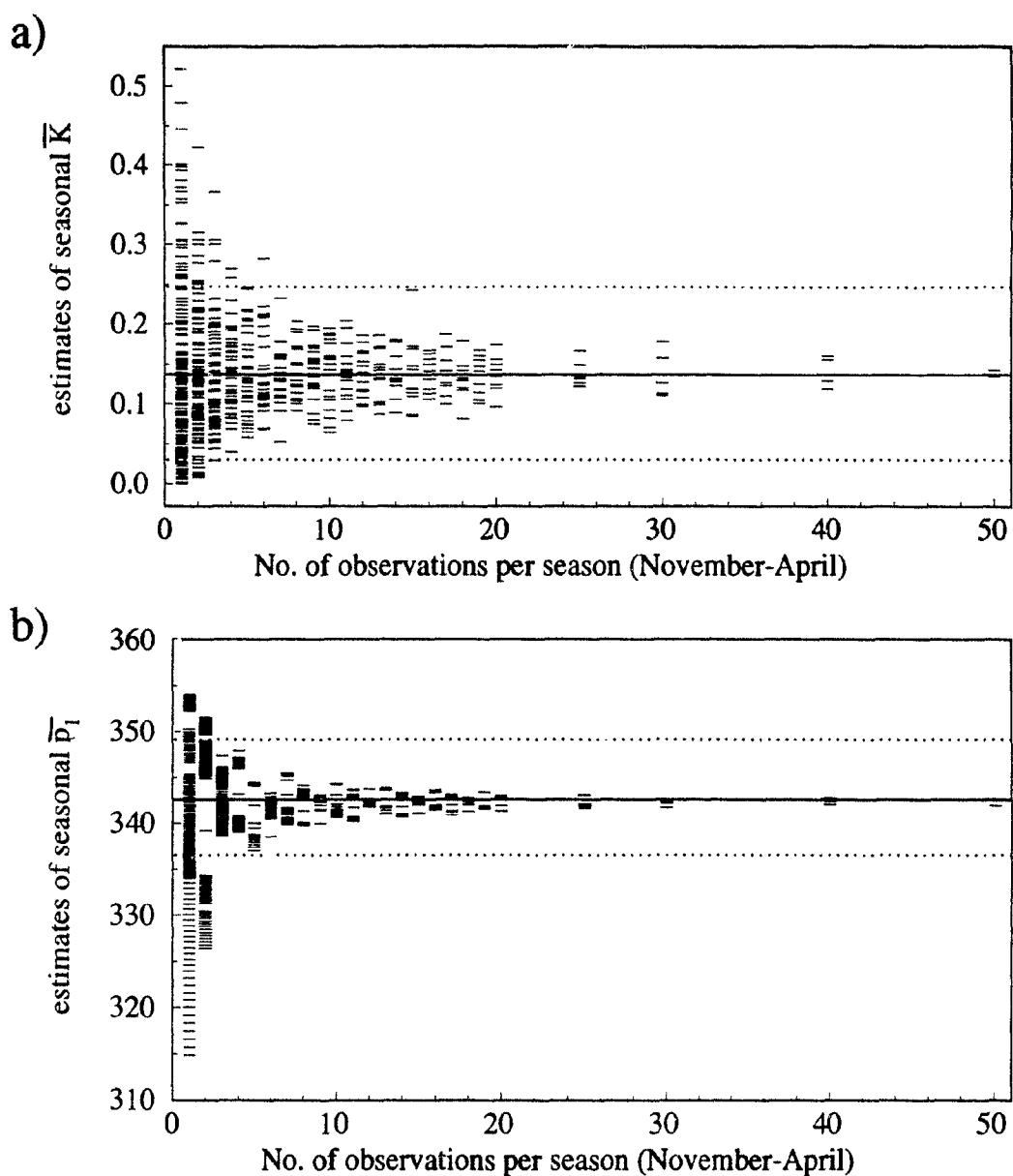


FIGURE 3-8. Distribution of the estimates of the seasonal means of K [$\text{mol CO}_2 \text{ m}^{-2} \text{ yr}^{-1} \mu\text{atm}^{-1}$] and p_1 [μatm], as a function of the number of observations used to compute a given estimate. The annual data were divided into two seasons: the warm season (May - October), and the cold season (November - April). Solid lines denote the true seasonal values. Broken lines mark the range of variability of a given variable which translates into an error of 0.8 mol C m^{-2} per season ($= 0.4 \text{ mol CO}_2 \text{ m}^{-2}$ per year, if this seasonal error is applied to the whole-year estimates of \bar{F}). For further details see Figure 3-7 and the text.

- (a) Estimates of the seasonal mean of K during the cold season.
- (b) Estimates of the seasonal mean of p_1 during the cold season.

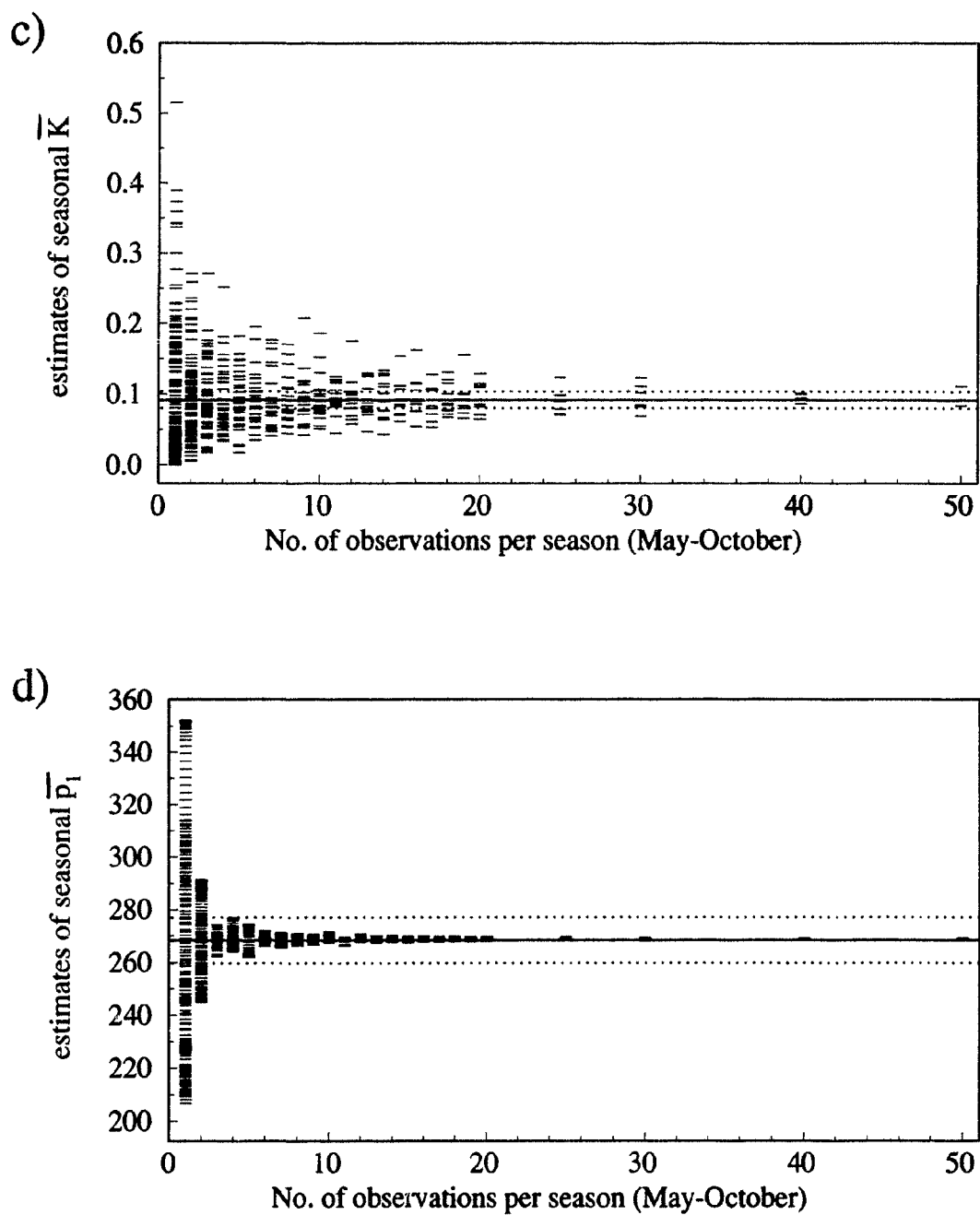


FIGURE 3-8 continued.

- (c) Estimates of the seasonal mean of K during the warm season.
(d) Estimates of the seasonal mean of p_1 during the warm season.

times larger deviation in the seasonal CO₂ fluxes in summer (when $\overline{\Delta p} = \overline{p_a} - \overline{p_1} = 67\mu\text{atm}$), than in the cold season (when $\overline{\Delta p} = -7\mu\text{atm}$). Therefore, to allow a comparison of the relative importance of the scatters in estimates of \overline{K} and $\overline{p_1}$, I have identified in Figures 3-8 the departures of a K of p_1 from their means that would translate into an error of $\pm 0.8 \text{ mol CO}_2 \text{ m}^{-2}$ per season ($= \pm 0.4 \text{ mol CO}_2 \text{ m}^{-2}$ per year, or 50% of annual uptake of anthropogenic CO₂ by the Labrador Sea, if this seasonal error is applied to the whole-year estimates of \overline{F}).

With increasing number of measurements, the scatter in the estimates of the seasonal values of Δp is reduced quickly. One needs 3-5 observations per season to remove most of the random error both in the cold and warm seasons (Figures 3-8b and 3-8d).

In contrast, the scatter in estimates of \overline{K} is reduced much more slowly. However, in the cold season (Figure 3-8a) most of this scatter does not translate into a scatter in the CO₂ fluxes, since $\overline{\Delta p}$ is low in the cold-season. Consequently, four observations of K per winter season were enough to remove most random errors associated with K . To achieve a similar effect in the warm season (Figure 3-8c), more than 40 observations were needed.

Comparison of the strategies

Both strategies for estimating the annual air-sea fluxes of CO₂ require at least 40-50 values of K per year. This should not pose a problem, since measurements of K can be computed from windspeeds, which are routinely measured at sea and could be obtained from satellites. On the other hand, Strategy B requires much fewer (6-8 per year) measurements of p_1 than Strategy A (about 40 per year). Therefore, for areas and periods without continuous measurements of p_1 , Strategy B is more practical than Strategy A, despite being subject to some bias caused by neglecting the covariance term at the seasonal scale.

3.6 Estimates of the CO₂ Fluxes by *Tans et al.* [1990]

I also subsampled the results of my model to test the representativeness of the data selection scheme used by *Tans et al.* [1990]. *Tans et al.* compiled archive data on the partial pressure of CO₂ and used them with the gas-transfer coefficient K , computed from climatological wind fields, to calculate the global air-sea fluxes of CO₂.

Tans et al. used only the data from the periods of January–April and July–October, which they assumed to be representative of the cold and the warm seasons, respectively. *Taylor et al.* [1991] argued that this data selection, omitting the May–June and the November–December periods, may result in a substantial underestimation of the annual CO₂ uptake by the North Atlantic. For instance, the uptake of atmospheric CO₂ at latitude 47°N computed by the model of *Taylor et al.* was underestimated by *Tans et al.* [1990] by 27%. This translates into an underestimation of the air-sea fluxes by 0.65 mol CO₂ m⁻² yr⁻¹ at this latitude.

To test whether a similar underestimation would hold for the Labrador Sea I divided the daily values of F , Δp and K from the Labrador Sea into two groups corresponding to the two seasons defined by *Tans et al.* [1990]. When average values of F for the two seasons were used, the estimated annual uptake of atmospheric CO₂ was 2.5 mol CO₂ m⁻² yr⁻¹. When the pooled and averaged values of Δp and K for the two seasons were used instead, the estimated uptake was 3.0 mol CO₂ m⁻² yr⁻¹. These results do not support the arguments of *Taylor et al.*, because both are *greater* than the uptake of 2.2 mol CO₂ m⁻² yr⁻¹ computed using all the data.

The underestimation described by *Taylor et al.* may well hold for the lower latitudes, where spring blooms occur early in the May–June period, and their effect on Δp does not last long (given that the concentration of nutrients in the surface layer after winter is lower than in the deeply-mixed waters of the Labrador Sea). In the Labrador Sea model, however, the bloom did not reach its maximum until the middle of June, and its strong effect on the dissolved inorganic carbon and the partial pressure was felt long into the July–October period. Therefore, the exclusion of the May–June period actually increased the estimated summer uptake of atmospheric CO₂ (Table 3-1).

3.7 Concluding Remarks

The one-dimensional, diagnostic model, developed here to simulate the cycles of oceanic variables affecting air-sea fluxes of CO_2 in the Labrador Sea reproduced the major features of the annual cycles of these variables. The results of the model were also consistent with observations in other localities with similar hydrological and biogeochemical regimes [Takahashi *et al.*, 1993].

Between the spring bloom of phytoplankton and the autumn mixing, changes in the surface-layer variables were dominated by biological activity. The partial pressure of CO_2 exhibited a strong annual cycle, with values falling by $160 \mu\text{atm}$ during the spring bloom. The annual cycle of partial pressure followed that of the dissolved inorganic carbon, since changes in other physico-chemical properties (temperature, salinity, alkalinity) were relatively small. The air-sea fluxes of CO_2 followed the cycle of the oceanic partial pressure, although changes in values of the gas-transfer coefficient played an important role in March–April and August–September.

The annual air-sea flux of CO_2 , \bar{F} , was $2.2 \text{ mol CO}_2 \text{ m}^{-2} \text{ yr}^{-1}$. If there were no covariance between K and Δp , the calculated flux would be considerably larger ($F_a = 3.7 \text{ mol CO}_2$). The flux computed neglecting both the covariance and the nonlinearity of the carbonate system would be even greater ($F_b = 4.6 \text{ mol CO}_2 \text{ m}^{-2} \text{ yr}^{-1}$). These results indicate that fluctuations in K and in the seawater properties determining the oceanic partial pressure of CO_2 may substantially affect air-sea fluxes of CO_2 . The magnitude of the covariance term was about twice the magnitude of the present anthropogenic flux of CO_2 in the Labrador Sea; the carbonate nonlinearity term had a similar magnitude to that of the anthropogenic flux.

During the cold season, both the covariance between K and Δp , and the nonlinearity of the carbonate system had negligible effects on the air-sea fluxes. In the warm season these effects were stronger, since the variability in the oceanic properties over this period was larger than in the cold season. Overall, when a year was split into two seasons, the effects of covariance between K and Δp , and of the nonlinearity of the carbonate system, on the estimates of the annual air-sea CO_2 fluxes were substantially reduced.

Partitioning the data into four seasons did not reduce the errors further. To achieve such a reduction, a partition of the year into 2- or 1-month periods would be necessary.

When observed properties of the surface ocean are used to estimate air-sea fluxes of CO_2 , the errors caused by neglecting the covariance between Δp and K can, in principle, be eliminated, by averaging individual values of F , computed from paired observations of K and Δp .

When the measurements of Δp are scarce this approach is not feasible. In such cases, the available data on K and Δp should be divided into at least two seasons. If the observations of oceanic properties were spread uniformly throughout the year, at least three measurements of Δp per season are required to increase the precision of the estimates of these averages. A large number (more than 40) of measurements of K is required during the warm season and about 4 measurements of K in the cold season.

The simulated annual cycles of oceanic variables were also used to test one of the explanations of the intensely debated results of *Tans et al.* [1990], who used synoptic data on oceanic properties to compute the oceanic uptake of anthropogenic CO_2 . The uptake computed from these data was much smaller than the values obtained from global carbon models and this discrepancy prompted *Tans et al.* to question the validity of present carbon models in which the ocean is an important sink of anthropogenic CO_2 .

In one of the attempts to reconcile this discrepancy, *Taylor et al.* [1991] suggested that the data selection scheme used by *Tans et al.* could cause underestimation of the CO_2 uptake by the North Atlantic. To test this hypothesis, the annual cycles of oceanic variables, computed by the Labrador Sea model, were subsampled to simulate the data selection scheme of *Tans et al.* The results do not support the hypothesis of *Taylor et al.* If anything, the data-selection scheme used by *Tans et al.* is likely to lead to a slight overestimation of the uptake of atmospheric CO_2 in the Labrador Sea and other high-latitudes waters. If air-sea fluxes of CO_2 were indeed overestimated, then it would appear that the calculations of the "missing" sink of anthropogenic carbon by *Tans et al.* [1990] are on the conservative side.

It is difficult to speculate on the reasons why the *Tans et al.* estimate of air-sea flux is much lower than that predicted by global carbon models. However, the results presented in this chapter suggest that the data-averaging strategy adopted by *Tans et al.* [1990] was an appropriate one in the sense that it would have accounted for the most of the effects of the covariance between K and Δp .

Chapter 4.

Sensitivity of Air-Sea Fluxes of CO₂ in the Labrador Sea to Changes in Oceanic Processes

4.1 Introduction

In this chapter I investigate the sensitivity of air-sea fluxes of CO₂ in the Labrador Sea to changes in physical and biogeochemical processes at present levels of atmospheric CO₂. The CO₂-rich environments of the future are explored in Chapter 5. I consider both the average annual flux, and the components of the annual flux associated with the covariance between K and Δp (the covariance term, defined in Chapter 3, equation 3-21) and with the nonlinearity of the carbonate system (the covariance term, see equation 3-23). It is hoped that the results may contribute to our understanding of the role of the oceans as a sink or source of CO₂. The study also yields some suggestions for strategies to adopt when analysing sparse observations related to CO₂ fluxes. Some guidelines for construction of carbon models also emerge from the study.

The importance of a given oceanic process for air-sea fluxes of CO₂ may be evaluated by studying the sensitivity of these fluxes to changes in the process. Various processes may then be ranked according their relative importance for air-sea fluxes of CO₂.

A shift in the balance between various oceanic processes may potentially alter air-sea fluxes of CO₂, and, consequently, affect the transfer of carbon between the atmosphere and the deep ocean. Such shifts may be of particular importance in

high-latitude waters. In these waters phytoplankton productivity is higher, the water exchange with the deep ocean stronger, and the gas-transfer between the surface waters and the atmosphere higher, than in low-latitude waters. Therefore, changes in the physical and biogeochemical processes in these waters could translate into large changes in air-sea fluxes of CO₂. For instance, it has been suggested that changes in the water circulation and biological production in high-latitude waters were responsible for the differences in atmospheric concentrations of CO₂, and in the air-sea CO₂ fluxes, between the glacial and interglacial periods [e.g., *Knox and McElroy*, 1984; *Sarmiento and Toggweiler*, 1984; *Siegenthaler and Wenk*, 1984].

Such changes in biogeochemical processes may occur at various time scales. To date, most of the research effort has focused on long-term changes (time scales from several hundreds to thousands of years). Such time scales allow for full adjustment in the composition of the deep ocean in response to the change. To this category belong the glacial/interglacial changes mentioned above.

The effects of potential changes in the physical and biological processes on the air-sea fluxes at the medium time scale (decades to a few centuries) and at the short time scale (one to several years) have received less attention. The medium-term changes may be of interest when the uptake of anthropogenic carbon is considered. To date, almost all transient-carbon models simulating this uptake have assumed that biological and physical processes in the ocean continue to function at their pre-industrial rates (but see evaluations of the iron-fertilization scheme by *Broecker and Peng* [1991] and *Joos et al.* [1991]). Nor have the effects of short-term variations in biological and physical processes on air-sea fluxes of CO₂ been discussed much (but see, for instance, the discussion of anomalous CO₂ fluxes observed during the El-Niño events by *Gaudry et al.* [1987]). That such short-term variations are common can be inferred from inter-annual differences in the timing of phytoplankton blooms in the CZCS satellite data or from large inter-annual variations in the amount of carbon exported into the deep ocean [e.g., *Boyd and Newton*, 1995].

The sensitivity analysis presented here primarily concentrates on the short-term effects of variations in the physical and biogeochemical processes on air-sea fluxes of CO₂. However, I will examine whether the conclusions on the relative importance of various processes to the CO₂ fluxes, drawn from the sensitivity analysis of short-term variations in oceanic processes, would be valid, to some extent, at longer time scales.

This sensitivity analysis also provides information on the stability of the present fluxes of CO₂ in the Labrador Sea. A high sensitivity of the CO₂ fluxes in this area to fluctuations in oceanic processes would suggest that the fluxes in this area could vary markedly from year to year.

Some knowledge of the possible range of inter-annual variability in air-sea fluxes of CO₂ may help the interpretation of the observational data on these fluxes. Such knowledge provides an insight into the representativeness of the CO₂ fluxes measured in any one year in an area, and, indirectly, into the reliability of the estimates of the annual air-sea fluxes of CO₂ based on the observational data that are available today. If fluxes of CO₂ in a given area are subject to high inter-annual variability caution should be exercised in using observations from one year as representative of the "typical" conditions in the area.

Understanding the sensitivity of air-sea fluxes of CO₂ to various oceanic processes may also help to distinguish between the natural inter-annual variability in these fluxes and potential long-term trends, which may be associated, for instance, with global climate change.

Sensitivity studies also have implications for the construction of carbon models. By their very nature, models can represent only a few physical and biogeochemical processes. Identification of the processes to which air-sea fluxes of CO₂ are most sensitive may be useful in determining which processes should be represented in future models.

4.2 Approach

This study was carried out using the one-dimensional model of the Labrador Sea introduced in Chapter 3. Sensitivity of the CO₂ fluxes was assessed through an analysis of differences between the air-sea fluxes of CO₂ in the standard model run (presented in Chapter 3) and those obtained by changing parameters describing various processes, one at a time. In some cases, potential effects of simultaneous alterations of more than one parameter were also examined.

The differences between the standard and the sensitivity runs provide information on the role of physical and biogeochemical processes in the real ocean. These insights could be used to design carbon models. For instance, if the change in computed fluxes resulting from an alteration of a given process in the Labrador Sea model is small, one may conclude from the model that potential changes in that process are not very important for the air-sea fluxes of CO₂ in this area, and the representation of this process in future carbon models may be omitted, or, at least, simplified.

The results presented in this chapter were obtained assuming an atmospheric concentration of CO₂ valid for late 1970s (335 μ atm). The CO₂ fluxes in future environments with much higher concentrations of atmospheric CO₂ are discussed in Chapter 5.

Most of the computations in this chapter are carried out for the first year after the alteration of a parameter (or an input variable). The computed difference between the altered and standard cases describes the short-term sensitivity of air-sea fluxes to a change in the parameter value (and in the process that given parameter represents). In reality, one expects that the effects of the alterations will evolve with passing time. For instance, if a higher phytoplankton productivity increased the air-sea fluxes of CO₂, there would be an initial increase in the drawdown CO₂ from the atmosphere into the ocean. However, the additional CO₂ drawn from

the atmosphere would enter the marine carbon cycle and eventually raise the seawater partial pressure of CO_2 , and gradually decrease the CO_2 fluxes until a new steady-state is achieved. Therefore, to test how the first-year response of the CO_2 fluxes would be modified if more time is allowed for adjustment, and consequently, to examine the extent to which the short-term sensitivity results may be extended to medium time scales, I followed the evolution of the CO_2 fluxes caused by hypothetical alterations in photosynthesis parameters over a 50-year period (section 4.4). Finally, some concluding remarks are presented.

4.3 Sensitivity of air-sea fluxes of CO_2 to changes in oceanic processes

In this section, the short-term sensitivity of the CO_2 fluxes to changes in oceanic processes is evaluated as follows. The model is first run in the “standard mode”, as in Chapter 3. After an inter-annual steady state is attained (that is, the annual cycles of the seawater properties are stabilized), one of the modelled oceanic processes is altered (by changing either an input variable or a parameter). The CO_2 fluxes are monitored for a simulated year following the alteration, and compared with the pre-alteration values.

With time the departure of the CO_2 fluxes from the pre-alteration values may be modified (as discussed in more detail in section 4.4). At this point, it suffices to say that the new steady state is usually approached slowly, given the large inventory of inorganic carbon in the water column that has to be adjusted. Therefore, although the results presented in this section best describe the sensitivity of air-sea fluxes to changes on the time scale of one year, the general conclusions on the importance of various processes, and on the direction of the resultant changes in air-sea fluxes of CO_2 should be valid, to some extent, at medium time scales also.

In evaluating the effects of modifications in physical and biological processes, I considered both the annual mean flux (\bar{F}), and the flux components associated with

the covariance between K and Δp (the covariance term, ΔF_a) and with nonlinearity of the carbonate system (the nonlinearity term, ΔF_b).

4.3.1 Physical processes

Sensitivity of air-sea CO₂ fluxes to changes in physical processes was evaluated by altering the depth and timing of winter convection, the annual cycle of the surface layer depth, and atmospheric forcing. The main results are summarized in Table 4-1 and discussed in detail here.

Winter deep convection: The depth of deep winter convection may vary from year to year. There are periods when no deep-water convection is observed in the Labrador Sea. In other periods the depth of the convection may reach in excess of 1000 m [Lazier, 1980; Ikeda, 1987]. To represent these extreme cases, H_c , the penetration depth of surface waters into the deep layer during the winter convection, was varied between 0 and 1000 m (Figure 4-1a).

First, the case with no deep winter convection ($H_c = 0$ m) was simulated (although the shallow convection between the top two layers was still allowed). The annual uptake of atmospheric CO₂ increased by $1.0 \text{ mol m}^{-2} \text{ yr}^{-1}$ relative to the standard uptake. Next, the depth of the convection was set at the maximum value ($H_c = 1000$ m). In years with such deep convection the uptake was smaller than the standard value, but only by $0.2 \text{ mol m}^{-2} \text{ yr}^{-1}$.

Note the asymmetry in the response to changes in H_c : the CO₂ fluxes were more sensitive to the reduction than to the increase in the depth of winter convection. The reduction in H_c substantially curtailed the contact of the surface layer with the carbon-rich deep layer, whereas the increase in H_c did not have a strong effect, because, at the standard value of $H_c = 400$ m, winter surface waters were already strongly influenced by the deep layer through convection, and a further increase in H_c had only a small effect on the carbon chemistry of the surface waters (Figure 4-1a).

TABLE 4-1. Sensitivity of the air-sea CO₂ fluxes to changes in the model parameters or inputs.

The departures of the CO₂ fluxes from the standard values \bar{F} , ΔF_a and ΔF_b , associated with averaging over the annual scale, during the first year after the change, are given in mol CO₂ m⁻² yr⁻¹. “-” denotes the departures smaller than ± 0.2 mol CO₂ m⁻² yr⁻¹; “s(...)” denotes standard deviation of a given property.

Parameter	Standard value	Alternative values	$\bar{F}=+2.2$	Departures from: $\Delta F_a=1.5$	$\Delta F_b=-0.9$	Comments
1. Physical processes						
Winter convection:						
- H_c [m]:	400	0/1000	+1.0/ 0.2	- / -	- / --	Fig. 4-1a
- timing:	28 Feb	2 Feb./31 Mar.	/ -	- / -	-- / ---	Fig. 4-1a
The surface layer:						
- summer thickness:	30 m	15 m/50 m	0.5/ 0.3	+0.3/+0.4	+0.2/+0.4	Fig. 4-1b
- spring shallowing:	May	Apr./Jun.	+0.5/ 0.4	-- / --	- / -	Fig. 4-1c
- autumn deepening:	Sep.	Aug./Oct.	0.4/+0.2	/ -	-- / --	Fig. 4-1c
Atmospheric forcing:						
Windspeed w :						
- without affecting H_c		$-s(w)/+s(w)$	-0.5/+0.3	+0.2/-0.2	-- / --	
- altered H_c		$-s(w)^0/+s(w)^{1000}$	+0.4/ --	+0.3/-0.3	+0.3/-0.2	
Air temperature T_a :						
- without affecting H_c		$-s(T_a)/+s(T_a)$	/ -	/	-- / --	
- altered H_c		$-s(T_a)^{1000}/+s(T_a)^0$	/+0.7	-- / -	-- / --	

⁰ and ¹⁰⁰⁰ denote simultaneous changes in the winter convection depth H_c to 0 m and 1000 m, respectively.

TABLE 4-1 -continued.

Parameter	Standard value	Alternative values	$\bar{F}=+2.2$	Departures from: $\Delta F_a=-1.5$ $\Delta F_b=-0.9$		Comments
Cloud cover cl :	0.82-0.90	$-s(cl)/+s(cl)$	- / -	- / -	- / -	
Humidity h_m :	0.5-0.8	-0.1/+0.1	+0.4/-0.3	- / -	- / -	
Precipitation		+50%/-50%	+0.2/-0.2	- / -	- / -	
2. Chemical composition						
Deep waters [mmol m ⁻³):						
C_3	2192	$-s(C_3)/+s(C_3)$	+0.4/-0.4	- / -	- / -	$s(C_3)=4$
A_3	2354	$-s(A_3)/+s(A_3)$	-0.3/+0.3	- / -	- / -	$s(A_3)=4$
N_3	16.8	$-s(N_3)/+s(N_3)$	- / -	- / -	- / -	$s(N_3)=0.5$
Biogenic matter:						
C:N	6.625-10	-25%/+25%	-0.5/+0.5	+0.2/-0.2	+0.3/-0.3	
C:chl	50-75	-25%/+25%	+0.3/-0.2	- / -	- / -	
C:N and C:chl		25%/+25%	-0.2/+0.2	-0.2/+0.2	-0.3/+0.3	
CaCO ₃ :C _{org} production:						
- throughout a year	0.02	0.25/0.25 ^a	2.0/- 2.7	+0.4/+0.9	+0.5/+0.7	Fig. 4-2
- in the post-bloom phase:	0.02	0.25/0.25 ^a	-0.6/ -0.6	- / -	- / -	Fig. 4-2
	0.02	1/1 ^a	-1.8/ -1.2	- / -	- / -	Fig. 4-2

^a denotes simulations using an increased attenuation coefficient (see text).

TABLE 4-1 -continued.

Parameter	Standard value	Alternative values	$\bar{F}=+2.2$	Departures from: $\Delta F_a=-1.5$	$\Delta F_b=-0.9$	Comments
3. Biological processes						
<i>Phytoplankton</i>						
Photosynthesis parameters		-50%/+50%	1.9/+1.1	+0.9/-0.2	+0.5/ -	Fig. 4-3, Tab. 4-2
Respiration:						
- R_d	0.08	-50%/+50%	+0.2/-0.2	-/-	-/-	
- R_L	1-2	-50%/+50%	+0.2/ 0.2	-/-	-/-	
- R_o [d^{-1}]:						
- in both layers	0.003	-50%/+50%	+0.9/ 0.5	-/ -	-/-	
- in layer 1 only	0.003	-50%/+50%	+0.4/-0.3	-/-	-/-	Fig. 4-4
- in layer 2 only	0.003	-50%/+50%	+0.4/ 0.2	-/	-/-	Fig. 4-4
Excretion \mathcal{E}	0.05	-100%/+100%	- / -	-/ -	-/-	
Sinking velocities [$m d^{-1}$]:						
- v_1 (layer 1)	0.5-3	0 / 0 ^{nz}	- / -0.3	- /	-/-	^{nz} no zoo-
	0.5-3	3	--	--	--	plankton
- v_2 (layer 2)	2	0/4	0.5/+0.2	/ -	-/-	
<i>Zooplankton</i>						
Λ [($mmol C m^{-3}$) $^{-1}$]	0.006	0.902/0.2	--/ --	- / 0.2	--/-0.2	Fig. 4-5
g_m [d^{-1}]	0.5	-25%/+25%	-/+0.2	/ 0.2	-/-0.2	Fig. 4-5
a	0.8	-25%/+25%	-/ 0.3	-/ 0.4	-/ 0.4	Fig. 4-3
m [d^{-1}]	0.03-0.3	-15%/+15%	-/+0.2	-/	-/-	
B_o [$mmol C m^{-3}$]	0.7	0		--	--	

TABLE 4-1 -continued.

Parameter	Standard value	Alternative values	$\bar{F}=+2.2$	Departures from: $\Delta F_a=-1.5$	$\Delta F_b=-0.9$	Comments
4. Other sensitivities						
No zooplankton			--/--	--/--	--/--	
Phytoplankton composition:						
- diatoms only			--	--	--	
- flagellates only			-0.5	+0.2	--	
Daily fluctuations in atmospheric forcing:						
- clouds			--	--	--	
- wind			--	+0.4	--	Fig. 4-6
Light attenuation:						
- \mathcal{K}^{chl} [(mg chl) ⁻¹ m ²]	0.023	-50%/+50%	+0.9/-0.4	- /+0.2	--/--	
Atmospheric CO ₂ :						
- mean p_a [μ atm]	335	+2	+0.2	--	--	
- seasonally variable p_a				--	--	
Oceanic CO ₂ :						
- dissociation constants of <i>Goyet and Poisson</i> [1987]			1.0	-	--	

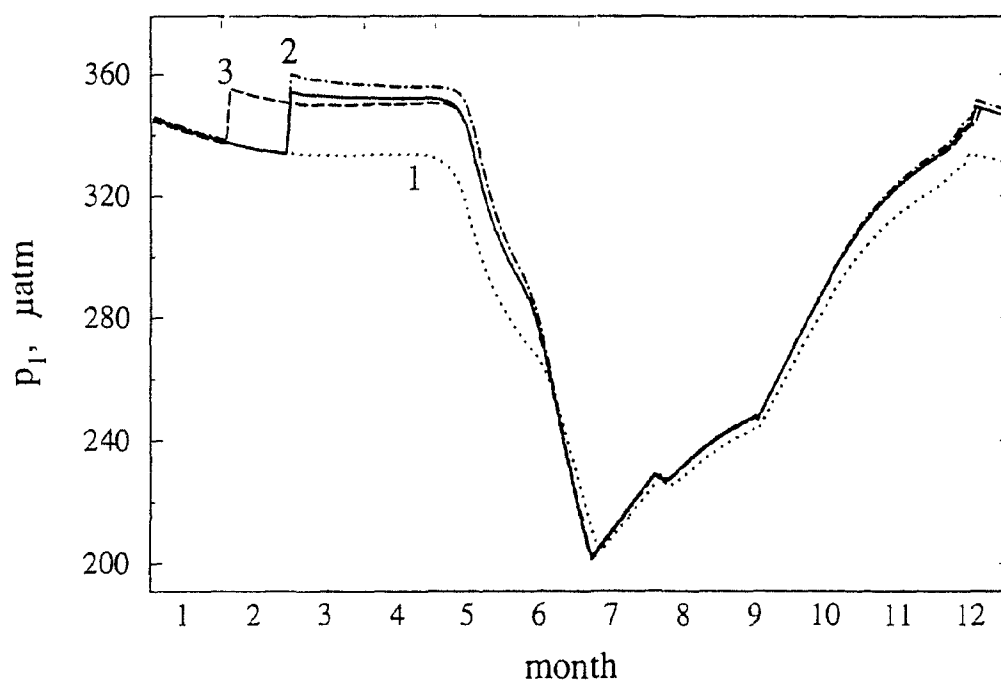


FIGURE 4-1. Effects of alterations in physical parameters of the model on the partial pressure of CO_2 in the surface layer:

- (a) Effects of the changes in the depth or timing of the deep winter convection. Solid line denotes the standard case, in which the convection takes place at the end of February and penetrates 400 m ($=H_c$) into the deep layer. Broken lines denote the simulations assuming: 1) no deep convection; 2) increase in H_c to 1000 m; 3) convection at the end of January.

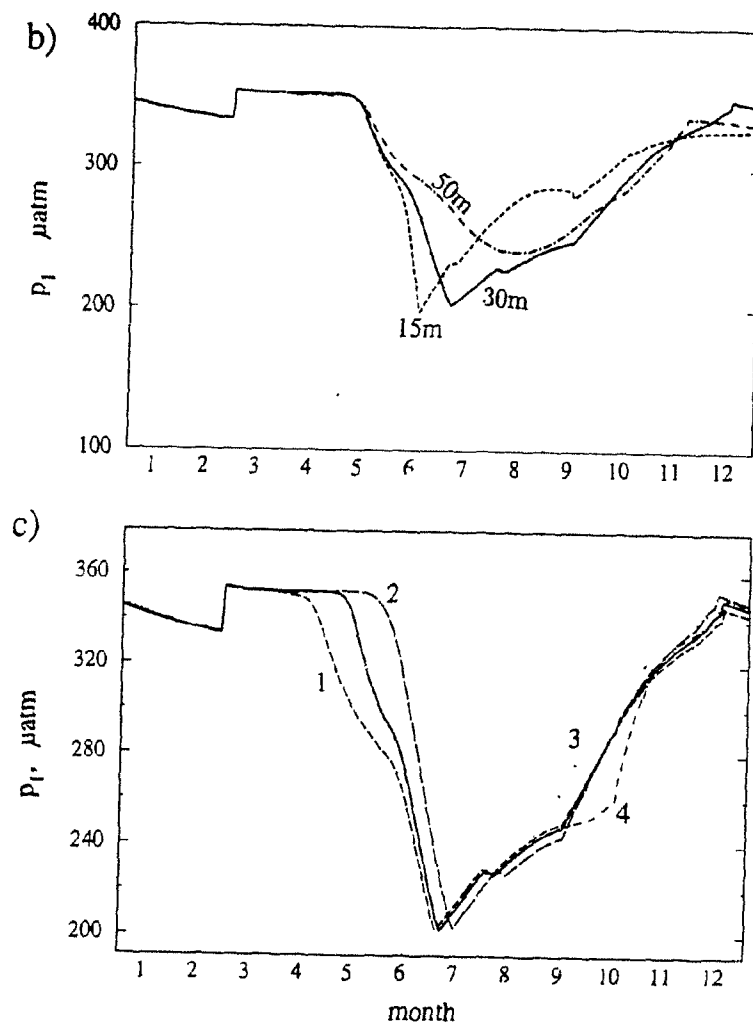


FIGURE 4-1 continued.

- (b) Effects of the changes in the depth of the surface layer thickness H_1 in summer. In the standard case (solid line), the summer values of H_1 were 30 m.
- (c) Effects of the changes in the duration of the summer stratification of the water column on the partial pressure of CO₂. Solid line denotes the standard case. Broken lines denote simulations assuming: the spring shallowing earlier (1) or later (2) by one month; the fall deepening earlier (3) or later (4) by one month.

Air-sea fluxes were insensitive to changes in the timing of the winter deep convection tested within a plausible range (one month earlier or later than the standard case). As long as the winter convection occurred, its exact timing was not very important: occurrence of the deep convection affects air-sea fluxes throughout the year, whereas the effect of a change in timing of the convection was mainly limited to a period of one month (the offset between the days in consecutive years when convection was assumed to take place) (Figure 4-1a).

Evolution of the surface layer: Changes in the annual evolution of the surface layer may moderately affect air-sea fluxes of CO_2 (Figure 4-1b). Either increasing or decreasing the summer surface layer depth from the standard value of 30 m lowered the mean flux \bar{F} by 0.3–0.5 mol $\text{CO}_2 \text{ m}^{-2} \text{ yr}^{-1}$. A shallower surface layer limited the amount of atmospheric CO_2 that could be absorbed by this layer during summer. On the other hand, a deeper surface layer slowed the development of the spring bloom, delaying the drawdown of atmospheric CO_2 . The flux components ΔF_a and ΔF_b were lower than in the standard case, because the variabilities in seawater properties during the year, on which the magnitudes of ΔF_a and ΔF_b depend, were reduced (Figure 4-1b).

Other modifications in the evolution of the surface layer considered here included changes in the timing of the spring shallowing and the autumn deepening of the surface layer (Figure 4-1c). A delay in the spring shallowing or an advance in the autumn deepening by one month would lower \bar{F} by 0.4–0.5 mol $\text{CO}_2 \text{ m}^{-2} \text{ yr}^{-1}$. An earlier spring shallowing and, to a lesser degree, a delayed autumn deepening, would have the opposite effect.

Atmospheric forcing:

The consequences of altering the atmospheric forcing were assessed next. In the standard run, the model was forced with climatological monthly means. To simulate plausible inter-annual variability in windspeed, air-temperature and cloudiness, I computed the monthly means of these properties for each year from 1950 to 1972,

and calculated the standard deviations of these means from the corresponding climatological monthly means (the climatological means being the averages of the individual monthly means for 1950-1972). The inter-annual variability was then simulated by forcing the model with monthly values which were allowed to deviate from the climatological monthly means by one standard deviation. Consequences of the day-to-day fluctuations in windspeed and cloudiness to air-sea fluxes of CO₂ are discussed later (section 4.3.4).

Windspeed: Changes in windspeed affect vertical mixing, water temperature and the gas-transfer coefficient of CO₂ (K). A substantial inter-annual variability in monthly mean winds can be observed in the data (standard deviations 4-5 m s⁻¹). An increase in windspeed by one standard deviation increased K by about 25%. This raises the air-sea fluxes of CO₂ (\bar{F}), as well the magnitude of the covariance and the carbonate-nonlinearity terms (ΔF_a and ΔF_b). Conversely, weaker winds lowered \bar{F} , ΔF_a and ΔF_b .

However, the changed winds are also likely to alter the winter convection depth [Ikeda, 1987]. As discussed before, possible increases in the winter convection depth would have little effect on \bar{F} . On the other hand, if weak winds prevented winter convection, the effect on the CO₂ fluxes would be strong (given the sensitivity of the CO₂ fluxes to reductions in the convection depth). As a result, the effect of lower K would be more than compensated by a weaker mixing of the surface layer with the carbon-rich deep layer. Thus, if the convection depth is affected, both an increase or a decrease in windspeeds may increase the uptake of atmospheric CO₂.

Air temperature: The air temperature T_a affects the surface water temperature and vertical mixing. Within the range of observed inter-annual variability in monthly values of T_a (standard deviations 0.6 – 1.6 °C), alterations in air temperature alone did not change the CO₂ fluxes strongly. However, an altered T_a may affect the depth of the winter convection via temperature and salinity changes in the surface layer [Ikeda, 1987]. Again, this effect would be substantial only if this depth

decreases, which might be expected when T_a is higher. In other words, changes in T_a affect the uptake of atmospheric CO_2 only if they reduce the winter convection depth.

Cloudiness: Changes in cloudiness modify the amount of solar energy entering the water column, potentially affecting the surface-water temperature, vertical water mixing and photosynthesis. However, the variability in the monthly cloud cover between different years was small (standard deviation of 0.02 - 0.06) and within this range the effect of variability in cloudiness on air-sea fluxes of CO_2 was negligible.

Other atmospheric variables: Two other atmospheric variables, precipitation and humidity, were directly prescribed from monthly values given by *Ikeda* [1987]. Changing the air humidity by 0.10 had a moderate effect ($0.4 \text{ mol m}^{-2} \text{ yr}^{-1}$) on air-sea CO_2 fluxes. Changes in precipitation by $\pm 50\%$ had a negligible effect on carbon fluxes.

4.3.2 Chemical composition of deep waters and biogenic material

Results of analyses on the sensitivity of air-sea fluxes of CO_2 to changes in the chemical composition of the deep waters and biogenic matter, discussed in this section, are summarized in Table 4-1.

Chemical composition of the deep waters

The sensitivity of the CO_2 fluxes to variations in the deep-ocean concentrations of dissolved inorganic carbon (C), alkalinity (A), and nutrients (N) were tested first, by changing these values by their corresponding standard deviations computed from the data. The standard deviations of these properties for the winter data set given by *Anderson et al.* [1985] did not differ much from those computed here from the TTO data from the central Labrador Sea, and were approximately 4 mmol m^{-3} , 4 meq m^{-3} , and 0.5 mmol m^{-3} for C , A and N , respectively. The model was run

using the deep-water concentrations C_3 , A_3 , or N_3 , increased or decreased by the respective standard deviation. When the deep ocean properties were changed one at a time, the CO_2 fluxes were moderately sensitive to changes in C_3 and A_3 ($\pm 0.4 \text{ mol CO}_2 \text{ m}^{-2} \text{ yr}^{-1}$), but not to changes in N_3 . When more than one of the deep ocean properties were changed at the same time, the air-sea fluxes of CO_2 were most strongly affected when a decrease in C_3 coincided with an increase in A_3 or vice versa (\bar{F} was then changed by $\pm 0.7 \text{ mol CO}_2 \text{ m}^{-2} \text{ yr}^{-1}$). On the other hand, when variations in C_3 and A_3 were positively correlated, the effects of these variations on the CO_2 fluxes tended to cancel each other. However, neither of these possibilities seems very likely, as in the TTO data from depth 230-1430 m, the variations in C and A were only weakly correlated (coefficient of correlation $r=+0.14$).

Chemical composition of biogenic matter

In the next step, the importance of the chemical composition of the biogenic matter was examined. The sensitivity of the CO_2 fluxes to changes in the relative concentrations of organic carbon, nitrogen and chlorophyll in the soft tissue, as well as to CaCO_3 formation, was evaluated.

Composition of the soft tissue: In the standard case, it was assumed (see Appendix C) that the C:N (carbon-to-nitrogen) molecular ratio in the organic matter corresponded to the typical Redfield value of 6.625 ($= 106/16$) when phytoplankton growth was not limited by biologically-usable nitrogen (i.e., nitrogen in form of nitrate, nitrite or ammonia), but increased to about 10 during the nitrogen-limited, post-bloom phase.

An increase in the C:N ratio by 25% throughout the year could increase moderately the mean flux of CO_2 (by $0.5 \text{ mol CO}_2 \text{ m}^{-2} \text{ yr}^{-1}$), as well as the flux components ΔF_a and ΔF_b . A decrease by the same amount would have opposite consequences. As might be expected, changes in the C:N ratio were particularly important shortly after the depletion of nutrients. Before the depletion, the phytoplankton uptake of inorganic carbon from the surface waters was not limited by

the availability of nitrogen (in the form of nitrate, nitrite or ammonium). whereas later, in the post-bloom phase, the pool of nitrogen available in the surface layer was depleted by the sinking of the spring phytoplankton. Therefore, any changes in the C:N ratio had only a small effect on the uptake of carbon by phytoplankton.

Changes in θ , the carbon-to-chlorophyll ratio, were seen to affect the CO_2 fluxes only to a small degree (from -0.2 to $+0.3 \text{ mol m}^{-2} \text{ yr}^{-1}$). Lower chlorophyll levels (i.e., higher θ) slowed the rate of increase in carbon biomass, as long as the growth was not being limited by the availability of nutrients.

Usually, the effects of variability in the C:N ratio would be partially compensated by those in the variability in θ , since these ratios are likely to covary. When light limits the growth, the C:N ratio and θ are low. When nutrients limit the growth, the C:N ratio and θ are high. As a result, at a given light level, the N:chl ratio is usually more stable than the C:N or the C:chl ratios [Cullen *et al.*, 1993]. Because of the covariance between the C:N ratio and θ , the CO_2 fluxes would be less sensitive to changes in the chemical composition of phytoplankton than the case when just one of these ratios is altered.

CaCO₃ formation: In the standard version of the model, it was assumed that Γ , the ratio of the production of CaCO_3 to gross primary production, is very low in the Labrador Sea ($\Gamma = 0.02$).

This assumption is consistent with the results of the analysis of the TTO data from the Labrador Sea, which showed a strong negative correlation between alkalinity A and nitrate concentration N ($r = -0.83$), a positive correlation between N and concentration of dissolved inorganic carbon C ($r = +0.56$) and a weak negative correlation between A and C ($r = -0.07$). Should the formation of organic carbon be accompanied by the formation of CaCO_3 in substantial quantities, one would expect that these correlations would have opposite signs, since the formation of CaCO_3 changes A and C in the proportion 2: 1, whereas the formation of

soft-tissue matter affects A and C in the proportion $+0.2:-1$ (Appendix C). Therefore, in the simulated standard case, it was assumed that much more carbon was incorporated into the soft-tissue matter than into CaCO_3 .

However, the TTO data represent only one year (and may be unrepresentative of other years). Besides, large blooms of coccolithophores have been observed in the waters surrounding the Labrador Sea [Trotte, 1985; Aiken and Bellan, 1990; Balch *et al.*, 1991; Holligan and Balch, 1991; Holligan, 1992; Brown and Yoder, 1994]. Therefore, it seems worthwhile to examine the consequences of a potential increase in CaCO_3 formation in the Labrador Sea.

Both the timing and the magnitude of the CaCO_3 production are important. For instance, if the production of CaCO_3 relative to organic carbon is increased to 0.25 throughout the year, it would increase the partial pressure of CO_2 (Figure 4-2) and decrease \bar{F} from 2.2 to 0.1 mol $\text{CO}_2 \text{ m}^{-2} \text{ yr}^{-1}$, removing most of the potential of the Labrador Sea to act as a sink for atmospheric CO_2 . The same value of Γ (0.25), when applied only to the portion of a year after the diatom bloom, would cause a much smaller decrease in annual fluxes of CO_2 (from 2.2 to 1.6 mol $\text{CO}_2 \text{ m}^{-2} \text{ yr}^{-1}$). The latter case seems more likely, since coccolithophore blooms typically develop in environments after the depletion of nutrients limits diatom growth [Brown and Yoder, 1994]).

If the magnitude of CaCO_3 production in the post-diatom phase are larger, the mean fluxes of CO_2 would be lowered by 1.6 mol $\text{CO}_2 \text{ m}^{-2} \text{ yr}^{-1}$ for $\Gamma = 1$ (this value of Γ is consistent with observations of Holligan and Balch [1991]), and by 2.0 mol $\text{CO}_2 \text{ m}^{-2} \text{ yr}^{-1}$ for $\Gamma = 2$ (the production ratio that can be computed from the results of Balch *et al.* [1991]).

The above estimates were arrived at assuming that photosynthesis is unaffected by the presence of CaCO_3 . However, carbonate shells and single coccoliths suspended in water may increase the attenuation of seawater and reduce the solar radiation penetrating the surface layer [Balch *et al.*, 1991]. This, in turn, could lower primary production in that part of the year when the growth is light-limited.

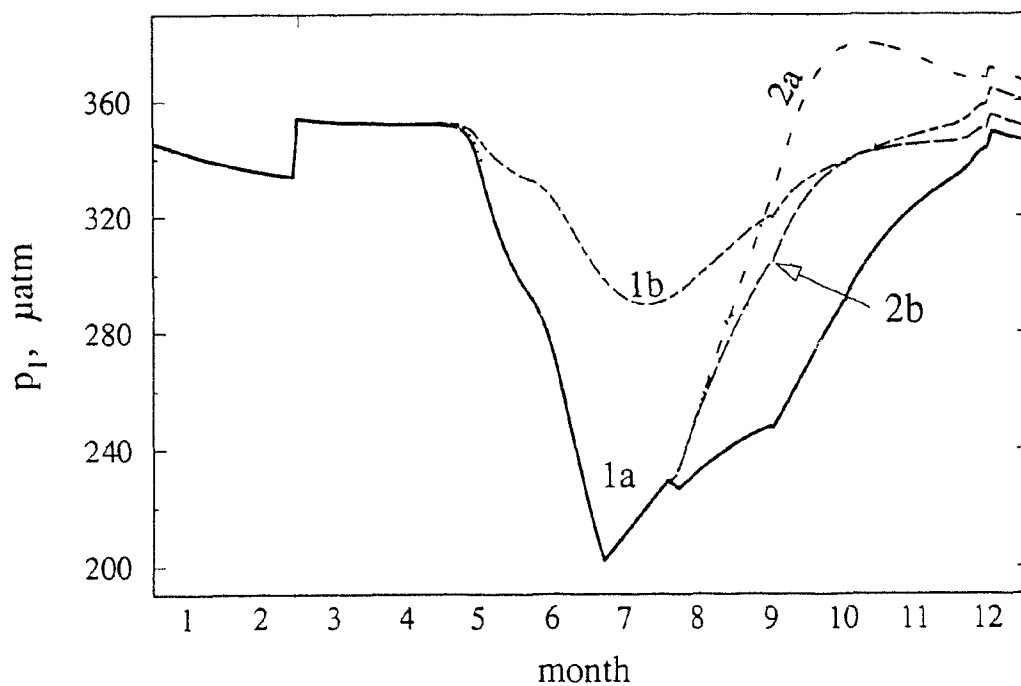


FIGURE 4-2. Effects of hypothetical increases in the ratio of the production of CaCO_3 to the gross primary production, Γ . Solid line denotes the standard case, in which $\Gamma = 0.02$. Broken lines denote the simulations using (1) $\Gamma = 0.25$ throughout the year, and (2) $\Gamma = 1.0$ during the post-bloom phase and $\Gamma = 0.02$ in the remaining portion of the year. Subscripts denote simulations without (a) and with (b) an increase in light attenuation (see text).

To quantify this effect, the light attenuation of seawater was increased to account for the light backscattered by CaCO_3 . I used the calcite-specific backscatter coefficient of $0.006 \text{ (mmol CaCO}_3\text{)}^{-1} \text{ m}^{-2}$ based on *Ackleson et al.* [1994]. Note that using such a coefficient requires knowledge of the standing stock of CaCO_3 . The present model computes only the production rate of CaCO_3 , but not the removal rate of CaCO_3 by grazing and sinking. Since the removal of CaCO_3 is likely to be less efficient than the removal of organic carbon respired by phytoplankton and assimilated by zooplankton, the residence time of CaCO_3 in the surface layer was assumed to be up to four times longer than that of organic carbon.

Increased light attenuation in the presence of CaCO_3 could have various effects on the CO_2 fluxes depending on Γ . At $\Gamma = 0.25$ throughout the year, accounting for increased light attenuation decreased the air-sea fluxes of CO_2 , because it slowed the development of the spring bloom (Figure 4-2). At $\Gamma = 1$ in the post-bloom phase, the effect was opposite: increased light attenuation effectively increased the uptake of CO_2 . Although primary production fell as a result of increased attenuation, so did the CaCO_3 formation, and the latter effect had a greater impact on the CO_2 fluxes.

The effect of CaCO_3 formation on the covariance term (ΔF_a) and the non-linearity term (ΔF_b) varied, depending on its temporal distribution. When the increase in CaCO_3 formation was spread throughout the year, values of ΔF_a and ΔF_b fell, because the annual variability in p_1 was smaller (in particular, the spring depression in p_1 was weaker; see Figure 4-2). On the other hand, when the CaCO_3 production was confined to the postbloom phase, ΔF_a and ΔF_b increased slightly, because the intra-annual variability in p_1 increased.

In summary, the CO_2 fluxes were moderately sensitive to changes in the composition of the deep ocean, within the range of variability of C , A and N seen in the data. The fluxes could be sensitive to the C:N ratio of organic matter, but this sensitivity is likely to be weakened by corresponding changes in the carbon-to-chlorophyll ratio. Although there are no indications of strong CaCO_3 production

in the open Labrador Sea in the available data on the water composition, should calcareous organisms become more abundant, the uptake of CO_2 from the atmosphere by this area could be seriously curtailed. Increased attenuation of light by the particulate CaCO_3 may provide a negative feedback to this effect by limiting further production of CaCO_3 . The strength of this feedback would depend on the efficiency of the mechanisms removing CaCO_3 from the surface waters.

4.3.3 Biological processes

Biological processes in the Labrador Sea affect the air-sea fluxes of CO_2 mainly by two routes. The first route is through a direct control of the composition of the surface layer as inorganic carbon is removed and incorporated into particulate matter. Biological processes control the timing of both this removal and its (partial) reversal when some of the organic carbon is remineralized. The second route is indirect, through modifications of the composition of the intermediate waters, which, when mixed or entrained into the surface layer, may affect the composition of the surface waters. Such modifications depend on biological processes, which control how much of the organic carbon, produced locally or imported from the surface layer, is remineralized within the intermediate layer.

I make the distinction between these two routes to indicate modelling implications: the first route is accounted for in all carbon models containing a biological component, but the second route is neglected in those carbon models that do not include an intermediate layer.

The consequences of changes in the phytoplankton gross growth rate on the water composition and on air-sea fluxes of CO_2 are described in detail below. Then, the sensitivity of the CO_2 fluxes to some other biological processes is briefly discussed.

Phytoplankton gross growth rate

Sensitivity of air-sea fluxes of CO_2 to the gross growth rate of phytoplankton was evaluated by alterations in the photosynthesis parameters: the chlorophyll-normalized, initial slope of the photosynthesis-light curve (α^{chl}) and the assimilation number (P_m^{chl}). These parameters were increased or decreased systematically by 50%, which is slightly greater than one standard deviation of the photosynthesis parameters from their seasonal means. The results are shown in Table 4-2.

The increase in α^{chl} and P_m^{chl} allowed stronger phytoplankton growth in poor light conditions, which accelerated the spring bloom (by two weeks) and slowed the autumn decline in biomass (Figure 4-3a). A close analysis of the effects of these changes in the photosynthesis parameters may illustrate the two routes by which the biological processes affect air-sea fluxes of CO_2 .

The direct route: An earlier spring bloom caused an earlier depression in the surface layer concentration of inorganic carbon (C_1) (Figure 4-3b), and an additional uptake of atmospheric CO_2 from April to early July (Figure 4-3c). When all the surface nutrients were used up, the potential for removal of inorganic carbon reached its limit, and there was not much difference in the CO_2 fluxes from the standard case throughout most of summer. In mid-September, however, under rapidly worsening light conditions, higher values of the photosynthesis parameters allowed higher phytoplankton production. The phytoplankton biomass initially increased and then declined more slowly than in the standard case. This delayed remineralization of organic carbon in the surface layer and allowed some additional uptake of atmospheric CO_2 .

The indirect route: After the onset of autumn mixing, the indirect route by which the photosynthesis parameters may affect air-sea fluxes of CO_2 also became apparent. At the beginning of autumn mixing the concentration of dissolved inorganic carbon in layer 2 (C_2) was lower than in the standard case (Figure 4-3b). The difference can be traced to the spring bloom. The increase in the photosynthesis

TABLE 4-2a. Departures of the annual air-sea CO₂ fluxes \bar{F} and of the day of the onset of nutrient limitation (in parentheses) from the values in the standard run (+2.2 mol CO₂ m⁻² yr⁻¹ and day 187, respectively) as a result of changes in the photosynthesis parameters.

	$P_m^{chl} \times 0.5$	$P_m^{chl} \times 1$	$P_m^{chl} \times 1.5$
$\alpha^{chl} \times 1.5$	-0.2 (+3)	+0.5 (-6)	+1.1 (-14)
$\alpha^{chl} \times 1$	-0.6 (+26)	0 (0)	+0.5 (-7)
$\alpha^{chl} \times 0.5$	-1.9 (*)	-0.7 (+23)	-0.4 (+10)

(*) — nutrients were not exhausted

TABLE 4-2b. Departures of the components of air-sea CO₂ fluxes associated with the covariance between K and Δp (the first number in the pair) and with nonlinearity of the carbonate system (the second number) from their standard values (-1.5 and -0.9 mol CO₂ m⁻² yr⁻¹, respectively) as a result of changes in the photosynthesis parameters.

	$P_m^{chl} \times 0.5$	$P_m^{chl} \times 1$	$P_m^{chl} \times 1.5$
$\alpha^{chl} \times 1.5$	+0.1/0	0 / 0	-0.2/0
$\alpha^{chl} \times 1$	+0.4/+0.1	0 / 0	-0.1/0
$\alpha^{chl} \times 0.5$	+0.9/+0.5	+0.3/+0.1	-0.2/-0.1

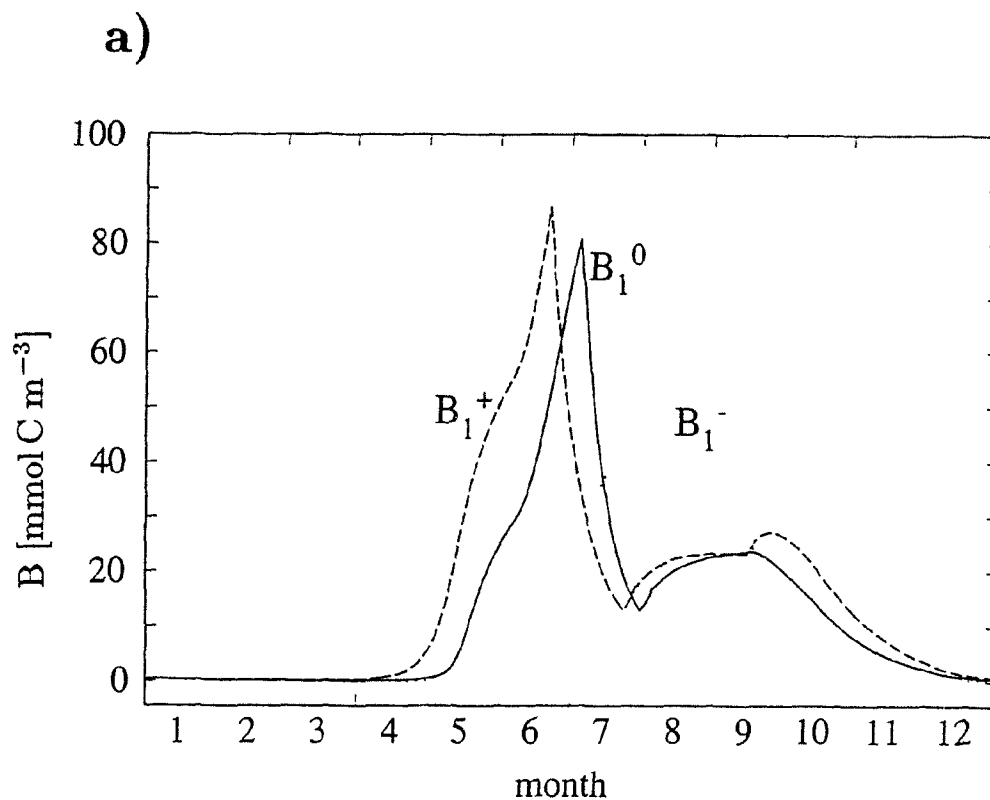


FIGURE 4-3. Effects of modifications in the photosynthesis parameters (α^{chl} and P_m^{chl}) on the seawater properties affecting the air-sea fluxes of CO_2 . Superscript 0 denotes the results obtained using the standard values of the photosynthesis parameters (solid lines); superscripts $^+$ and $^-$ denote the results obtained by increasing (dashed lines) and decreasing (dotted lines) the parameters by 50%, respectively.

(a) Phytoplankton concentration in the surface layer (B_1), in mmol C m^{-3} .

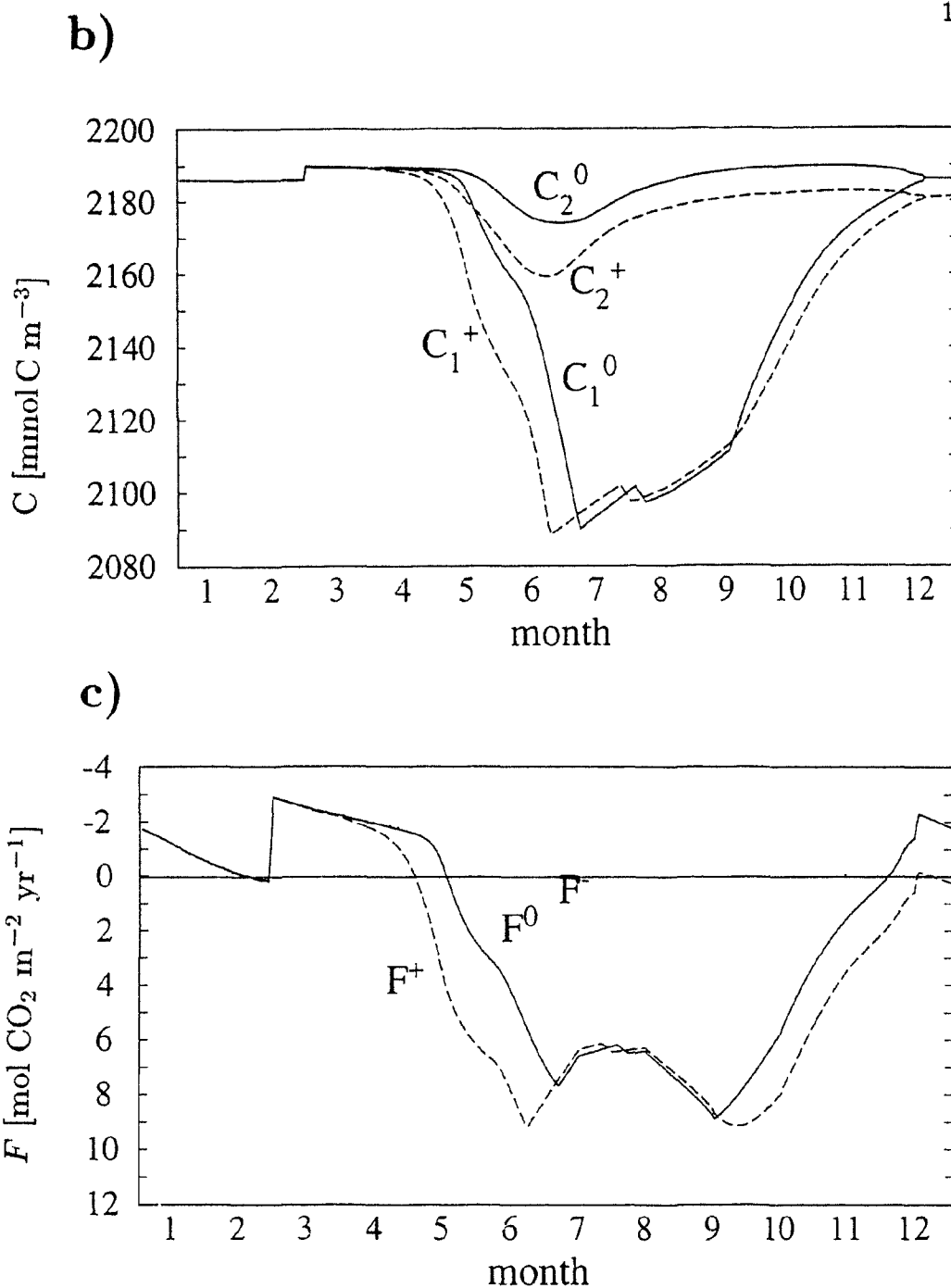


FIGURE 4-3 continued.

- (b) Dissolved inorganic carbon concentration in the surface layer (C_1) and in the intermediate layer (C_2), both in mmol C m^{-3} (results of the reduction in the photosynthetic parameters were omitted from the graph for clarity).
- (c) Air-sea fluxes of CO_2 , in $\text{mol CO}_2 \text{ m}^{-2} \text{ yr}^{-1}$. Positive values of F correspond to the net uptake of CO_2 by the ocean.

parameters allowed phytoplankton production to begin when the surface layer was still deep. As the shallowing of the surface layer progressed, some of the water, with lowered concentration of inorganic carbon, was left behind and was incorporated into the intermediate layer. This lowered C_2 compared with the standard case. In autumn, when mixing and entrainment brought the intermediate waters into the surface layer, the resulting increase in C_1 was lower than in the standard case (Figure 4-3b). Therefore, the increase in the uptake of CO_2 in autumn (Figure 4-3c) was associated not only with the direct route (slower decay of organic matter in the surface layer), but also with the indirect one (lower supply of inorganic carbon from the intermediate layer).

In total, an increase in α^{chl} and P_m^{chl} by 50%, led to an increase in the annual mean flux \bar{F} by $1.2 \text{ mol CO}_2 \text{ m}^{-2} \text{ yr}^{-1}$. On the other hand, a 50% drop in the values of the photosynthesis parameters lowered the annual uptake of atmospheric CO_2 by $1.9 \text{ mol CO}_2 \text{ m}^{-2} \text{ yr}^{-1}$. The decrease in the photosynthesis parameters slowed the growth of the phytoplankton (Figure 4-3a), and caused a delayed, weaker depression in C_1 (Figure 4-3b) (because not all the nutrients in the surface waters were utilized).

These values, $+1.2$ and $-1.9 \text{ mol CO}_2 \text{ m}^{-2} \text{ yr}^{-1}$, resulting from changes in the photosynthesis parameters within a realistic range (about one standard deviation from the seasonal means), may be compared with the magnitude of the uptake of anthropogenic CO_2 by the Labrador Sea, which is likely to be about $0.8 \text{ mol CO}_2 \text{ m}^{-2} \text{ yr}^{-1}$ (see Chapter 5). Therefore, the fluctuations in air-sea fluxes of CO_2 in response to changes in the photosynthesis parameters at the annual time scale, may be indeed significant in the context of climate change. Effects of similar variations over longer time scales are discussed in section 4.4.

Other combinations of changes in the photosynthesis parameters produced smaller departures from the standard values of CO_2 fluxes. The CO_2 fluxes were most sensitive to proportional changes in α^{chl} and P_m^{chl} , that is, when the photoadaptation parameter $I_k (= P_m^{chl}/\alpha^{chl})$ was unchanged.

Changes in the photosynthesis parameters in most cases did not affect strongly the terms associated with the covariance (ΔF_a) or the carbonate nonlinearity (ΔF_b) (Table 4-2b). The only exception was the case of low α^{chl} and P_m^{chl} , where the incomplete utilization of nutrients caused a lower depression in the concentration of dissolved inorganic carbon, which in turn reduced ΔF_a and ΔF_b .

Other biological parameters may affect the CO₂ fluxes in a similar manner: either directly, by affecting conversions between inorganic carbon and organic matter in the surface layer, or indirectly, by affecting the inorganic carbon concentration in the intermediate layer. Sensitivity of the CO₂ fluxes to some of these parameters is discussed briefly below.

Phytoplankton losses

Respiration and excretion: Sensitivity of the CO₂ fluxes to production-dependent and production-independent components of phytoplankton respiration was evaluated by altering the parameters describing these components by $\pm 50\%$. Such a range seems reasonable given that the respiration parameters vary substantially, depending on species and environmental conditions [Langdon, 1992].

Within the 50% range, the CO₂ fluxes were not very sensitive to changes in the parameters describing the production-dependent respiration, either to the dark respiration coefficient, R_d , or its enhancement in light, R_L (Table 4-1). The CO₂ fluxes were also not sensitive to large changes in the production-dependent excretion rate \mathcal{E} .

On the other hand, changes in the production-independent component of respiration, R_o , may alter the CO₂ fluxes. The value of this parameter becomes important when primary production is low, which occurs in spring and autumn in layer 1 and throughout the year in layer 2. Changes in R_o in either of the layers modified air-sea fluxes of CO₂ by similar amounts ($0.4 - 0.5 \text{ mol CO}_2 \text{ m}^{-2} \text{ yr}^{-1}$), although the mechanisms of these modifications were different:

- **In layer 1**, lower values of R_o accelerated the phytoplankton bloom in spring and slowed the phytoplankton decline in autumn. This increased the CO_2 uptake by the Labrador Sea in two ways: *directly*, by extending the period of the uptake of atmospheric CO_2 by the surface layer, and *indirectly*, by affecting the composition of the intermediate layer (an earlier spring phytoplankton bloom in waters destined to be incorporated into layer 2 during the subsequent shallowing of the surface layer) (Figure 4-4).
- **In layer 2**, lower values of R_o increased the uptake of CO_2 indirectly: lower respiration in layer 2 decreased the degree to which organic carbon, exported from layer 1 by sinking or detrainment, was remineralized in this layer, and, therefore, lowered the amount of inorganic carbon reaching the surface layer after the onset of autumn mixing (Table 4-1).

Increasing R_o decreased the CO_2 fluxes, although the magnitude of change was smaller than for a comparable decrease in R_o (Figure 4-4).

Sinking: The CO_2 fluxes were not very sensitive to small changes in sinking velocities. A decrease in all sinking velocities by 0.5 m d^{-1} changed the CO_2 fluxes by less than $-0.3 \text{ mol CO}_2 \text{ m}^{-2} \text{ yr}^{-1}$. A comparable increase in the sinking velocities had an even smaller impact (Table 4-1). When changes in sinking velocities were larger, the CO_2 fluxes seemed to be affected mainly by the sinking velocity in layer 2 (v_2). Changes in the sinking velocity in layer 1 (v_1) within a realistic range of $0\text{-}3 \text{ m d}^{-1}$, had negligible effects on the CO_2 fluxes. For instance, when v_1 was reduced to zero, the annual CO_2 fluxes were hardly affected. In this case, lack of sinking of organic carbon from the surface layer was compensated by an increased export of organic carbon by zooplankton which, given high concentrations of food, could attain much higher biomass than in the standard case.

A similar mechanism cannot be invoked for the intermediate layer, where there is much less food than in layer 1 to support a large zooplankton biomass. Consequently, if sinking of organic material from layer 2 was substantially reduced, more

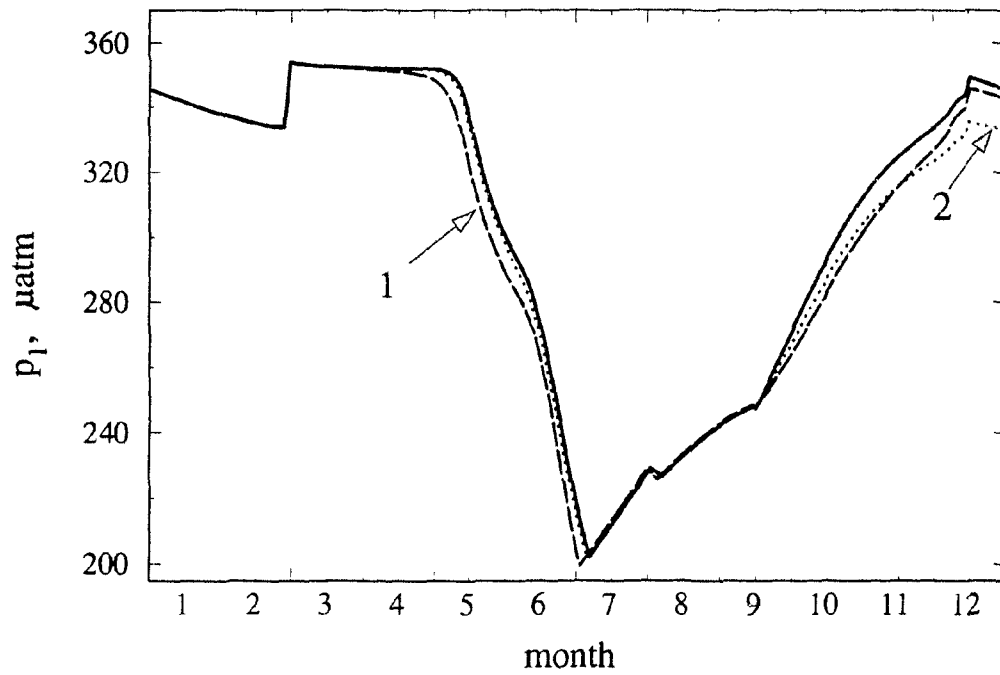


FIGURE 4-4. Effects of changes in the production-independent component of respiration, R_o , on the partial pressure of CO_2 . Solid line denotes the standard case in which $R_o = 0.003 \text{ d}^{-1}$. Broken lines denote the simulations in which R_o was increased by 50% in surface layer (1) or in the intermediate layer (2).

organic carbon would be remineralized in this layer and more CO₂ would degas after the onset of autumn mixing.

On the other hand, an increase in the sinking velocity v_2 had a weaker effect on the CO₂ fluxes than a decrease in v_2 . For instance, the reference value of v_2 would have to increase 400% to produce an effect similar in magnitude (but opposite in sign) to that of reducing v_2 by 50%.

Zooplankton: The effect of zooplankton on the CO₂ fluxes was evaluated by altering zooplankton parameters within a large range, corresponding to the large potential variability in the zooplankton community. In the standard case, the zooplankton concentrations (which were consistent with the observations of *Longhurst and Williams* [1993]) had only a weak effect on the CO₂ fluxes. When the model was run without zooplankton, the CO₂ fluxes were hardly affected (Table 4-1). In general, changes in zooplankton parameters that did not lead to an increase in zooplankton biomass by at least one order of magnitude from the standard values had negligible effects on the CO₂ fluxes.

However, a large range of the zooplankton biomass is possible, given uncertainties in estimates of zooplankton parameters [*Parsons et al.*, 1984], as well as the large variability in zooplankton biomass reported in the Labrador Sea (some samples from NORTHWESTATLANT cruises (ICNAF Report, 1968) and BIO 1994-1995 cruises (Les Harris, unpublished data) contain such high concentrations of zooplankton).

Therefore, I tested the effect of zooplankton on CO₂ fluxes when its biomass was allowed to increase by one order of magnitude compared with the values computed in the standard case. Figure 4-5 shows several ways in which such large increases in zooplankton biomass may be achieved:

- by increasing the Ivlev parameter Λ ,
- by increasing the assimilation efficiency a , or
- by increasing the maximum grazing ration g_m (lowering the zooplankton specific loss rate m had a similar effect as increasing g_m).

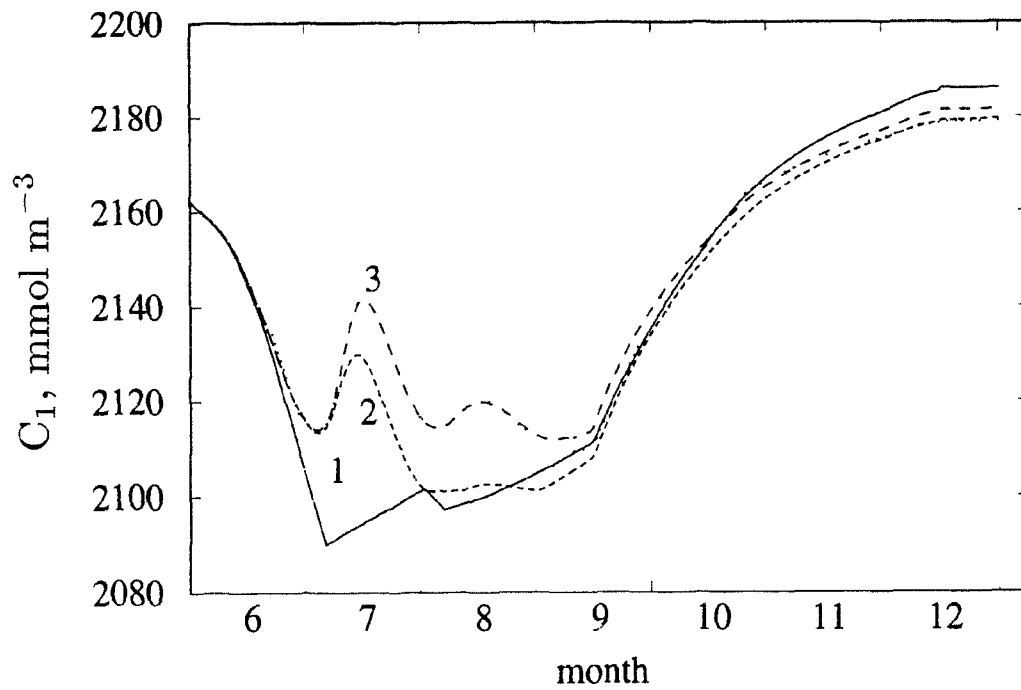


FIGURE 4-5. Effects of changes in the zooplankton parameters on the dissolved inorganic concentration in the surface layer. Solid line denotes the standard case. Broken lines denote simulations with altered parameters: 1) Λ : $0.006 \rightarrow 0.2$ (mmol C m^{-3}) $^{-1}$; 2) g_m : $0.5 \rightarrow 0.6$ d^{-1} ; 3) a : $0.8 \rightarrow 1$.

In the first case, the annual flux of atmospheric CO₂ (\bar{F}) was almost unchanged, in the second case \bar{F} decreased, whereas in the third case \bar{F} increased. These different responses reflect different impacts of the alterations on the compositions of layers 1 and 2.

In layer 1, more zooplankton respired more organic matter, thus remineralizing more carbon and reducing the uptake of atmospheric CO₂ during summer. In layer 2, on the other hand, less organic carbon was respired, since some organic carbon was either remineralized before entering layer 2, or exported into the deep ocean (by rapidly-sinking fecal pellets, or by downward migration of zooplankton). As a result, the inorganic carbon concentration in layer 2 was lower than in the standard case, which, in turn, increased the uptake of atmospheric CO₂ after autumn mixing brought intermediate waters to the surface. The net effect of changes in a given zooplankton parameter depended therefore on the balance between the summer increase and the autumn decrease in air-sea fluxes of CO₂.

The flux components associated with the covariance between K and Δp (ΔF_a) and with the nonlinearity of the carbonate system (ΔF_b) were substantially reduced in all three cases, as more intensive grazing lowered the annual variability in the oceanic properties (e.g., a smaller depression in p_1 in summer).

In conclusion, the CO₂ fluxes were sensitive to changes in some phytoplankton loss terms. The fluxes were affected by changes in the production-independent (maintenance) respiration R_o in both layers and in sinking velocity in layer 2. An increase of zooplankton biomass may signal a change of the CO₂ fluxes, but the direction and magnitude of the change depend on the mechanism by which the increase in zooplankton biomass was achieved.

4.3.4 Other considerations

Sensitivity of the results to some other parameters and input values, as well as to the modelling approach adopted, was also evaluated.

Zooplankton component: In the standard version, the model would function quite well even if the zooplankton component were omitted. However, the zooplankton component would be necessary if new observational data indicated presence of much higher zooplankton concentrations in the area than was assumed here. Furthermore, retaining the zooplankton component in the model may be important in cases where the model parameters constraining the phytoplankton growth or export of organic matter from the surface layer are modified. For instance, the presence of zooplankton mitigates potential changes in the CO₂ fluxes resulting from lowering the velocity with which phytoplankton sinks from the surface layer (as discussed in more detail in section 4.3.3).

Phytoplankton succession:

Representation of the succession of phytoplankton communities from the diatom-dominated to the flagellate-dominated phase (e.g., by increasing the carbon-to-chlorophyll and C:N ratios, lowering the sinking rate and modifying the phytoplankton respiration rates) was not critical to the estimates of the CO₂ fluxes. If the phytoplankton community were dominated by diatoms throughout the year, the CO₂ fluxes would not be modified much from the standard case. The simulated shift to the flagellate-dominated community occurred after most the particulate carbon and nitrogen pools had already been removed from the surface waters. If the phytoplankton composition shifted earlier during the annual cycle, before the sinking of the spring-bloom phytoplankton into deeper waters, the consequences for the CO₂ fluxes could be larger. However, such a possibility seems unrealistic, since it is the same condition (onset of nutrient depletion) that is likely to trigger both the sinking of phytoplankton and the shifting of composition.

Atmospheric partial pressure of CO₂: One of the prescribed inputs was the atmospheric partial pressure of CO₂ (p_a), fixed at 335 μ atm.

In reality, the atmospheric partial pressure of CO_2 varies between seasons. *Wong et al.* [1984] found, between 1974 and 1981, that the peak-to-trough differences in p_a measured at Sable Island and Alert (that is, at sites to the south and to the north of the Labrador Sea) were $\pm 11\text{-}18 \mu\text{atm}$. To test whether neglecting such seasonal variability affects the model estimates of air-sea fluxes of CO_2 , I computed monthly departures in p_a from annual means for different years at these two sites and overlaid these departures on the prescribed mean value of $p_a = 335 \mu\text{atm}$.

In all cases, the CO_2 fluxes computed using such modified values of p_a were almost identical to the fluxes computed in the standard case. This indicates that the model is not sensitive to the seasonal variations in p_a .

This low sensitivity may be due to two main factors (see Figure 4-6):

- 1) the magnitude of the intra-annual variations in p_a was one order of magnitude lower than that in p_1 ,
- 2) the covariance between p_1 and K was more strongly pronounced (with lowest values of p_1 in early summer coinciding with lowest values of K) than the covariance between p_a and K (p_a reaches its minimum at the end of summer when K is close to its annual mean value).

The prescribed *mean value* of p_a may also be subject to error: the value used here approximated p_a in the period 1979-80, from which most of the data on the carbonate system originate. A difference of $2 \mu\text{atm}$, which is more than the typical difference in p_a between two consecutive years, would not strongly affect the CO_2 fluxes.

Light attenuation by phytoplankton: Estimates of air-sea fluxes of CO_2 were sensitive to the chlorophyll-specific vertical attenuation coefficient of phytoplankton (κ^{chl}). This coefficient describes apparent optical properties of the water column and depends on the angular and spectral composition of light, the phytoplankton community structure, and the presence of other absorbing and scattering material that covary with chlorophyll. The CO_2 fluxes were more sensitive to a reduction

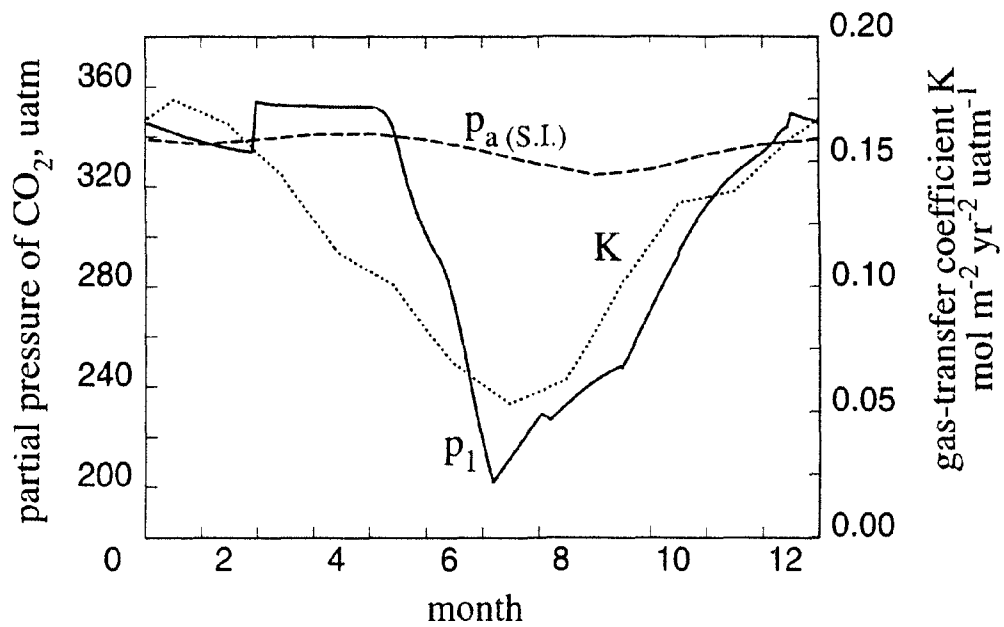


FIGURE 4-6. The partial pressure of atmospheric CO₂ at Sable Island ($p_{a(S.I.)}$), based on data from 1978 by *Wong et al.* [1984]. Also shown are the modelled values of the partial pressures in the surface layer (p_1) and the gas-transfer coefficient K (see also Figure 3-4 f).

than to an increase in κ^{chl} . Reducing κ^{chl} by 50%, well within the range cited in the literature, would increase the uptake of CO_2 by $0.9 \text{ mol m}^{-2} \text{ yr}^{-1}$. In this case, the spring bloom would be accelerated and the autumn decrease in the CO_2 uptake delayed. Increasing κ^{chl} by 50% would lower the annual uptake only by $0.4 \text{ mol m}^{-2} \text{ yr}^{-1}$.

Abiotic case: To test the role of biological processes in creating the variability of seawater properties responsible for the covariance and the carbonate nonlinearity terms, I ran the model in an abiotic mode. Without the biological processes the carbonate nonlinearity term was highly reduced, and the covariance term had a different sign and a much reduced magnitude.

Carbonate dissociation constants: The partial pressure of CO_2 was computed using the carbonate dissociation constants of *Mehrbach et al.* [1973]. When the dissociation constants of *Goyet and Poisson* [1989] were used instead, the partial pressure of CO_2 was lower throughout the year, and consequently the annual CO_2 uptake \bar{F} was higher by $1 \text{ mol CO}_2 \text{ m}^{-2} \text{ yr}^{-1}$ than in the standard case. At the same time, values of the covariance term (ΔF_a) and the carbonate nonlinearity term (ΔF_b) were not substantially affected.

The lack of sensitivity of ΔF_b to the dissociation constants was somewhat unexpected: in the analysis of the spatial data, values of the nonlinear contribution c associated with a one-box model of the global ocean computed using the dissociation constants of *Goyet and Poisson* [1989] were half the magnitude of c based on the constants of *Mehrbach et al.* [1973] (Chapter 2). This difference probably reflects different variability in temperature between a single-ocean box, which contains both cold and warm waters. and the Labrador Sea data set, which has relatively stable temperatures. When p is a function of T , the difference between the algorithm using the constants of *Mehrbach et al.* and that based on the constants of *Poisson and Goyet* is more pronounced than in the case when p is a function of C , as is the case in the Labrador Sea. Therefore, the estimates of the nonlinear contribution were

quite sensitive to dissociation constants in the large-scale spatial computations, but much less so in the temporal computations.

Short-term variability of atmospheric forcing: The model uses “smoothed” atmospheric forcing: inputs on any given day were interpolated linearly from the monthly averages. I tested some consequence of neglecting the day-to-day variations in windspeed and cloud cover.

To simulate the day-to-day variability in windspeed w , I used the 1964 record of winds measured at 3-hour intervals at Station Bravo in the Labrador Sea. Each day in this year was represented by one of the instantaneous wind measurements from that day.

These data were not used directly to compute air-sea fluxes of CO_2 , since the monthly means of windspeed (w) in 1964 were different from the climatological monthly means employed in the standard case. Instead, I overlaid the 1964 day-to-day variations on the “smoothed” windspeeds used in the standard run (interpolated from climatological monthly means). First, I computed the 1964 monthly means of windspeed. Next, I interpolated from them the “smoothed counterparts” of the actual 1964 daily values, in the same way that the “smoothed” climatological daily windspeeds were interpolated from climatological monthly means in the standard version of the model. Finally, I subtracted from the 1964 daily values their 1964 “smoothed counterparts”, and added in their place the climatological values. This ensured that the day-to-day values of w would average to monthly means that were identical to those used in the standard case.

To run the model with rapidly changing windspeeds one has to change the coefficients in the formula for the gas-transfer coefficient K from the one applicable to the climatological means ($K \propto 0.094 \times w^2$, where w is windspeed in m s^{-1}) to another, applicable to instantaneous windspeeds ($K \propto 0.075 \times w^2$) (see section 3.3.4 in Chapter 3 and *Wanninkhof* [1992]).

The annual evolution of daily values of K is shown in Figure 4-7 a. The annual average of K computed from the daily-changing windspeed ($=0.114 \text{ mol CO}_2 \text{ m}^{-2} \text{ yr}^{-1}$) was close to the value computed from winds interpolated from monthly averages ($=0.117 \text{ mol CO}_2 \text{ m}^{-2} \text{ yr}^{-1}$). This agreement indicates that by using the proportionality coefficient \mathcal{A} (see equation 3-16) of 0.094 instead of 0.075, following *Wanninkhof* [1992], I implicitly accounted for most of the effects of the smaller variability in the “smoothed” windspeeds on K , at least at the annual scale.

Unlike K , values of p_1 did not vary much from day to day (Figure 4-7 b): air-sea fluxes of CO_2 on any single day did not change p_1 much, since the daily influx of CO_2 was distributed over at least 30 m of the water column. Because of the slow changes in p_1 , the day-to-day variability in $F (= K(p_a - p_1))$ depended mainly on the variability in K .

In reality, during periods of weaker winds only a portion of the surface layer may be in effective contact with the atmosphere. This would result in a faster increase in the partial pressure of the seawater and consequently would lower air-sea fluxes of CO_2 , at least until stronger winds would bring waters from lower portion of the surface layer into the contact with the atmosphere. Evaluation of the effects of such temporary stratifications within the surface layer for air-sea fluxes of CO_2 merits special attention (see suggestions for future work in Chapter 6).

If daily variations in F were “smoothed out”, (by computing monthly means from daily F values and then interpolating the “smoothed” F values from these monthly means), the remaining differences in F between this and the standard case included a stronger air-sea flux in summer and a weaker flux in winter. At the annual scale, these differences nearly cancelled each other; therefore the annual mean flux \bar{F} did not change much. Nor did the nonlinearity term, ΔF_b : since the annual mean K and the mean properties of the surface layer (T_1 , S_1 , C_1 , A_1) were not changed substantially by the daily fluctuations in windspeed, ΔF_b was close to its value in the standard case. On the other hand, the smaller difference in K

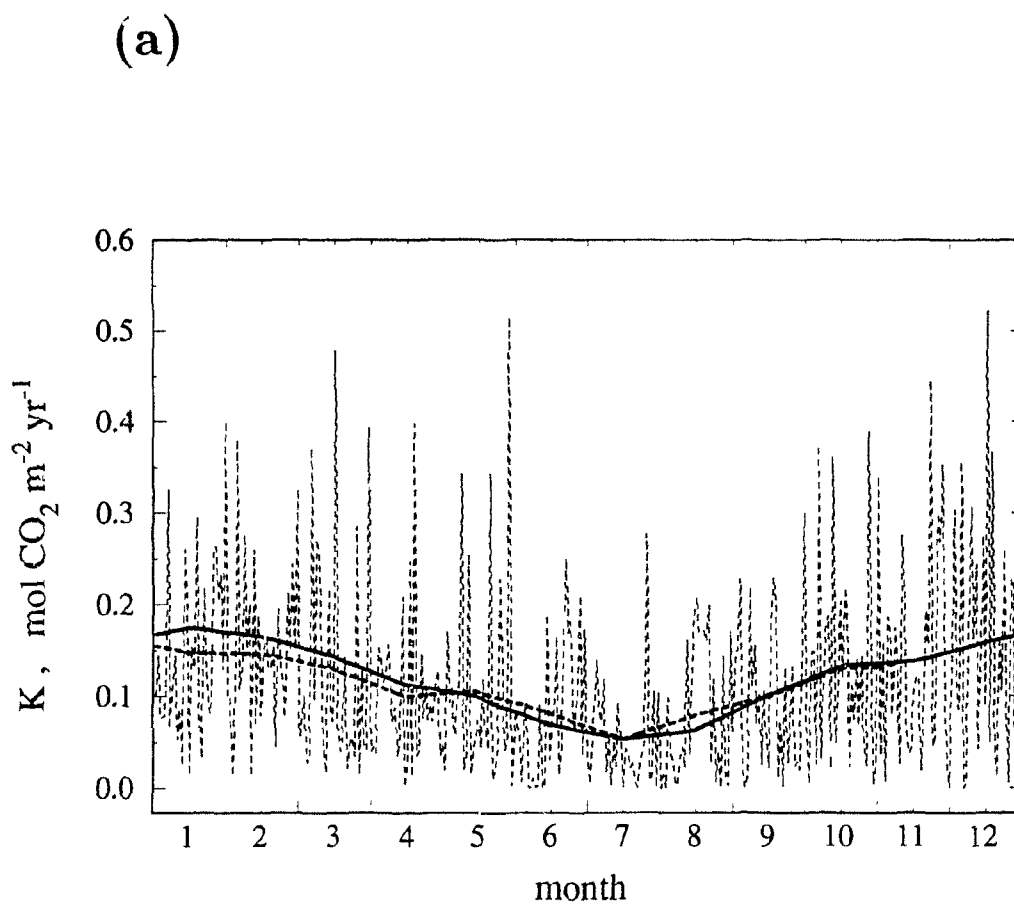
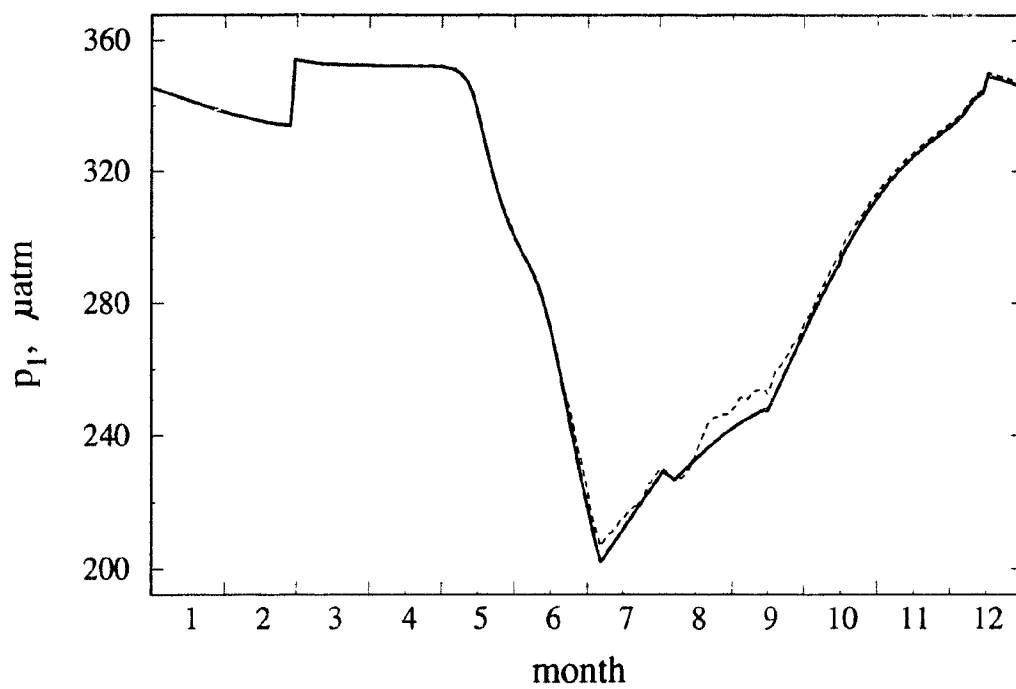


FIGURE 4-7 a). The gas-transfer coefficient K as a function of instantaneous windspeeds. Broken lines denote K computed from instantaneous windspeeds, before (thin line) and after (thick line) "smoothing" to remove the day-to-day variations in K (see text). Solid line denotes results of the standard run, in which "smoothing" is performed on windspeeds instead of K .

(b)**FIGURE 4-7 continued.**

(b) Partial pressures of CO₂ in the surface layer computed with the gas-transfer coefficient K as a function of instantaneous windspeeds (broken line) and "smoothed" windspeeds used in the standard run (solid line).

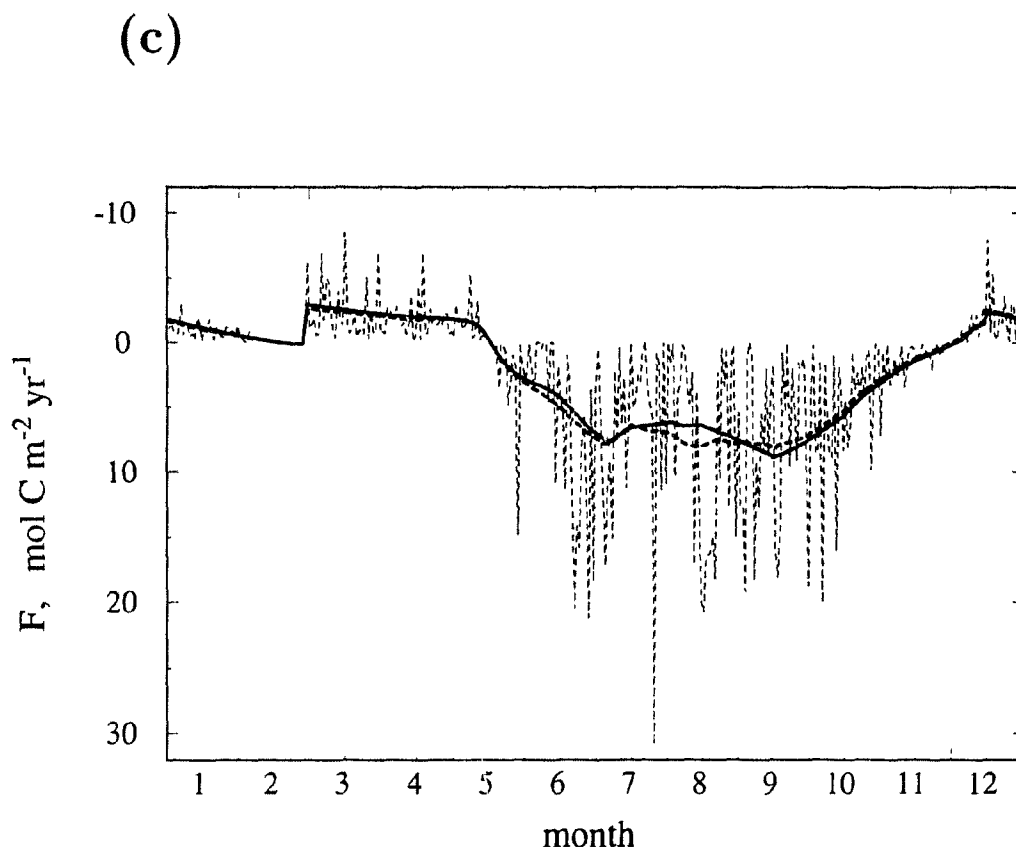


FIGURE 4-7 continued.

(c) Air-sea fluxes of CO₂ computed using instantaneous windspeeds, before (thin broken line) and after (thick broken line) "smoothing" to remove the day-to-day variations in F . Solid line denotes results of the standard run.

between winter and summer caused the covariance term, ΔF_a , to fall from 1.5 to 1.1 mol CO₂ m⁻² yr⁻¹.

Note that these computations accounted only for the effect of changes in wind-speed on the gas-transfer coefficient. Possible effects of increased vertical mixing on the depth and composition of the surface layer are not addressed here.

Daily variations in cloud cover were simulated similarly to windspeed. When the cloud cover was allowed to vary following the pattern observed in 1964, \bar{F} , ΔF_a and ΔF_b were almost identical to those in the standard case.

Nonlinear contribution as a function of variability in seawater properties:

In Chapter 2, I found that the magnitude of the nonlinear contribution c was better correlated with the standard deviation of the partial pressure of CO₂ within a region than with the standard deviation of C or T (see Figure 2-4). I investigated the applicability of a similar approach to temporal fluctuations in the Labrador Sea. I examined whether the magnitude of the temporal nonlinear contribution c_t associated with the annual cycle in seawater properties in any given year could be predicted from standard deviations of T_1 , C_1 or p_1 during this year.

The oceanic data are too scant to re-create an annual cycle of oceanic properties of the Labrador Sea. However, some insight into this matter can be gained by additional analysis of the sensitivity runs that were introduced earlier in this section (Table 4-1). They cover much of the range of variability in physical and biotic properties in the Labrador Sea. I examined whether the magnitude of the nonlinear contribution in these runs could be predicted from variability in T_1 , C_1 or p_1 .

For each sensitivity run, I computed the nonlinear contribution, as well as the standard deviations of T_1 , C_1 and p_1 (denoted here as $s(T_1)$, $s(C_1)$ and $s(p_1)$, respectively). There was no correlation between $s(T_1)$ and c in this dataset ($r^2 = 0.05$), because:

- (a) many modifications of chemical and biological processes altered c_t without affecting T_1 , and

(b) changes in $s(T_1)$ caused by modifications of physical processes were not correlated with changes in c_t .

On the other hand, the nonlinear contribution was closely correlated with $s(p_1)$, and, in most cases, with $s(C_1)$ (Figure 4-8). If the runs with increased production of CaCO_3 (denoted by squares in Figure 4-8) were excluded from the analysis, the nonlinear contribution was closely correlated with both standard deviations of C_1 and p_1 ($r^2 = 0.97$ and $r^2 = 0.96$, respectively). However, when the runs with elevated production of CaCO_3 were included, the correlation between $s(C_1)$ and c broke down. At the same time, the correlation between $s(p_1)$ and c remained very high ($r^2 = 0.96$), indicating that the variability in p is a more reliable predictor of the nonlinear contribution than the variability in C . This finding is consistent with the observations made with respect to spatial fluctuations of oceanic properties in Chapter 2.

4.4 Medium-term effects of alterations in processes determining air-sea fluxes of CO_2

So far, the effects of alterations in biogeochemical and physical processes have been evaluated on a short time scale: air-sea fluxes of CO_2 were computed during the first year after the model parameters or inputs were changed. However, the fluxes computed in the first year may differ from the fluxes in the subsequent years. For instance, an uptake of additional CO_2 in one year would increase the dissolved inorganic carbon inventory of the water column in the following year. Since the carbon-enriched waters absorb less atmospheric CO_2 , the annual fluxes of CO_2 would decrease with time.

To gain some insight into the effects of changes in the modelled processes on air-sea fluxes of CO_2 over several decades, I followed the evolution of the model system during 50 years after the alteration of a few selected parameters. This would also

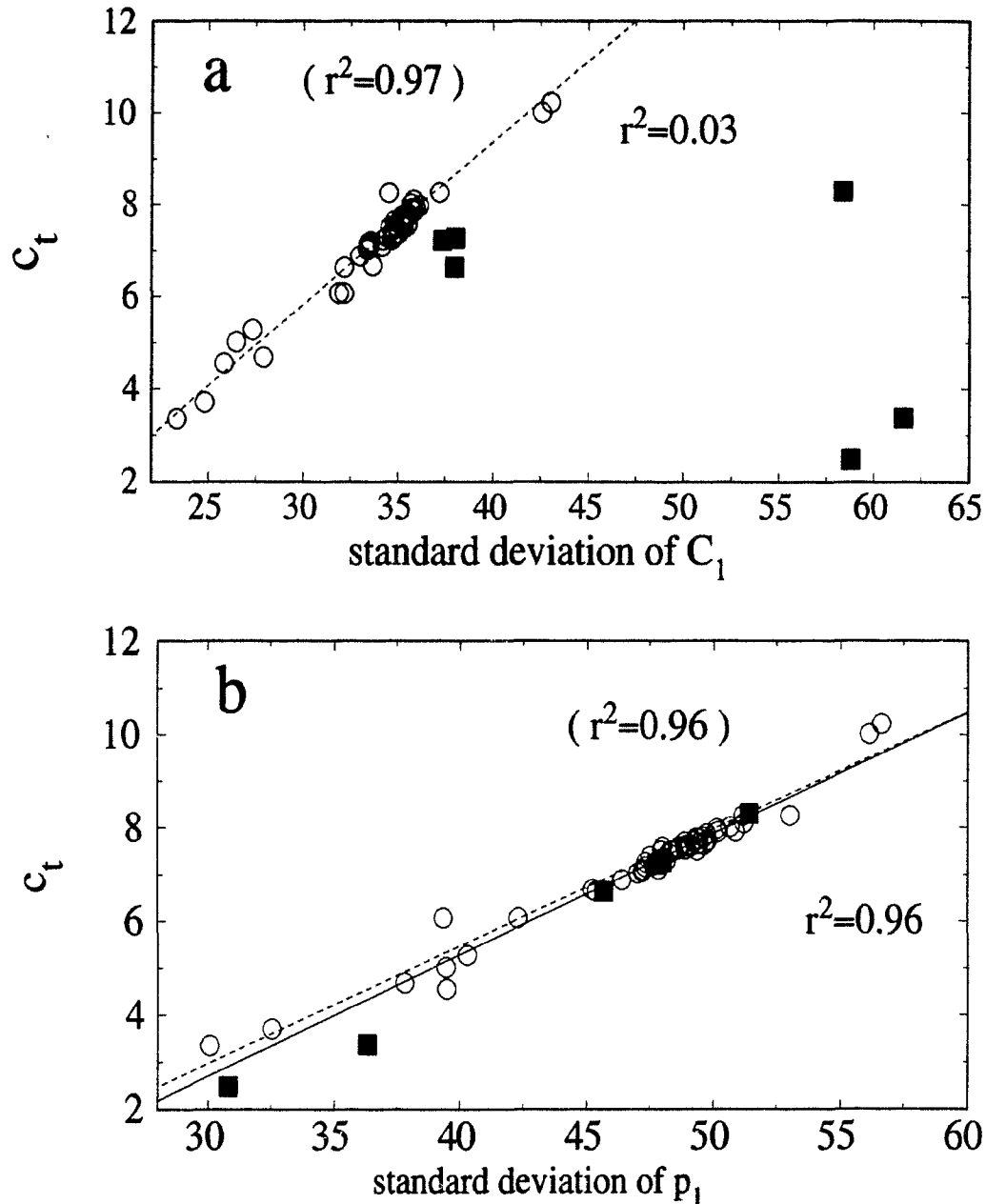


FIGURE 4-8. The temporal nonlinear contribution, c_t [μatm], as a function of standard deviations of the properties of the surface layer of the Labrador Sea. Each symbol represents one of the sensitivity simulations summarized in Table 4-1: squares denote simulations with increased production of CaCO_3 , circles represent the remaining simulations. Solid line represents the linear regression calculated using all the simulations (this line is not shown in *a*) as in this case $r^2 = 0.03$, dashed lines were computed when the simulations of increased production of CaCO_3 were omitted.

(a) Dissolved inorganic carbon, C_1 [mmol m^{-3}].

(b) Partial pressure of CO_2 , p_1 [μatm].

help to ascertain whether the conclusions on the importance of various processes to the CO_2 fluxes that were reached for short time scales are valid for a medium time scale.

As a test case, I used the modifications in the air-sea fluxes of CO_2 caused by hypothetical changes in the photosynthesis parameters of the phytoplankton community by $\pm 50\%$. The assumption of constant composition of the deep-ocean box, used in the short-term sensitivity analysis, may no longer be valid over 50 years. Therefore, the concentrations of dissolved inorganic carbon C , nutrients N and alkalinity A were allowed to change in all three modelled layers.

In general, the evolution of the air-sea CO_2 fluxes, following an alteration in oceanic processes, depended on the exchanges of water between the modelled layers of the Labrador Sea and the adjacent waters (including the waters from the adjacent geographic regions as well as the bottom waters of the Labrador Sea, residing below the top 1430 m represented in the model).

Two cases were considered. First, a no-export case was analysed, in which all the additional fluxes of CO_2 were taken up by (or released from) the three ocean layers modelled here. In other words, there was no net export of the additional CO_2 from the top 1430 m of the Labrador Sea. Later, I considered an alternative case in which export (or import) into the adjacent waters was allowed.

Two elements of the carbon system were examined: the annual air-sea fluxes of CO_2 and the total inorganic carbon inventory of the modelled waters. The departure from the pre-alteration values of the annual CO_2 fluxes is denoted as $\Delta\bar{F}(t)$ and given by:

$$\Delta\bar{F}(t) = \bar{F}(t) - \bar{F}(0), \quad (4-1)$$

where t is the year of simulation and 0 denotes the pre-alteration values.

At any given time, the total inorganic carbon inventory, denoted as $\sum C$ can be expressed as

$$\sum C = C_1H_1 + C_2H_2 + C_3H_3, \quad (4-2)$$

where C_i and H_i are, respectively, the inorganic carbon concentration in, and the thickness of, the i th layer ($i = 1, 2, 3$). The accumulation of the additional carbon in the modelled waters (that is, the departure from the pre-alteration carbon inventory, denoted as $\Delta \sum C(t)$) is given by:

$$\Delta \sum C(t) = \sum C(t) - \sum C(0). \quad (4-3)$$

4.4.1 The no-export case

Applicability: The no-export case was computed on the assumption that all the additional CO_2 remained within the three modelled layers. Such an assumption would be valid if one of the two conditions were met:

- 1) no water exchange with the adjacent waters, or:
- 2) the concentration of C in the adjacent waters was equally affected, so there is no net export (or import) of any additional C to the adjacent waters.

High-latitude waters are usually regarded as sinks of atmospheric carbon and to fulfil this role they have to export inorganic carbon into adjacent waters. Furthermore, the heat and salinity budgets of the Labrador Sea require some exchange of water with the adjacent water bodies (Appendix B; *Ikeda* [1987]). Therefore, the first condition is not likely to hold for the Labrador Sea, and so would be of little interest, except for those studies designed to explore the consequences of reducing the exchanges with adjacent waters.

The second condition could be met if changes in the physical or biogeochemical processes are widespread, thus affecting not only the water composition in the studied area, but also the composition of the adjacent water masses.

Results: To simulate the evolution of the CO_2 fluxes in the no-export case, the total inventory of the inorganic carbon $\sum C(t)$ was allowed to accommodate all the additional air-sea fluxes of CO_2 in year t :

$$\sum C(t+1) = \sum C(t) + \Delta \bar{F}(t). \quad (4-4)$$

The total inventories of nutrients and alkalinity were maintained constant within the top 1430 m (although redistribution of these properties between individual layers, resulting from changes in the biological processes, was allowed).

The results of the increase in the photosynthesis parameters by 50% are shown as line 1a in Figure 4-9. In the first two years, changes in the biological productivity dominated the evolution of the air-sea fluxes of CO₂. In year 1, the increase in α^{chl} and P_m^{chl} raised the annual air-sea flux by $\Delta\bar{F}(1) = +1.2 \text{ mol CO}_2 \text{ m}^{-2} \text{ yr}^{-1}$ (as already shown in 4.3.3). The increased phytoplankton biomass during the first year allowed more biomass to survive till early spring of year 2. The larger concentration of phytoplankton in early spring accelerated the onset of the phytoplankton bloom and, consequently, increased the departure from the standard CO₂ fluxes: $\Delta\bar{F}(2) = +1.4 \text{ mol CO}_2 \text{ m}^{-2} \text{ yr}^{-1}$. In year 3, the phytoplankton concentration C (as well as the concentrations of nutrients N and alkalinity A) reached a new inter-annual steady state, in the sense that the cycles of B , N and A were repeated from year to year with respect to both the phase and the magnitude.

The further evolution of the carbonate system depended only on the physical exchanges with the atmosphere. As the additional CO₂ accumulated, the partial pressure of CO₂ in seawater rose, which, in turn, reduced the air-sea fluxes of CO₂.

The new steady-state of inorganic carbon was approached slowly, because of the large amount of carbon in the water column that had to be adjusted. In year 10, $\Delta\bar{F}(t)$ was $+0.6 \text{ mol CO}_2 \text{ m}^{-2} \text{ yr}^{-1}$, that is, after 10 years, 50% of the initial change in the CO₂ fluxes was still present. After another 10 years, the departure from the pre-alteration values was reduced to 20% ($\Delta\bar{F}(20) = 0.20 \times \Delta\bar{F}(1)$). Ultimately, the new steady state of C was approached asymptotically, where $\Delta\bar{F}(t) \rightarrow \Delta\bar{F}(\infty) = 0$ and $\Delta \sum C(t) \rightarrow \Delta \sum C(\infty) = +15.7 \text{ mol CO}_2 \text{ m}^{-2}$, where ∞ denotes the final, steady-state values. In other words, the increase in the photosynthesis parameters allowed an additional $15.7 \text{ mol CO}_2 \text{ m}^{-2}$ to be stored within the top 1430 m of the water column.

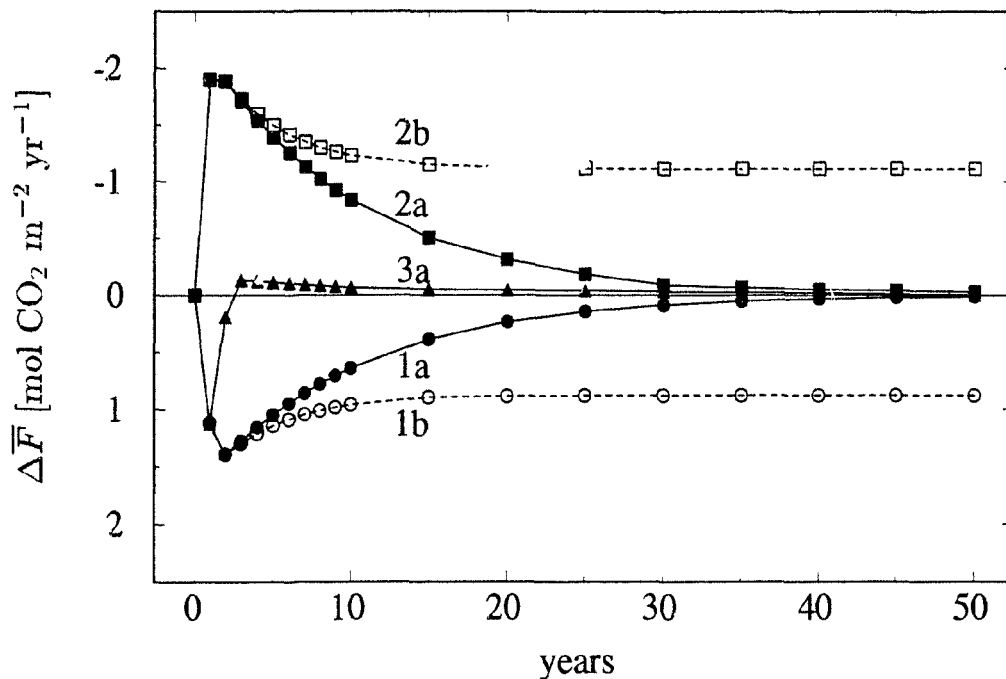


FIGURE 4-9. Evolution of the air-sea fluxes of CO_2 ($\Delta\bar{F}$) following hypothetical changes in the photosynthetic parameters. $\Delta\bar{F}$ denotes the departure from the standard values of the air-sea fluxes of CO_2 . Solid lines (denoted by subscripts "a") were computed neglecting exchanges with adjacent waters; broken lines (subscripts "b") were calculated including the effect of the exchanges (see text). Lines 1a and 1b were obtained by increasing both α^{chl} and P_m^{chl} by 50% throughout the simulation; lines 2a and 2b were calculated by decreasing the photosynthetic parameters by 50%. In case 3a, the photosynthetic parameters were increased by 50% (as in case 1a) during the first year, but afterwards were returned to the standard values. Positive values of $\Delta\bar{F}$ correspond to the net uptake of CO_2 by the ocean.

Similar tendencies, although of opposite sign, resulted from decreasing the photosynthesis parameters by 50% (line 2a): large negative departure in \bar{F} during the first year was gradually reduced to zero in the following years. Over this time the negative fluxes, representing degassing of CO_2 , lowered the carbon inventory of the Labrador Sea by $\Delta \sum C(\infty) = -20 \text{ mol CO}_2 \text{ m}^{-2}$.

Medium-term effects of a short-term perturbation: In the computations above, the change in the photosynthesis parameters persisted throughout the simulation. For a comparison, line 3a in Figure 4-9 shows the medium-term results of a short-term perturbation: after the 50% increase in the photosynthesis parameters in the first year, they were restored to the standard, pre-alteration, values. In year 2, there was still some additional uptake of CO_2 because of an earlier spring bloom caused by higher biomass surviving from the first year. However, from year 3 onwards, the phytoplankton biomass stayed at its pre-modification levels and the water column began releasing the inorganic carbon accumulated during the first two years.

4.4.2 The export case

Applicability: The export-case, in which some of the additional CO_2 is exported into (or imported from) the adjacent waters, was also considered. This case differed from the previous one in assuming that the adjacent waters were not substantially affected by the simulated changes in the physical or biological processes affecting the top 1430 m of the Labrador Sea. This may be a reasonable assumption when:

- 1) the changes are local, and do not affect waters in other locations; or
- 2) the exchange of properties with the adjacent waters includes a substantial exchange with the bottom layer, located below the depth of 1430 m (given the large volume of the bottom layer, it would take some time until its composition changes in the response to changes in the processes occurring in the top 1430 m).

Results: If one assumes that the typical mixing rate between the top three layers of the Labrador Sea and the adjacent waters is of order of 5 Sv and the area of the open Labrador Sea is $0.86 \times 10^{12} \text{ m}^2$ (Appendix B; Ikeda [1987]), then about 13% of the top 1430 m of the Labrador Sea is exchanged each year with the adjacent waters. If the composition of the adjacent waters were unchanged, the amount of the additional C exported annually by mixing between the modified Labrador Sea waters and the adjacent waters would equal $[\sum C(t) - \sum C(0)] \times 0.13$. Results of the simulation incorporating this removal are shown as broken lines *1b* and *2b* in Figure 4-9.

In case *1b*, mixing with adjacent waters removed some of the additional inorganic carbon drawn from the atmosphere. This slowed the increase in the carbon inventory and the decrease in the CO_2 fluxes, compared with case *1a* in which the mixing was neglected. After 10 years, $\Delta \bar{F}(t)$ was still 85% of the first-year departure. After a few additional years, the departure stabilized at 75% of $\Delta \bar{F}(1)$. In other words, a new steady state was approached in which air-sea fluxes of CO_2 were permanently increased by $\Delta \bar{F}(\infty) = +0.9 \text{ mol CO}_2 \text{ m}^{-2} \text{ yr}^{-1}$. Note that all these additional fluxes of CO_2 were channeled into the adjacent waters, as the inorganic carbon inventory in the top 1430 m of the Labrador Sea stabilized at a value $7.7 \text{ mol CO}_2 \text{ m}^{-2}$ ($= \Delta \sum C(\infty)$) higher than the pre-alteration inventory.

Similar tendencies were observed in the case of the reduction of the photosynthesis parameters (*2b*). Mixing slowed the reduction in the magnitude of $\Delta \bar{F}(t)$ and led to an end-state that was different from that in the no-export case. In this new end-state the CO_2 uptake remained lower by $\Delta \bar{F}(\infty) = 1.1 \text{ mol CO}_2 \text{ m}^{-2} \text{ yr}^{-1}$ from the pre-alteration value.

4.4.3 Implications

Time scale of the response: The results presented in this section indicate that a sustained change in the phytoplankton productivity (and other oceanic processes)

may affect the air-sea fluxes of CO_2 and the amount of carbon stored in the ocean on medium-time scales.

If the export of the additional carbon from the top three layers of the Labrador Sea (0-1430 m) were small, it would take about 30 years to restore the air-sea fluxes of CO_2 to within $\pm 0.1 \text{ mol CO}_2 \text{ m}^{-2} \text{ yr}^{-1}$ from the pre-alteration values. This restoration of the pre-alteration fluxes would be achieved through a permanent change in the inorganic carbon inventory.

If the export of the additional carbon from the top three layers were substantial, the air-sea fluxes of CO_2 could be altered permanently: in the analysed cases, after 10-15 years the carbon system approached a new steady state, in which air-sea CO_2 fluxes differed from those prior to the alteration. These differences were balanced by the additional exports of inorganic carbon into the adjacent waters.

The new steady state in inorganic carbon was reached much more slowly than in the case of the other model variables. Perturbations in concentrations of nutrients, alkalinity, phytoplankton and zooplankton were limited here to the modelled waters and the interactions between these variables usually brought them to a new steady state within 2-3 years after the alteration. In the case of inorganic carbon, the response time was much longer, because, in addition to responding to changes in the seawater variables, the inorganic carbon had to adjust to changes in the external input from the atmosphere. When some of the altered CO_2 fluxes were exported into the adjacent waters, the change in the carbon inventory that was required to achieve the new steady state was smaller and, consequently, the adjustment period was shorter (10-15 years instead of 30 years).

Extrapolation of the short-term sensitivity results to medium-term scales: One of the aims of this section was to evaluate the extent to which the conclusions derived from the short-term changes in the CO_2 fluxes in section 4.3 would be valid over longer time scales.

The sign and the magnitude of the change in the mean CO₂ fluxes during the first year ($\Delta\bar{F}(1)$) are good indicators of the sign and the magnitude of both $\Delta\bar{F}(t)$ and $\Delta\sum C(t)$ during several years following a change in the oceanic processes (Figure 4-9). Further extrapolation of the information contained in $\Delta\bar{F}(1)$ over the time scale of decades depends on the case considered to be adequate to describe the changes.

If the *no-export case* better approximates the real situation, the annual air-sea fluxes of CO₂ would return ultimately to the pre-alteration values ($\bar{F}(\infty) = \bar{F}(0)$). Still, the first-year results indicate the sign and magnitude of the changes in the inorganic carbon inventory required to approach this new steady-state. In general, larger values of $\Delta\bar{F}(1)$ result in larger values of $\sum C(\infty)$.

If the *export case* is more appropriate, the first-year results indicate not only the amount of carbon stored in (or removed from) the modelled layers, but also the permanent change in the air-sea fluxes of CO₂ and the amount of inorganic carbon exported into the adjacent waters associated with the new steady state. Typically, larger $\Delta\bar{F}(1)$ values result in

- larger $\Delta\bar{F}(\infty)$ values,
- higher $(\bar{F}(\infty) - \bar{F}(0))$ values, and
- higher exports of C into the adjacent waters.

In view of these arguments, one may conclude that the results of the sensitivity analysis, based on the short-term changes in air-sea fluxes of CO₂ (section 4.3), contain some information on changes occurring at longer time scales as well.

4.5 Concluding remarks

The calculated mean annual fluxes \overline{F} in the Labrador Sea were sensitive to a number of physical and biogeochemical processes, whereas the flux components associated with the covariance between K and Δp and with the nonlinearity of the carbonate system, ΔF_a and ΔF_b , were more stable, provided the partial pressure of atmospheric CO_2 did not change much.

Results of the sensitivity analysis allow various oceanic processes to be ranked according to their potential to alter mean annual CO_2 fluxes. The **first group**, which contains the processes to which the fluxes were **most sensitive**, would include:

- photosynthesis efficiency in spring,
- growth-independent respiration in the surface and the intermediate layers,
- light attenuation in the water,
- presence or absence of deep winter convection, and
- timing and magnitude of CaCO_3 production.

Realistic changes in these processes altered \overline{F} by amounts comparable to, or greater than, the typical anthropogenic flux of CO_2 in this area, estimated to be about $0.8 \text{ mol CO}_2 \text{ m}^{-2} \text{ yr}^{-1}$. Therefore, any model of the CO_2 uptake in high latitudes should simulate these processes carefully.

Changes in some of these processes may manifest themselves through a change in the timing of the spring bloom. A shift in this timing by merely two or three weeks, which may be observable from ships or from satellites, may indicate large changes in the annual CO_2 fluxes in the area.

The **second group** comprises the processes which were identified in this study as having a **moderate influence** on the CO_2 fluxes. Reasonable changes in these processes altered the CO_2 fluxes by amounts comparable to about half that of the anthropogenic flux of CO_2 in the area. This group includes:

- winds,
- humidity,
- duration of the warm-season stratification,
- thickness of the summer surface layer.

- concentrations of dissolved inorganic carbon and alkalinity in the deep layer, and
- sinking of organic matter from the intermediate layer.

Finally, the **third group**, consists of processes that, *within the context of this model*, had small effects on air-sea fluxes of CO₂. This group includes:

- sinking rate of organic matter from the surface layer;
- chemical composition of the soft-tissue matter (the C:N:chl ratio in phytoplankton),
- zooplankton dynamics,
- changes in monthly means of cloudiness, air-temperature and precipitation,
- the day-to-day variability in cloudiness and in the gas-transfer coefficient K , and
- the deepening of the winter convection beyond several hundred meters and changes in the timing of the convection.

Processes in the last group may be omitted or simplified in models evaluating the uptake of CO₂ in the Labrador Sea and in other, similar, high-latitude waters. For instance, one may use a single phytoplankton species, with a constant C:N:chl ratio, constant sinking velocity in the surface layer and a simplified zooplankton component. Detailed prescription of cloudiness, air-temperature and precipitation would not be critical either, as long as the occurrence of winter convection were properly simulated.

Two caveats should be mentioned at this point. First, sensitivity analyses that led to these conclusions were done, for most part, by alterations of one parameter at a time. If two or more parameters are changed simultaneously, the effect of the changes could be different from that expected from changes in any one parameters. Second, the processes which could be omitted or simplified when the annual (net) fluxes of CO₂ are of interest, could still be important when other elements of the carbon cycle (such as total primary production or carbon fluxes between trophic levels) are assessed.

The results of many of the sensitivity analyses presented here would be very different if the intermediate layer separating the surface layer from deep layer were not

modelled. This work, therefore, underscores the need for including an intermediate layer in carbon models.

The strong sensitivity of \bar{F} to a number of processes also indicates that the annual air-sea fluxes of CO₂ in high latitudes could be susceptible to large inter-annual variability. Therefore, obtaining reliable estimates of fluxes of CO₂ in high latitudes may require compiling observations from many years. Given the potentially large range of natural variability in \bar{F} , it may also be difficult to discern possible effects of any anthropogenic climate change.

The choice of the carbonate dissociation constants to be used in a model is important (e.g., between those of *Mehrbach et al.* [1973] and *Goyet and Poisson* [1989]) because it may produce large differences in the computed partial pressure of CO₂ and, consequently, affect model estimates of \bar{F} . Unlike the mean fluxes, values of ΔF_a and ΔF_b were not sensitive to the choice of the carbonate dissociation constants: in the Labrador Sea, computations of the partial pressure of CO₂ using the constants of *Goyet and Poisson* [1989] were almost as sensitive to the nonlinear effects as those using the constants of *Mehrbach et al.* [1973]. The advantage of the weaker nonlinearity of the constants of Goyet and Poisson, noted in the analysis of the global spatial data in Chapter 2, is apparent only when dealing with waters having strongly variable temperatures.

In general, values of the covariance term (ΔF_a) and the nonlinearity term (ΔF_b) in the Labrador Sea were less sensitive than average annual fluxes (\bar{F}) to changes in oceanic processes. Magnitudes of ΔF_a and ΔF_b depend mainly on biological processes creating the intra-annual variability in the partial pressure of CO₂. The value of ΔF_b was found to be closely correlated with the annual standard deviations in p_1 , which is consistent with the observation made in Chapter 2, linking the carbonate nonlinearity with spatial variability in the partial pressure of CO₂. The magnitude of ΔF_a was somewhat reduced when realistic day-to-day windspeeds were used.

When changes in the processes determining air-sea fluxes of CO₂ were simulated over several decades, the whole system approached a new steady state. In most cases, nutrients, alkalinity, phytoplankton and zooplankton in the Labrador

Sea achieved a new equilibrium within a few years, whereas the adjustment of the inorganic carbon required at least 10–30 years. During the adjustment, the inventory of dissolved inorganic carbon of the water column changed and the air-sea fluxes of CO_2 were altered. The flux alteration could be permanent or temporary, depending on whether the change was limited to the modelled waters of the Labrador Sea, or affected the adjacent water masses as well. Changes in biogeochemical or physical processes may therefore modify the uptake of anthropogenic CO_2 by high latitude waters.

Chapter 5.

Effects of Temporal Fluctuations in Oceanic Properties on Air-Sea Fluxes of CO₂ in High-CO₂ Environments

5.1 Introduction

Accumulation of anthropogenic CO₂ in the ocean-atmosphere system modifies interactions between various components of the carbon system. In the future, CO₂-rich, environment, a given change in the properties of seawater, such as temperature, salinity, concentration of dissolved inorganic carbon concentration or alkalinity, may have a different effect on the seawater partial pressure of CO₂ (p) than at present.

In the present-day ocean there is a certain degree of spatial and intra-annual variability in the seawater properties, created by the spatial and intra-annual variability in the oceanic processes (such as mixing or primary production). The relationship between p and seawater properties is such that the same variability in these oceanic properties would produce a larger variability in p in the future, CO₂-rich, conditions. As a result, the *covariance term*, defined as the component of the CO₂ flux associated with the covariance between the gas-transfer coefficient K and air-sea difference in the partial pressure of CO₂ (Δp), is likely to increase in the future. Moreover, under CO₂-rich conditions, the partial pressure of CO₂ becomes a more nonlinear function of seawater properties. As a result, the *nonlinearity term*, defined as the component of the CO₂ flux associated with the nonlinearity of the carbonate system, is likely to increase in the future as well.

In other words, the difference between the actual uptake of atmospheric CO₂ and that expected from mean oceanic properties (which can be attributed to the

covariance and the nonlinearity terms), will increase in the future, even if the biogeochemical processes responsible for the spatial and intra-annual variability in the oceanic properties remain unchanged.

In this chapter I quantify the increase in the covariance and nonlinearity terms (denoted as ΔF_a and ΔF_b , respectively; see equations 3-21 and 3-23) in the future environments by computing them for a range of atmospheric partial pressure of CO_2 (p_a) varying from the pre-industrial value to four times that value.

In Chapter 3, it was found that most of the covariance and the nonlinearity terms were implicitly accounted for, if the annual data were partitioned into seasons. In this chapter, I test whether this finding would hold in the future, CO_2 -rich environments.

The cases considered above concern changes in air-sea fluxes of CO_2 with increasing p_a , assuming that physical and biological processes determining the seawater properties are *unchanged* from their present-day spatial and temporal patterns. However, the CO_2 -rich conditions may also affect the way in which the future air-sea fluxes of CO_2 respond to potential *changes* in these patterns. I explore this issue through an analysis of short- and medium-term responses of annual air-sea fluxes of CO_2 to a hypothetical change in primary production in a CO_2 -rich environment.

Next I discuss some consequences of potential changes in ΔF_a and ΔF_b for diagnostic and transient carbon models. In carbon models, the covariance and the nonlinearity terms are neglected at time scales below the temporal resolution of the model. Since most carbon models have a resolution of one year, the consequences of intra-annual variability in oceanic properties are usually not accounted for explicitly. The problems with an implicit accounting, through calibration of the air-sea gas exchange in these models using data on tracers, are also examined. Finally, some general conclusions are presented.

5.2 Approach

Future changes in air-sea fluxes of CO_2 are evaluated using the one-dimensional model of the Labrador Sea described in Chapter 3. This area was chosen because high-latitude waters are believed to be important for the present and future uptake of anthropogenic carbon. Many transient models, which follow the evolution of the carbon cycle over a wide range of partial pressure of CO_2 in the atmosphere (p_a), recognize this importance by assigning a separate compartment to represent high-latitude waters [e.g., *Joss et al.*, 1991; *Peng and Broecker*, 1991; *Shaffer and Sarmiento*, 1995]. Future changes in the covariance and the nonlinearity terms in high-latitude waters may influence the accuracy of these models.

I simulate of the annual cycles of the oceanic variables controlling air-sea fluxes of CO_2 for environments with an atmospheric partial pressure of CO_2 (p_a) different from the present-day value.

To simulate future conditions, two modifications are made to the model:

- 1) the partial pressure of CO_2 in the atmosphere (p_a) is set at arbitrary levels (up to four times the preindustrial value), and
- 2) the total inventory of dissolved inorganic carbon ($\sum C$) is changed. The change reflects the accumulation of anthropogenic CO_2 in the modelled 1430 m of the water column between the present time and the time when the atmospheric partial pressure achieves the prescribed value.

It is not easy to modify the inventory of dissolved inorganic carbon. It requires a knowledge of the rate of increase in p_a and the rate of accumulation of anthropogenic CO_2 in the adjacent waters with which the Labrador Sea waters are exchanged. Without this information, changes in $\sum C$ have to be prescribed. Fortunately, as will be shown in section 5.3, it is not crucial to the objectives of this analysis that the inventory of dissolved inorganic carbon be represented very accurately.

Results of each simulation are used to calculate three annual fluxes of CO₂:

- \bar{F} , the annual mean flux (i.e., the sum of daily fluxes),
- F_a , the product of mean K and mean Δp (see equation 3-21), and
- F_b , the product of mean K and the Δp computed as the difference between mean p_a and the partial pressure of seawater (p) computed from the mean values of T , S , C and A of seawater (see equation 3-23).

Future values of the covariance term (ΔF_a) are computed as the differences between \bar{F} and F_a at a given p_a . Similarly, future values of the carbonate nonlinearity term (ΔF_b) are computed as the differences between F_a and F_b . Values of ΔF_a and ΔF_b are computed for p_a ranging from the preindustrial value (assumed to be 280 μatm [Neftel *et al.*, 1986]) to four times that value.

To evaluate whether partitioning of the annual cycle into seasons could remove most of averaging errors caused by neglecting ΔF_a and ΔF_b , I partition the data into cold and warm seasons. The covariance and the carbonate nonlinearity terms within these seasons are calculated. These seasonal values are then added and their sum is compared with the standard values of ΔF_a and ΔF_b obtained by pooling all the daily data into a single annual dataset.

I also examine changes in the sensitivity of the mean CO₂ fluxes (\bar{F}) to alterations in the physical and biogeochemical processes at higher p_a . This is achieved by a simulation of the response of the annual CO₂ fluxes to a change in primary production at $p_a = 840 \mu\text{atm}$ (three times the preindustrial value), over 50 years. Results of this simulation are then compared with the response of the CO₂ fluxes to an identical change in primary production simulated at the present-day p_a in Chapter 4.

5.3 The covariance and the nonlinearity terms under various atmospheric partial pressures of CO₂

5.3.1 Adjustment of the inorganic carbon inventory

As indicated in the previous section, to run the model at various p_a one should modify the total inventory of dissolved inorganic carbon ($\sum C$ – see equation 4-2) to reflect the accumulation of anthropogenic CO₂ in the sea with time. The modification of $\sum C$ was achieved by adjusting the concentration of dissolved inorganic carbon in the deep layer (C_3) until the mean annual flux of CO₂ at partial pressure p_a (\bar{F}_{p_a}) achieved a prescribed value.

Fortunately, values of ΔF_a and ΔF_b , unlike values of \bar{F} , are not sensitive to (reasonable) changes in C_3 (as shown in Table 4-1). Therefore, I modified C_3 until the computed values of \bar{F}_{p_a} were identical to the present-day \bar{F} (that is, until $\bar{F}_{p_a} = \bar{F}_{335}$).

In section 5.3.3 I show that allowing for a reasonable increase in \bar{F} would have negligible effects on the computed values of ΔF_a and ΔF_b .

5.3.2 The covariance and the nonlinearity terms at atmospheric partial pressure of CO₂ of 560, 840, and 1120 μatm

The covariance and the nonlinearity terms (ΔF_a and ΔF_b , respectively) were computed for atmospheric partial pressure (p_a) equal to two, three and four times the preindustrial values (that is, for $p_a = 560, 840$ and $1120 \mu\text{atm}$). In these calculations I used the simplifying assumption that the carbon inventory of seawater increased in such a way that the mean annual fluxes remained at their present values (see the previous subsection). I found that the magnitudes of the covariance term

ΔF_a and, for the most part, the nonlinearity term ΔF_b , increased with p_a (Figure 5-1).

The present value of ΔF_a ($-1.5 \text{ mol C m}^{-2} \text{ yr}^{-1}$) nearly doubled at $560 \mu\text{atm}$, and more than tripled when p_a reached $1120 \mu\text{atm}$. The magnitude of ΔF_b increased from the present value of $-0.9 \text{ mol C m}^{-2} \text{ yr}^{-1}$ to more than two times that value at $840 \mu\text{atm}$, and slightly declined at $1120 \mu\text{atm}$ (Figure 5-1).

The increase in the covariance term ΔF_a can be understood if one compares the annual cycles of the partial pressure of CO_2 in the surface layer at various levels of p_a . For instance, the removal of the same amount of inorganic carbon by the spring bloom (Figure 5-2 a) causes a much deeper depression in p (and a larger Δp) at $p_a = 840 \mu\text{atm}$ than at $p_a = 335 \mu\text{atm}$ (Figure 5-2 b).

Low values of \bar{K} during late spring and summer coincide with higher values of Δp at higher p_a . Therefore, ΔF_a , the component of the CO_2 flux associated with the covariance between \bar{K} and Δp , is expected to increase in the future.

The evolution of the nonlinearity term ΔF_b with p_a is more complicated. Equation (3-23) in Chapter 3 shows that $\Delta F_b = -\bar{K} c_t$. Since \bar{K} , the mean gas-transfer coefficient of CO_2 , is assumed to be constant here, the evolution of ΔF_b with p_a (shown in Figure 5-1) mirrors changes in the nonlinear contribution c_t . The nonlinear contribution reached a maximum ($16 \mu\text{atm}$, compared with $7.5 \mu\text{atm}$ at present) at $p_a = 840 \mu\text{atm}$, and then slightly decreased.

The rise and fall of c_t (and, consequently, of ΔF_b) can be understood if the partial pressure of CO_2 of seawater is treated solely a function of dissolved inorganic carbon C (a reasonable assumption in the Labrador Sea where changes in C are by far the dominant source of variability in p). When the partial pressure p is a function of a single seawater property, be it temperature (as discussed in Chapter 2), or dissolved inorganic carbon (as discussed here), the nonlinear contribution increases with the convexity of p and with the variability of the property controlling p .

In the case examined here, the convexity of $p(C)$ can be quantified by the second derivative of p with respect to C (dp^2/dC^2 , plotted in Figure 5-3). For T , A

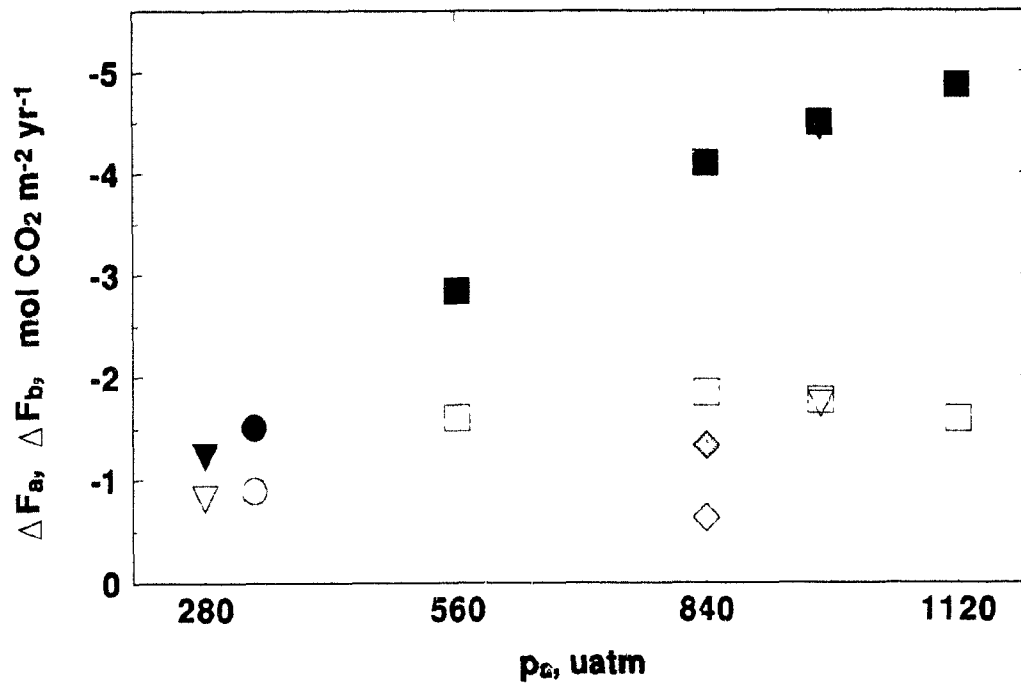


FIGURE 5-1. Values of ΔF_a (filled symbols) and ΔF_b (empty symbols) as a function of atmospheric partial pressure of CO_2 . Circles denote the present-day values, squares represent the values derived assuming the anthropogenic fluxes at the present levels, and triangles depict the values computed assuming the anthropogenic fluxes consistent with those given by *Maier-Reimer* [1991]. Also shown are ΔF_a and ΔF_b after the partitioning of the annual cycle into two seasons (diamonds). Negative values of ΔF_a and ΔF_b indicate that these terms reduce the uptake (or increase loss) of CO_2 by the ocean.

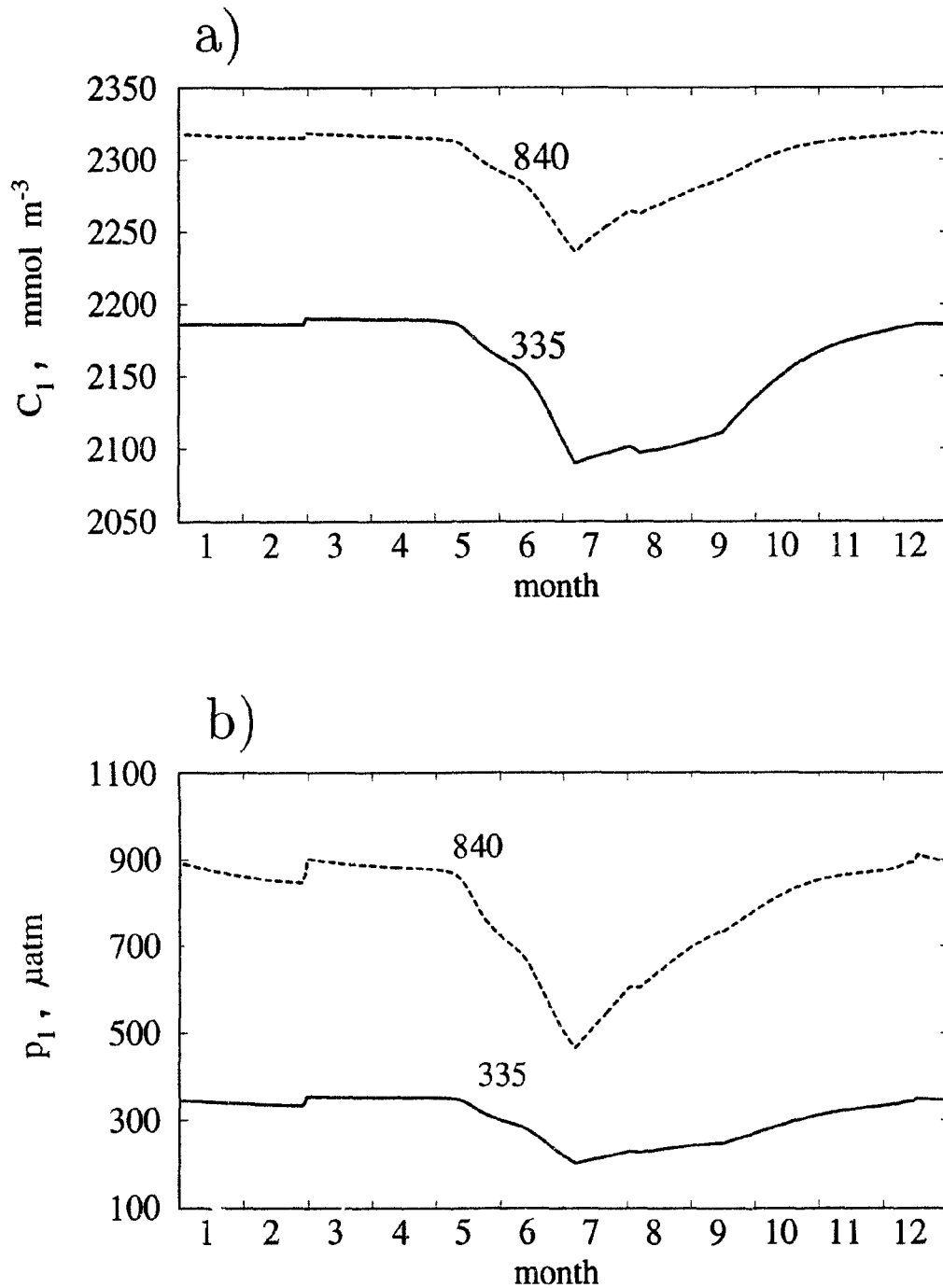


FIGURE 5-2. Annual cycles of (a) dissolved inorganic carbon (C_1) and (b) partial pressure of CO_2 (p_1) in the surface waters of the Labrador Sea at the atmospheric partial pressure of CO_2 of $335 \mu\text{atm}$ (the standard case) and $840 \mu\text{atm}$ (three times the preindustrial value).

and S typical of the Labrador Sea. dp^2/dC^2 initially increases with C and p , then levels off and finally decreases at high values of p .

The second element, the intra-annual variability in C , decreases with p_a (Figure 5-2 a): in the CO₂-rich environment, large departures in C from an equilibrium value are of a shorter duration than in the present-day environment. This can be seen in Figure 5-2: the removal of the same amount of carbon by the spring bloom (Figure 5-2 a) causes a much deeper depression in p_1 at $p_a = 840 \mu\text{atm}$ than at $p_a = 335 \mu\text{atm}$ (Figure 5-2 b). The higher Δp ensures that the air-sea fluxes of CO₂ are stronger and that the departures in C_1 from the equilibrium value are reduced much faster than at the present-day p_a (Figure 5-2 a). In other words, the resistance of the air-sea interface to the CO₂ fluxes is weaker in the CO₂-rich environments, where $K\Delta p$ are larger than at present.

Consequently, although the variability in p_1 increases sharply with p_a , the variability in C_1 decreases: the standard deviation in daily values of C_1 decreases from 35 mmol m^{-3} at $p_a = 335 \mu\text{atm}$, through 23.5 mmol m^{-3} at $p_a = 840 \mu\text{atm}$ at $p_a = 1120 \mu\text{atm}$, to 19.5 mmol m^{-3} at $p_a = 1120 \mu\text{atm}$.

The initial rise in the nonlinear contribution c_t when p_a increases from 280 to $840 \mu\text{atm}$ (reflected in the increase in ΔF_b shown in Figure 5-1), corresponds to the rising values of dp^2/dC^2 (Figure 5-3). Within this range of p_a , the increasing curvature of $p(C)$ more than compensates for the decreasing variability in concentrations of dissolved inorganic carbon C . However, for p_a greater than $840 \mu\text{atm}$, dp^2/dC^2 stabilizes and eventually decreases (Figure 5-3), and the convexity of $p(C)$ can no longer compensate the decreasing variability in C . As a result, the nonlinear contribution c_t declines at high values of p_a (Figure 5-1).

The decline in c_t at high p_a may be limited to cold waters: in waters with typical global-ocean properties, dp^2/dC^2 continues to rise well beyond $840 \mu\text{atm}$ (Figure 5-3). Therefore, at the global scale, the values of ΔF_b are likely to continue to increase with p_a .

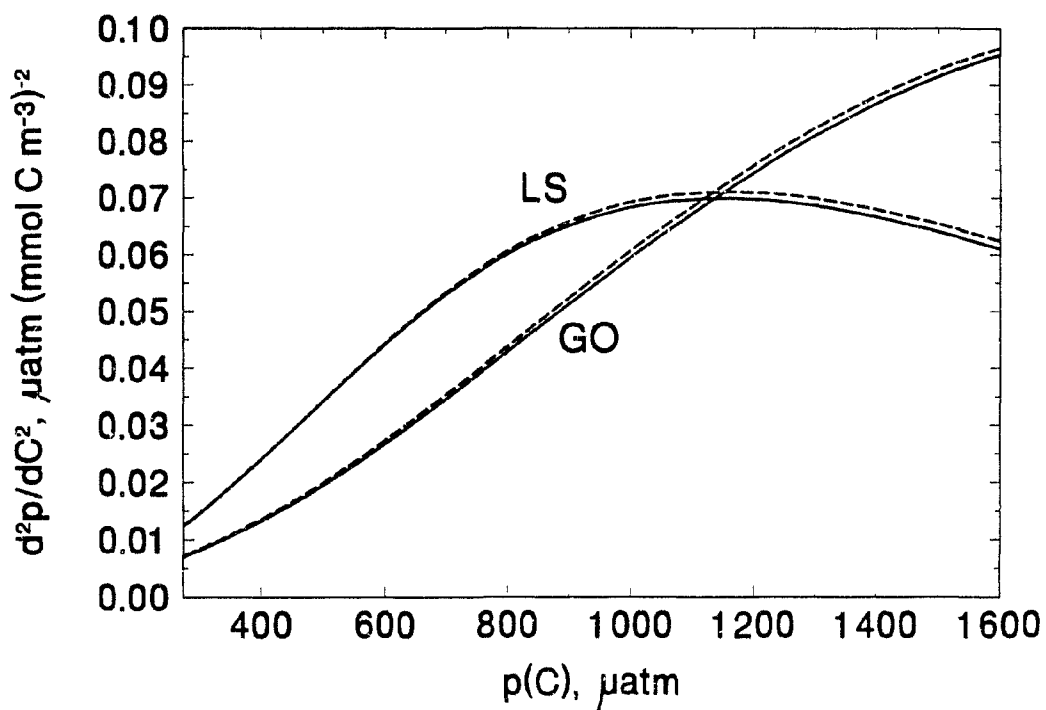


FIGURE 5-3. The second derivative of p with respect to C as function of $p(C)$, with T , S and A set at their average values for the Labrador Sea (LS) or the global ocean (GO). Note the good agreement between d^2p/dC^2 obtained using the carbonate dissociation constants of Mehrbach *et al.* [1973] (solid lines) and Goyet and Poisson [1989] (broken lines), while their respective $d^2p(T)/dT^2$ differ significantly as shown in Figure 2-1b.

Note also that the values of dp^2/dC^2 computed using the carbonate dissociation constants of *Goyet and Poisson* [1987] are in a close agreement with those computed using the dissociation constants of *Mehrbach et al.* [1973] (Figure 5-3). The conclusion from Chapter 4 that computations of p using the constants of *Goyet and Poisson* [1987] were almost as susceptible to the nonlinear errors as the computations using the constants of *Mehrbach et al.* [1973] (provided the variability in seawater temperature is small) seems to be applicable to the future environments as well.

5.3.3 Air-sea fluxes of CO₂ at 968 μatm

Next I examined the sensitivity of the covariance and the nonlinearity terms to the assumptions made regarding the mean fluxes in the high-CO₂ environments. For this purpose, I ran the model with the deep-layer carbon concentration (C_3) adjusted to reproduce the estimate of the annual mean flux \bar{F} obtained by *Maier-Reimer* [1991] from 3-D model simulations, and compared the new estimates of ΔF_a and ΔF_b with those obtained using the assumption of constant \bar{F} , which was presented in the previous subsection.

The model of *Maier-Reimer* predicts the evolution of p_a and \bar{F} associated with the “business-as-usual” CO₂-emission scenario (emission increases by 1.5% per year). According to this model, p_a would rise to 968 μatm in year 2100. From Figure 8 in *Maier-Reimer* [1991] one can roughly estimate that the increase in \bar{F} by year 2100 over the present-day value would be about $2 \text{ mol C m}^{-2} \text{ yr}^{-1}$:

$$\bar{F}(2100) = \bar{F}_{968} \approx \bar{F}_{335} + 2 \text{ mol C m}^{-2} \text{ yr}^{-1}. \quad (5-1)$$

With \bar{F}_{968} fixed at the value given by equation (5-1), the calculated ΔF_a and ΔF_b turn out to be -4.5 and $-1.7 \text{ mol CO}_2 \text{ m}^{-2} \text{ yr}^{-1}$, respectively (Figure 5-1). These answers are remarkably similar to the results obtained when the $2 \text{ mol CO}_2 \text{ m}^{-2} \text{ yr}^{-1}$ increase in \bar{F} over the present-day values were neglected: the differences were only -0.05 and $0.04 \text{ mmol m}^{-2} \text{ yr}^{-1}$ (or 1% and 2%), respectively (see also Figure

5-1). These results suggest that ΔF_a and ΔF_b are not sensitive to changes in \bar{F} (and the total inventory of dissolved inorganic carbon) and the simplifying assumption on the future values of \bar{F} used in this work does not introduce any appreciable errors.

5.3.4 Preindustrial fluxes of CO₂

The analysis of the evolution of the covariance term ΔF_a and the nonlinearity term ΔF_b with p_a can be also extended in the other direction – from the present-day to preindustrial values. Again using the results of the 3-D model of *Maier-Reimer* [1991] (his Figure 6), I inferred the present-day value of anthropogenic flux in the Labrador Sea to be about 0.8 mol CO₂ m⁻² yr⁻¹. This value is consistent with my estimates of the uptake of atmospheric CO₂ by the top 1430 m of the Labrador Sea: to maintain \bar{F} at the present level, the total inventory of inorganic carbon in the top 1430 m of the water column should increase each year by 0.6–0.9 mol CO₂ m⁻² yr⁻¹ to match the rise in p_a , assumed to be 1–1.5 μatm per year the early 1980s.

After adjusting C_3 so that $\bar{F}_{280} = \bar{F}_{335} - 0.8 \text{ mol C m}^{-2} \text{ yr}^{-1}$, I computed the preindustrial values of ΔF_a and ΔF_b to be -1.2 and -0.8 mol CO₂ m⁻² yr⁻¹, respectively. These magnitudes are smaller than those at $p_a = 335 \text{ μatm}$, which fits well (see Figure 5-1) the trend established previously.

5.3.5 Effect of partitioning of the oceanic properties into seasons

Under the present-day atmospheric concentration of CO₂, partition of the simulated variables of the Labrador Sea into warm and cold seasons removed most of the potential errors associated with neglecting the covariance between K and Δp and the nonlinearity of the carbonate system (Chapter 3). I tested whether this would also be the case in CO₂-rich environments.

When the daily variables obtained for the Labrador Sea at $p_a = 840 \text{ μatm}$ were divided into the November–April and the May–October seasons, the annual sums of

seasonal values of ΔF_a and ΔF_b were about one third of the values of ΔF_a and ΔF_b obtained from a single annual dataset (Figure 5-1). Therefore, the recommendation on the division of the annual data sets into at least two seasons, made in Chapter 3, is valid for the future as well.

5.4 Sensitivity of future fluxes of CO₂ to biogeochemical processes

In an environment with high values of the partial pressure of CO₂ one may expect a different sensitivity of the CO₂ fluxes to changes in the physical or biogeochemical processes. Modifications in temperature or the composition of the seawater in the CO₂-rich environment may cause larger fluctuations in the partial pressure of CO₂ than at present.

To explore this point, I repeated some of the previous calculations (section 4.4) of the 50-year evolution of the CO₂ fluxes following hypothetical modifications in the photosynthesis parameters for high p_a . The consequences of an increase in P_m^{chl} and α^{chl} by 50% at $p_a = 840 \mu\text{atm}$ are shown in Figure 5-4.

Both the no-export case (line *1c*) and the export case (line *1d*) were simulated (for definitions of the cases see section 4.4). The computed values were compared with the corresponding cases *1a* and *1b* computed at $p_a = 335 \mu\text{atm}$. Two observations can be made:

1. At $p_a = 840 \mu\text{atm}$, a given modification in primary production would change \bar{F} initially, as in the case for $p_a = 335 \mu\text{atm}$. However, the first-year departure in \bar{F} from the pre-alteration value for $p_a = 840 \mu\text{atm}$ was twice the magnitude of the first-year departure at $p_a = 335 \mu\text{atm}$.
2. The approach to the new-steady state in the years following the initial departure would be faster in the CO₂-rich environments.

Both these effects can be traced to the properties of the carbonate system: a given change in C causes larger changes in p in the CO₂-rich environment (as

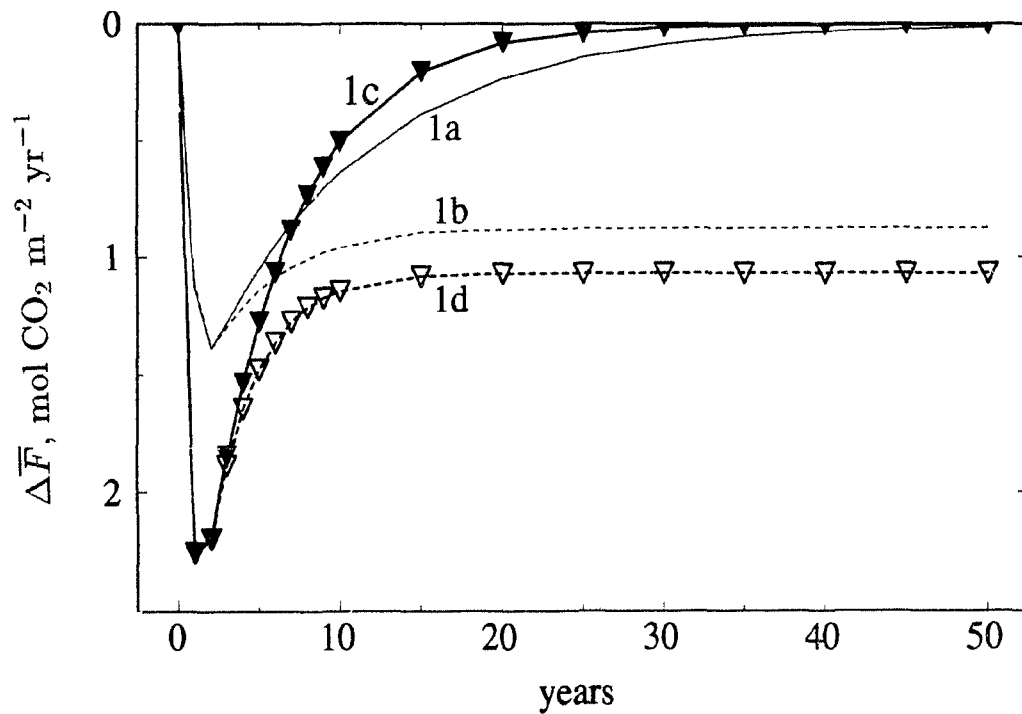


FIGURE 5-4. Evolution of the air-sea fluxes of CO_2 following hypothetical increase in α^{chl} and P_m^{chl} by 50% throughout the simulation for the partial pressure of atmospheric CO_2 (p_a) of $840 \mu\text{atm}$. $\Delta\bar{F}$ denotes the departure from the mean air-sea fluxes of CO_2 (\bar{F}) computed using the standard values of α^{chl} and P_m^{chl} : 1c is the case without exchanges with adjacent water; 1d is the case including the effect of the exchanges. For comparison, the corresponding cases 1a and 1b from Figure 4-5, computed under $p_a = 335 \mu\text{atm}$, are also shown. Positive values of $\Delta\bar{F}$ indicate additional uptake of CO_2 by the ocean.

dp/dC increases with C). Larger changes in p translate into larger changes in the CO_2 fluxes. Therefore, the first-year departure in \bar{F} is stronger. On the other hand, as more CO_2 is drawn into the water, the partial pressure of CO_2 approaches the levels corresponding to a new steady state more quickly.

These results indicate that the nature of interannual-to-interdecadal fluctuations in the air-sea fluxes of CO_2 may change in the future: the fluctuations are likely to become larger in magnitude and shorter in duration.

The new-steady states approached by the system at different p_a can be different as well. For instance, in the export case, the difference between the new steady-state annual uptake of CO_2 and the pre-alteration value, $\Delta F(\infty)$, is equal to $+1.1 \text{ mol C m}^{-2} \text{ yr}^{-1}$ at $p_a = 840 \mu\text{atm}$, compared with $\Delta F(\infty) = +0.9 \text{ mol C m}^{-2} \text{ yr}^{-1}$ at $p_a = 335 \mu\text{atm}$ (Figure 5-4). The reason for this change is that the enhanced primary production causes a deeper depression in p_1 at higher p_a , which allows more CO_2 to be taken up from the atmosphere in late spring and summer, despite relatively low K . In other words, in the CO_2 -rich environment, the same increase in formation of organic carbon translates into a stronger fluxes of CO_2 from the atmosphere. The same will be true for alterations in other biogeochemical or physical processes.

5.5 Some consequences for carbon modelling

The results of this work indicate that the effects of the fluctuations in the properties controlling air-sea fluxes of CO_2 could potentially affect the accuracy of carbon models and the empirical formulations of the gas-exchange coefficients.

5.5.1 Calibration by tracers

Carbon models have limited temporal and spatial resolution and therefore do not account explicitly for the effects of fluctuations at scales below the model resolution. One might argue, however, that these effects are accounted for implicitly, through calibration of the exchange coefficients for CO_2 between the atmosphere

and the ocean with tracer data. The distribution of a tracer reflects the actual fluxes of this tracer into the ocean and might, in theory, account for the effects of the fluctuations in oceanic properties.

However, there are several problems with such an argument. Let us first consider the tracers other than carbon isotopes, such as ^3H , CFCs, radon, or argon. The distributions of these tracers may account for covariance between the tracer transfer coefficient and air-sea differences in tracer concentration, but this covariance is not likely to be the same as the corresponding covariance term for CO_2 . Besides, the nonlinear term discussed here is specific to the nonlinear dependence of the partial pressure of CO_2 on several seawater properties. The study of non-carbon tracers would not throw any light on this consequence of the nonlinearity of the carbonate system.

Even the exchange of carbon radioisotopes across the air-sea interface may not reflect all mechanisms determining the exchange of ^{12}C . The net flux of ^{14}C into the ocean per unit area, ^{14}F , can be expressed as the difference between the invasion and the evasion fluxes:

$$^{14}F = K p_a \mathcal{R}_a - K p_m \mathcal{R}_m, \quad (5-2)$$

where K is the gas-transfer coefficient of CO_2 , p is the partial pressure of CO_2 , \mathcal{R} is the isotopic ratio ^{14}C to ^{12}C , and subscripts a and m denote the atmosphere and oceanic mixed layer respectively.

Note that the covariance and the carbonate nonlinearity terms affect primarily the evasion fluxes ($= K p_m \mathcal{R}_m$). On the other hand, the invasion fluxes ($= K p_a \mathcal{R}_a$) are practically unaffected by these terms. Since p_a does not vary much in space or in time, within a year, the covariance between K and p_a is likely to be small and to have a negligible effect on the CO_2 fluxes. The nonlinearity of the seawater carbonate system does not affect directly the invasion flux either.

In the case of the bomb ^{14}C , produced by atmospheric nuclear testing in the late 1950s and early 1960s, the values of \mathcal{R}_m are much lower than those of \mathcal{R}_a , since the ratio of bomb ^{14}C to ^{12}C is much higher in the atmosphere than in the oceanic

mixed layer. Therefore, the net flux of bomb ^{14}C is dominated by the invasion flux. Since the invasion flux is not affected by covariance between K and p_m or by the nonlinearity of the carbonate system of seawater, the CO_2 exchange coefficients computed from the oceanic inventory of bomb ^{14}C measured by the GEOSECS program [Broecker, 1985] do not reflect well these effects either.

On the other hand, for the natural ^{14}C , values of the invasion and the evasion fluxes are of similar magnitude: the natural ^{14}C to ^{12}C ratio in the mixed layer is about 95% of that in the atmosphere ($\mathcal{R}_m \approx 0.95\mathcal{R}_a$). Consequently, the air-sea gas exchange coefficients derived from the observed distribution of the natural ^{14}C would account for most of the effects of the covariance and carbonate nonlinearity (during the pre-industrial period over which natural ^{14}C was being taken up by the ocean).

However, one should exercise caution when results from studies of natural ^{14}C are extrapolated to situations other than the pre-industrial state. Results of this work indicate that the covariance and the nonlinearity terms may change with changes in oceanic processes and with changes in the atmospheric concentrations of CO_2 . The former effect is particularly relevant to diagnostic models, and the latter to transient models.

5.5.2 Diagnostic models

By their very nature, diagnostic models have to vary physical and biogeochemical processes to achieve their objective of examining the relative importance of various oceanic processes to the carbon cycle. However, as these processes are varied, values of ΔF_a and ΔF_b are likely to change as well, and such changes may influence the results of the simulations.

For instance, some diagnostic models were used to evaluate the sensitivity of the global carbon cycle to changes in the supply or uptake of nutrients (and associated inorganic carbon) in high-latitude waters [e.g., Knox and McElroy, 1984]. In the standard case, the nutrient concentration in the high-latitude box was set at the

present-day annual mean values. In the modified cases, the nutrient concentration in the high-latitude box was set to zero to reflect one of two cases

- a) no mixing with deep waters, or
- b) biological removal of nutrients at its maximum efficiency.

Changing patterns of physical and biological processes in high-latitudes changes ΔF_a and ΔF_b as well (as seen in Chapter 4). Therefore the differences between the standard and modified cases depend not only on the differences in the fluxes associated with mean properties (as computed by these models), but also on the differences in the respective values of ΔF_a and ΔF_b . To quantify these effects one would have to run a diagnostic model, which is beyond the scope of this thesis.

If diagnostic models simulate conditions at various p_a , ΔF_a and ΔF_b could be influenced not only by alterations in the processes causing temporal variability in oceanic properties, but also by changes in p_a . In the example discussed above, the lower concentrations of nutrients (and inorganic carbon) in the high-latitude box may lead to lower p_a [Knox and McElroy, 1984]. This would additionally reduce the magnitudes of ΔF_a and ΔF_b . Still, in most diagnostic models, changes in p_a would play a secondary role to changes in the oceanic processes, unlike in transient models, where this situation is reversed.

5.5.3 Transient carbon models

Transient carbon models typically use physical and biological processes at their present-day rates to simulate the evolution of the carbon cycle over a wide range of atmospheric partial pressure of CO_2 . Variabilities at time-scales less than one year are typically neglected. Even if the exchanges between the model reservoirs were calibrated with the natural ^{14}C , the effects of ΔF_a and ΔF_b would be accounted for only at their preindustrial levels. Results presented in this chapter indicate that ΔF_a and ΔF_b associated with these intra-annual variabilities increase strongly with

p_a . Therefore, when future environments are modelled, the preindustrial calibration may no longer be valid.

The situation may further complicate if some biological or physical processes in the transient models are altered in the future, as in the case of models of long-term effects of the iron-fertilization scheme [Peng and Broecker, 1991; Joos et al., 1991]. Iron fertilization would modify not only the mean values, but also the temporal variability in the properties of the Antarctic waters, and therefore, values ΔF_a and ΔF_b , at any given p_a .

5.6 Concluding remarks

With increasing partial pressure of CO_2 in the atmosphere (p_a), a given change in the composition of the surface waters is likely to result in a larger change in the seawater partial pressure of CO_2 (p_1). Consequently, in the CO_2 -rich environment, values of ΔF_a and ΔF_b , which depend on the variability in p_1 , would increase, even if the biological and physical processes remained unchanged.

In the future environments, interannual-to-interdecadal fluctuations in air-sea flux of CO_2 will be modified: a given change in a physical or biogeochemical process would cause a stronger initial perturbation, a shorter period of adjustment of the carbonate system and a different, new, steady-state CO_2 flux, when p_a are higher. Partitioning the annual cycle into at least two seasons is again recommended, because it would reduce some of the errors associated with neglecting ΔF_a and ΔF_b .

Estimates of the CO_2 exchanges between the ocean and the atmosphere, which are based on the uptake of tracers by the oceans, are subject to errors because they neglect, or inadequately account for, the covariance between K and Δp and for the nonlinearity of the carbonate system. This may introduce errors when the tracer-derived CO_2 gas-exchange coefficients are employed to compute carbon fluxes in diagnostic and transient carbon models.

Most of the lessons from this work, although derived for the Labrador Sea, should be applicable, at least to some extent, to other areas of the ocean: the

increase in the atmospheric concentration of CO_2 would probably increase ΔF_a and ΔF_v in other parts of the global ocean, even if the absolute magnitude of these terms, and the nature of variability in oceanic properties (for instance, spatial rather than temporal) were different.

Chapter 6.

Summary and Suggestions for Further Work

This thesis focused on the effects of spatial and temporal fluctuations in the seawater composition and in the air-sea gas-transfer coefficient on the fluxes of CO₂ between the ocean and the atmosphere. I also examined the sensitivity of various components of air-sea fluxes of CO₂ to physical and biogeochemical processes, using the Labrador Sea as a case study. This analysis was also extended to examine the future, CO₂-rich, conditions. The main results are summarized here and some directions for further work are indicated.

Summary

Air-sea fluxes of CO₂ are determined by the gas-transfer coefficient K and Δp , the difference in the partial pressure of CO₂ in the air (p_a) and surface ocean (p). In turn, the partial pressure of CO₂ in seawater is a nonlinear function of several seawater properties, such as temperature (T), salinity (S), concentration of dissolved inorganic carbon (C) and alkalinity (A).

The air-sea fluxes from a uniform ocean may be different from those from a nonuniform ocean with the same bulk properties. Fluxes in the nonuniform ocean are not only affected by the means, but also by fluctuations of the oceanic values. These fluctuations affect the fluxes through:

- 1) the covariance term, which is the difference between the mean flux and the flux computed from mean values of K and Δp .
- 2) the carbonate nonlinearity term, which is the difference between air-sea fluxes computed using mean values of p and the fluxes calculated using p computed from mean values of T , S , C and A .

I quantified the magnitude of the covariance and the nonlinearity terms, using oceanic spatial data (Chapter 2) and temporal simulations from a model of the Labrador Sea (Chapters 3, 4, and 5). Implications for direct estimates of air-sea fluxes of CO_2 from surface-ocean data and for carbon models were discussed.

Using the surface-ocean data averaged over global or annual scales to compute air-sea fluxes of CO_2 may lead to a systematic overestimation of these fluxes by amount comparable to, or larger than, the total estimated oceanic uptake of anthropogenic CO_2 . The value of the error is likely to increase strongly in the future, CO_2 -rich, environments.

This systematic error could, in principle, be eliminated if the average fluxes of CO_2 were computed directly from individually values of F (calculated as a product of paired measurements of K and Δp). However, when measurements of Δp are scarce (thus the number of paired observations of K and Δp is low) this approach was shown (Chapter 3) to be impractical, since it is subject to large random errors. For such situations, an alternative strategy was recommended. In this strategy the systematic error associated with averaging is reduced by partitioning the global and annual datasets into subsets representing high- and low-latitude waters, and warm and cold seasons, respectively.

Carbon models, which idealize the ocean as a set of internally-uniform boxes and use finite time-steps, may be subject to errors caused by neglecting fluctuations in oceanic properties below the spatial and temporal resolution of the models. Preliminary computations indicated that accounting for the present-day carbonate nonlinearity effects reduced the oceanic uptake computed by transient carbon models by 3%. In reality, this effect may be stronger, since in these computations the effects of nonlinearity associated with intra-annual variability, as well as the covariance effects, were not included. Moreover, it was shown (Chapter 5) that the covariance and the nonlinearity terms increase strongly with p_a . Therefore, carbon models simulating the future, CO_2 -rich, environments should attempt to reduce the errors caused by neglecting these terms. The results of this work indicate that most

of the errors would be removed if carbon models included a separate high-latitude box and used a time-step not longer than half-a-year, to represent cold and warm seasons.

Some general conclusions on the effect of the carbonate nonlinearity were reached:

- The standard deviation in p was found to be a good indicator of the magnitude of the carbonate nonlinearity effect, both in the data and in the model simulations (although this correlation may not hold when the nonlinearity effects from environments with very different levels of p_a are compared).
- The computations of the partial pressure of CO_2 using the dissociation constants of *Gouet and Poisson* [1989] were less sensitive to the nonlinear effects than those using the constants of *Mehrbach et al.* [1973], but only when the fluctuations in temperature were large.

I also explored the sensitivity of the CO_2 fluxes in high-latitude waters, associated with the mean and the fluctuating components of oceanic properties, to hypothetical changes in temporal patterns of physical and biogeochemical processes (Chapter 4).

The fluxes associated with the fluctuating components were not sensitive to most of these changes, suggesting that the estimates of the magnitude of the covariance and the carbonate nonlinearity terms made in this work are relatively robust.

The mean component of the CO_2 fluxes, on the other hand, was much more sensitive to changes in the modelled processes. Consequently, realistic changes in some of these processes (such as the timing of spring bloom, presence of deep winter convection or CaCO_3 production by marine organisms) may result in large changes in the calculated total annual fluxes of CO_2 , comparable to, or greater than, the total anthropogenic flux of CO_2 in this area.

This strong sensitivity of the CO_2 fluxes to various processes also indicates a potential for large inter-annual variations in these fluxes in high latitudes. Consequently, the CO_2 fluxes computed from observations from one or a few years (a

very common procedure, given very scant data coverage) may be unrepresentative of "typical" values of the fluxes of CO_2 in the area.

I examined the decadal-scale response of the CO_2 fluxes in high latitudes to hypothetical alterations in the primary production at higher values of p_a . In the future environments, the magnitude of the initial response to such an alteration will be larger, and the approach to the new equilibrium faster, than at present.

The results of the sensitivity analysis may also be used in the optimization of carbon models of high-latitude waters:

1. I identified the most important processes that should be carefully represented in such models: the spring photosynthesis efficiency and growth-independent respiration of phytoplankton, light attenuation in the water, presence or absence of deep winter convection and timing and magnitude of CaCO_3 production.
2. I suggest that an intermediate layer (separating the surface and the deep-ocean layers) be included in such models, given the sensitivity of air-sea fluxes of CO_2 to processes occurring in this layer.
3. I found that the CO_2 fluxes in the Labrador Sea, were not sensitive to a number of other processes. Therefore, simplified models, using single phytoplankton species with a constant C:N:chl ratio and a constant sinking velocity from the surface layer, a simplified zooplankton component, and approximate values of cloudiness, air-temperature and precipitation, should be suitable for simulating air-sea fluxes of CO_2 in the Labrador Sea and similar waters. Note, however, that these simplifications are only justified within the range of tested parameters. Besides, processes that have negligible effect of the annual fluxes of CO_2 could still be important when other elements of the carbon cycle (such as total primary production) are assessed.
4. Accounting for the day-to-day variability in the gas-transfer coefficient K does not seem crucial for estimating of the annual CO_2 fluxes, provided that proper proportionality constants relating K with windspeed are used.

The representativeness of the synoptic estimates of the oceanic uptake of anthropogenic CO_2 by *Tans et al.* [1990] was also tested. The results did not support

the criticism of these estimates based on the data selection scheme used by Tans *et al.*, at least for high-latitude waters.

Suggestions for Further Work

New questions have emerged from this study. The results presented here have also highlighted some problems not addressed in this thesis.

The Labrador Sea model can be further developed, for instance, by adding an oxygen component, which could be used to constrain primary production and remineralization processes (by testing the result of the model against relatively abundant measurements of oxygen concentration in the Labrador Sea).

Another clear direction for further work is evaluation of the effects of variability in oceanic properties in other regions of the oceans. The Labrador Sea model may be adapted for use in other waters, or its biogeochemical component can be coupled physical models previously developed for a given location. For instance, the biogeochemical component can be coupled with physical models of Antarctic waters including effects of ice formation (such as the Weddell Polynya model by *Martinson et al.* [1981]).

One may also apply the model to compute the temporal covariance and carbonate nonlinearity effects in warm waters (e.g., in the Sargasso Sea). Although the magnitudes of these effects per unit area are likely to be much smaller than in high latitudes, they may still translate into a substantial correction of the global CO₂ fluxes given the much larger area of warm waters. Besides, as indicated in the present work, the increase in the nonlinear contribution with p_a may be more pronounced in warm than in cold waters.

As mentioned, the effects of oceanic variability for diagnostic and transient models of carbon flux (e.g., the models containing separate high-latitude compartments, such as the model of *Knox and McElroy*, [1984], or the HILDA model of *Shaffer and Sarmiento* [1995]) merits careful consideration.

Another possible direction of future work is further exploration of the consequences of the day-to-day fluctuations in windspeed. In the present work it was shown that the accounting for the day-to-day changes in K , caused by the day-to-day changes in windspeed, had minor effect on the annual CO_2 fluxes, if an appropriate formula is used for the computation of K . However, other consequences of the day-to-day variability in windspeed, for instance, for the depth of the surface layer and for mixing with the intermediate layer, have not been addressed here.

During days with weak winds, the depth of effectively-mixed water may be only a fraction of the depth of the surface layer prescribed from long-term observations [Brainerd and Gregg, 1995]. This may affect air-sea fluxes of CO_2 directly or indirectly:

- directly, by limiting the volume of the water effectively in the contact with the atmosphere, thus causing faster reduction in Δp and consequently in air-sea fluxes of CO_2 ; and
- indirectly, by affecting the timing of the spring bloom.

To quantify the effect of temporary stratification as a function of frequency of storm events, one may modify the Labrador Sea model, by overlaying the short-term variations in the depth of the surface layer on the long-term trends in the surface-layer depth prescribed from climatological data. In the absence of frequent *in-situ* measurements, the day-to-day variations in the effective depth of the surface layer may be simulated by a mixed-layer model [e.g., Niiler and Kraus, 1977; Denman, 1973; Price et al., 1986].

Appendices

Appendix A: Sensitivity of the Estimates of the Spatial Nonlinear Effects to the Computational Procedure

When computing the effects of nonlinearity for the partial pressure of the surface ocean (see subsection 2.4.3). I employed the 10-region partition of the GEOSECS data from the depths 0-49 m, (as given by *Takahashi et al.* [1981b]) with area weights based on *Moiseev* [1971], and partial pressure of CO₂ calculated according to *Peng et al.* [1987]. To assess the sensitivity of my results to these assumptions. I repeated some of the computations altering the conditions of this scheme, one at a time.

Table A-1 shows how my estimates may be affected by alterations in this basic procedure. I present the results of the alterations for three models described in Table 2-2: models 1 and 2a, representing the most frequently-used box models and model 4, a likely upper limit of the horizontal resolution of simple carbon models.

Note that modifications of the procedure also change the reference value, which is the estimated global value of partial pressure in the nonuniform ocean (p_t). In each case the nonlinear error \mathbf{E} is calculated with respect to the corresponding p_t . I do not discuss at this point which value of p_t is most representative of the actual ocean but merely assess whether any of the modified procedures is less vulnerable to nonlinear errors.

In all cases one-box representations of the global ocean were more susceptible to the nonlinear error, and more sensitive to changes in the computational procedure, than the corresponding two-box or multi-box representations. All but one of the modifications yielded no substantial change in the nonlinear error.

Table A-1. Sensitivity of Global Estimates of Partial Pressure of CO₂ and the Nonlinear Error in Selected Model Representations

	i	ii	iii	iv	v	vi	vii	viii	ix
<i>Global Mean Partial Pressure (above 300 μatm) Directly Estimated From Data (p_t)</i>									
	35.9	33.6	25.5	21.9	32.9	33.9	32.9	34.6	32.2
<i>Global Mean Partial Pressure (above 300 μatm) Estimated From Models (p_e)</i>									
one-box model	25.0	23.2	16.6	17.7	23.9	24.1	20.4	24.2	20.7
two-box model*	31.1	29.0	21.6	18.8	28.8	30.1	28.5	29.9	26.5
ten-box model [†]	31.5	29.4	21.8	19.0	29.2	30.6	28.6	30.4	27.4
<i>Global Nonlinear Error ($E = p_t - p_e$)</i>									
one-box model	10.9	10.4	8.9	4.2	9.1	9.8	12.5	10.4	11.5
two-box model*	4.8	4.6	3.9	3.1	4.1	3.8	4.4	4.7	5.7
10-box model [†]	4.4	4.2	3.7	2.9	3.7	3.3	4.3	4.2	4.7

Column i contains the reference values extracted from Table 2-2, based on the 10-region partition of the GEOSECS data from the depths 0-49 m (following *Takahashi et al.* [1981b]), with area weights based on *Moisev* [1971] and partial pressure of CO₂ calculated according to *Peng et al.* [1987]. Columns ii-iv were obtained by modification of the algorithm of *Peng et al.*: ii, alkalinity was approximated as a sum of the carbonate, borate and water contributions; iii, alkalinity was approximated as a sum of the carbonate and borate contributions only; iv, carbonic acid dissociation constants of *Goyet and Poisson* [1989] were used. Columns v-ix were computed using an alternative data selection: v, values of *A*, *C*, *Si*, and *P* were standardized to salinity *S*=34.78; vi, the data from the depths 0-24 m were used only; vii, the 7-region partition of the data and area weights based on *Takahashi et al.* [1981a] were employed; viii, a station instead of a sample was the basis of calculation of regional averages of the seawater properties; ix, the Arctic region was added and the TTO data were included. All values are in microatmospheres.

* Here represented by model 2a from Table 2-2

[†] Except column vii, where the ten-box model is replaced by the seven-box one, and column ix, where the eleven-box model was used.

A.1 Alternative Algorithms of Calculations of Partial Pressure of CO₂

The only modification that resulted in substantially lower nonlinear error **E** (computed using equation 2-7b) was replacing the carbonic acid dissociation constants of *Mehrbach et al.* [1973] with those of *Goyet and Poisson* [1989].

Simplified formulations of the carbonate system that approximate total alkalinity as the sum of the carbonate, borate, and water contributions ($A = [\text{HCO}_3^-] + 2[\text{CO}_3^{2-}] + [\text{H}_4\text{BO}_4^-] + [\text{OH}^-] - [\text{H}^+]$), or as the sum of the carbonate and borate contribution only ($A = [\text{HCO}_3^-] + 2[\text{CO}_3^{2-}] + [\text{H}_4\text{BO}_4^-]$), were still prone to the nonlinear errors.

A2. Alternative Selection of the Data

Changing the procedure of selection of the data (described in subsection 2.2.1) did not strongly affect the estimates of the nonlinear error. First, I modified the values of *A*, *C*, *S_i*, and *P*, by standardization to the GEOSECS average oceanic salinity of 34.78 [*Takahashi et al.*, 1981a]. As standardization eliminates variations in salinity and reduces variability of alkalinity (which is determined mainly by the addition or removal of fresh water), one might expect weaker nonlinear effects. However, the temperature variations are unaffected. Also, since the concentration of *C* may be strongly influenced by processes other than the addition or removal of fresh water (mixing, gas exchange with the atmosphere, and biological activity), standardization to a constant salinity may actually increase variability of *C*. As a result, variability in *p* is only slightly reduced (as seen in Figure 2-4) and nonlinear errors are not substantially lower than in the nonstandardized case.

Next, I computed the nonlinear errors when observations from the depth range of 0-24 m only were used. Estimates of **E** were not altered substantially, suggesting that the influence of deep waters in the data from depths 0-49 m is weak.

Then, I considered a station as the basis of computations instead of a sample, i.e., all samples from a given station were averaged and a single value from each station was used in the computation. Although averaging of the observations obtained from different depths within a single location removed part of the data variability associated with differences in seawater within a station, it did not substantially reduce the nonlinear error, since the differences between different stations were still present.

Finally, an alternative scheme for defining regions was examined. Instead of using the 10-box partition of *Takahashi et al.* [1981b], I partitioned the GEOSECS data after *Takahashi et al.* [1981a] into seven boxes. Each ocean was divided at the equator into a northern and a southern part, and all data south of 45°S were pooled into an Antarctic region. The computations using this set of regions yielded similar values of \mathbf{E} for the two-box and multibox representations, and somewhat larger \mathbf{E} for the single-box representation.

A.3 The Effect of Incorporation of the TTO Data

I assessed the effect of supplementing the GEOSECS data with those from the TTO cruises (subsection 2.2.2). To this point I had not combined these data sets because of methodological differences (for instance, the need of correction of the GEOSECS titration data discussed by *Takahashi et al.* [1981a]) and the time gap between these sampling programs. I made an exception to evaluate how the estimates of the nonlinear error at global scale would change, if the data coverage was extended in the North Atlantic beyond 36°N. I expanded the range of the North Atlantic region from 10°-36°N to 10°-50°N and assigned it an area weight of 9.3%. I also added an eleventh region representing ice-free Arctic waters with area weight of 4.9%. This weight was obtained assuming the Arctic sea ice in its minimal range covers $8 \times 10^{12} \text{ m}^2$ [*Parkinson et al.*, 1987]. The weights of the remaining nine regions were proportionately reduced.

Assuming that the TTO data from latitudes 50°-80°N and 15°-50°N are representative of the Arctic and the North Atlantic region, respectively, I computed the nonlinear errors using those values and the properties of the remaining nine regions based on the GEOSECS data. I also calculated the nonlinear errors after supplementing the GEOSECS data with the TTO observations. As expected, the addition of the Arctic data, with properties strongly differing from the low-latitude waters, increased the variability of the seawater properties and the nonlinear error in models that pool the high-latitude data with those from low-latitudes into single boxes (models 1, 2b, and 2c). The nonlinear error increased even in the case of the remaining models which isolate the high-latitude waters from the rest of the ocean. As the properties of the Arctic region differ from properties of the Antarctic region, pooling together data from these regions into a single high-latitude box (models 2a and 3) increases the nonlinear contribution in this box to 7.3 μatm , more than doubling the value computed for this box when only the GEOSECS Antarctic data were used.

Appendix B: Computation of Vertical Exchanges and the Surface-Layer Temperatures in the Labrador Sea

The vertical exchanges of water between the three oceanic layers and the annual cycles of surface water temperature were obtained by balancing the budgets of temperature and salinity in the Labrador Sea, which were computed using the approach of *Ikeda* [1987] with some modifications. The computational procedure was summarized in section 3.3.2 (Chapter 3). The properties of the horizontally mixed waters, justifications for the modifications of the *Ikeda* model, and results of the fitting procedure are described here.

B.1 Properties of the horizontally-mixed waters

The horizontal exchanges of temperature T and salinity S were calculated according to *Ikeda* [1987]. In this approach (see also section 3.3) atmospheric forcing and the properties of waters adjacent to the Labrador Sea are prescribed; vertical diffusive mixing between the modelled layers of the Labrador Sea is then adjusted until the annual cycles of temperature and salinity meet prescribed criteria.

The properties of the adjacent waters, used in these calculations, are summarized in Table B-1. In this table, LC2 denotes the cold and low salinity water from the Labrador shelf and the West Greenland Current, delivered to layers 1 and 2 in the model, with the volume of input to each layer per unit time being proportional to the thickness of the layer.

Another cold and low salinity water affecting the Labrador Sea is denoted as LC1. The input of this water, formed as a result of the melting of Arctic ice and the outflow of fresher water from the Hudson Bay, affects mainly the surface layer and occurs seasonally. Therefore, it was assumed in the model that this water enters only layer 1, between April and October (with the October flow being half the volume of flow during the other months).

Table B-1. Temperatures and salinities of the waters adjacent to the Labrador Sea (based on *Ikeda* [1987]).

Waters	Layer Affected	Temperature	Salinity
LC1	1	$T_1 - 4 (\pm 0.5) ^\circ\text{C}$	32.5 (± 0.25)
LC2	1, 2	$T_i - 4 (\pm 0.5) ^\circ\text{C}$	33.0 (± 0.25)
NC	1, 2	$T_i + 6 (\pm 0.5) ^\circ\text{C}$	35.1 (± 0.10)
IC	3	4.5 (± 0.5) $^\circ\text{C}$	35.1 (± 0.10)

The top two layers also receive warm, saline waters from the North Atlantic Current and the upper part of the Irminger Current. The input of this water, denoted as NC, was divided between the top two layers in proportion to their thicknesses. Finally, layer 3 is affected by the horizontal exchanges with the core of the Irminger Current (IC).

The effect of the horizontal mixing on the properties of the Labrador Sea water column were calculated by dividing the inputs of the adjacent waters by the area of the open Labrador Sea (with depths over 1000 m), which was assumed to be $0.86 \times 10^{12} \text{ m}^2$ [Ikeda, 1987].

B.2 Modifications of the model of Ikeda

The modifications to the Ikeda approach include an altered vertical structure (i.e., a variable surface-layer depth and the omission of the bottom-water layer), a different specification of the upper limit of the eddy diffusivity and modified initial conditions, atmospheric inputs, fitting criteria and the computational time-step.

B.2.1 Variable depth of the surface layer

The depth of the surface-layer in this model was allowed to vary, because fixing the surface layer depth at 30 m throughout the year as in Ikeda [1987] was inadequate for the modelling of the biological productivity in the Labrador Sea. For example, the average light in a 30-m layer would be higher than that in a deeper mixed layer in spring. I found that, in this model, a 30-m surface layer would lead to the development of a bloom in mid-April, which is at least one month earlier than that expected from the monthly composites of the CZCS images [Feldman *et al.*, 1989] or from the nutrient and chlorophyll data [Irwin *et al.*, 1983, 1984, 1986], or from the timing of blooms at other locations of comparable latitudes [Takahashi *et al.*, 1993].

B.2.2 Omission of the bottom layer

The bottom-waters, represented in the Ikeda model as a layer of thickness 1800 m directly below layer 3, was omitted in the present model in the interest of simplicity. This omission is not likely to affect the values of the properties affecting the air-sea fluxes of CO₂ in the upper three layers, which are of main interest here, as the mixing between layer 3 and the bottom layer in the model of *Ikeda* [1987] was very weak and the properties of these two layers were similar.

B.2.3 Upper limit of the vertical eddy diffusivity

When the difference in density ρ is very small, the values of d_i , the vertical eddy diffusivity at the bottom of the i th layer, could become unreasonably high. To avoid this, the maximum value of d_i was set here at $864 \text{ m}^2 \text{ d}^{-1} = 1 \times 10^{-2} \text{ m}^2 \text{ s}^{-1}$, for all layers, corresponding to the diffusivity in a non-stratified ocean [*Munk and Anderson*, 1948]. This limit is slightly different from that used by *Ikeda* [1987], who assumed that when the density difference falls below 0.05 kg m^{-3} , $d_i = L_i \times 0.05^{-1.5} \text{ m}^2 \text{ s}^{-1}$ (where L_i , is the proportionality constant linking the difference in density with the diffusivity). This assumption is equivalent to the one used here only when L_i is equal $1.1 \times 10^{-4} \text{ m}^2 \text{ s}^{-1} (\text{kg m}^{-3})^{1.5}$.

I modified the upper limit because assuming a single maximum diffusivity, corresponding to that of a non-stratified ocean, seems to be more realistic than the situation in which, by adjusting L_i to fit the temperature and salinity criteria for summer, one also alters the maximum diffusivity in winter.

B.2.4 Initial conditions, atmospheric forcing, fitting criteria and computational time-step

The initial values of seawater temperatures, as well as the annual cycle of air temperature were changed to be more consistent with the long-term data of *Lazier and Hackett* [1986] and *Smith and Dobson* [1984], respectively.

The fitting criteria constraining inter-annual variabilities in T and S were modified here as well. The present model approximates the inter-annual steady state, which requires temperatures and salinities to change little between consecutive years of simulation, while the original model of Ikeda attempted to reproduce the inter-annual trends in T and S observed during the periods 1964–1967 and 1968–71.

To be consistent with the time-step used to model the biogeochemical variables, the time-step used in the computation of T and S was one day, instead of the 5-day time-step used by Ikeda. The time-step difference would mainly affect the frequency of the shallow overturnings, which are simulated at the end of each time-step if the density of layer 1 is greater than the density of layer 2. In winter, a shorter time-step implies more frequent shallow overturnings between the top two layers. However, since the properties of the top two layers after the first overturning become quite similar to each other, the difference in frequency of the following overturnings do not affect the budgets of T and S strongly.

B.3 Results of the fitting procedure

Results of fitting the proportionality coefficients L_i and the horizontal water inputs are given in Table B-2. Using these parameters allowed the simulation of temperature and salinity cycles with low inter-annual variabilities, as expected for a steady-state situation. These parameters also reproduce well the observed summer differences in temperature and salinity between the top two layers computed from the Labrador Sea data of *Lazier and Hackett* [1986]. For a comparison, the parameter values fitted by *Ikeda* [1987] are also shown (Table B-3).

Table B-2. Fitted parameters of the present model and model of *Ikeda* [1987].

Parameter	This work	<i>Ikeda</i> [1987]
$L_{12} [\times 10^{-4}]$	0.83	0.9
$L_{23} [\times 10^{-4}]$	0.50	1.1
LC1 [Sv]	0.57	0.4-0.8
LC2 [Sv]	0.23	0.3-0.8
NC [Sv]	0.55	1.3-1.5
IC [Sv]	4.2	3.0

Table B-3. Inter-annual and annual variabilities in temperature T [$^{\circ}\text{C}$] and salinity S obtained by applying the parameters from Table B-2.

Inter-annual variabilities:			
ΔT_1	-0.0002	ΔS_1	0.0001
ΔT_2	-0.0002	ΔS_2	0.0001
ΔT_3	-0.0002	ΔS_3	- 0.0050
Annual variabilities:			
$T_1 - T_2$ (31 Aug.)	3.89 (3.95)	$S_2 - S_1$ (30 Sept.)	0.31 (0.34)

The inter-annual variabilities (ΔT and ΔS) were measured as differences in T and S in each of the three layers on February 1 of two consecutive years of simulation. The modelling approximates the inter-annual steady state. The annual variabilities are measured as differences between the top two layers in T in S at the end of summer (following *Ikeda* [1987]). The corresponding values of the annual variabilities in T and S computed from the data from the Ocean Weather Station Bravo [*Lazier and Hackett*, 1986] are given in the parentheses.

Appendix C: Details of biogeochemical components of the model of the Labrador Sea

A general description of the biogeochemical variables was given in section 3.3 (Chapter 3). Here only details of the computation and justifications for the assumptions made in the model are presented.

C.1 Zooplankton

Changes in zooplankton concentration depend on gross growth and losses, which determine net growth of zooplankton within a layer, and on migrations of zooplankton between layers. These processes, and the parameters describing them, are reported to vary widely in the natural environment. Therefore, the main concern in the selection of particular values of the parameters was that they be within the reported range from the literature and that the zooplankton biomass computed using these parameters be of a similar order of magnitude as the biomass reported for high latitudes of the North Atlantic. *Longhurst and Williams* [1993] observed the zooplankton biomass near Iceland between 80 (winter) and 345 (summer) mg C m⁻².

C.1.1. Gross growth rate

The gross growth rate of zooplankton is the product of grazing rate g , expressed in d⁻¹, and dimensionless assimilation efficiency a . The grazing rate depends on the concentration of prey: grazing is assumed to take place only above the threshold prey concentration B_o , and the dependence of grazing rate on concentration of food is described by:

$$dg/dB = \Lambda(g_m - g),$$

where g_m is the maximum daily ration, and Λ is the proportionality constant (the Ivlev parameter). Integrated, this equation gives

$$g = g_m \left[1 - \exp(-\Lambda(B - B_o)) \right]. \quad (\text{C} - 1)$$

A wide range of values has been reported in the literature [*Parsons et al.*, 1984] for the parameters describing grazing: g_m : 0.01–0.6 d⁻¹, Λ : 0.024–2.4 (mmol C m⁻³)⁻¹, and B_o : 0–11 mmol C m⁻³. The assimilation efficiency a was generally reported to be 0.60–0.95 [*Conover*, 1968] (although for some zooplankton a could be as low as 0.10–0.20 [*Parsons et al.*, 1984]).

The standard version of the model uses $g_m = 0.5$ d⁻¹, $\Lambda = 0.07$ m³ (mmol C m⁻³)⁻¹, $B_o = 0.66$ mmol C m⁻³ and $a = 0.75$, following the values used by *Wroblewski et al.* [1988] in their model of the North Atlantic plankton.

C.1.2 Loss rate

The specific loss rate for zooplankton m , expressed in d⁻¹, is difficult to determine as it encompasses losses due to various processes, such as respiration, excretion and mortality. The largest mortality rate was assigned to the zooplankton in layer 1 ($m_1 = 0.30$ d⁻¹), because of higher rates of metabolism (stimulated by higher temperatures and active feeding) and possible larger losses to predation (predators may be more efficient in locating the prey because of higher concentrations of zooplankton in the layer and good illumination). The loss term in layer 2 is somewhat smaller ($m_2 = 0.25$ d⁻¹) given lower temperatures and less light in this layer. Finally, the loss rate in layer 3 is assumed to be very small ($m_3 = 0.01$ d⁻¹) to reflect low metabolic losses, possible because of low temperatures, little energy spent on grazing [*Conover*, 1962] and zooplankton physiology being in the state of diapause [*Longhurst et al.*, 1989; *Vinogradov*, 1968]. Furthermore, losses to predation are likely to be much lower, because of darkness and low zooplankton concentrations.

C.1.3 Migrations

The zooplankton concentration is affected not only by the balance between the growth and the loss terms, but also by vertical migration. Most of the ecosystem models assume either no vertical migration, or migrations within the surface layer. For instance, *Sarmiento et al.* [1993] neglect movement of zooplankton by treating

it as a non-motile tracer, passively transferred between layers through the water mixing. Other models, such as those of *Evans and Parslow* [1985], or *Fasham et al.* [1990], assume that zooplankton actively maintains itself within the layer in which phytoplankton growth takes place. Therefore, vertical migrations in these models are limited to the surface layer.

However, observations in the high-latitude North Atlantic indicate that vertical migrations of zooplankton are not limited to surface waters. Calanids, the main component of zooplankton in the Labrador Sea, undertake large migrations associated with their developmental cycle: after overwintering at depths, zooplankton ascends to the surface, grazes on phytoplankton and gradually descends to deep waters [*Conover*, 1976; *Longhurst et al.*, 1989].

In the present model these ontogenic migrations are represented by allowing zooplankton, after overwintering in layer 3, to migrate to the upper layers, when the net growth rate ($ag - m$) in these layers exceeds those in layer 3. The gradual descent occurring later in the season is then represented as a migration of a fixed fraction of zooplankton per day, which is arbitrarily set at 0.04 d^{-1} .

Daily migrations are not represented in the model. Although *Vinogradov* [1968] reports migrations of older stages of *Calanus finmarchicus* in autumn in several regions of the North Atlantic, in general, daily migrations in high latitudes are deemed unimportant or nonexistent [*Longhurst et al.*, 1989].

C.2 Phytoplankton

C.2.1 Gross Growth Rate

The phytoplankton gross growth rate is computed from daily production of phytoplankton within a layer (P_T), divided by the depth of the layer and concentration of phytoplankton within the layer (eq. 3-10 in subsection 3.3.3). The daily production depends on the amount of light available for photosynthesis and on other limiting factors.

Light limitation: The daily phytoplankton productions in layers 1 and 2 were computed as a function of noon irradiance following *Platt et al.* [1990] and *Platt and Sathyendranath* [1991], who integrated phytoplankton production analytically over an arbitrary layer and over the day, assuming a vertically-uniform distribution of biomass, and approximated the solution by a fifth-order polynomial to within 0.5% .

The attenuation coefficient for photosynthetically active radiation \mathcal{K} , appearing in this solution, was computed following *Sathyendranath and Platt* [1988]:

$$\mathcal{K} = \mathcal{K}_w + \mathcal{K}_{chl} [12 \times B/\theta] + \mathcal{K}_x, \quad (\text{C} - 2)$$

where \mathcal{K}_w denotes the attenuation coefficient of pure seawater, expressed in m^{-1} , \mathcal{K}_{chl} is the chlorophyll-specific coefficient of attenuation of phytoplankton and co-varying substances (expressed in $(\text{mg chl m}^{-3})^{-1}$), biomass B is converted from mmol C m^{-3} to mg chl m^{-3} by multiplication by the molecular weight of carbon (12) and by division by the carbon-to-chlorophyll ratio θ , and \mathcal{K}_x , expressed in m^{-1} , describes the attenuation caused by all other substances. As the model is run for a location away from the coast, the contribution of the other substances should be negligible, hence $\mathcal{K}_x \approx 0$. After *Sathyendranath and Platt* [1988] it was assumed that \mathcal{K}_w is 0.06 m^{-1} and \mathcal{K}_{chl} $0.023 \text{ m}^{-1} (\text{mg chl m}^{-3})^{-1}$.

Limitations by other factors – justification of the implicit approach: The limitation of the daily phytoplankton production by factors other than light can be represented using one of two approaches. In the explicit approach the phytoplankton production at a given irradiance is reduced by additional limiting factors, usually according to the Michaelis–Menten kinetics (as in models of *Evans and Parslow* [1985], *Fasham et al.* [1990], and *Taylor et al.*, [1991]). This approach has some limitations. First, only a few functional dependencies can be represented in the model. In *Evans and Parslow* [1985] and in *Fasham et al.* [1990] nutrients are the only other limiting factor in addition to light; in *Taylor et al.* [1991] growth rate is

influenced additionally by temperature. All other factors, such as the light history and changes in taxonomic composition, are neglected.

In the available data from the Labrador Sea no strong correlation between the photosynthesis parameters and amount of nutrients or temperature (Figure C-1) could be found, which indicates that for the most of the year phytoplankton production in this area, or at least its chlorophyll-normalized component, may be strongly affected by a combination of other factors.

The lack of correlation between P_m^{chl} and temperature differs from the findings of *Harrison and Platt* [1980] in temperate waters of Bedford Basin, a small inlet on the coast of Nova Scotia, south of the Labrador Sea, where temperature was the most important co-variate of P_m^{chl} . The difference may be caused by more than two times smaller range of temperature in the Labrador Sea, making any possible relation with temperature more "noisy", and the origin of samples, from much larger, thus less homogenous, area.

Second, there are potential errors in the parameters used to define the relationship between the photosynthesis and the limiting factors. The maximum growth rate, the half-saturation constant of nutrients, and the temperature quotient (used to describe the effect of temperature by *Taylor et al.* [1991]) are derived mainly on the basis of a limited number of laboratory experiments, and their applicability to the natural phytoplankton communities is doubtful. For instance, *Harrison et al.* [1995, in press], in their recent study, found the half-saturation constants for nitrate and ammonia to be one order of magnitude lower than those typically used in ecosystem modeling.

Therefore, I use an alternative approach in which all growth constraints other than light are dealt with implicitly by using the *in situ* measured photosynthesis parameters: the assimilation number (P_m^{chl}) and the initial slope of the photosynthesis-irradiance curve (α^{chl}), and by the prescribed values of the carbon-to-chlorophyll ratio (θ).

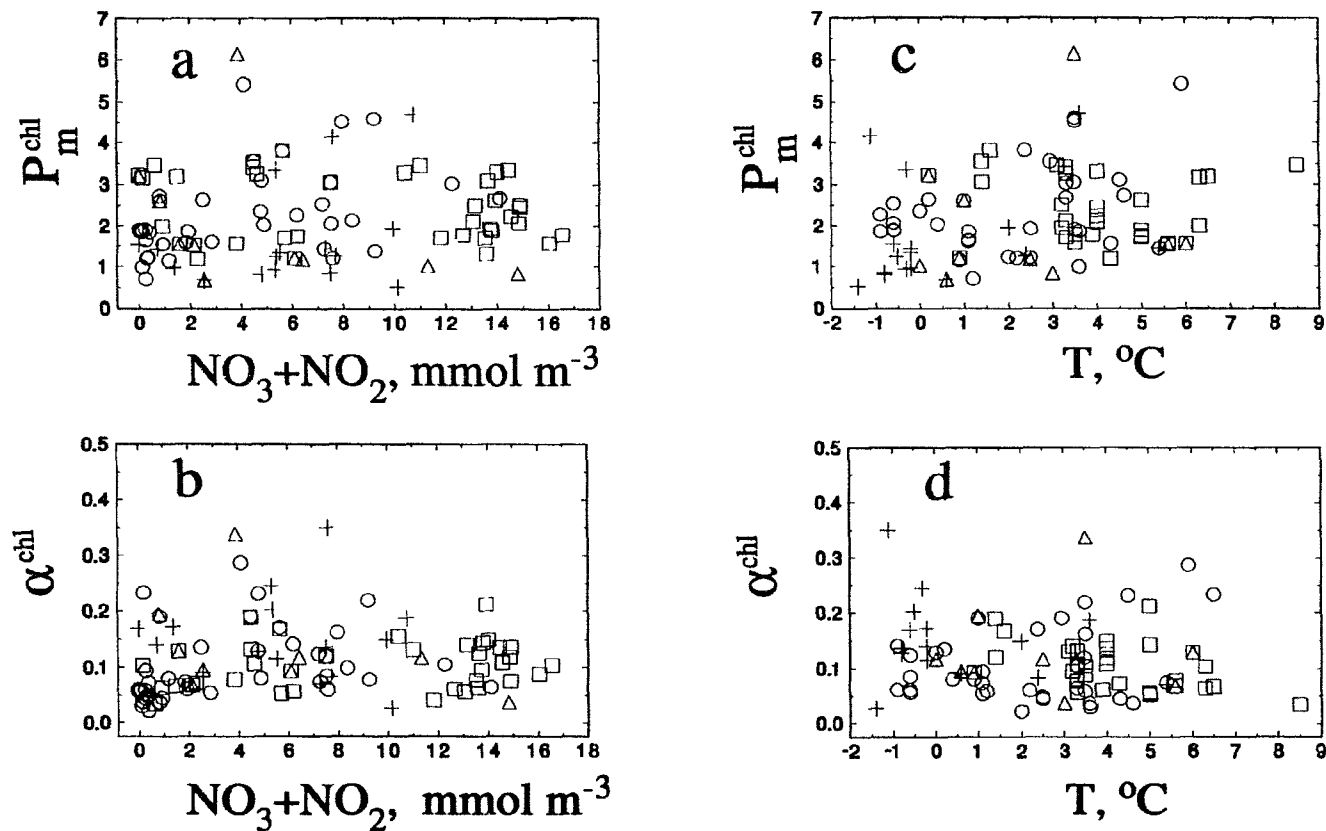


FIGURE C-1. The photosynthesis parameters as a function of the nitrate concentration (a,b) and seawater temperature (c,d) in the Labrador Sea, based on the data collected by the Bedford Institute of Oceanography [Irwin *et al.*, 1978, 1980, 1983, 1984, 1986, 1988]. Circles and triangles denote the samples from the surface and intermediate waters of the open Labrador Sea, circles and crosses denote the samples from the surface and subsurface waters from margins of the sea, respectively. The assimilation number P_m^{chl} is in $\text{mg C (mg chl)}^{-1} \text{ hr}^{-1}$ and the chlorophyll-normalized initial slope of the photosynthesis-light curve α^{chl} is in $\text{mg C (mg chl)}^{-1} \text{ hr}^{-1} (\text{W m}^{-2})$.

At a given irradiance, values of these parameters are assumed to reflect limitations on the gross growth exerted by all environmental and biotic factors.

Values of photosynthesis parameters: The seasonal averages of the photosynthesis parameters were computed from the data collected by Bedford Institute of Oceanography [Irwin *et al.*, 1978, 1980, 1983, 1984, 1986, 1988], and the daily values were interpolated from them (Figure C-2).

In the surface layer, the assimilation number P_m^{chl} (Figure C-2 a) was about 2.5 mg C (mg chl)⁻¹ hr⁻¹ throughout most of the year, with the exception of autumn when it dropped to 1.6 mg C (mg chl)⁻¹ hr⁻¹. The initial slope α^{chl} (Figure C-2 b) in the same layer was higher during the first half of year at 0.12 mg C (mg chl)⁻¹ hr⁻¹ (W m⁻²)⁻¹, and fell to about half of that value later in the year (about 0.07 mg C (mg chl)⁻¹ hr⁻¹). These values are similar to those computed by Platt *et al.* [1991] from the BIO data for subarctic, open, Atlantic Ocean (51–70°N). The value of the photoadaptation parameter I_k (Figure C-2 c) was between 20–25 W m⁻², except in summer when it was somewhat higher (36 W m⁻²), reflecting probably the adaptation of phytoplankton to higher levels of irradiance.

There were few measurements of the photosynthesis parameters from depths corresponding to those of layer 2 in the model outside the summer season, so the summer values of these parameters were prescribed throughout the year: $P_m^{chl} = 2.25$ mg C (mg chl)⁻¹ hr⁻¹, $\alpha^{chl} = 0.15$ mg C (mg chl)⁻¹ hr⁻¹ (W m⁻²)⁻¹ and $I_k = 15$ W m⁻². The higher values of α^{chl} and lower values of I_k reflect adaptations to low light levels in this layer.

Temporal changes in photosynthesis parameters computed in this way may not reflect exactly the evolution of the photosynthesis parameters in the real ocean, given that the *in situ* data were collected in different years and at different locations. In particular, during transitions between seasons, the interpolated values of the photosynthesis parameters might not change fast enough. For instance, after the

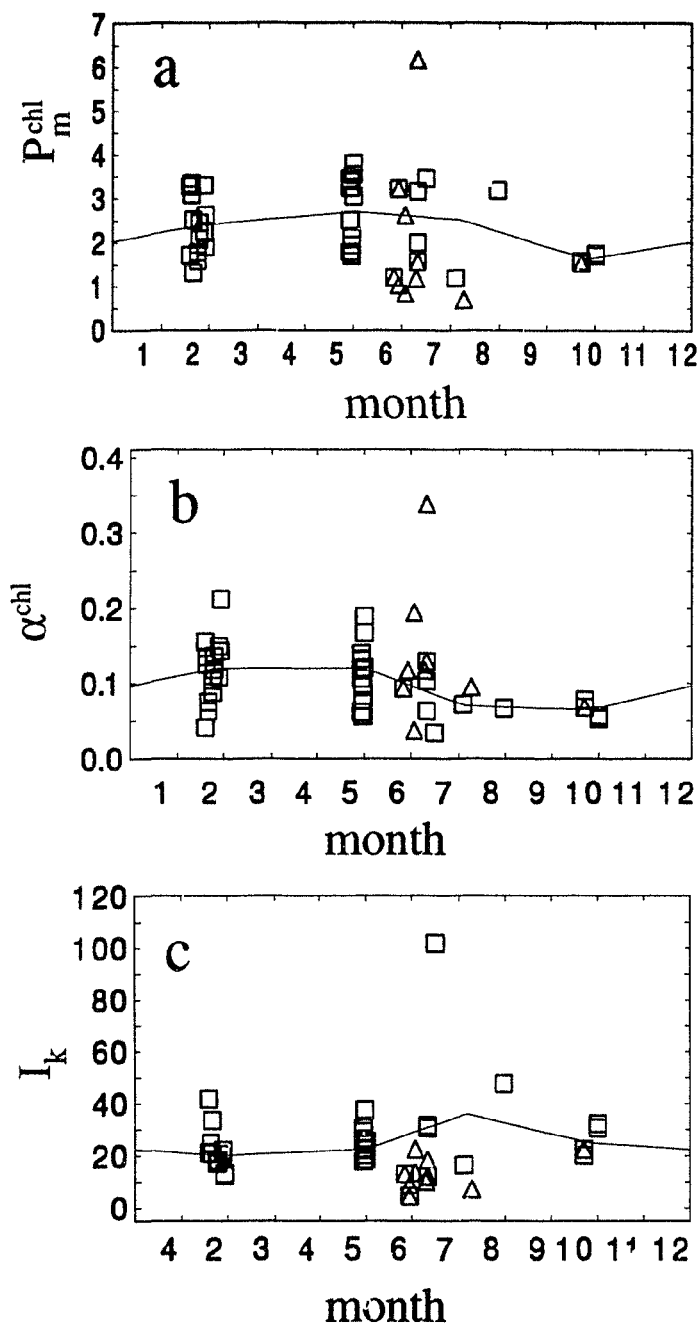


FIGURE C-2. The photosynthesis parameters in the open Labrador Sea as a function of time, based on the data collected by the Bedford Institute of Oceanography [Irwin *et al.*, 1978, 1980, 1983, 1984, 1986, 1988]. Squares and triangles denote the samples from the surface and subsurface waters of the open Labrador Sea, circles and crosses denote the samples from the surface and intermediate waters, respectively. Solid line denotes the daily values of the parameters used in the model, interpolated from the seasonal data. The assimilation number P_m^{chl} is in $\text{mg C (mg chl)}^{-1} \text{ hr}^{-1}$, the chlorophyll-normalized initial slope of the photosynthesis-light curve α^{chl} is in $\text{mg C (mg chl)}^{-1} \text{ hr}^{-1} (\text{W m}^{-2})$ and the photoadaptation parameter I_k is in W m^{-2} .

onset of nutrient limitation at the end of spring bloom. the photosynthesis parameters in the real ocean might decrease faster than the interpolation from seasonal values of the photosynthesis parameters would indicate. Consequently, the model nutrient uptake deduced from these interpolated parameters may occasionally become larger than the amount of nutrients available. To prevent such an error, a numerical safeguard in the computer program reduces the growth rate to the level at which the concentration of nutrients can be maintained just above zero.

This numerical safeguard was used between early July and mid-September: during this period to prevent nutrient concentration from falling below zero, the phytoplankton growth rate had to be reduced to about 30-40% of the potential growth rate, computed using prescribed values of the photosynthesis parameters (P_m^{chl} and α^{chl}) and the carbon-to-chlorophyll ratio (θ).

As an alternative solution one may consider limiting the phytoplankton growth rate through an increase in θ . For given values of P_m^{chl} and α^{chl} the primary production at depth z and time t , $P(z, t)$ (expressed in $\text{mol C m}^{-3} \text{ hr}^{-1}$) is inversely proportional to θ (equation 3-11). The reduction in the realized phytoplankton growth rate (30-40% of the potential growth rate at prescribed values of θ) would require an increase in θ to $150\text{-}200 \text{ mg C (mg chl)}^{-1}$, which is within the upper limit of $200 \text{ mg C (mg chl)}^{-1}$ measured in polar phytoplankton by *Sakschaug* [1989].

C.2.2 Other Phytoplankton Parameters

Other phytoplankton parameters describe chemical composition (the carbon-to-chlorophyll and carbon-to-nitrogen ratios), metabolic losses (respiration and excretion) and sinking. Different values of these parameters are prescribed to characterize different stages in phytoplankton growth in the surface layer, and to describe the difference between the surface and the intermediate layers.

Parameters typical to diatoms, which dominate the early part of the year [*Longhurst et al.*, 1989], are used to characterize the surface phytoplankton community in the period between the deep convection at the end of February and

the peak of spring bloom. After the onset of nutrient-depletion, the sinking rate strongly increases and the diatom bloom declines. Once the phytoplankton concentration falls to $0.7 \text{ mmol C m}^{-3}$ (corresponding to 3 mg chl m^{-3}) the parameters describing phytoplankton respiration, sinking and chemical composition are gradually modified to the "post-bloom" values, characteristic to the community adapted to the low-nutrient environment. The "post-bloom" values are used to parametrize phytoplankton until the next deep-water convection event. Although changes in environmental conditions in autumn may alter the phytoplankton parameters, any such alterations are ignored in the model, because the influence of phytoplankton on the properties of the ocean at this time of year is minimal (because of low biomass and low primary production).

Chemical composition: The description of the chemical composition of phytoplankton includes relationships between cellular carbon, chlorophyll and nitrogen. The carbon-to-chlorophyll ratio (θ) affects conversion of the chlorophyll-normalized photosynthesis parameters into phytoplankton gross growth rate, while the carbon-to-nitrogen ratio affects how much organic carbon could be formed given the available pool of nitrogen.

Both these ratios are highly variable, depending on the availability of light and nutrients, light history and species composition. In polar waters values of θ were found to range from 20 to $200 \text{ mg C (mg chl)}^{-1}$ [Sakshaug, 1989]. Similarly, the C:N molecular ratio varies widely: for instance, in diatoms it was found to vary from 6 in the nitrogen-replete cultures, to 20 in the nitrogen-limited cultures [Chalup and Laws, 1990; Cullen *et al.* 1993].

Direct estimates of chemical composition in natural phytoplankton are subject to serious uncertainties [Eppley, 1980] given difficulties in separating the phytoplankton from detritus, bacteria or microzooplankton. For instance, in the BIO data from the Labrador Sea the ratio between the particulate organic carbon (POC)

and chlorophyll varies from less than 10 to several hundreds, reflecting both the differences in phytoplankton composition and in the ratio between the phytoplankton and non-phytoplankton components of POC.

The laboratory results, on the other hand, impose growth conditions different from those prevailing in the natural environment, and are affected by the experimental design (see *Cullen et al.* [1993] for a discussion of differences between the results of batch and continuous cultures).

Consequently, to describe the composition of the phytoplankton in the model I assigned arbitrary values within the range of observed values and with differences between communities reflecting known adaptation mechanisms.

The carbon-to-chlorophyll ratio in the surface layer is set at 50 during the diatom-dominated phase. This value was chosen to be between the values of 60-65 reported in high-latitude bloom diatoms by *Sakshaug* [1989], the typical values of 30-40 in the POC-to-chlorophyll ratios in the BIO samples from the Labrador Sea from waters with high concentrations of phytoplankton (thus, presumably, with relatively lower errors caused by the presence of the non-phytoplankton carbon), and the range of 30-75 for shipboard cultures of diatoms from the Barents Sea [*Sakshaug*, 1989].

In the post-bloom phase, θ is assumed to increase to 75 to reflect adaptation to high-light and low-nutrients environment [*Geider*, 1987; *Langdon*, 1988; *Cullen et al.*, 1993]. In the intermediate layer θ is set at 35 throughout the year, because of low-light, high-nutrient, conditions prevailing there.

The carbon-to-nitrogen ratio is assumed, except the post-bloom phase, to be close to the Redfield ratio (106:16=6.625), which is to be expected for the phytoplankton growth of which is not limited by nitrogen [*Eppley*, 1980; *Laws and Chakrap*, 1990]. In the post-bloom phase the C:N ratio increases to 10, to reflect adaptations to the nitrogen-limiting environment.

Note that the chosen values of C:chl and C:N imply a constant N:chl ratio (= 8.8) in the surface waters. This is consistent with the findings of *Laws and*

Chalup [1990] and *Cullen et al.* [1993], who showed that in continuous cultures, this ratio is relatively constant over a wide range of nutrient-limited growth rates, as long as the light conditions are not very different. In the low-light environment, the N:chl ratio is lower (albeit this decrease is not very dramatic), leading to a lower value for N:chl in the intermediate layer (= 6.1).

Modelling the chemical composition during transitions: Representing the variable chemical composition of phytoplankton requires an adjustment of the model variables when a) the bloom phase changes into the post-bloom phase and b) when phytoplankton is transferred from layer 1 to layer 2.

- a) During the transition from the diatom-dominated conditions and the post-bloom conditions in the surface layer, the model conserves the phytoplankton nitrogen, allowing additional carbon to be synthesized to bring the C:N ratio to the higher post-bloom level. As the nitrogen-to-chlorophyll ratio remains unchanged, there is no increase in the amount of chlorophyll.
- b) When phytoplankton is exported from layer 1 to layer 2, the model conserves the phytoplankton carbon. As the carbon-to-chlorophyll ratio is lower in layer 2, the amount chlorophyll is increased. Similarly, when the post-bloom phytoplankton sinks, its nitrogen content is increased to bring the high post-bloom carbon-to-nitrogen ratio to the layer 2 value (there is no need to adjust the C:N ratio during the earlier, diatom-dominated stage, when the surface C:N ratio is assumed to be the same as that in layer 2).

The difference in the modelling of the “seasonal” and the “vertical” transitions reflects different adaptation mechanisms operating in these two cases. In the surface layer, after the onset of nutrient-limitation, phytoplankton has a photosynthesis “overcapacity” — there is enough light to synthesize more organic carbon, but the growth is limited by available nitrogen. For this reason, during the transition between the diatom-dominated and the post-bloom phytoplankton communities, model tracks nitrogen, not carbon. In layer 2, on the other hand, there is enough available nitrogen, but the synthesis of organic carbon is low because of insufficient light. Therefore, when phytoplankton sinks, the model tracks carbon. As more

chlorophyll allows better utilization of available light, the amount of chlorophyll increases. When the post-bloom plankton sinks in layer 2, given the availability of nitrogen, the elevated C:N ratio may be brought down to the Redfield ratio. The simulated changes in chlorophyll (nitrogen) reflect adaptation to the low-light (high-nutrient) environment, which may occur either through the synthesis of additional chlorophyll (uptake of additional nitrogen) or a faster rate of decomposition of carbon than chlorophyll (nitrogen).

Respiration and excretion: The losses by phytoplankton l are the sum of respiration R and excretion E :

$$l = R + E.$$

Following *Platt et al.* [1991a] and *Langdon* [1993], the daily respiration per unit biomass is split into a maintenance respiration R_o and a growth-dependent respiration:

$$R = R_o + \left(\frac{24 - D}{24} R_d + \frac{D}{24} R_d R_L \right) \sigma \quad (C - 3)$$

where D is daylength (in hours), R_d describes the dark respiration as a fraction of the gross growth rate σ , and R_L denotes the enhancement of dark respiration in the presence of light.

Values of the growth-related parameters, R_L and R_d , are based on *Langdon* [1993]. For diatom-dominated plankton, R_L was set at 2, and R_d at 0.08, which is somewhat higher than the value of 0.06 given for diatoms by *Langdon* [1993]. *Langdon's* average value for diatoms was strongly influenced by the contribution of low R_D ($=0.047$) measured in *Leptocylindricus danicus* (*C. Langdon*, personal communication): other diatom species have considerably higher R_D (see Table 3 in *Langdon* [1993]). Although *Leptocylindricus danicus* dominated some of the Labrador Sea samples [e.g., *MacLaren Report*, 1976] the value of R_D was set at 0.08, to account for the other species as well.

The post-bloom community in high latitudes are often dominated by flagellates and other taxonomic groups [MacLaren Report, 1976; *Longhurst et al.*, 1989], that typically have higher values of R_d than diatoms [*Langdon*, 1993]. Therefore, the value of R_d was set at 0.20 for the post-bloom phase.

In his review, *Langdon* [1993] cites R_L for only one non-diatom group – chlorophytes ($R_L \approx 1$). For lack of other estimates, R_L is assumed to take this value in the post-bloom phase.

In layer 2, values of R_d and R_L were set to the same values as in the pre-bloom surface community. As in the case of the photosynthesis parameters, uncertainty in the growth-related respiration parameters in this layer had negligible effect on the composition of seawater, given low growth rates in this layer.

Values of the growth-independent maintenance respiration R_o was set at 0.03, within the range observed in various taxonomic groups [*Langdon*, 1993]. The importance of the maintenance respiration in the model lies in its effect on the decomposition of organic matter in the intermediate layer. Its rate, together with the sinking rate and zooplankton grazing, determine how much of the phytoplankton biomass is decomposed before sinking to the deep-ocean layer. This, in turn, affects the air-sea fluxes of CO_2 .

In addition to respiration, the phytoplankton losses are also caused by excretion of organic material. It is assumed that the excretion is a constant fraction of the gross growth rate:

$$E = \mathcal{E}\sigma$$

where \mathcal{E} is the proportionality coefficient, assumed to 0.05 [*Platt et al.*, 1991a].

During winter the computed losses of phytoplankton could sometimes cause the phytoplankton biomass to fall below the minimum value. In such cases the loss rates were reduced to maintain the minimum phytoplankton biomass. This numerical safeguard would reflect lowering of metabolism losses in an inhospitable environment (for instance, through forming overwintering spores with low rates of metabolism).

Sinking: Sinking removes phytoplankton from the surface and the intermediate layers. The sinking velocity v depends on many biological factors, such as size of organisms, their nutritional status, species composition, [e.g., *Smayda*, 1970; *Bienfang*, 1981; *Granata*, 1987; *Waite et al.*, 1992a,b] and on physical properties of seawater such as viscosity and density.

In the surface layer various sinking velocities were prescribed depending on the stage of phytoplankton growth:

- slow sinking ($v_1 = 0.5 \text{ m d}^{-1}$) during winter and during the initial, nutrient-unlimited phase of spring bloom;
- fast sinking ($v_1 = 3 \text{ m d}^{-1}$) during the declining phase of spring bloom (after the onset of nutrient limitation);
- slow sinking ($v_1 = 0.5 \text{ m d}^{-1}$) in the post-bloom phase, with phytoplankton community adapted to low-nutrient levels, likely to be dominated by smaller phytoplankton, often with some ability to swim actively (flagellates).

In the intermediate layer the sinking velocity v_2 was set between the two extremes of the sinking velocities in the surface layer. On the one hand, v_2 should be higher than 0.5 m d^{-1} prescribed for the actively-growing diatoms (and for the post-bloom community growing at the maximum rate permitted by the availability of nutrients). Phytoplankton production in layer 2 was low (respiration and excretion losses exceeded the photosynthesis rate throughout most of the year, because of strong light limitation), therefore the growth status of phytoplankton would favor fast sinking (senescent organisms sink faster than those growing actively [*Smayda*, 1970]). On the other hand, v_2 may be lower than 3 m d^{-1} prescribed for the declining phase of spring bloom in the surface layer. On average, the phytoplankton community in the intermediate layer is likely to contain smaller organisms than the community present in the surface layer during the spring bloom, which is dominated by large diatoms. With a smaller particle size and with the density and viscosity of the surrounding water being slightly higher than those in the surface layer, the phytoplankton sinking should be slower. Therefore, v_2 was set at 2 m d^{-1} .

C.2.3 Effects of formation of organic matter on alkalinity

The formation of organic matter affects alkalinity of seawater (subsection 3.3.3). If nitrate and sulfate are used in the formation of organic matter, then assuming the C:N molecular ratio of 106:16 [Redfield, 1934], and the N:S molecular ratio of 10:1 [Chen, 1978], formation of 1 mole of organic carbon would increase the seawater alkalinity by $\gamma_A = 0.18$ equivalents

$$\gamma_A = (16 : 106) \times 1 + (1.6 : 106) \times 2 = 0.18, \quad (\text{C} - 4)$$

where multiplication by one and by two reflects the increase by one and two equivalents of alkalinity, respectively, for every mole of nitrate and sulfate removed.

If ammonium were used as a source of nitrogen instead of nitrate, the effect on alkalinity would be different. since the uptake of one mole of NH_4^+ decreases A by 1 equivalent. Therefore, a more detailed treatment of alkalinity would require separate modelling of ammonium, with a description of the uptake preferences by phytoplankton and bacteria. Such modeling is a part of the ecosystem nitrogen budgets of *Fasham et al.* [1990] (see also *Sarmiento et al.* [1993]). However, in the context of this work I am ultimately interested in the fate of nutrients brought to the surface waters from the deep ocean, in which nitrate are the dominant form of the biologically-usable nitrogen.

Even if a large fraction of the phytoplankton production were ammonium-based, only the ammonium remaining in seawater affects directly the air-sea fluxes of CO_2 . Concentration of ammonium is likely to be low: in summer, when all species of biologically-available nitrogen are taken up by the nutrient-starved phytoplankton, and in spring and autumn, because of preferential uptake of ammonium over nitrates.

Concentrations of ammonium measured in the surface waters of the open Labrador Sea are typically below 1 mmol m^{-3} , so the effect of treating all dissolved nitrogen available to phytoplankton as nitrate has hardly any effect on the estimates of the seawater partial pressure of CO_2 .

Furthermore, the overestimation of the partial pressure of CO_2 by neglecting ammonium is roughly compensated by the underestimation of the partial pressure caused by neglecting the effect of phosphates and silicates.

For instance, in winter the partial pressure of CO_2 computed by representing 1 mmol m^{-3} of ammonium as nitrates, would overestimate the partial pressure of CO_2 by $3 \text{ } \mu\text{atm}$. At the same time, neglecting the presence of silicates and phosphates in their winter concentrations (about 10 mmol m^{-3} and 1 mmol m^{-3} , respectively [Anderson *et al.*, 1985]), would cause underestimating the partial pressure by $4 \text{ } \mu\text{atm}$, so the two errors nearly cancel each other. During other seasons both the effects are likely to be smaller, since ammonium, silicates and phosphates are likely to be smaller.

Therefore, for the sake of simplicity in the model, in computation of partial pressure of CO_2 all biologically-usable nitrogen in seawater is treated as nitrate, and silicates and phosphates are not simulated.

C.2.4 Recycling

Some of the nutrients, dissolved inorganic carbon and alkalinity sequestered by phytoplankton production are later lost from the system (subsection 3.3.3). They may be either removed physically from a layer (in the phytoplankton exported from the layer by sinking and mixing, or in migrating zooplankton and in zooplankton feces), or locked in the refractory dissolved organic matter (DOM), in which form it is inaccessible to phytoplankton and no longer affects the inorganic carbon fluxes. The remaining part is recycled within the layer and is either reused by phytoplankton, or released into the seawater. The recycled N , C and A are contained in the recycled fractions of the phytoplankton and zooplankton losses.

The recycled fraction of the phytoplankton losses, ϵ_l , is given by

$$\epsilon_l = \frac{R + \epsilon_e E}{R + E}, \quad (\text{C} - 5)$$

where ϵ_e is the recycled fraction of the excretion E . Note that equation (C-5) implies that all products of phytoplankton respiration R are recyclable (as implicitly assumed by *Fasham et al.* [1990]). Since the estimates of the refractory fraction of the phytoplankton excretion in the literature vary, I used $\epsilon_e=0.5$.

I assumed that the recycled fraction of the zooplankton losses, ϵ_m , is 0.75, the same as the ammonium fraction of the zooplankton nitrogen excretion in *Fasham et al.* [1990]. The remaining 0.25 of the zooplankton losses include zooplankton migrating away from the layer and zooplankton excretion of refractory organic material. The unassimilated fraction of zooplankton grazing ($0.25=1-a$) is not recycled, since it is likely to leave the layer as part of fast-sinking fecal pellets.

Note that I did not specify separate recycling efficiencies for nutrients and carbon. Such a differentiation would be important if the non-recycled material had a Redfield ratio different from that of the recycled portion. Although refractive DOM has typically a much higher C:N ratio than living biomass, the same recycling efficiencies are used for N and C , given that most of non-recycled material in my model is lost through export of intact cells or unassimilated zooplankton food.

References

- Ackleson S. G., W. M. Balch, and P. M. Holligan, Response of water-leaving radiance to particulate calcite and chlorophyll *a* concentrations: A model for Gulf of Maine coccolithophore blooms, *J. Geophys. Res.*, *99*, 7483-7499, 1994.
- Aiken, J., and I. Bellan, Optical oceanography: an assessment of a towed method, in: *Light and Life in the Sea*, edited by P. J. Herring, A. K. Campbell, M. Whitfield, and L. Maddock, pp. 39-57, Cambridge Univ. Press, Cambridge, 1990.
- Anderson, L. G., A. R. Coote, and E. P. Jones, Nutrient and alkalinity in the Labrador Sea, *J. Geophys. Res.*, *90*, 7355-7360, 1985.
- Antoine, D., and A. Morel, Modelling the seasonal course of the upper ocean pCO₂ (I). Development of a one-dimensional model, *Tellus*, *47B*, 103-121, 1995a.
- Antoine, D., and A. Morel, Modelling the seasonal course of the upper ocean pCO₂ (II). Validation of the model and sensitivity studies, *Tellus*, *47B*, 122-144, 1995b.
- Bacastow, R., and A. Björkström, Comparison of ocean models for the carbon cycle, in *Carbon Cycle Modelling (SCOPE 16)*, edited by B. Bolin, pp. 29-79, John Wiley, New York, 1981.
- Bacastow, R., and C. D. Keeling, Atmospheric carbon dioxide and radio-carbon in the natural carbon cycle, II; Changes from A.D. 1700 to 2070 as deduced from a geochemical model, in *Carbon in the Biosphere*, AEC Symp. Ser. vol. 30, edited by G. M. Woodwell and E. V. Pecan, pp. 86-136, U.S. Department of Commerce, Washington, D. C., 1973.
- Bacastow, R., and C. D. Keeling, Atmospheric carbon dioxide concentration and the observed airborne fraction, in *Carbon Cycle Modelling (SCOPE 16)*, edited by B. Bolin, pp. 103-112, John Wiley, New York, 1981.
- Bacastow, R., and E. Maier-Reimer, Ocean-circulation model of the carbon cycle, *Climate Dynamics*, *4*, 95-125, 1990.
- Bainbridge, A.E. (Ed.), *GEOSECS Atlantic Expedition, Vol. 1, Hydrographic Data 1972-1973*, 121 pp., International Decade of Ocean Exploration, National Science Foundation, Washington, D. C., 1981.

- Balch, W. M., J. M. Holligan, S. G. Ackleson, and K. J. Voss, Biological and optical properties of mesoscale coccolithophore blooms in the Gulf of Maine, *Limnol. Oceanogr.*, *36*, 629-643, 1991.
- Baumgartner, A., and E. Reichel, *The World Water Balance*, Elsevier Sci. Publ. Co., 182 pp., 1975.
- Bienfang, P. K., Sinking rates of heterogeneous, temperate phytoplankton populations, *J. Plankton Res.*, *3*, 235-253, 1981.
- Björkström, A., A model of CO₂ interaction between atmosphere, oceans, and land biota, in *The Global Carbon Cycle (SCOPE 13)*, edited by B. Bolin, E. T. Degens, S. Kempe and P. Ketner, pp. 403-457, John Wiley, New York, 1979.
- Bolin, B., Steady state and response characteristics of a simple model of the carbon cycle, in *Carbon Cycle Modelling (SCOPE 16)*, edited by B. Bolin, pp. 287-305, John Wiley, New York, 1981.
- Bolin, B., and E. Eriksson, Changes in the carbon dioxide content of the atmosphere and the sea due to fossil fuel combustion, in *Atmosphere and Sea in Motion*, edited by B. Bolin, pp. 130-142, Rockefeller Institute Press, New York, 1959.
- Boyd, P., and P. Newton, Evidence of the potential influence of planktonic community structure on the interannual variability of particulate organic carbon flux, *Deep-Sea Res.*, *42(5)*, 619-639, 1995.
- Brainerd, K. E., and M. C. Gregg, Surface mixed and mixing layer depths, *Deep-Sea Res.*, *42(9)*, 1521-1543, 1995.
- Broecker, W. S., and T.-H. Peng, Interhemispheric transport of carbon dioxide by ocean circulation, *Nature*, *356*, 587-589, 1992.
- Broecker, W. S., D. W. Spencer, and H. Craig (Eds.), *GEOSECS Pacific Expedition. Vol. 3. Hydrographic Data 1973-1974*, 137 pp., International Decade of Ocean Exploration, National Science Foundation, Washington, D. C., 1982.
- Broecker, W. S., T.-H. Peng, G. Ostlund, and M. Stuiver, The distribution of bomb radiocarbon in the ocean, *J. Geophys. Res.*, *90*, 693-6970, 1985.
- Brown C. W., and J. A. Yoder, Coccolithophorid blooms in the global ocean, *J. Geophys. Res.*, *99*, 7467-7482, 1994.
- Chalup, M. S., and E. A. Laws, A test of the assumptions and predictions of recent microalgal growth models with the marine phytoplankter *Pavlova lutheri*, *Limnol. Oceanogr.*, *35*, 1555-1577, 1990.

- Chen, C.-T. A., Decomposition of calcium carbonate and organic carbon in the deep oceans, *Nature* 201, 735-736, 1978.
- Conover, R. J., Metabolism and growth in *Calanus hyperboreus* in relation to its life cycle, *Rapp. et proces-verbaux Conseil internat. explorat. mer.*, 153, 1962.
- Conover, R. J., Zooplankton - life in a nutritionally dilute environment. *Amer. Zoologist*, 8, 107-118, 1968.
- Conover, R. J., Comparative life histories in the genera *Calanus* and *Neocalanus* in high latitudes of the northern hemisphere, *Hydrobiologia*, 167/168, 127-142, 1988.
- Craig, H., The natural distribution of radiocarbon and the exchange time of carbon dioxide between atmosphere and sea, *Tellus*, 9, 1-17, 1957.
- Craig, S. G., and K. J. Holmen, Uncertainties in future CO₂ projections, *Global Biogeochem. Cycles*, 9, 139-152, 1995.
- Cullen, J. J., Toward a general description of phytoplankton growth for biogeochemical models. in: *Towards a Model of Ocean Biogeochemical Processes*, edited by G. T. Evans and M. J. R. Fasham, Springer-Verlag, Berlin, 1993.
- Denman, K. L., A time-dependent model of the upper ocean, *J. Phys. Oceanogr.*, 3, 173-184, 1973.
- Eppley, R. W., Temperature and phytoplankton growth in the sea, *Fish. Bull.*, 70, 1063-1085, 1972.
- Eppley, R. W., Temperature and phytoplankton growth in the sea, in: *Primary Productivity in the Sea*, edited by P. G. Falkowski, Plenum, New York, p. 47-67, 1980.
- Erickson, D. J., A stability dependent theory for air-sea gas exchange, *J. Geophys. Res.*, 98, 8471-8488, 1993.
- Esbenson, S. K., and Y. Kushnir, *The Heat Budget of the Global Oceans: An Atlas Based on Estimates from the Surface Marine Observations (Clim. Res. Inst. Rep. 29)*. Oregon State Univ., Corvallis, OR, 1981.
- Etcheto, J., and L. Merlivat, Satellite determination of the carbon dioxide exchange coefficient at the ocean-atmosphere interface: A first step, *J. Geophys. Res.*, 93, 15,669 - 15,678, 1988.
- Evans, G. T., and J. S. Parslow, A model of annual plankton cycles, *Biol. Oceanogr.*, 3, 327-347, 1985.

- Fasham, M. J. R., H. W. Ducklow, and D. S. McKelvie, A nitrogen-based model of plankton dynamics in the oceanic mixed layer, *J. Mar. Res.*, *48*, 591-639, 1990.
- Feldman, G., N. Kuring, C. Ng, W. Esaias, C. McClain, J. Elrod, N. Maynard, D. Endres, R. Evans, J. Brown, S. Walsh, M. Carle and G. Podesta, Ocean color: Availability of the global data set, *EOS* *70*, 634-635, 640-641, 1989.
- Friederich G. E., P. G. Brewer, R. Herlien, and F. P. Chavez, Measurement of sea surface partial pressure of CO₂ from a moored buoy, *Deep-Sea Res.* *42*, 1117-1186, 1995.
- Garçon, V. C., L. Martinon, C. Andrie, P. Andrich J.-F. Minster, Kinematics of CO₂ fluxes in the tropical Atlantic Ocean during the 1993 northern summer, *J. Geophys. Res.*, *94*, 855-870, 1989.
- Gaudry, A., P. Monfray, G. Polian and G. Lambert, The 1982-1983 El Niño: a 6 billion ton CO₂ release, *Tellus*, *39B*, 1987.
- Geider, R. J., Light and temperature dependence of the carbon to chlorophyll ratio in microalgae and cyanobacteria: implications for physiology and growth of phytoplankton, *New Phytol.*, *106*, 1-34, 1987.
- Goyet, C., and A. Poisson, New determination of carbonic acid dissociation constants in seawater as a function of temperature and salinity, *Deep Sea Res.*, *36*, 1635-1654, 1989.
- Granata, T. C., Measurements of phytoplankton sinking and growth under varied light intensities and mixing regimes, Ph.D. Thesis, University of California, Berkeley, 175 pp., 1987.
- Harris, R. P., Zooplankton grazing on the coccolithophore *Emiliana huxleyi* and its role in inorganic carbon flux, *Mar. Biol.*, *119*, 431-439, 1994.
- Harrison, W. G., and T. Platt, Variations in assimilation number of coastal marine phytoplankton: effects of environmental co-variates, *J. Plankton Res.*, *2*, 249-260, 1980.
- Harrison, W. G., L. R. Harris, and B. D. Irwin, The kinetics of nitrogen utilization in the oceanic mixed layer: nitrate and ammonium interactions at nanomolar concentrations, *Limnol. and Oceanogr.*, in press.
- Hoffert, M. I., A. J. Callegari, and C.-T. Hsieh, A box-diffusion carbon cycle model with upwelling, polar bottom water formation and marine biosphere, in *Carbon*

- Cycle Modelling (SCOPE 16)*, edited by B. Bolin, pp. 287-305, John Wiley, New York, 1981.
- Holligan, P. M., Do marine phytoplankton influence global climate?, in: *Primary Productivity and Biogeochemical Cycles in the Sea*, edited by P. G. Falkowski and A. D. Woodhead, pp. 487-499. Plenum Press, New York 1992.
- Holligan, P. M., and W. M. Balch, From the ocean to cells: Coccolithophore optics and biogeochemistry, in: *Particle Analysis in Oceanography*, NATO ASI Ser. Vol. G27, edited by S. Demers, p. 301-324, Springer Verlag, New York, 1991.
- ICNAF (International Commission for the Northwest Atlantic Fisheries), Environmental Surveys - NORTHWESTLANT 1-3, 1963, part 4. Biological Data Record, edited by J. Corlett, Dartmouth, N.S., Canada. 1968.
- Ikedo, M., Salt and heat balances in the Labrador Sea Using a Box Model, *Atmosphere-Ocean*, 25, 197-223, 1987.
- Ingri, N., Equilibrium studies of polyanions. IV. Silicate ions in NaCl medium, *Acta Chem. Scand.* 13, 758-775, 1959.
- Irwin B., P. Evans, and T. Platt, Phytoplankton productivity experiments and nutrient measurements in the Labrador Sea from 11 February to 28 February 1978, *Fish. Mar. Serv. Data Rept. No. 114*, 38pp., 1978.
- Irwin B., W. G. Harrison, C. L. Gallegos, and T. Platt, Phytoplankton productivity experiments and nutrient measurements in the Labrador Sea, Davis Strait, Baffin Bay and Lancaster Sound from 26 August to 14 September 1978, *Can. Data Rept. Fish. Aquat. Sci. No. 213*, 103 pp., 1980.
- Irwin B., L. Harris, P. Dickie, P. Lindley, and T. Platt, Phytoplankton productivity in Eastern Canadian Arctic during July and August 1980, *Can. Data Rept. Fish. Aquat. Sci. No. 386*, 157 pp., 1983.
- Irwin B., P. Dickie, P. Lindley, and T. Platt, Phytoplankton productivity in Lancaster Sound and approaches during summer 1979, *Can. Data Rept. Fish. Aquat. Sci. No. 423*, 103 pp., 1984.
- Irwin B., C. Caverhill, P. Dickie, E. Horne, and T. Platt, Phytoplankton productivity on the Labrador Shelf during June and July, 1984, *Can. Data Rept. Fish. Aquat. Sci. No. 577*, 162 pp., 1986.

- Irwin B., P. Dickie, M. Hodgson, and T. Platt, Primary production and nutrients on the Labrador Shelf, in Hudson Strait, and Hudson Bay in August and September 1982, *Can. Data Rept. Fish. Aquat. Sci. No. 692*, 139 pp., 1988.
- Ivlev, V. S., The biological productivity of waters, *Usp. Sovrem. Biol.*, 19, 98-120, 1945.
- Jain, A. K., H. S. Kheshgi, M. I. Hoffert, and D. J. Wuebbles, Distribution of radiocarbon as a test of global carbon cycle models, *Global Biogeochem. Cycles*, 9, 153-166, 1995.
- Joos, F., J. L. Sarmiento, and U. Siegenthaler, Estimates of the effect of Southern Ocean iron fertilization on atmospheric CO₂ concentrations, *Nature*, 349, 772-775, 1991.
- Keeling, C. D., The carbon dioxide cycle, Reservoir models to depict the exchange of atmospheric carbon dioxide with the oceans and land plants, in *Chemistry of the Lower Atmosphere*, edited by S. J. Rasool, pp. 251-329, Plenum, New York, 1973.
- Kester, D. R., and R. M. Pytkowich, Determination of the apparent dissociation constants of phosphoric acid in seawater, *Limnol. Oceanogr.*, 12, 243-252, 1967.
- Knox, F., and M. B. McElroy, Changes in atmospheric CO₂: Influence of the marine biota at high latitude, *J. Geophys. Res.*, 89, 4629-4637, 1984.
- Langdon, C., On the causes of interspecific differences in the growth-irradiance relationship for phytoplankton II. A general review, *J. Plankton. Res.*, 10, 1291-1312, 1988.
- Langdon, C., The significance of respiration in production measurements, *ICES mar. Sci. Symp.*, 197, 69-78, 1993.
- Laws, E. A., and M. S. Chalup, A microalgal growth model, *Limnol. Oceanogr.*, 32, 597-608, 1990.
- Lazier, J. R., Oceanographic conditions at ocean weather station ship *Bravo*, 1964-1974, *Atmosphere-Ocean* 18, 227-238, 1980.
- Lazier, J. R., and J. R. Hackett, Monthly mean values of potential temperature, salinity and sigma-theta at ocean weather ships Bravo, Charley, Delta, and Echo, *Can. Data Rep. Hydrogr. Ocean Sci. No. 44*, 38 pp., 1986.

- Lefevre, N., A first step towards a reference $\Delta p\text{CO}_2$ map for the North Atlantic Ocean, IGBP-DIS Working Paper 11, Universite Pierre et Marie Curie, Paris, France, 1995.
- Levitus, S., *Climatological atlas of the world ocean*, NOAA Profess. Pap. 13, US Govt. Printing Off., Washington, D.C., 1982.
- Longhurst, A., and R. Williams, Carbon flux by seasonal vertical migrant copepods is a small number, *J. Plankton. Res.*, 14, 1495-1509, 1993.
- Longhurst, A., T. Platt, W. G. Harrison, E. J. H. Head, A. W. Herman, E. Horne, R. J. Conover, W. K. W. Li, D. V. Subba Rao, D. Sameoto, J. C. Smith, and R. E. Smith. Biological oceanography in the Canadian High Arctic. *Rapp. P.-v. Reun. Cons. int. Explor. Mer.*, 188, 80-89, 1989.
- Longhurst, A., A. W. Bedo, W. G. Harrison, E. J. H. Head, and D. Sameoto, Vertical flux of respiratory carbon by oceanic diel migrant biota, *Deep-Sea Res.*, 37, 685-694, 1990
- Lyman, J., Buffer mechanism of sea water. PH.D. Thesis, Univ. of Calif., Los Angeles, 1956.
- MacLaren Atlantic Ltd, Imperial Oil Report on Cruise II, July, 1976: Environmental aspects of Imperial Oil cruise to Flemish Pass and Davis Strait, 84 pp., MacLaren Atlantic Limited, 1976.
- Maier-Reimer, E., Carbonate buffering of anthropogenic CO_2 , in: *Strategies for Future Climate Research*, edited by Mojib Latif, pp. 287-318, Max-Planck-Institut für Meteorologie, Hamburg, 1991.
- Maier-Reimer, E., and K. Hasselmann, Transport and storage of CO_2 in the ocean — An inorganic ocean-circulation carbon cycle model, *Clim. Dyn.*, 2, 63-90, 1987.
- Martinson, D. G., P. D. Killworth, and A. L. Gordon, A convective model of the Weddell Polynya, *J. Phys. Oceanogr.* (11), 466-488, 1981.
- Mehrbach, C., C. H. Culberson, J. E. Hawley, and R. M. Pytkowicz, Measurements of apparent dissociation constants of carbonic acid in seawater at atmospheric pressure, *Limnol. Oceanogr.*, 18, 897-907, 1973.
- Memery L., and L. Merlivat, Influence of gas transfer on the CO_2 uptake by the ocean, *J. Geophys. Res.*, 90, 7361-7366, 1985.

- Moiseev, P. A., *The Living Resources of the World Ocean*, translated from Russian by N. Kaner and W. E. Ricker, Washington D. C., 1971.
- Munk, W. H., and E. R. Anderson, Notes on a theory of the thermocline, *J. Mar. Res.*, 276-295, 1948.
- Neftel, A., E. Moor, H. Oeschger, and B. Stauffer, Evidence from polar ice cores for the increase in atmospheric CO₂ in the past two centuries, *Nature*, 45-47, 1986.
- Niiler, P. P., and E. B. Kraus, One-dimensional models, In: *Modeling and Prediction of the Upper Layers of the Ocean*, edited by E. B. Kraus, 143-172, Pergamon Press, New York, 1977.
- Nydal, R., Further investigation on the transfer of radiocarbon in nature, *J. Geophys. Res.*, 73, 3617-3635, 1968.
- Oeschger, H., U. Siegenthaler, U. Schotterer, and A. Gugelman, A box diffusion model to study the carbon dioxide exchange in nature, *Tellus*, 27, 168-192, 1975.
- Parkinson, C. L., J. C. Comiso, H. J. Zwally, D. J. Cavalieri, P. Gloersen, and W. J. Campbell, Arctic Sea Ice, 1973-76: Satellite Passive-Microwave Observations, NASA Spec. Publ. SP-489, 239 pp., 1987.
- Parsons, T. R., M. Takahashi, and B. Hargrave (Eds.), *Biological Oceanographic Processes*, 330 pp., Pergamon Press, New York, 1984.
- Pavshchik, E. A., The influence of currents upon seasonal fluctuations in the plankton of the Davis Strait. *Sarsia*, 34, 383-392, 1968.
- Peng, T.-H., and W. S. Broecker, Dynamic limitations on the Antarctic iron fertilization strategy. *Nature* 349, 227-229, 1991.
- Peng, T.-H., T. Takahashi, and W. S. Broecker, Seasonal variability of carbon dioxide in the northern North Atlantic surface water: Observation and a model. *Tellus*, 39B, 439-458, 1987.
- Platt, T., and S. Sathyendranath, Biological production models as elements of coupled, atmosphere-ocean models for climate research, *J. Geophys. Res.*, 96, 2585-2592, 1991.
- Platt T., and S. Sathyendranath, Estimators of primary production for interpretation of remotely-sensed data on ocean color, *J. Geophys. Res.*, 98, 14561-14576, 1993.

- Platt, T., C. L. Gallegos, and W. G. Harrison, Photoinhibition of photosynthesis in natural assemblages of marine phytoplankton, *J. Mar. Res.*, *38*, 687-701, 1980.
- Platt, T., S. Sathyendranath, and P. Ravindran, Primary production of phytoplankton: Analytic solutions for daily rates per unit area of water surface, *Proc. R. Soc. London, Ser. B*, *241*, 101-111, 1990.
- Platt, T., D. F. Bird, and S. Sathyendranath, Critical depth and marine primary production. *Proc. R. Soc. Lond. B*, *246*, 205-217, 1991a.
- Platt, T., C. Caverhill, and S. Sathyendranath, Basin-scale estimates of oceanic primary production by remote sensing: the North Atlantic, *J. Geophys. Res.*, *96*, 15147-15159, 1991b.
- Platt, T., O. Ulloa, W. G. Harrison, N. Hoepffner, and J. Goes, Nutrient control of phytoplankton photosynthesis in the Western North Atlantic, *Nature*, *356*, 229-231, 1992.
- Price, J. F., R. A. Walker, and R. Pinkel, Diurnal cycling: Observations and models of the upper ocean response to diurnal heating, cooling, and wind mixing, *J. Geophys. Res.*, 8411-8427, 1986.
- Redfield, On the proportions of organic derivatives in sea water and their relation to the composition of phytoplankton, *James Johnstone Memorial Volume (Liverpool)*, 176 pp., 1934.
- Revelle, R., and H. E. Suess, Carbon dioxide exchange between atmosphere and ocean and the question of an increase of atmospheric CO₂ during the past decade, *Tellus*, *9*, 18-27, 1957.
- Rintoul, S. R., Towards coupled physical-biogeochemical models of the ocean carbon cycle, in *Modeling the Earth System*, edited by D. Ojima, pp. 39-75. University Corporation for Atmospheric Research/Office for Interdisciplinary Earth Studies, Boulder, Colo., 1992.
- Robertson, J. and A. J. Watson, Thermal skin effect of the surface ocean and its implications for CO₂ uptake, *Nature*, *358*, 738-740, 1992.
- Rotty, R. M., A look at 1983 CO₂ emissions from fossil fuels (with preliminary data for 1984), *Tellus*, *39B*, 203-208, 1987.

- Sakshaug, E., The physiological ecology of polar phytoplankton, in: *Proceedings of the sixth conference of the Comité Arctique International, 19-1 May 1985*, edited by L. Rey and V. Alexander, pp. 61-89, E. J. Brill, New York, 1989.
- Sarmiento, J. L., and E. T. Sundquist, Revised budget for the oceanic uptake of anthropogenic carbon dioxide, *Nature*, *356*, 589-593, 1992.
- Sarmiento, J. L., and J. R. Toggweiler, A new model for the role of the oceans in determining atmospheric pCO₂, *Nature*, *308*, 622-624, 1984.
- Sarmiento, J. L., J. C. Orr, and U. Siegenthaler, A perturbation simulation of CO₂ uptake in an ocean general circulation model, *J. Geophys. Res.*, *97*, 3621-3645, 1992.
- Sarmiento, J. L., R. D. Slater, M. J. R. Fasham, H. W. Ducklow, J. R. Toggweiler, and G. T. Evans, A seasonal three-dimensional model of nitrogen cycling in the North Atlantic euphotic zone, *Global Biogeochem. Cycles* *7*, 417-450, 1993.
- Sarmiento, J. L., C. Le Querre, and S. W. Pacala, Limiting future atmospheric carbon dioxide, *Global Biogeochem. Cycles*, *9(1)*, 121-137, 1995.
- Sathyendranath, S., and T. Platt, The spectral irradiance field at the surface and in the interior of the ocean: a model for applications in oceanography and remote sensing, *J. Geophys. Res.*, *93*, 9270-9280, 1988.
- Shaffer, G., and J. L. Sarmiento, Biogeochemical cycling in the global ocean. 1. A new, analytical model with continuous vertical resolution and high-latitude dynamics, *J. Geophys. Res.*, *100*, 2659-2672, 1995.
- Shuly, J. L., Oceanographic observations. North Atlantic ocean station Bravo. Terminal report 1964-1974. Oceanographic Report No. CG 373-72, U. S. Coast Guard Oceanographic Unit, Washington, D. C., 1978.
- Siegenthaler, U., Uptake of excess CO₂ by an outcrop-diffusion model of the ocean *J. Geophys. Res.*, *88*, 3599-3608, 1983.
- Siegenthaler, U., and T. Wenk, Rapid atmospheric CO₂ variations and ocean circulation, *Nature*, *308*, 624-626, 1984.
- Simpson, J. J., and A. Zirino, Biological control of pH in the Peruvian coastal upwelling area, *Deep-Sea Res.*, *27*, 733-744, 1980.

- Simpson J. J., Air-Sea exchange of carbon dioxide and oxygen induced by phytoplankton. Methods and interpretations. In: *Mapping Strategies in Chemical Oceanography*; edited by A. Zirino; *Advances in Chemistry Series, 209*, Am.Chemical Soc., Washington, D. C., 1985.
- Smayda, T. J., The suspension and sinking of phytoplankton in the sea, *Oceanogr. Mar. Biol.*, 8, 353-414, 1970.
- Smith, E. L. Photosynthesis in relation to light and carbon dioxide, *Proc. Natl. Acad. Sci.* 22, 504-511, 1936.
- Smith, S. D., and F. W. Dobson. The heat budget at Ocean Weather Station *Bravo*, *Atmosphere-Ocean.* 22, 1-22, 1984.
- Takahashi, T., W. S. Broecker, and A. E. Bainbridge. The alkalinity and total carbon dioxide concentration in the world oceans, In: *Carbon Cycle Modelling (SCOPE 16)*, edited by B. Bolin. pp. 271-286, John Wiley, New York, 1981a.
- Takahashi, T., W. S. Broecker, and A. E. Bainbridge. Supplement to the alkalinity and total carbon dioxide concentration in the world oceans, In: *Carbon Cycle Modelling (SCOPE 16)*, edited by B. Bolin, pp. 159-199, John Wiley, New York, 1981b.
- Takahashi, T., J. Olafsson, W. S. Broecker, J. G. Goddard, D. W. Chipman, and J. White. Seasonal variability of the carbon-nutrient chemistry in the ocean areas west and north of Iceland. In: *Chemical tracers for studying water masses and physical processes in the sea.* edited by U. Stefansson. *Rit Fiskideildar (J. of the Marine Research Institute, Reykjavik)* 9, 20-36.
- Takahashi, T., C. Goyet, D. W. Chipman, E. Peltzer, J. Goddard, and P. G. Brewer. Ratio of organic carbon and calcium carbonate productions observed at the JGOFS 47°N, 20°W site, JGOFS Report No 7, Abstracts, JGOFS North Atlantic Bloom Experiment International Scientific Symposium, SCOR/ICSU, 76-77, 1990.
- Takahashi, T., J. Olafsson, J. G. Goddard, D. W. Chipman, and S. C. Sutherland. Seasonal variations of CO₂ and nutrients in the high-latitude surface oceans: A comparative study, *Global Biogeochem. Cycles.* 7, 843-878, 1993.
- Takahashi, T., T. T. Takahashi, and S. C. Sutherland, An assessment of the role of the North Atlantic as a CO₂ sink, *Phil. Trans. R. Soc. Lond. B*, 143-151, 1995.

- Talley, L. D., and M. S. McCartney, Distribution and circulation of Labrador Sea water, *J. Physical Oceanogr.*, *12*, 1189-1204, 1982.
- Tans, P. P., I. Y. Fung, and T. Takahashi, Observational constraints on the global atmospheric CO₂ budget, *Science*, *247*, 1431-1438, 1990.
- Taylor, A. H., and I. Joint, A steady-state analysis of the "microbial loop" in stratified systems, *Marine Ecol. Prog. Ser.*, *59*, 1-17, 1990.
- Taylor, A. H., A. J. Watson, M. Ainsworth, J. E. Robertson, and D. R. Turner, A modelling investigation of the role of phytoplankton in the balance of carbon at the surface of the North Atlantic, *Global Biogeochem. Cycles*, *5*, 151-171, 1991.
- Taylor N. K., Seasonal uptake of anthropogenic CO₂ in an ocean general circulation model, *Tellus*, *47*, 145-169, 1995.
- Toggweiler, J. R., K. Dixon, and K. Bryan, Simulations of radiocarbon in a coarse-resolution, world ocean model, I, Steady state, pre-bomb distribution, *J. Geophys. Res.*, *94*, 8217-8242, 1989.
- Trenberth, K. E., W. G. Large, and J. G. Olson, The effective drag coefficient for evaluating wind stress over the oceans, *J. Clim.*, *2*, 1507-1516, 1989.
- Trotte, J. R., Phytoplankton floristic composition and size-specific photosynthesis in the eastern Canadian Arctic, M. Sc. thesis, Dalhousie University, Halifax, Nova Scotia, Canada, 1985.
- Van Scoy, K. A., K. P. Morris, J. E. Robertson, and A. J. Watson, Thermal skin effect and the air-sea flux of carbon dioxide: A seasonal high-resolution estimate, *Global Biogeochem. Cycles*, *9*, 253-262, 1991.
- Vinogradov, M.E., (Ed.), *Vertical distribution of the oceanic zooplankton*, (In Russian), 320 pp., Publishing House "Nauka", Moscow, 1968.
- Volk, T., and Z. Liu, Controls of CO₂ sources and sinks in the Earth scale surface ocean: temperature and nutrients, *Global Biogeochem. Cycles*, *2*, 73-89, 1988.
- Wagener, K., The carbonate system of the ocean, in *The Global Carbon Cycle (SCOPE 13)*, edited by B. Bolin, E. T. Degens, S. Kempe, and P. Ketner, pp. 251-258, John Wiley, New York, 1979.
- Waite A., P. K. Bienfang, and P. J. Harrison, Spring bloom sedimentation in a subarctic ecosystem. I. Nutrient sensitivity, *Mar. Biol.*, *114*, 119-129, 1992a.

- Waite A., P. K. Bienfang, and P. J. Harrison, Spring bloom sedimentation in a subarctic ecosystem. II. Succession and sedimentation, *Mar. Biol.*, 114, 131-138, 1992b.
- Wanninkhof, R., Relationship between wind speed and gas exchange over the ocean, *J. Geophys. Res.*, 97, 7373-7382, 1992.
- Watson, A. J., C. Robinson, J. E. Robertson, P. J. le B. Williams, and M. J. R. Fasham, Spatial variability in the sink for atmospheric carbon dioxide in the North Atlantic, *Nature*, 350, 50-53, 1991.
- Webb, W. L., M. Newton, and D. Starr, Carbon dioxide exchange of *Alnus rubra*: A mathematical model, *Oecologia*, 17, 281-291, 1974.
- Weiss, R. F., Carbon dioxide in water and sea water: The solubility of a non-ideal gas, *Mar. Chem.*, 2, 203-215, 1974.
- Weiss, R. F., W. S. Broecker, H. Craig, and D. W. Spencer (Eds.), *GEOSECS Indian Ocean Expedition. Vol. 5, Hydrographic Data 1977-1978*, 42 pp., International Decade of Ocean Exploration, National Science Foundation, Washington, D. C., 1983.
- Wiebe, P. H., S. Boyd, and J. L. Cox, Relationship between zooplankton displacement volumes, wet weight, dry weight and carbon, *Fish. Bull.*, 53, 777-786, 1975.
- Wong, C. S., Y. -H. Chan, J. S. Page, R. D. Bellegay, and K. G. Pettit, Trends of atmospheric CO₂ over Canadian WMO background stations at Ocean Weather Station P, Sable Island, and Alert, *J. Geophys. Res.*, 89, 9527-9539, 1984.
- Wroblewski, J. S., J. L. Sarmiento, and G. R. Flierl, An ocean basin scale model of plankton dynamics in the North Atlantic. 1. Solutions for the climatological oceanographic conditions in May, *Global Biogeochem. Cycles*, 2, 199-218, 1988.
- Zwally, H. J., J. C. Comiso, C. L. Parkinson, W. J. Campbell, F. D. Carsey, and P. Gloersen, Antarctic Sea Ice, 1973-76: Satellite Passive-Microwave Observations, NASA Spec. Publ., SP-459, 206 pp., 1983.